UNIVERSITY OF
BIRMINGHAM

THE DISTRIBUTION AND PRO-INFLAMMATORY IMPACT OF TITANIUM DEBRIS ACCUMULATION IN THE PERI-IMPLANT ENVIRONMENT

by

Sonam Kalra

A thesis submitted to
The University of Birmingham
for the degree of
DOCTOR OF PHILOSOPHY

Biomaterials Unit
School of Dentistry
College of Medicine & Dentistry
The University of Birmingham
September 2013

ABSTRACT

Titanium (Ti) and its alloys have many properties and behaviour characteristics which make them a suitable group of materials to be used for biomedical implants. Ti implant materials are used in both indwelling sites such as parts of joint replacements or in sites that penetrate the epithelium such as dental implants. In both contexts, device failure which is often associated with chronic inflammation is a significant problem. For indwelling devices, the build-up of particles and implant derived ions in the peri-implant tissues has been identified to significantly have impact on inflammation and clinical outcomes. For skin or mucosa penetrating Ti implants, little consideration is given to the potential role that Ti has in particulate or ionic form in modifying or indeed initiating inflammatory responses.

In the current thesis, state of the art elemental detection methods were adopted to firstly probe tissues surrounding Ti implants where wear processes would not be expected. The discovery of Ti distributions in forms indicative of corrosion processes suggests that indeed Ti should be considered as a potential modifier of the peri-implant physiological processes. Subsequent analysis of inflamed peri-implant tissues from indwelling, percutaneous and transmucosal sites demonstrated the presence of Ti in all samples studied. Characterisation of the Ti speciation preceded electrochemical simulations which confirmed that all Ti that had been observed in the tissues could be accounted for by crevice corrosion processes.

Neutrophils are the predominant acute inflammatory cells in percutaneous and transmucosal peri-implant sites. Therefore, an array of neutrophil immune responses (phagocytosis, respiratory burst, NETosis, cytokine secretion and chemotaxis) were studied following stimulation with Ti in forms identified in the peri-implant tissues. Finally, the modification of neutrophil immune responses to known periodontal pathogens following Ti exposures was explored. The findings strongly indicated that neutrophil responses can be modified by Ti species found in peri-implant sites and further work is needed to identify the role that ‘free Ti’ has on implant outcomes.

ACKNOWLEDGEMENTS

I would like to express great gratitude to my supervisors, Dr. Owen Addison and Professor Iain Chapple for their endless patience, support, guidance and encouragement. Special thanks to Dr. Alison Davenport, Dr. John Mathews, Dr. Melissa Grant and Dr. Helen Wright for their beneficial innovative ideas, suggestions and feedback.

I would also like to convey great thanks and appreciation to co-team members Dr. Richard Martin (Aston University), Dr. Mehdi Monir (University of Birmingham, Metallurgy and Materials Department) and Dr. Fred Mosselmans and Ms. Tina Geraki (I-18 Beamline scientists) for their help in synchrotron experiments and Ms. Helen Roberts for her help in chemotaxis assays. Sincere thanks to Dr. Kevin Carter and Mrs. Michelle Holder for their helpful laboratory assistance at all times.

Most importantly I would like to thank all the volunteers who willingly donated blood. Equally, I would like to thank the nurses of the periodontology unit for their expert venepuncture skills.

Lastly, but not the least a big thank you to my parents for always believing in me and my friends for making me laugh at stressful times.

TABLE OF CONTENTS

LIST OF FIGURES

LIST OF TABLES

ABBREVIATIONS

3-Amino-1,2,4 Triazole	3-AT
4-Aminobenzoic Acid Hydrazide	4-ABAH
Alpha	α
Aluminium	Al
American Society for Testing and Materials	ASTM
Antigen Presenting Cells	APCs
Antimicrobial Protein	AMP
Arbitrary Fluorescent Units	AFU
Approximate	~
Base Pairs	bp
Beta	β
Bone Anchored Hearing Aid	BAHA
Bovine Serum Albumin	BSA
Calcium	Ca
Carbon	C
Carbon Dioxide	CO_2
Centimetre cubed	cm^3
Chloride	Cl
Chromium	Cr
Chronic Granulomatous Disease	CGD
Cobalt	Co
Commercially Pure	Cp
Cystic Fibrosis	CF
Cytochalasin B	cytoB
Degree Celsius	°C
Dendritic Cells	DCs
Deoxyribonuclease	DNase
Deoxyribonucleic acid	DNA
Diacylglycerol	DAG
Dimethyl Sulfoxide	DMSO
Diphenyl-Eneiodonium	DPI
Electrochemical Impedance Spectroscopy	EIS
Electron Volt	eV
Energy Dispersive X-ray	EDX
Energy Filtered Transmission Electron Microscopy	EFTEM
Enzyme Linked Immunosorbant Assay	ELISA
Ethylene Diamine Tetraacetic Acid	EDTA
Extended X-ray Absorption Fine Structure	EXAFS
Extracellular signal Regulated Kinase	ERK
Fc-gamma Receptor	Fc-γR
Foetal Calf Serum	FCS
Fusobacterium Nucleatum	*FN*
Gamma	γ
Giga Electron Volt	GeV

Glucose supplemented Phosphate Buffer Saline	GPBS
Glutathianione	GSH
Grams	g
Granulocyte Macrophage Colony Stimulating Factor	GM-CSF
Greater than	>
Greater than or equal to	≥
Haematoxylin and Eosin	H & E
Horseradish Peroxidase	HRP
Hour	hr
Human Aortic Endothelial Cells	HAECs
Human Mesenchymal Stem Cells	hMSCs
Hydrochloric Acid	HCl
Hydrogen Peroxide	H_2O_2
Hydroxide	OH
Hydroxyl Radical	·OH
Hypochlorous acid	HOCl
Immunoglobulin	Ig
Inductively Couple Plasma	ICP
Inflammatory infiltrate	ICT
Insertion Device	ID
Interferon	IFN
Interleukin	IL
Iron	Fe
Kilo Electron Volt	KeV
Less than	<
Less than or equal to	≤
Lipopolysaccharide	LPS
Litre	L
Magnesium	Mg
Magnetic Resonance Imaging	MRI
Major Histocompatibility Complex	MHC
Mannitol Salt Agar	MSA
Mass Spectroscopy	MS
Matrix Metalloproteinase	MMP
Mechanically Assisted Crevice Corrosion	MACC
Megapascal	MPa
Mesenchymal Stem Cell	MSC
Micrococccal Nuclease	Mnase
Microgram	µg
Microlitre	µL
Micrometer	µm
Micron	µ
Miligram	mg
Millilitre	mL
Millimetre	mm
Millimolar	mM
Minutes	mins
Mitogen Activated Protein Kinase	MAPK

Molar	M
Molybdenum	Mo
Mouse Stem Cell Factor	M-SCF
Multiplicity of Infection	MOI
Myeloperoxidase	MPO
N-Formyl-Metionyl-Leucyl-Phenylalanine	fMLP
Nanometer	nm
Neutrophil Attractant Protein-1	NAP-1
Neutrophil Elastase	NE
Neutrophil Extracellular Traps	NETs
Nicotinamide Adenine Dinucleotide Phosphate	NADPH
Niobium	Nb
Nitrogen	N
Non-Steroidal Anti-Inflammatory Drugs	NSAID's
Nuclear Factor-kB	NF-kB
Opsonised *Staphylococcus aureus*	Ops *Sa*
Optical Density	OD
Oxygen	O
Oxygen Molecule	O_2
Particle Induced X-ray Emission	PIXE
Parts Per Billion	ppb
Parts Per Million	ppm
Pathogen Associated Molecular Patterns	PAMPs
Pattern Recognition Receptors	PRRs
Peptidoglycans	PGN
Percent	%
Peripheral Blood Neutrophils	PBN
Pico grams	pg
Phorbol 12-Myristate 13-Acetate	PMA
Phosphate Buffered Saline	PBS
Phosphatidylinositide 3-Kinases	PI3K
Phosphorous	P
Platelet Activating Factor	PAF
Polymorphonuclear leukocyte	PMNL
Polyvinylchloride	PVC
Polyvinylpyrrolidone	PVP
Potassium	K
Prostaglandin E2	PGE2
Protein Kinase C	PKC
Reactive Oxygen Species	ROS
Receptor Activator of NF-kB ligand	RANKL
Relative Centrifugal Force	rcf
Relative Light Units	RLU
Scanning Electron Microscope	SEM
Seconds	secs
Signal Transducers and Activators of Transcription	STAT
Silicon Carbide	SiC
Silver	Ag

Sodium	Na
Standard Deviation	SD
Superoxide Anion Radical	O_2^-
Superoxide Dismutase	SOD
Synchrotron Radiation	SR
Systemic Lupus Erythamatosis	SLE
Titanium	Ti
Titanium chloride	$TiCl_3$
Titanium dioxide	TiO_2
Toll Like Receptor	TLR
Transmission Electron Microscope	TEM
Tumour Necrosis Factor-alpha	TNF-α
Units	U
Vanadium	V
Volts	V (Ch5)
Water	H_2O
Wavelength	λ
White Blood Cell	WBC
X-ray Absorption Fine Structure	XAFS
X-ray Absorption Spectroscopy	XAS
X-ray Fluorescence Mapping	XRF
X-ray Near Edge Structure	XANES
Years	yrs
Zirconium	Zr

CHAPTER 1

GENERAL INTRODUCTION

1.1 Titanium (Ti) and Ti alloys as biomaterials

Titanium (Ti) is a transitional metal with silver colour, possessing an atomic number of 22 and atomic weight of 47.9 (McQuillan, 1970). Ti is generally considered as one of the most biocompatible metallic materials used for biomedical applications (Williams, 1987). However, the term 'biocompatibility' is often loosely used by the biomaterials community and the general population and is frequently ill-defined. Biocompatibility is best considered as a state of mutual coexistence between the biomaterial and the physiological environment such that neither has an undesirable effect on the other (Tang & Eaton, 1995). However, a material may be biocompatible in one form in a specific environment but elicit an unfavourable response when presented in a different form or placed into a different environment (Williams, 1994). Therefore, biocompatibility of a material must be contextualised to a specific application (Brunette, 2001).

Ti has been successfully used in a wide variety of surgical applications including orthopaedics (Cook et al., 1988), maxillofacial (Williams, 1981), craniofacial (Albrektsson et al., 1983), cardiovascular and neurosurgery (Sunny & Sharma, 1991) rehabilitation purposes. Ti is a suitable substrate for a variety of manufacturing routes including casting, sintering or machining (lathing, milling, threading) which are all currently used for the manufacture of Ti medical devices (Brunette, 2001). Alongside the versatility in processing Ti, it has favourable

mechanical properties including a high tensile strength, high toughness, low elastic modulus and low density of 4.54 (g/cm^3) (Elias et al., 2008). These characteristics of Ti confer a light weight to fabricated devices (Elias et al., 2008) and suitable chemical properties including corrosion resistance and thermal stability (Albrektsson et al., 1981) which ensure that they are also highly damage tolerant (Hallam et al., 2004). In addition, Ti was the first metallic biomaterial which was demonstrated to have the ability to osseointegrate (Brånemark, 1977). Osseointegration is a time dependent process and is defined as the dynamic interaction of living bone with an implanted biomaterial which occurs with the absence of an interposing soft tissue layer (Brånemark et al., 1985). A further favourable property of Ti for biomedical applications includes that it is relatively radiolucent (Mudali et al., 2003) enabling patients with indwelling Ti implant(s) to be examined with Magnetic Resonance Imaging (MRI) (Hettige & Norris, 2012). As a consequence Ti is being increasingly used as a biomedical material.

1.1.1 Classification of biomedical Ti

The American Society for Testing and Materials (ASTM) International recognizes 31 grades of Ti and Ti alloys of which 23 are classified as biomedical materials (Brunnette, 2001). Biomedical Ti is used in either commercially pure (Cp) forms or alloyed with elements such as aluminium (Al), vanadium (V) or niobium (Nb) (Elias et al., 2008) in order to modify the mechanical and surface properties. CpTi is itself not completely pure, containing metallic impurities of which iron (Fe) is the most common and which can modify the mechanical and chemical material properties. The two most commonly used biomedical forms of Ti include CpTi

and the alloy Ti-6Al-4V (Elias et al., 2008). Both grades are paramagnetic, have low electrical and thermal conductivity and a significantly higher strength to weight ratio in comparison to other competing metallic implant materials such as stainless steel or Cobalt-Chromium-Molybdenum (Co-Cr-Mo) (Elias et al., 2008).

1.1.2 CpTi (unalloyed) biomedical implants

CpTi is classified by ASTM as Grades I-IV which are suitable for the manufacture of long term craniofacial and dental devices and for which the mechanical demands are considered less than for orthopaedic applications (Elias et al., 2008). Grades I-IV are distinguished by their varying degrees of tensile strength which is influenced by the oxygen content (itself dictated by the impurity level). Grade I is the most ductile (lowest tensile strength of 240 MPa with an oxygen content of 0.18%) and Grade IV the least ductile (highest tensile strength of 550 MPa with an oxygen content of 0.40%).

1.1.3 Ti-6Al-4V alloyed biomedical implants

Ti-6Al-4V is the ASTM Grade V alloy and was originally developed for aerospace applications but has historically been the most attractive for indwelling (orthopaedic) implant applications because of its high tensile strength of 910 MPa (Elias et al., 2008). The alloy is less commonly used in dental applications but is extensively used for craniofacial fixation devices (Neumann, 2009) following trauma or elective surgeries for fracture stabilisation.

1.1.4 Biological and biomechanical differences between CpTi (unalloyed) and Ti-6Al-4V alloyed implants

Differences between the biological responses to CpTi (unalloyed) and Ti-6Al-4V alloyed implants have been observed in *in-vivo* studies. Following osseous insertion into rabbit bone, it was observed that the CpTi implants had higher removal torque values than the Ti-6Al-4V alloyed implants and a significantly increased number of bone contacts were observed (Johansson et al., 1998 & Elias et al., 2008). It has subsequently been proposed that the increased elasticity of CpTi results in more evenly shared loading between bone and the implant (Wang et al., 2007) thus leading to a lower incidence of bone degradation (Niinomi, 2003). However, CpTi implants possess lower shear strengths (240-550 MPa) than Ti-6Al-4V and are therefore largely precluded in orthopedic applications (Elias et al., 2008). The corrosion resistance of Ti-6Al-4V implants is also lower and therefore for permanent implant applications, the alloy has been proposed to have toxic effects on host tissues but to date this has largely been associated with the release of Al and V ions (Mudali et al., 2003 & Elias et al., 2008). For this reason, Al- and V- free alloys including Ti-6Al-7Nb (ASTM F1295), Ti-13Nb-13Zr (ASTM F1713) and Ti-12Mo-6Zr (ASTM F1813) have been introduced (Elias et al., 2008). It is important to note that the potential toxicity of Ti itself is rarely considered.

1.2 The Ti surface

Ti is a highly reactive metal and its stability in physiological environments and the biological response to it are conferred by the presence of a resilient surface

oxide layer (Kasemo, 1983). Cellular responses to Ti, including the highly favourable phenomenon of osseointegration are determined by the interaction with the Ti oxide surface which is extremely thin at a thickness of 5-20 nm (Schroeder et al., 1981). Disruption of this oxide surface either mechanically or chemically leads to rapid reformation (re-passivation) of the surface (Kasemo, 1983) wherever moisture and oxygen are present due to the strong affinity of Ti for oxygen (Joshi & Eley, 1988). It is important to recognise that the formation of such a robust oxide layer on Ti implants accounts for the perceived benign nature of Ti as a biomaterial (Sunny & Sharma, 1991 & Olmedo et al., 2008).

The chemical composition and structure of the surface oxide film is complex and can be highly heterogeneous. Simplistically, it can be considered as comprising of three layers where the first layer adjacent to metallic Ti is TiO, the intermediary layer is Ti_2O_3, and the third layer, which is in contact with the external environment, displays the passive oxide (TiO_2) film (Gemelli et al., 2007). The composition, structure and morphological variability of biomedical Ti surfaces have been shown to impact on the surface hydrophobicity (influencing protein interactions) (Rae, 1978 & Varmanu et al., 2008), cellular adhesion and proliferation (Sunny & Sharma, 1991) and corrosion resistance properties (Koike & Fujii, 2001).

1.2.1 The composition of the surface oxide layer (TiO_2) on Ti implants

The passive surface exhibits TiO_2 which is a naturally occurring, highly insoluble (Driscoll et al., 1997), thermally stable Ti compound found in minerals as rutile,

anatase, brookite as well as in iron-containing ilmenite (Jolivet et al., 2010). Although they share the same chemistry, each form of TiO_2 has a distinctive structure due to its atomic co-ordination (Hedenborg, 1988 & Rahman et al., 2002). In nature, ilmenite is the most common form of TiO_2 (Duan et al., 2010 & Iavicoli et al., 2011) however, the passive film formed on biomedical Ti has been characterised as composed of mainly rutile and anatase polymorphs (Effah et al., 1995 & Olmedo et al., 2008). Structurally, the Ti atoms in rutile and anatase are surrounded octahedrally in a distorted structure by six oxygen atoms (Figure 1.1) (Jolivet et al., 2010).

Figure 1.1 Crystal structure representations of (a) rutile and (b) anatase polymorphs of TiO_2 (Jolivet et al., 2010)

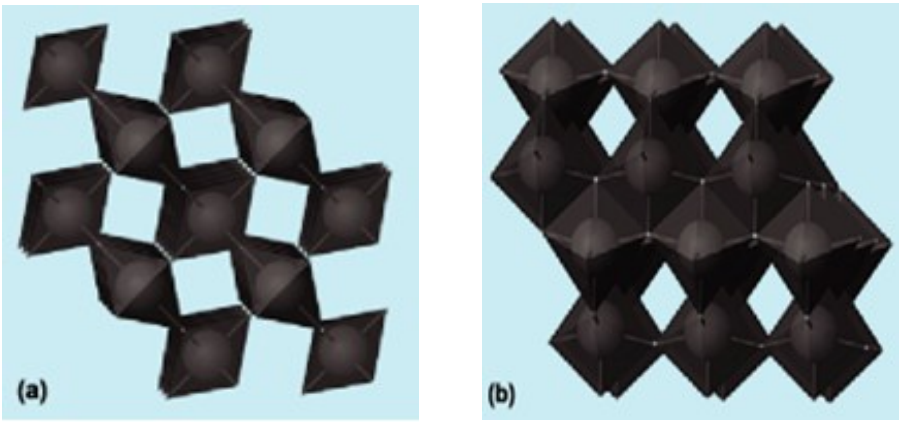

Both rutile and anatase polymorphs of TiO_2 possess tetragonal symmetry and have similar physical properties although their stability differs (Iavicoli et al., 2011). Rutile has been assumed to be the most thermodynamically stable form because of its significantly naturally increased occurrence as compared with anatase (Iavicoli et al., 2011).

1.3 Ti prosthesis failure

Despite the extensive use of Ti implant devices which have revolutionised treatment options in dentistry and many surgical disciplines (Albretktsson, 1983), failure of the device and its management remains, the key clinical concern. Several people worldwide annually undergo revision procedures, for maintenance or replacement of a Ti prosthesis. Complications are predominately biological (Ratner, 2001) which have raised concerns regarding the biocompatibility of Ti as an implant material (Li et al., 2010). Biological complications are frequently ill-defined but include pathological inflammatory changes in the tissues surrounding a functional Ti implant. In dentistry, adverse biological responses associated with implants are termed as peri-implant disease (Albretktsson & Isidor, 1994).

1.3.1 Peri-implant disease

Peri-implant disease encompasses two distinct entities. Establishment of a reversible inflammatory lesion in the peri-implant mucosa is referred to as 'peri-implant mucositis' (Albrektsson & Isidor, 1994 & Klokkevold & Newman, 2000). However, this lesion may spread in an 'apical' direction to involve bone, compromising osseointegration, with varying degrees of bone loss and is referred to as 'peri-implantitis' (Albrektsson & Isidor, 1994 & Klokkevold & Newman, 2000). Bone loss associated with peri-implantitis is typically circumferential and the shape of the bony defects appears to be influenced by the macroscopic shape of the implant. Peri-implantitis, like most inflammatory diseases, exhibits

discontinuous progression so that episodes of disease progression are interspersed with periods of quiescence (Klinge et al., 2005).

1.3.2 Prevalence of dental peri-implant disease

According to the 6th European workshop on periodontology, it is estimated that around 80% subjects with Ti dental implants suffer from peri-implant mucositis and up to 46% subjects suffer from peri-implantitis (Lindhe & Meyle, 2008). Mucositis and peri-implantitis are likened to gingivitis and periodontitis respectively (Mombelli et al., 1987). However, the extent and composition of the inflammatory infiltrate (ICT) into the lesion has been demonstrated to differ suggesting the mediators of the inflammation may also be different (Meffert, 1996).

1.3.3 Failure of skin penetrating Ti implants

It is estimated that around 25,000 percutaneous Ti implants require revision procedures annually worldwide (Ratner, 2001) which have raised concerns regarding the use of Ti in skin accessible systems. One such system where complications are frequent are Bone Anchored Hearing Aids (BAHA) used for the treatment of unilateral sensorineural hearing impairment (Wazen et al., 2008). BAHA's are dependent on a Ti implant which is inserted into the outer table of the post-auricular skull and connected via a modular percutaneous CpTi abutment to a sound processor (Addison et al., 2012). It is reported that ~33% patients suffer from peri-implant skin inflammation and ~3% extrude the prosthesis (Grant

et al., 2010) following chronic peri-implant inflammation. The prevalence of adverse complications manifested for Ti skin penetrating devices are similar to those for Ti indwelling prostheses (Ratner, 2001).

1.3.4 Failure of orthopaedic Ti implants

Ti and Ti alloys are extensively used in orthopaedic surgery as indwelling devices forming components of hip and knee joints (Sargeant & Goswami, 2007). It is estimated that over 300,000 patients with indwelling Ti prostheses undergo revision annually worldwide due to implant associated complications (Ratner, 2001). Symptoms associated with failing Ti devices include significant pain; clinical swelling and implant mobility are often detected (Hallam et al., 2004). Radiographic imaging can reveal cortical hypertrophy associated with intra-osseous Ti which has been described as resembling osteoid osteoma (Figure 1.2) (MDA, 2002 & Hallam et al., 2004).

Figure 1.2 Radiographs of a Ti hip replacement. Left: 2 days after implantation. Right: 2 years after implantation showing femoral loosening, thickening of the femoral cortices, similar to osteoid osteoma (Hallam et al., 2004)

Clinical signs associated with failing indwelling Ti prostheses include architectural modification of the tissues (Agins et al., 1988 & Black et al., 1990); discoloration of the surrounding bone and fibrous tissues known as metallosis (Scales, 1991); and inflammation of the surrounding tissues (Hallam et al., 2004). The current understanding of adverse inflammatory reactions surrounding orthopaedic indwelling Ti prostheses is that implant failure is multifactorial (Hallab & Jacobs, 2009) but failure is usually aseptic (Hallam et al., 2004). One of the major factors implicated is the presence of wear and/or corrosion processes (Mudali et al., 2003) leading to the accumulation of metal debris in the surrounding tissues. Therefore, considering Ti as a biologically inactive and physiological inert material in the human body is a false assumption (Warheit, 1997). The release of metal debris is itself complex and is mediated by mechanisms ranging from obvious wear processes to crevice corrosion and bio-corrosion. The combination of mechanisms which contribute to the release of Ti ions and particles (Ingham & Fischer, 2000 & Hallab et al., 2004) into the peri-prosthetic environment determine the characteristics of the metal release and are influenced by physiochemical processes which may be specific to a particular physiological environment (Sargeant & Goswami, 2007).

1.4 Aetiology of the failure of skin and mucosal penetrating Ti implants

The current understanding of the aetiology of skin and mucosal penetrating devices suggests multifactorial mechanisms, implicating both the presence of a bacterial biofilm (Fransson, 2009) and a dysregulated host-response (Flatebø et al., 2006).

1.4.1 The role and composition of microflora in the peri-implant *milieu*

The current understanding is that the presence of a biofilm on the implant surface is necessary for peri-implant 'mucositis' and 'implantitis' to occur (Berglundh et al., 1992 & Meffert, 1996). This cause and effect relationship is similar to that observed between bacterial plaque and periodontal inflammation (Bundy et al., 1980) in which plaque components express virulence factors which stimulate an array of inflammatory responses within the host that directly disturb tissue homeostasis (Amano, 2003). Similar to periodontal disease, the microbial flora comprises a multitude of microorganisms and a single causative pathogen for peri-implantitis cannot be identified (Socransky et al., 1998 & Haffajee et al., 2008). Early microbial colonisation studies of the 'pristine' peri-implant pocket identified that similar proportions of coccoid cells, motile rods and spirochetes become established within one to three weeks of implant insertion (Ponteriero et al., 1994 & Quirynen et al., 2006). The biofilm composition on the implant surfaces subsequently increases in complexity with time and is modified in the presence of peri-implant disease. Studies on Ti dental implants, after 6 years of service life associated with probing depths greater than 6 mm found higher percentages of both anaerobic gram positive and negative bacteria (George et al., 1995 & Renvert et al., 2007). Some of the pathogens dominating inflamed Ti implant sites identified using DNA probe analysis include gram positive *Staphylococci* species (Bundy et al., 1980 & Rams & Feik, 1990) and *Actinobacillus actinomycetemcomitans* (Leonhardt et al., 1993); and/or gram negative bacteria as *Fusobacterium nucleatum* (*FN*) (Mombelli et al., 1995), *Porphyromonas gingivalis* and *Bacterioides forsythus* (Becker et al., 1990).

1.4.2 The host response role in the progression of peri-implant disease and the impact of Ti implant derivatives

In common with periodontal disease, the host response is also implicated in determining an individual's susceptibility to the progression of peri-implant disease. The host-response can significantly influence the nature or magnitude of tissue destruction and inflammation. To date, studies have focused on the response(s) to periodontal pathogens, however, factors intrinsic to the implant environment including the potential release of Ti ions or particles which may act to stimulate or modulate the host response contributing in progression of the peri-implant disease are less well understood (Cobelli et al., 2011).

A limited number of studies have documented the potential cellular and molecular consequences of Ti ions and particles. Investigations have studied cell viability, differentiation and proliferation on variety of cell types with a variety of stimuli (Table 1.1). Ti particles have been reported to cause increased production of pro-inflammatory and pro-osteoclastogenic cytokines including interleukins such as IL-1α/β, IL-6, IL-8, IL-12; interferons such as IFN-α/γ, tumour necrosis factor-alpha (TNF-α); receptor activator of nuclear factor kappa-B ligand (RANKL) (Tuan et al., 2008) and many more which have been addressed to mediate enhanced bone resorption, contributing to peri-implant disease progression (Iavicoli et al., 2011). However, the mechanisms by which Ti particulate debris mediate such biological responses remain incompletely addressed (Iavicoli et al., 2011).

Table 1.1 Documented toxicological effects of Ti particles (Listed in alphabetical chronological order)

Ti Species	Cell Type	Reference
TiO_2 (anatase)	Human bronchial cells (BEAS-2B)	Bhattacharya et al., 2009
$Ti_{(iv)}$ ions	Human osteoclasts and osteoblasts	Cadosch et al., 2009
TiO_2 (unspecified)	Human dendritic cells	Chan et al., 2009
$Ti_{(iv)}$ ions	Wistar rats osteoblasts	Choi et al., 2005
TiO_2 (anatase)	Rat osteosarcoma	Di Virgilio et al., 2010
TiO_2 (anatase)	Chinese hamster ovary	Dodd & Jha, 2009
TiO_2 (anatase & rutile)	Human bronchial cells (BEAS-2B)	Falck et al., 2009
TiO_2 (anatase)	Human neutrophils	Goncalves et al., 2010
TiO_2 (anatase)	Human bronchial cells (BEAS-2B)	Gurr et al., 2005
TiO_2 (anatase)	Murine alveolar macrophages	Hamilton et al., 2009
TiO_2 (unspecified)	Rat macrophages	Hirayama et al., 2011
TiO_2 (anatase & rutile)	Human bronchial epithelial cells	Hussain et al., 2009
TiO_2 (anatase & rutile)	Mouse fibroblasts	Jin et al., 2008
TiO_2 (unspecified)	Fish neutrophils	Jovanovic et al., 2011
TiO_2 (unspecified)	Human lymphocytes	Kang et al., 2009
TiO_2 (anatase & rutile)	Human neutrophils	Kumazawa et al., 2002
TiO_2 (anatase & rutile)	Human fibroblasts	Lai et al., 2008
TiO_2 (anatase & rutile)	Human mesagial	L'Azou et al., 2008
TiO_2 (unspecified)	Human osteoblast-like cells ($SaOS_2$)	Li et al., 2010
TiO_2 (anatase & rutile)	Mouse neuronal cells	Liu et al., 2010
Metallic Ti	Rat brain microglia	Long et al., 2007
TiO_2 (unspecified)	Human mesenchymal stem cells (hMSCs)	Okafor et al., 2006
TiO_2 (anatase & rutile)	Male Wistar rats	Olmedo et al., 2008
TiO_2 (rutile)	Rat whole blood	Onuma et al., 2009
TiO_2 (rutile)	Human bronchial cells (BEAS-2B)	Park et al., 2008
TiO_2 (unspecified)	Human aortic endothelial cells (HAECs)	Peng et al., 2010
TiO_2 (unspecified)	Human muscle cells	Peters et al., 2004
Metallic Ti	Rat osteoblasts	Pioletti et al., 1999
TiO_2 (unspecified)	Hamster embryo cells	Rahman et al., 2002
TiO_2 (unspecified)	Mouse fibroblasts	Renwick et al., 2001
TiO_2 (anatase & rutile)	Human fibroblasts	Rothen-Rutishauser et al., 2008
TiO_2 (anatase)	Human monocytes,	Sayes et al., 2006

	macrophages and dendritic cells	
TiO_2 (anatase)	Human dendritic cells	Schanen et al., 2009
TiO_2 (anatase)	Human macrophages (THB-1)	Soto et al., 2007
TiO_2 (anatase & rutile)	Human epithelial cells	Stearns et al., 2001
TiO_2 (unspecified)	Hamster ovary cells	Uchino et al., 2002
TiO_2 (unspecified)	Human mesenchymal stem cells (hMSCs) and lymph cells	Wang et al., 2007 & 2009

The current understanding is that Ti particles can alter cell function and phenotype with effects regulated by particle size (Choi et al., 2005 & Cobelli et al., 2011). In particular, nanoparticles with dimensions <100 nm, have been shown to interact differently with various proteins and subsequently with cells when compared with larger sized particles (Liu and Webster, 2006). Further studies have demonstrated that nanoparticles bind to serum proteins which enables the transport of Ti debris into surrounding tissues and to organs far from the implant site (Rubio et al., 2008). *In-vivo* studies measuring Ti debris accumulation in sites distant from the implant including the kidneys, livers, lungs, spleens and lymph nodes (Rubio et al., 2008) revealed Ti localised within these organs and the concentrations significantly increased with implantation time. Using energy filtered transmission electron microscopy (EFTEM) and mass spectrometry (MS), it has been demonstrated that Ti possesses a strong affinity for phosphorous containing molecules (Chan et al., 2009). This could have particular relevance to euchromatin in the nucleus, ribosomes in the cytoplasm, and phospholipids in the cell membrane (Carvalho et al., 2007). It has been suggested that the attachment of Ti to phosphorylated intercellular proteins and phospholipids (corresponding to the active functional states of enzymes or signalling proteins) could alter cellular

and metabolic functions of the cell such as migration and protein secretion (Carvalho et al., 2007 & Chan et al., 2009).

1.5 Role of neutrophils in inflammation

Amongst the innate immune cells; neutrophils have been significantly associated with the progression of periodontitis (Kantarci et al., 2003) and are found in high numbers in mucosa and skin penetrating implant sites (Holgers, 2000). When compared with chronic periodontitis, neutrophils are proportionally found in increased numbers in peri-implant disease sites (Klinge et al., 2005 & Teronen et al., 1997). Initially neutrophils are attracted to the inflamed site following a chemotactic gradient from the blood with the aim of infiltrating the tissue and phagocytosing the pathogen or foreign material, to prevent its spread (Witko-Sarsat et al., 2000). The process involves margination, tethering and rolling, adhesion and finally transmigration (Witko-Sarsat et al., 2000). Bacterial products such as lipopolysaccharides (LPS) (Edwards, 1994); formyl peptides (Amulic et al., 2012); and endogenous signals such as pro-inflammatory cytokines released by other immune cells are known chemoattractants (Tuan et al., 2008 & Kumar & Sharma, 2010).

Neutrophils constitute ~40-60% of the white blood cell (WBC) population and are considered as the first line of defence in the inflammatory response providing a relatively non-specific response (Segal, 2005). These cells are also known as polymorphonuclear leukocytes (PMNL) due to their multi-lobed (3-5 lobes) nuclei (Metchnikoff, 1905) and their cytosol is densely populated with four

different types of granules containing cytotoxic contents such as hydrolytic enzymes, defensins, proteolytic enzymes and antimicrobial proteins (AMP's) (Hampton et al., 1998) which are released upon microbial challenge to kill the internalised microorganism (Borregaard & Cowland, 1997) and/or in the process of eliminating foreign stimuli such as cellular debris (Cicchetti et al., 2002).

1.5.1 Neutrophil activation

An abundance of neutrophils (5 x 10^{10} cells/day) circulate in the blood of normal healthy individuals and the cells are short lived (~12 hr in circulation), and are not present in normal healthy tissue sites (Edwards, 1994). During an inflammatory response, neutrophils leave the blood volume and infiltrate the site of tissue injury or infection (Stevens et al., 2002). Following migration to the site, the activated cells execute a variety of specialised tasks including phagocytosis, degranulation and secretion of variety of pro-inflammatory cytokines (Metchinikoff, 1893 & Wright et al., 2010). Neutrophils have significant antimicrobial activity through the secretion of reactive oxygen species (ROS) (Larsson et al., 2003) and/or through degranulation releasing antimicrobial agents such as neutrophil elastase (NE) into the extracellular space (Parsonage et al., 2008). A variety of cell surface receptors including pattern recognition receptors (PRRs) including toll like receptors (TLRs) and Fc-γ receptors (Fc-γR) for the Fc region antibodies, and receptors for C3b, an opsonising molecule of the complement system have been identified as routes by which neutrophils can target and internalise a pathogen within a vacuole called the phagosome (Figure 1.3) (Garcia-Garcia, 2005). Once formed, the phagosomes can fuse with endosomes and lysosomes which contain

active lipases and proteases to produce phagolysosome (Figure 1.3) (Tapper, 1996).

Figure 1.3 Schematic representations of neutrophil phagosome and phagolysosome formation (Tapper, 1996)

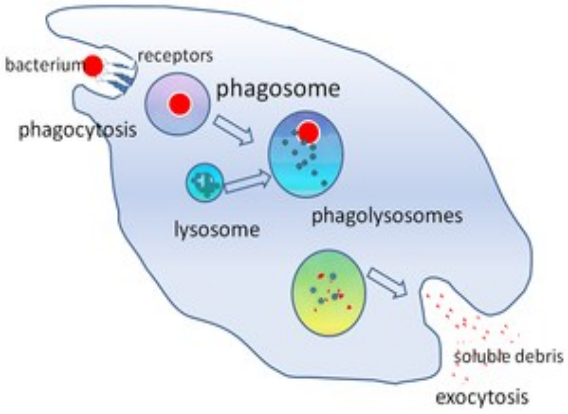

1.5.2 Neutrophil killing mechanism

Following engulfment of the foreign material, the neutrophil generates antimicrobial agents to combat its spread (Hampton et al., 1998). The antimicrobial activity is via two routes involving either oxidative or non-oxidative mediated killing mechanisms (Hampton et al., 1998). The release of proteases and AMPs within neutrophil granules is known as the non-oxidative killing mechanism (Hampton et al., 1998). The process occurs by fusing of the granule with the phagosome leading to exposure of the engulfed body to antimicrobial peptides and enzymes (Hampton et al., 1998). In addition, an oxidative killing mechanism known as oxidative burst (Griffiths & Lunec, 1988) involves the generation of ROS (Larsson et al., 2003). Such species are chemically reactive

molecules and free radicals such as singlet oxygen, superoxides, peroxides, hydroxyl radical (·OH) and hypochlorous acid (HOCl) are generated as by-products from cellular metabolism of oxygen (Nathan, 2006). ROS are capable of oxidizing various types of molecules including nucleic acids (Park et al., 1992), lipids (Battino et al., 1999) and proteins (Roberfroid & Calderon, 1995) and if released into the extracellular space, can damage components of the connective tissue leading to destruction of tissues such as alveolar bone and the periodontium (Moseley et al., 1997). The release of ROS can also cause activation of other cells such as osteoclasts and evidence has shown that ROS are capable of both increasing osteoclast numbers and osteoclasts activity (Garrett et al., 1990 & Pioletti et al., 1999).

1.5.3 Extracellular killing mechanism

Neutrophils are also capable of mediating extracellular killing mechanism by actively protruding fragile fibril complexes called Neutrophil Extracellular Traps (NETs) into the extracellular matrix (Brinkmann et al., 2004). NETs are web-like strands of decondensed chromatin packaged with antimicrobial components such as NE and myeloperoxidase (MPO) (Brinkmann & Zychlinsky, 2007) secreted to trap and kill micro-organisms extracellulary (Remijsen et al., 2010 & Menegazzi et al., 2012). Recent studies over the past years have implicated NETs to play an important role in immune defence (Beiter et al., 2006 & Buchananan et al., 2006).

1.6 Neutrophil responses to Ti particles

Surprisingly, despite the significant presence of neutrophils at peri-implant disease sites, there have been limited studies to evaluate the potential effects of Ti particles exposure on neutrophil responses (Table 1.1) (Kumazawa et al., 2002, Goncalves et al., 2010, & Jovanovic et al., 2011). However, the evidence that has been reported strongly suggests that should these species be present in the peri-implant tissues, they can significantly affect neutrophil function. *In-vitro* studies have demonstrated that TiO_2 of up to 3 μm diameter can be phagocytised by mammalian neutrophils (Kumazawa et al., 2002) and stimulate respiratory burst release (Jovanovic et al., 2011). Neutrophils exposed to nano TiO_2 (0-100 μg/mL) have been reported to induce phosphorylation of p38 Mitogen Activated Protein Kinase (MAPK) and Extracellular signal Regulated Kinases-½ (ERK-1/2) (Goncalves et al., 2010). In addition, TiO_2 exposure (≥20 μg/mL) has been shown to significantly inhibit neutrophil apoptosis in a concentration dependent manner and stimulate IL-8 cytokine release (Goncalves et al., 2010). Moreover, NET release which is associated with the neutrophil respiratory burst process has been demonstrated in TiO_2 stimulated fish neutrophils (Jovanovic et al., 2011).

1.7 Summary and aims

Clinical concern remains regarding the performance of biomedical Ti implants largely due to the development of chronic inflammation in the peri-implant tissues necessitating removal or revision of the device (Hallab & Jacobs, 2009). The perceived biocompatibility of Ti is conferred by a resilient surface oxide film

(Kasemo, 1983). However, the composition, structure and morphology of the layer have been shown to be sensitive to the alloy type and the environment into which it is placed (Williams, 1994). The failure of indwelling Ti devices is often aseptic (Caicedo et al., 2010) and associated with the generation of micron and nano sized implant debris released into the peri-implant tissues (Choi et al., 2005 & Hallab & Jacobs, 2009). In common with orthopaedic devices, chronic inflammation in peri-implant tissues surrounding skin and/or mucosal penetrating Ti implants is of significant concern. To date all research into chronic inflammation associated with these devices has implicated implant surface microflora (section 1.4.1) and the host response (section 1.4.2) in the pathogenesis of peri-implant disease. Although, it is strongly hypothesized, but it is not known whether Ti implant derivatives are formed or whether they can contribute to pathophysiology of the inflammation present surrounding skin or mucosal penetrating Ti implants. However, Ti products identified or hypothesised to be released into these environments have been previously shown to be pro-inflammatory and have been studied *in-vitro* (Table 1.1). Very few studies have focused on cell types which are identified to be of primary importance in the progression of the inflammation surrounding Ti skin or mucosal penetrating implants, such as human neutrophils. The current evidence suggests that should such Ti implant derivatives be present, they are likely to have an impact on neutrophil phagocytosis, ROS and NET generation mechanisms.

The overall objectives of this thesis are to:

- Identify whether Ti is found in soft tissues surrounding percutaneous/trans-mucosal implants.

- Identify whether Ti species found in tissues can be accounted for release by mechanically assisted crevice corrosion (MACC) mechanism.

- Study the responses of human neutrophils to representative Ti stimuli identified from the peri-implant tissues in terms of ROS production, NET formation and chemotaxis.

- Study how Ti implant derivatives may disrupt or modify responses of neutrophils to known peri-implant pathogens.

CHAPTER 2

MATERIALS AND METHODS

2.1 Raw materials

3 mm wide strips of 5 μm (TI2279) and 50 μm thick (TI2276) commercially pure titanium (CpTi) foils [Carbon (C) 200 ppm, Nitrogen (N) 120 ppm, Iron (Fe) 1500 ppm and Oxygen (O) 1500 ppm] were purchased from Advent Materials, Oxford, UK. Titanium chloride ($TiCl_3$) solution (14010) was purchased from Sigma-Aldrich, UK. Ultra-pure silica plates (Spectrosil 2000) were ordered from HeraeusQuarzglas GmbH & Co., Hanau, Germany. Polyimide films (PC500FILM-0500) were purchased from Kapton, Dupont, Wilmington, NC, USA. Vacutainer (GRI454247) and lithium heparin coated tubes (171 U/mL) (GRI454008) were purchased from Greiner, Bio-one Ltd, Stonehouse, UK. Needles (SN2170) and syringes (BS-120527) were purchased from Terumo Europe, Leuven, Belgium. Percoll 1.13 g/mL (17-0891-01) was purchased from GE Healthcare, Buckinghamshire, UK. Distilled sterile water (10977-023) was purchased from Versol, Somerset, UK. Sodium chloride (NaCl) (S9625) was from Sigma-Aldrich, UK. Trypan blue (T8154) was purchased from Sigma-Aldrich, UK. Bovine Serum Albumin (BSA) (A4530) was purchased from Sigma-Aldrich, UK. 96-well white plates (15041) were purchased from Immunolon2, Chantilly, USA. 30% hydrogen peroxide (H_2O_2) (H1009) was purchased from Sigma-Aldrich, UK. Mannitol Salt Agar (MSA) (CM0085), Tryptone Soya Agar (CM0131) and Tryptone Soya Broth (CM0129) were purchased from ThermoFisher Scientific, Oxford, UK. Petri dishes (101VR20) were from Sterilin,

Newport, UK. Formaldehyde (P6148) was from Sigma-Aldrich, UK. Vigam liquid (5 mg/mL IgG) (2620102) was purchased from Bio Products Laboratory, Hertfordshire, UK. *Fusobacterium Nucleatum* (*FN*) (ATCC 10953) in freeze dried format was supplied by LGC Standards, Germany. Crystal violet (C0775) was purchased from Sigma-Aldrich, UK. RPMI-1640 (R2405) was obtained from Sigma-Aldrich, UK. SYTOX® Green nucleic acid stain (S7020) was purchased from Invitrogen, Paisley, UK. 96-well black plates (3340) were ordered from Corning, Lowell, MA, USA. Micrococcal nuclease (MNase) (LS004797) was from Worthington Biochemical Corporation, Lakewood, NJ, USA. Ti discs Grade II, IV and V (Ø 14 mm*1 mm) (143238-954) were purchased from Titanium Products Ltd, England. Silicon carbide (SiC) abrasive paper (40800005) from P320 through P500, P800, P1200, P2400 to P4000 grit were purchased from Struers, UK. Transparent 24-well sterile plates (CLS3527) were purchased from Corning Costar, Dorset, UK. RPMI-1640 with ultraglutamine-1, Foetal Calf Serum (FCS) and penicillin (1000 U/mL)/streptomycin (10,000 μg/mL) (BE12-702F/U1) were obtained from Lonza Wokingham Ltd, Berkshire, UK. Interferon-alpha (IFN-α) (500 pg/mL) (I4784) was purchased from Sigma-Aldrich, UK. Transparent 6 (CC010) and 12 (BC311) well cell culture plastic plates were purchased from Appleton Woods (Birmingham, UK). All the other reagents were obtained from Sigma-Aldrich Chemical Company, Poole, UK and solvents from Fisher, Loughborough, UK unless otherwise stated. Furthermore, range of Ti powders utilised within the study (Table 2.1) were purchased from Sigma-Aldrich or Alfa-Aesar, UK.

2.2 Ti stimuli preparation and storage

The dispersions of Ti stimuli (Table 2.1) were prepared in either phosphate buffered saline (PBS) (Appendix I) or in RPMI-1640 and stored at 4 °C until used. 0.1 g of each respective Ti powder was weighed out and dispersed in 10 mL of PBS or RPMI-1640 resulting in 2000 ppm Ti dispersion. A set of serial dilutions was performed by transferring 1 mL of the higher Ti concentration dispersion to 9 mL of PBS or RPMI-1640 resulting in 200, 20 and 2 ppm Ti dispersions respectively. Prepared dispersions were then autoclaved and prior to being used were sonicated using an electric sonicator (Clifton MU-22, Progen Scientific, London, UK) at 25 °C for 15 mins.

Table 2.1 Ti stimuli used in this study

Ti stimuli	Application	Particle size	Supplier (Product Code)
Anatase	Chemiluminescence, MNase and ELISA assays	~30 nm	Alfa-Aesar (039953)
Rutile	Chemiluminescence, MNase, TEM, chemotaxis and ELISA assays	~50 nm	Sigma-Aldrich (1317802)
Mix oxide (anatase-rutile)	Chemiluminescence, MNase and ELISA assays	~66 nm	Sigma-Aldrich (13463677)
Anatase mesh	TEM and EDX analysis	≤45 nm	Sigma-Aldrich (248576)
Peroxy	Chemiluminescence assays	Unknown	Produced in house (section 2.2.1)
Metallic	Chemiluminescence, MNase, chemotaxis and ELISA assays	~5 µm	Prepared in house (section 2.2.2)
Metallic	Chemiluminescence, MNase and ELISA assays	~20 µm	Alfa-Aesar (744032)

2.2.1 Ti peroxy (Ti stimuli produced in house)

Ti peroxy compounds are yellow powders prepared by exposing the surfaces of mirror-like Grade IV Ti discs to physiological saline (0.9% NaCl solution) and 10% H_2O_2 (H1009; Sigma-Aldrich, UK). Ti Grade IV identical disc specimens (Ø 14 mm*1 mm, Titanium Products Limited, England) were ground in distilled water using sequential grades of SiC abrasive paper from P320 through P500, P800, P1200, P2400 to P4000 grit (Struers, UK). All specimens were polished with MD-Chem polishing cloth using OP-S colloidal silica suspension (Struers, UK) prior to thorough cleaning in acetone, ethanol and distilled water using ultrasonic agitation for 10 mins at each stage. All the samples were then dried in an oil and water free air stream prior to treatment. The prepared mirror-like Ti discs specimens were immersed in 3 mL of physiological saline and exposed to 10% H_2O_2 in a 30 mL universal tube which was covered with a cap and sealed with parafilm in order to prevent any evaporation. These were then incubated at 37 °C and shaken every day on A500 orbital mixer (Denley, England) for 1 hr daily. In addition, the physiological saline was replenished every week and the colour of the surface of the samples after immersion was visually examined and recorded with optical camera. After 4 weeks of immersion, the Ti precipitate yellow in colour is formed on the surface of the Ti discs which is easily separated and then dispersions in PBS similarly to other Ti stimuli were prepared (section 2.2) for *ex-vivo* chemiluminescence assays (section 5.4.3).

2.2.2 Preparation of ~5 μm metallic Ti dispersions (Ti stimuli prepared in house)

Metallic Ti dispersions of concentrations 2000, 200, 20 and 2 ppm in PBS or RPMI-1640 were prepared using ~20 μm particles (section 2.2). Particles ranging between 2.5 μm and 5 μm were separated using 5 and 2.5 μm pore size filters (Appleton Woods, UK) and the collected particles were then dispersed in PBS or RPMI-1640 (section 2.2). The prepared dispersions were then autoclaved and prior to being used were sonicated using an electric sonicator (Clifton MU-22, Progen Scietific, London, UK) at 25 °C for 15 mins.

The purity of sourced Ti oxide powders was verified using Raman spectroscopy (Appendix III) and the particulate sizes and morphology following dispersions were studied in section 5.4.1.

CHAPTER 3

DETECTION OF TITANIUM IN TISSUES ASSOCIATED WITH IMPLANTS NOT SUBJECTED TO SIGNIFICANT WEAR

3.1 PREFACE

Significant limitations exist in current methods used to detect implant derived metals in peri-implant tissues and therefore the stability of implant surfaces in physiological environments may be being over-estimated. Using a beyond-state-of-the-art technique –namely micro-focus synchrotron X-ray spectroscopy, the distribution and chemical speciation of Ti in peri-implant tissues was studied. The Ti implant component of Bone Anchored Hearing Aids (BAHA) was used as a model system to explore whether commercially pure Ti implant surfaces could deteriorate releasing Ti into the surrounding tissues in the absence of wear. Measurements of explanted inflamed tissues taken from around BAHA implants demonstrated a heterogeneous distribution of Ti debris in oxide states such as anatase and rutile and in Ti-metallic and intermediary forms. The abundance of oxide species suggests that corrosion processes are operative. Basic haematoxylin and eosin (H & E) histology of the studied tissues confirmed the distribution of Ti to be non-exclusively associated with PMNL infiltrates suggesting that interactions of such cells with the Ti debris may be of interest when considering the biological consequences of 'free Ti' in these tissues.

Published in: Addison et al. (2012). Do 'passive' medical titanium surfaces deteriorate in service in the absence of wear? *R. Soc. Interface,* 9, 3161-3164.
Included in: Highlights of the Diamond Light Source 2012/2013.

3.2 INTRODUCTION

3.2.1 Stability of passive Ti-oxide surfaces

Accumulation of Ti in the soft tissues that surround indwelling implants subjected to obvious wear processes (e.g. articulating joints used in orthopaedic rehabilitations) is well documented (Ektessabi et al., 1994, Doorn et al., 1998, Coen et al., 2003, Kasai et al., 2003, Sargeant & Goswami, 2007 & Jacobs et al., 2011). However, to date there is little evidence that demonstrates the presence of implant derived Ti in the tissues or in fluids surrounding skin or mucosa penetrating devices such as dental implants or craniofacial anchorage devices where wear processes are minimal (Ektessabi et al., 1994 & Uo et al., 2007). These implants are assumed to have Ti oxide surfaces which are highly stable in the environment into which they are placed, but studies have reported elevated serum and urine Ti levels in both animals (Bianco et al., 1996 & Sarmieno-González et al., 2008) and humans (Bölükbaş et al., 2013) which have been implanted with such devices. The question that arises is whether there is actually only minimal Ti release into the surrounding tissues or whether the current detection methods and experimental approaches lack the required sensitivity to determine the presence of Ti.

3.2.2 Detection of peri-implant Ti

A variety of imaging/detection methods are available to probe tissues for the presence of metal ions and/or particles (Punshon et al., 2005 & McRae et al., 2009). The optimal approach for the identification of metal ions in tissues will

provide high sensitivity and specificity for the element of interest and will enable spatial correlation of the element with the underlying structures (Lobnski et al., 2006 & Ortega et al., 2009). Histology is the first experimental approach to study the microscopic anatomy of cells and tissues (Willmott, 2011) and has previously been used to explore peri-implant tissues (Lalor et al., 1991 & Lang et al., 1994). Studies using simple staining methods such as haematoxylin and eosin (H & E) have reported metal particle associations (assumed to be Ti) with multi-nucleated cells including neutrophils, macrophages and also with T and B lymphocytes (Lalor et al., 1991). Light microscopy and basic histology provides some insight into the presence of implant debris but fails to provide the necessary chemical and spatial characterisation to elucidate both the mechanism of metal release and the biological consequences. Combining these histological techniques with scanning electron microscopy (SEM) (Maloney et al., 1993 & Ichinose et al., 2003) and transmission electron microscopy (TEM) (Wu et al., 2005) has provided insight into the morphology of particulate debris but has provided little information on the presence of Ti in ionic forms (Ferguson et al., 1960 & Koike & Fujii, 2001). Quantification of Ti concentrations in peri-implant tissues and in distant organs can be performed using Mass Spectrometry (MS) (Griffin & Schnitzer, 2011) and the technique takes into account both particulate and soluble Ti (Wang et al., 2007). Most MS studies on tissues associated with Ti implants that have been reported have used Inductively Couple Plasma techniques (ICP-MS) which have confirmed the presence of elemental Ti in concentrations of up to 100 ppm (Rubio et al., 2008, Sarmieno-González et al., 2008 & Bölükbaşı et al., 2013). However, ICP-MS provides a measurement of elemental concentration averaged across the

tissue bulk and may significantly underestimate local concentrations of an element should it be heterogeneously distributed (Griffin & Schnitzer, 2011). Moreover, ICP-MS techniques are sensitive to polyatom effects whereby failure for atoms to dissociate in the plasma field can lead to over or underestimations (Bradford & Cook, 1997). This is a particular problem for Ti whose common isotope mass is 47 (Barbalace, 2006) and therefore is difficult to differentiate from a common and biologically relevant polyatom, P-O whose combined mass (P (31) and O (16)) is equivalent (Barbalace, 2006). Therefore, both MS and EM techniques have limitations in detection ability and cannot relate a characterised Ti distribution to the cellular and subcellular structures with a wide field of view (Griffin & Schnitzer, 2011). Furthermore, the specimen preparation requirements for these techniques is either destructive or can modify the location of Ti in the tissues before or during the test (Hanlon et al., 1992 & Doorn et al., 1998).

3.2.3 X-ray microscopy

X-ray microscopy offers a possible solution to achieve highly sensitive imaging for metallic elements on a micron and submicron scale within peri-implant tissues that are preserved close to their natural hydrated state (Ektessabi, 1998, Carvalho et al., 2007 & McRae et al., 2009). X-ray microscopy is advantageous as it is highly specific for an element and works by probing a sample with ionising radiation (Newville, 2006). X-rays of energy greater than the atom's ionising potential will cause ejection of one or more electrons from a quantum core level through a phenomenon known as the photoelectric effect (Figure 3.1) (Newville, 2006). The removal of an electron destabilises the atom and consequently an

electron from a higher orbit drops into the lower orbit. As the electron drops, energy is released in the form of a photon which has a characteristic energy and this photon and its specific energy can subsequently be detected (Newville, 2006).

Figure 3.1 Photoelectric effect of an X-ray absorbed and a core level electron is prompted out of an atom (Newville, 2006)

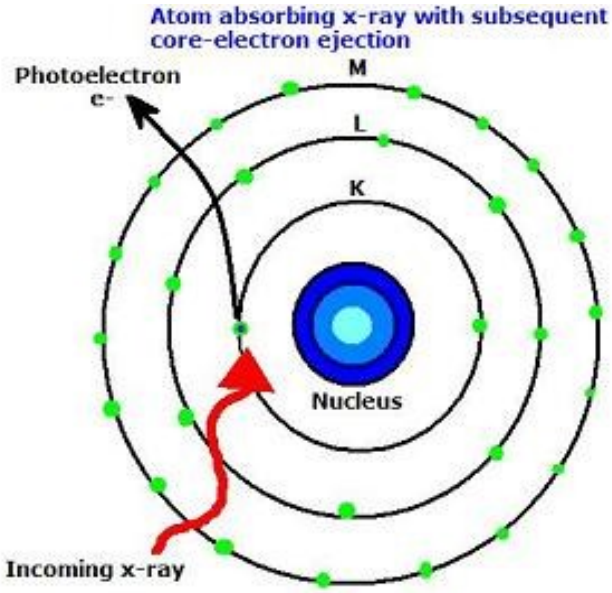

The primary limitation of X-ray microscopy using laboratory sources is a lack of lateral resolution (inability to focus the X-ray beam) and a low X-ray flux, so that detailed mapping of a sample where elemental concentrations are dilute is often not possible (Willmott, 2011). However, these limitations can be surmounted with the use of synchrotron X-ray sources.

3.2.4 Synchrotron sources

Synchrotron facilities produce X-rays up to ten thousand billion times brighter than the X-rays produced by a conventional hospital source (McRae et al., 2009). Such X-rays allow sensitive detection of trace levels of elements in samples in a natural hydrated state and through considerable advances in optics can provide spatial resolutions of <50 nm (Petibois & Guidi, 2008 & McRae et al., 2009).

3.2.4.1 Generation of synchrotron radiation (SR)

A synchrotron consists of an evacuated storage ring into which high energy electrons are injected (Willmott, 2011). The electrons are then accelerated to just below the speed of light (Figure 3.2) (Willmott, 2011). The electrons travel in straight lines and so in order that they can follow the curvature of the storage ring, an array of bending magnets is used to modify their trajectory. As the electron passes through the magnetic field their velocity is changed which results in the emission of photons which range in wavelength from X-rays to microwaves. It is these photons which are considered the Synchrotron Light and which are then guided through sophisticated optics to an experimental end-station to probe a sample. Although the brilliance of the light emitted from bending magnets far exceeds that of laboratory X-ray sources (McRae et al., 2009), further orders of magnitude of increase in brilliance can be achieved by the use of insertion devices (ID) (Willmott, 2011) and it is these levels of brightness that are often required to detect ultra-trace concentrations of an element. IDs are positioned between bending magnets on straight sections of the storage ring and employ sets of

permanent magnets to produce magnetic fields that point alternatively in perpendicular directions to each other (Willmott, 2011). IDs are found in two forms and can be distinguished by the degree to which the direction of the electrons is moved away from a straight path (Willmott, 2011). Wigglers cause large angular excursions from which the emitted radiation cones of each 'wiggle' do not overlap and the intensities are added. The radiation is enhanced by a factor of 2N where N is the number of magnetic periods in the ID and the radiation produced is both of a high power and a broad spectrum (Willmott, 2011). In contrast, Undulators cause gentler electron excursions creating spectra consisting of regularly separated narrow bands of highly intense radiation (Willmott, 2011).

Figure 3.2 Schematic representation of a synchrotron source (Willmott, 2011)

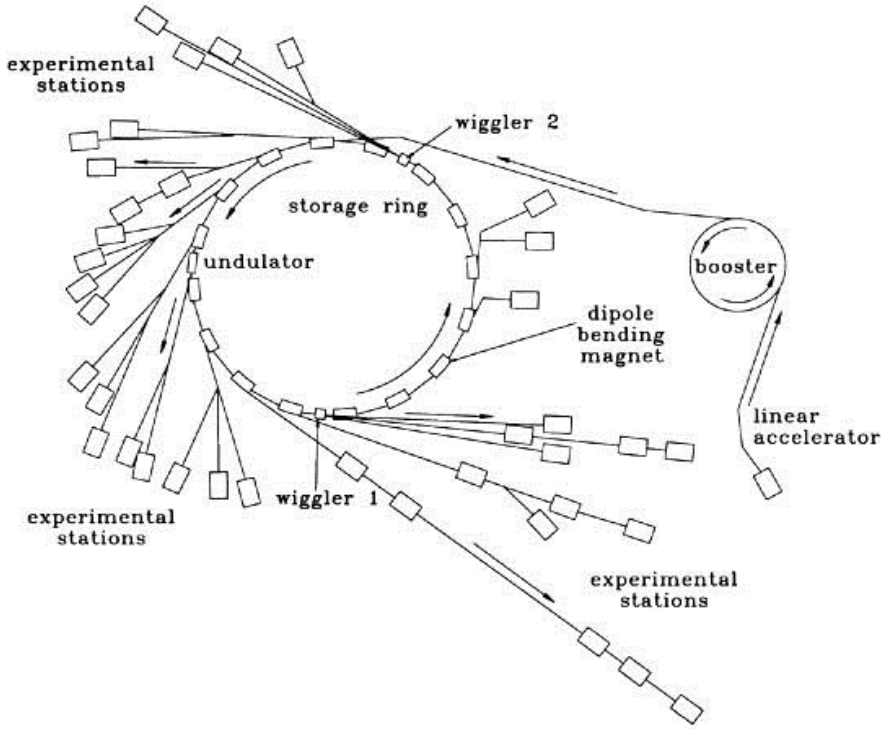

3.2.4.2 Use of synchrotron radiation for imaging biological samples

In the past two decades there has been increased use of SR for the microanalysis and mapping of elemental distributions in biological samples (Chen et al., 1999, Ektessabi, 1998, Bacquart et al., 2007, Carvalho et al., 2007, Petibois & Guid, 2008, Ortega et al., 2010 & Hart et al., 2012). Related to the objectives of this thesis a multi-disciplinary team recently used SR to study tissues surrounding failing Co-Cr-Mo implants used for total hip replacements (Hart et al., 2012). SR techniques enabled identification of particle sizes, chemical compositions and localisation of implant elements with inflammatory cells (Hart et al., 2012). Studies utilising SR to study Ti associated with implants have been limited to measurements on bulk tissues with a relatively low resolution (Uo et al., 2007). Ti however, is a particularly interesting element to study using X-ray methods as it has well characterised X-ray absorption behaviours enabling simple separation of different Ti-O co-ordinations (Mountjoy et al., 1999) and hence identification of the chemical speciation of Ti within the sample.

3.2.5 I-18 beamline, the Diamond Light source

The Diamond Light source is the United Kingdom's (UK) 3rd generation, 3 GeV synchrotron facility and the I-18 beamline which takes light from an ID has been developed as a world-leading micro-focus spectroscopy instrument with an accessible X-ray energy range from 2.0 to 20.7 KeV. The I-18 beamline is able to analyse heterogeneous materials and is capable of exciting the K-edges of elements from P to Mo and the L_3-edges from Sr to Pu. To date the instrument has

been applied in multiple fields of science including cultural heritage, geology and biomedicine (Mosselmans et al., 2009). The I-18 optics takes advantage of the high brightness of the Diamond lattice combined with a 27 mm period undulator providing an energy tunable X-ray microbeam to perform micro-X-ray fluorescence (XRF) (section 3.2.6) and micro-X-ray absorption spectroscopy (XAS) (section 3.2.7) measurements with an average spot size of around 3 μm at the sample (Mosselmans et al., 2009). As part of the beamline commissioning and exploration of its capabilities, Ti debris was identified in thin sections (6 μm) of oral epithelium taken from adjacent to Ti dental implants which had been *in-situ* for 3 months (Mosselmans et al., 2009).

3.2.6 X-ray Fluorescence (XRF) for mapping elements within biological samples

XRF is a highly sensitive technique for multi-elemental and quantitative imaging (Punson et al., 2005, Lobinski et al., 2006 & Ortega et al., 2009). XRF is achieved by focussing an X-ray beam onto the sample whereby the incident X-ray photon knocks out electrons from the inner shells of all elements with lower ionising energies than the energy of the incident X-rays (Punson et al., 2005 & Ortega et al., 2009). In doing so an electron hole is created which is immediately filled by a higher orbit electron which drops into the lower shell and simultaneously emits a fluorescence photon which is then detected for imaging using a detector (Punson et al., 2005 & Ortega et al., 2009). The number of fluorescence photons can be quantified in order to provide a surrogate measure of concentration and can be

further calibrated against standards to provide absolute elemental concentrations (Punson et al., 2005, Lobinski et al., 2006 & McRae et al., 2009).

3.2.7 X-ray Absorption Spectroscopy (XAS)

Measurement of X-ray absorption spectra is referred to as X-ray absorption spectroscopy (XAS) and can provide information on the organisation of atoms and chemical bonds surrounding the absorbing atom in all of the possible environmental states that it may be in i.e. a solid, liquid, and/or gas (Ortega et al., 2009 & Willmott, 2011). XAS relies on repeatedly scanning the sample with a monochromatic beam with the energies increasing from just below to just above the absorption energy for the element under investigation (Ortega et al., 2009). XAS can be performed in a fluorescence mode or by transmission through the sample (Kruger et al., 1990) and the technique is typically divided into two parts, namely X-ray absorption near edge structure (XANES) and extended X-ray absorption fine structure (EXAFS) (Figure 3.3) (Kruger et al., 1990, Punson et al., 2005, Petibois & Guidi, 2008 & Willmott, 2011). The principle of EXAFS which provides information regarding the metal atom site ligation (Willmott, 2011) is not discussed in detail as the technique is not employed within this investigation.

Figure 3.3 Schematic representations of XANES and EXAFS regions (Willmott, 2011)

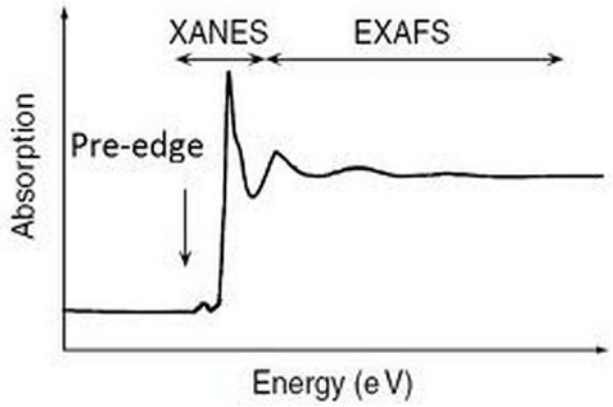

3.2.8 XANES

XANES is a highly sensitive detection method for the oxidation state, coordination environment and bonding characteristics of a specific element (Ektessabi, 1998 & Baccquart et al., 2007). In combination with a micro-focussed beam it can be used to probe subcellular compartments thereby avoiding cell fractionation and other preparation steps that might modify the chemical species (Ektessabi et al., 2005 & Baccquart et al., 2007). A XANES spectrum is typically divided into three regions, namely the pre-edge, edge and above the edge region (Figure 3.4) (Ravel & Newville, 2005 & Weng et al., 2005). The pre-edge area is sensitive to the local structure surrounding the element of interest and its oxidation state and the edge energy position is a specific characteristic of the absorbing atom, again dependent on its oxidation state (Baccquart et al., 2007).

Figure 3.4 Schematic representations of XANES regions of a metallic Ti spectrum

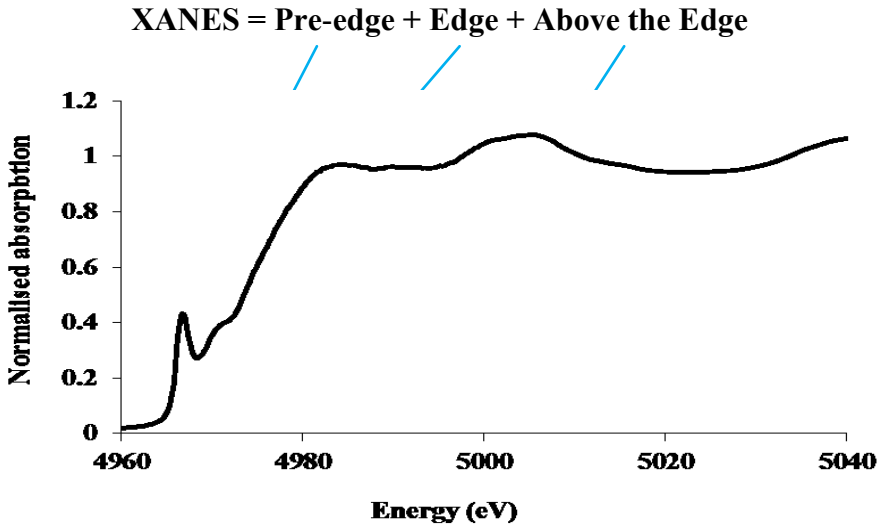

3.2.8.1 XANES studies on Ti

Previous XANES studies for Ti (K-edge) have focused on the pre-edge area of the spectrum as the pre-edge heights/intensities and positions vary considerably between common Ti species (Farges et al., 1996 & Mountjoy et al., 1999). Three different coordination states of Ti have been characterised including tetrahedral (four-fold), square-pyramid (five-fold) and octahedral (six-fold) (Figure 3.5) (Farges et al., 1996 & Mountjoy et al., 1999). The height/intensity of the pre-edge peak decreases sequentially from a tetrahedral coordination to square pyramid to octahedral fold due to the increasing centrosymmetry (Figure 3.5) (Farges et al., 1996 & Mountjoy et al., 1999). Furthermore, the pre-edge features are modified by Ti-O bond length, coordination and bond angles (Farges et al., 1996 & Mountjoy et al., 1999). All these features are considered as fingerprints for qualitatively identifying Ti coordination states in unknown samples.

Anatase and rutile which are reported as the main polymorphs of the passive oxide layer formed on Ti implants (Effah et al., 1995) belong to tetrahedral coordination (Iavicoli et al., 2011) but have differing arrangement of the Ti atoms (Figure 1.1) (Jolivet et al., 2010) which consequently results in differing pre-edge peak heights/intensities (Mountjoy et al., 1999 & Farges et al., 1996) (Figure 3.5).

Figure 3.5 Ti K-edge XANES spectra of (a) tetrahedral (b) square pyramid and (c) octahedral coordination states (Farges et al., 1996)

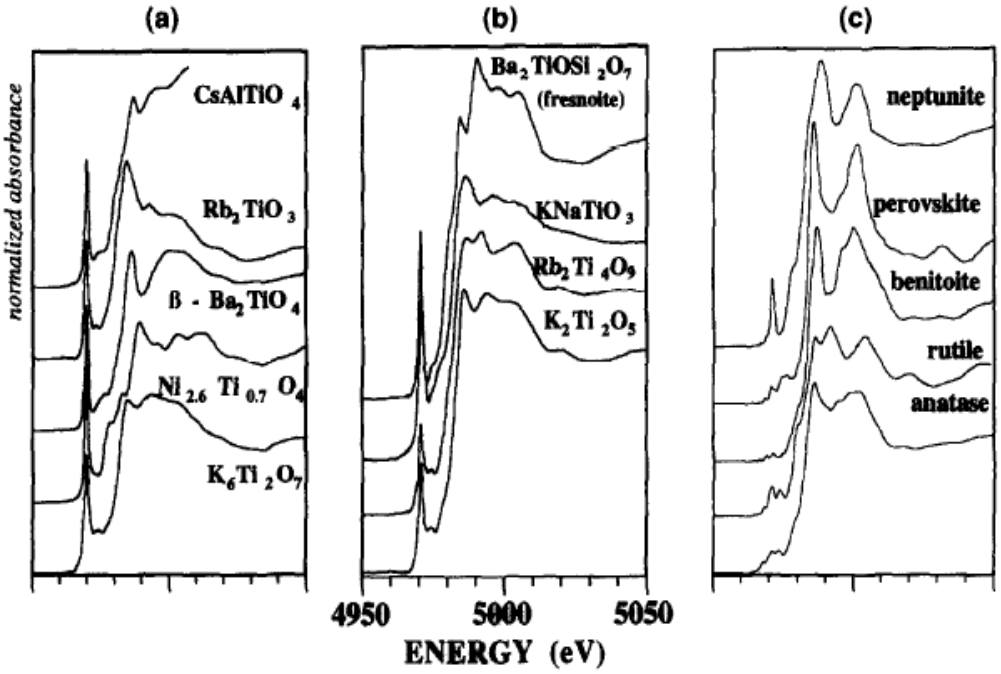

Previous studies investigating the structure of TiO_2 nanoparticles by probing the Ti K-edge and studying XANES have revealed severe distortions in the Ti environments when compared to bulk particles (Chen et al., 1999). The distorted Ti sites have been associated with distortions in the TiO_2 lattice located on the surface of the particles (Chen et al., 1999). As the particles decrease in size the surface atoms have proportionally greater influence on the spectra when compared

with the bulk (Chen et al., 1999). Therefore, the presence of distorted Ti sites in spectra from an unknown sample can possibly provide additional information on particle size (Chen et al., 1999).

The objective of the current investigation was to apply this beyond-state-of-the-art instrumentation to identify whether there is a detectable Ti distribution in the soft tissues which surround Ti implants that are not subjected to significant wear processes.

3.3 METHODS

3.3.1 Model system selection

Ti cranial anchorage implants were selected as a model system to study whether passive Ti surfaces can deteriorate in the absence of wear. Epithelial tissues from surrounding Ti implants used as part of Bone Anchored Hearing Aids (BAHA) were studied. The BAHA offers an ideal model system to test the experimental null hypothesis that there is no discernible Ti distribution in tissues surrounding implants not subjected to wear. The system is useful to study as all implants are placed in anatomically the same site; the implants are fabricated from Grade IV CpTi in common with most dental implants but in contrast with dental implants there is little geometrical variability with only the abutment component provided in different lengths. The implants are provided by a single manufacturer (Cochlear Ltd, Sydney, Australia). Furthermore, the abutments are pre-connected and torqued by the manufacturer prior to surgical insertion removing the risk of introduction of Ti from abutment insertion at a later stage. The Ti implants are percutaneous but surrounded by a relatively thick soft tissue cuff which prevents the surface(s) from being exposed to wear processes from foreign objects (as dental implants which may be brushed during oral hygiene measures). Finally, tissue from around these implants is readily available from surgical debulking procedures during palliative treatments of chronically inflamed implants.

3.3.2 Tissue excision and preparation

Peri-implant inflamed skin tissue was obtained from six consented competent adults undergoing scheduled revision surgery associated with a BAHA at University Hospital Birmingham NHS Foundation Trust (Ethical approval REC 08/H1203/128). The inflamed tissue was surgically retrieved from around the percutaneous Grade IV CpTi implants (BAHA, Cochlear Ltd, Sydney, Australia) using a full thickness circumferential excision. Skin was retrieved from around implants that remained firm and well osseointegrated but associated with a hypertrophic reaction surrounding the Ti implant that necessitated skin reduction surgery. The implants were present for between 2 and 6 years prior to revision surgery. During tissue excision, metallic contamination was prevented and tissue sections were immediately orientated and snap-frozen prior to cryo-preparation. Sequential frozen sections of 4-6 μm thickness were cut using tungsten carbide knives and were mounted on ultra-pure fused silica plates (<10 ppb Ti) (Spectrosil 2000, Heraeus Quarzglas GmbH & Co., Hanau, Germany); desiccated, then covered with 25 μm kapton film (Kapton, Dupont, Wilmington, NC, USA) and sealed peripherally with epoxy resin. Alternating sections were fixed and H & E stained to provide a histological reference for each experimental section. In addition, supplementary tissue sections which had not been exposed to Ti were prepared in an identical manner as a control in order to determine if any contamination had occurred during sample preparation.

3.3.3 Ti reference standards preparation and calibration

In addition to the explanted human tissue samples, spectra were also collected in transmission mode from Ti standards, including Ti foil (metallic) and several containing Ti^{4+} ions in different coordination environments: cristobalite (four-fold), Na_2TiSiO_5 (five-fold); and anatase, rutile and $CaTiSiO_5$ (all six-fold).

3.3.4 XRF measurements

Using the micro-focus capability of I-18 beamline (Diamond Light Source, UK) each experimental tissue section (section 3.3.2) was initially fluorescence mapped with an incident beam of 5.7 KeV at a 50 μm resolution to identify areas of interest. Fluorescence data were collected using a four element Si drift detector (Oxford Instruments, Oxford, UK). The beam was then focused to give a spot size 5 μm (height) by 3.4 μm (width) and the sample was mounted at a 45° angle to the incident beam, thus resulting in a resolution of 5 μm by 5 μm. The measurements were undertaken in reflection mode at room temperature. The fluorescence intensity under the Kα and Kβ emission peaks were integrated to give the total number of counts.

3.3.5 XANES measurements

To determine Ti speciation from regions where Ti was detected, Ti K-edge XANES spectra were acquired for specimens (section 3.3.2) in fluorescence mode at room temperature. Measurements were taken using Si (111) crystal monochromator giving an energy range 4950 to 5050 eV with a 9 element Ge

detector. The beam size was maintained at 5 µm (H) x 5 µm (V) at the sample allowing accurate localisation on discrete particles/groups of small particles. Spectra acquired were compared with Ti standards of known coordination (section 3.3.3).

3.3.6 Data analysis

XANES data analysis was carried out using ATHENA (version 0.8.061, 2001-2009). All data was normalised by selecting two points which had the best fit in pre-edge and post-edge regions (Figure 3.6). Consistency in normalising the data was maintained throughout to avoid fluctuations in the acquired results. Reference standards (section 3.3.3) were compared with experimental measurements (section 3.3.2) acquired using ATHENA to determine Ti speciation.

Figure 3.6 Normalisation of XANES spectra using Athena (Version 0.8.061, 2001-2009) (a) a typical raw data plot (b) selection of pre-edge and post-edge range for normalisation and (c) normalised data plot

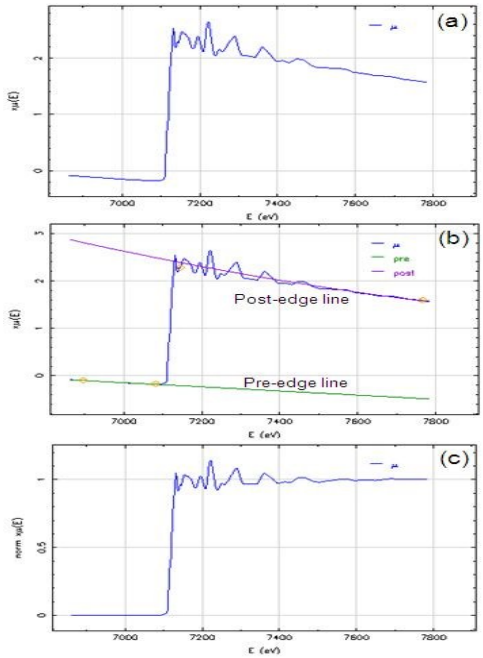

3.4 RESULTS

3.4.1 SR-XRF mapping of inflamed peri-implant (BAHA) tissues

Synchrotron X-ray fluorescence mapping of thin (4-6 µm) sections of the inflamed skin tissue recovered from adjacent to percutaneous CpTi implants demonstrated a widespread scattered distribution of Ti in all tissue sections studied (6 patients and 1-3 sections from each patient) (Figure 3.7). The Ti distribution was heterogeneous in both the size of the particles (areas of fluorescence intensity) of Ti observed and in their chemical speciation. Areas of Ti concentration varied in size from 5 µm (highest resolution of detection) to 150 µm.

Figure 3.7 An X-ray fluorescence map (5300 × 2000 µm) of the associated distribution of Ti in peri-implant soft tissue (6 µm thickness) taken at greater than 25 µm from a CpTi BAHA. Legend refers to increasing Ti fluorescence values

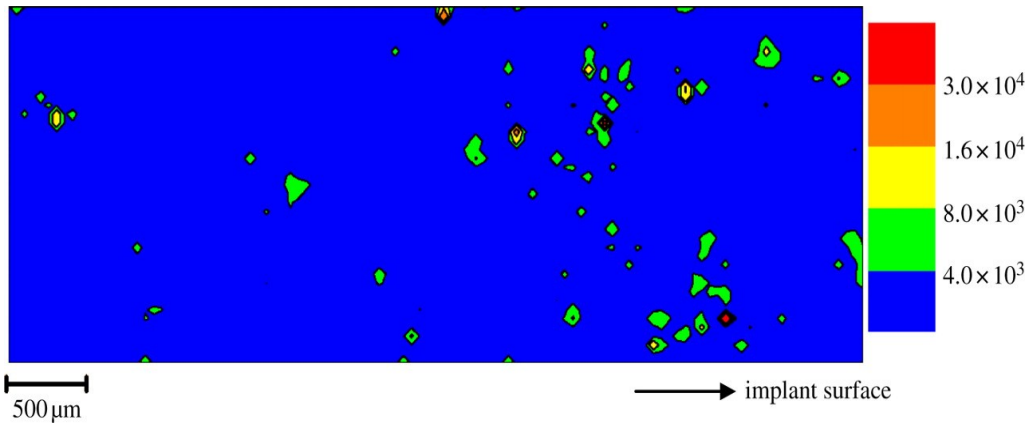

Orientation of the tissue prior to snap-freezing allowed the Ti distribution to be co-ordinated relative to the adjacent Ti implant surface which demonstrated that the Ti was scattered radially outwards from the tissue-implant interface to

distances > 2000 μm (Figure 3.7). Tissue sections immediately adjacent to those mapped for Ti fluorescence and stained with H & E and were observed with optical microscopy (Figure 3.8). No obvious relationship between the Ti maps and the underlying cell types and tissue architecture were observed. However, PMNLs were seen in a zone close to the implant surface where an abundance of Ti had been demonstrated (Figure 3.8).

Figure 3.8 An optical micrograph of the H & E stained tissue section taken from immediately adjacent to a section mapped for Ti using X-ray fluorescence as presented in Figure 3.7. A mixed inflammatory infiltrate including the presence of PMNLs was seen adjacent to the implant surface with densely packed plasma cells at a greater distance from the Ti surface

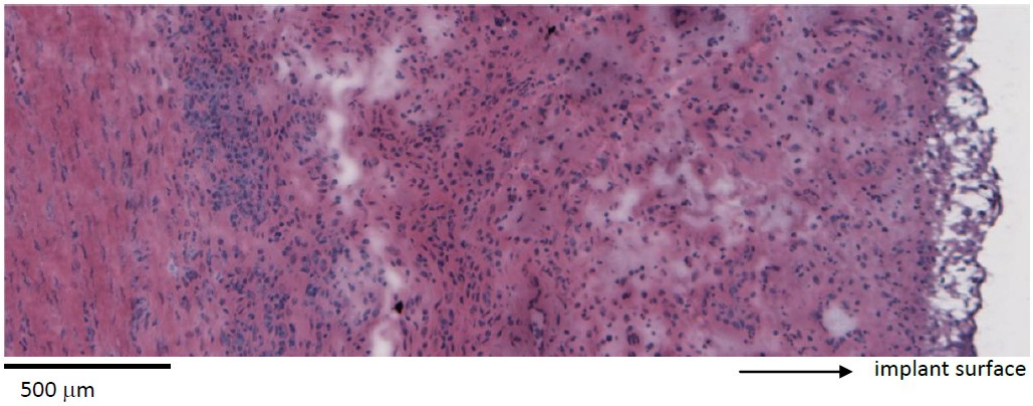

No Ti was detected by X-ray fluorescence mapping performed on the control tissue, which had no known Ti exposure and had been collected, stored and prepared according to an identical experimental protocol.

3.4.2 Calibration of Ti standards

XANES spectra were acquired in transmission mode for all Ti reference standards. Spectra were calibrated to the inflection point of Ti at 4960 eV. Ti oxides as rutile

and anatase have three well resolved pre-edge features at ~4968.7 eV, 4971.5 eV and 4974.2 eV. Ti as metallic form exhibits one well resolved pre-edge peak of higher intensity at around 4966 eV (Figure 3.9).

Figure 3.9 Normalised Ti K-edge XANES spectra pre-edge features acquired in transmission mode of high purity (99.9 %) Ti standards in forms of oxide and metallic species

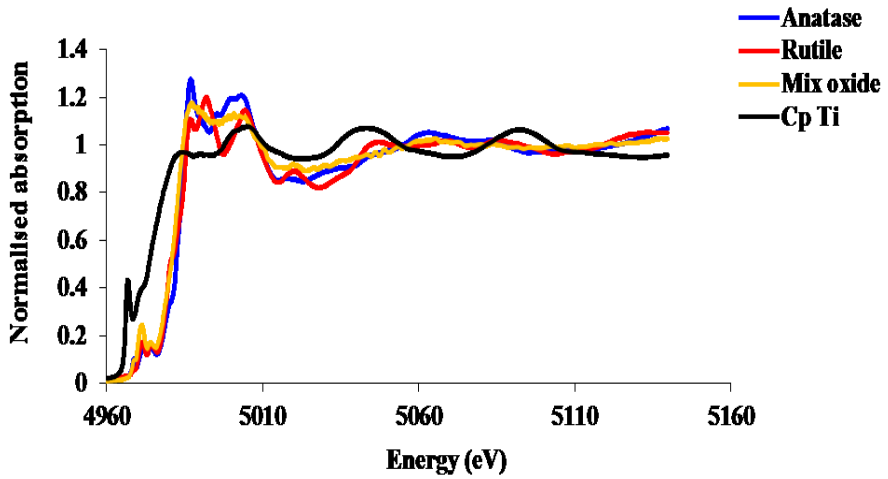

3.4.3 XANES spectra of inflamed Ti peri-implant soft tissues

Comparison of the XANES spectra of the Ti standards with spectra taken from areas of high, medium and low relative Ti fluorescence intensity, as identified by XRF mapping, revealed that the Ti was present in a number of forms. Metallic particles were detected only in small quantities and there was a considerable quantity of Ti species exhibiting six-fold coordination states analogous to anatase and rutile (Ti oxide species) (Figures 3.10 & 3.11). Furthermore, spectra resembling Ti-peroxo complexes and intermediary between oxide and metallic states were frequently encountered.

Figure 3.10 A representative plot showing a normalised Ti K-edge XANES spectra for BAHA tissues (BAHA 1 and 2) compared with anatase and rutile (Ti-oxide) reference standards

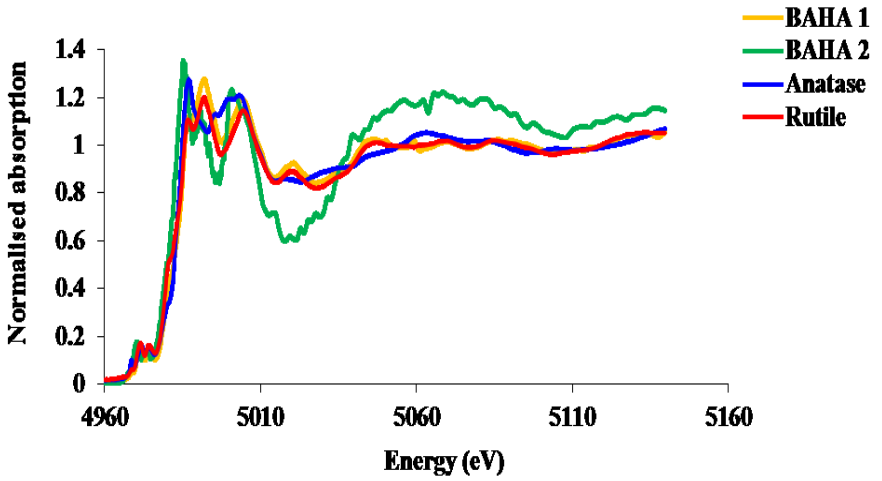

Figure 3.11 Normalised Ti K-edge XANES spectra above edge features for BAHA tissues (BAHA 3-5) compared with Ti metallic and rutile (oxide) reference standards suggesting combination of both metallic and oxide states

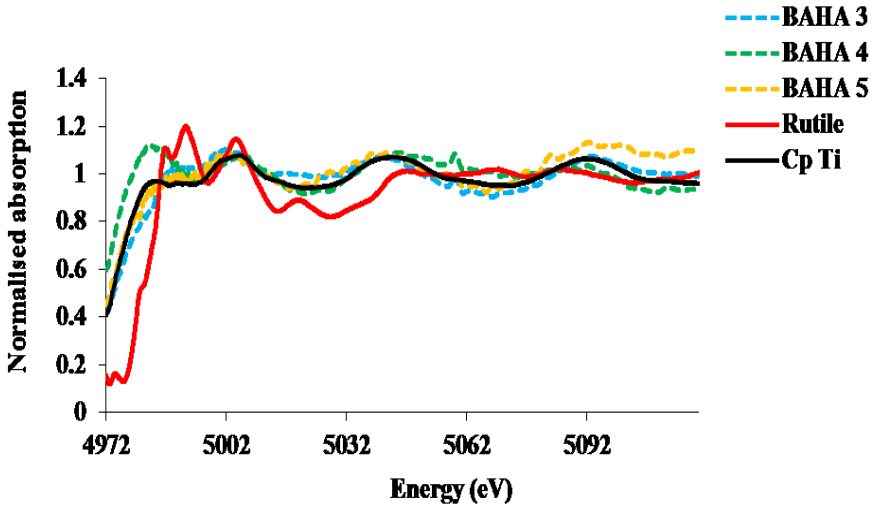

Over 30 XANES spectra were acquired from areas of high, medium and low Ti fluorescence intensity from peri-BAHA tissues. The majority of XANES spectra acquired suggested that Ti was present as Ti-oxide with predominance for a rutile state and intermediary species (mixed oxide and/or oxide-metallic) were observed.

3.5 DISCUSSION

Previously investigators have used microscopy, optical spectroscopy and MS techniques to confirm the existence of Ti in peri-prosthetic orthopaedic soft tissues (Hallab et al., 2004, Kasai et al., 2003, Sargeant & Goswami, 2005 & Baldwin & Hunt, 2006). The techniques have limited resolution or an inability to relate the quantity, size and chemical speciation of Ti to cellular and sub-cellular structures that would be required to inform biological investigations (McRae et al., 2009).

Accordingly, synchrotron X-ray micro-focus spectroscopy was used in the current investigation and conferred the ability to detect trace distributions of Ti in thin tissue sections at a high resolution (section 3.4) (Mosselmans et al., 2009). The observation of Ti in all of the tissue sections probed apart from the control tissues was confirmatory that the implant surfaces were deteriorating in service. A small number of tissue sections of thin thickness (4-6 μm) were prepared from relatively large tissue blocks from 6 different patients. Multiple tissue sections from each patient were prepared and the sections for XRF mapping (which is a limited resource) were randomly selected with Ti discovered in all without any pre-screening methods being applied. Given the small tissue volumes probed it is highly unlikely that the findings were therefore fortuitous and it can also be safely extrapolated that the Ti is likely to be found in a 3 dimensional distribution around the implant itself.

For the first time, a scattered and heterogeneous distribution of Ti in inflamed tissues taken from around failing skin-penetrating Ti implants has been observed (Figure 3.7). The tissue taken was adjacent to a CpTi device that was not exposed to obvious macroscopic wear or loading in service. Furthermore, the location of the distributed Ti was deep with respect to the skin surface which suggests that wear processes were unlikely to be a major contributor. Debris from implant insertion is also highly unlikely to lead to the observed widespread distribution of fine fragments of both oxide and metal forms of Ti that were observed. The predominance of oxide forms (section 3.4.3) is strongly suggestive that chemical or physiochemical mechanisms underpin metal release.

In the absence of obvious macroscopic wear or loading processes, we propose that the Ti in the tissue results from micro-motion and localized corrosion in surface crevices (Griess, 1968). This is supported by previous observations of systemically distributed Ti that has been detected in serum in ionic states (Kasai et al., 2003) and bound to proteins (Vamanu et al., 2008) and that implant debris in the form of nanoparticles ranging from 10-50 nm has been localised with inflammatory cells in tissues surrounding implants (Broggini et al., 2006). Localised corrosion which is mechanically assisted will lead to transient depassivation of the Ti surface oxide layer resulting in the burst release of Ti ions (Mudali et al., 2003). These will either bind to biomolecules or rapidly oxidise and where oxidation occurs insoluble particles will be formed. In the absence of wear, only small numbers of Ti ions are likely to be generated at any one instance so that following oxidation the insoluble particle formed is likely to be of a nano-

scale. The current methodology did not permit size discrimination to the nano-scale but chemical evidence derived from the XANES spectra was strongly indicative of the formation of oxidised particles on this scale (Uo et al., 2007).

The results provide primary evidence that the expected passive surface of skin-penetrating Ti implants can deteriorate in clinical service, leading to the accumulation of Ti debris in the surrounding tissue. The quantities, size and speciation of Ti debris reflect stimuli that have previously been demonstrated to be pro-inflammatory in nature (Iavicoli et al., 2011). In the current study, the tissues were examined close to their native state and referenced against histological images taken from immediately adjacent section taken during cryo-preparation (section 3.4.1). Measurements on H & E stained specimens themselves were avoided because of the risk of moving Ti through the tissue section during staining or due to the risk of modifying the chemical state of any Ti that may be present. The tissues sections cannot therefore be explicitly correlated with the XRF maps but were indicative that some of the Ti distribution was found in close proximity to PMNLs which were found in abundance in regions close to the implant surface. These findings suggest that PMNL interactions with Ti implant debris may be of significance in the pathogenesis of chronic peri-implant inflammation.

3.6 CONCLUSION

For the first time synchrotron micro-focus XRF and XAS measurements have been successfully performed on tissues surrounding Ti implants. A chemically and geographically heterogeneous distribution of Ti has been demonstrated to be associated with Ti implants that are not subjected to significant wear. The results challenge previous assumptions of the chemical stability of “passive” biomedical Ti oxide surfaces and given findings from the orthopaedic literature highlight that implant metal debris must be considered as a potential factor in the failure of skin penetrating Ti implants. The results highlight the need to understand both the physical and the chemical mechanisms leading to the generation and dispersal of Ti species in the tissue surrounding implants and then their subsequent potential to exacerbate inflammation. Similar processes are likely to contribute to the failure of other metal implants in soft tissues where macroscopic wear is not traditionally considered to be a risk.

CHAPTER 4

ACCOUNTING FOR THE TITANIUM SPECIES OBSERVED IN PERI-IMPLANT TISSUES

4.1 PREFACE

In Chapter 3, it was demonstrated that a heterogeneous distribution of Ti can be detected in inflamed peri-implant soft tissues surrounding percutaneous Ti devices. It is essential for both the purposes of improving biomedical materials and for informing appropriate biological modelling of the consequences of the released Ti, that the mechanisms underpinning the generation of such debris are understood. The mechanism or mechanisms will dictate the morphological and chemical characteristics of Ti implant derivatives and the release process itself may have biological consequences (e.g. through the generation of localised acidity). A preliminary electrochemical investigation was undertaken using a Ti artificial pit model in various media, including physiologically representative, in order to identify whether the species observed in a range of peri-implant environments can be generated by a non-tribological (non-wear) process. In addition, a further preliminary investigation was undertaken to identify whether cellular products could further modify Ti when it is in particulate form in the peri-implant soft tissues. It was demonstrated that all Ti species observed in peri-implant soft tissues can be accounted for its release by crevice corrosion processes. In addition, the capacity of human neutrophils to chemically modify Ti nanoparticles was suggested.

4.2 INTRODUCTION

4.2.1 Corrosion of biomedical Ti

It is acknowledged that in certain conditions all metals are susceptible to corrosion (Shreir et al., 1993) but for Ti and Ti alloys such conditions are not predicted in physiological environments (Hansen, 2008). Therefore, when Ti has been detected in fluids and tissues (Bölükbaş et al., 2013), wear processes are normally attributed (Mudali et al., 2003). However, a small body of evidence exists which demonstrates Ti binding to biomolecules and the accumulation of Ti in structures and organs and for this to occur Ti must at some point have been in ionic state, in solution (Beck, 1973). This has been further supported by the findings of Chapter 3 which demonstrate a significant distribution of oxide particles which again can only have formed from the oxidation of Ti^{3+} or Ti^{4+} released from the Ti surface (Vicentini et al., 1975).

Corrosion encompasses groups of chemical phenomena which results in the progressive dissolution of a metal in an environment via electrochemical reactions (Kruger, 1979 & Mudali et al., 2003). These electrochemical reactions occur at the surface of the implant which acts as an anode and where the metallic components are oxidised to their ionic forms and any dissolved oxygen is reduced to hydroxyl ions (Kruger, 1979). Prolonged hydrolysis and dissolution of a metallic biomaterial leads to build up of metal ions and compounds including chloride products which consequently reduce the pH and can prevent re-passivation of metal surface leading to prolongation of the process (Kruger, 1979

& Geringer et al., 2005). Corrosion processes pertinent to current implant alloys include crevice, galvanic, intergranular, stress-corrosion cracking, corrosion fatigue and fretting corrosion (Mudali et al., 2003 & Sargeant & Goswami, 2007). The consequences of these processes include mechanical deterioration of the implant and the generation of particulate debris and ions ranging from nano- to macro- scale which are then released into the peri-prosthetic *milieu* (Hallam et al., 2004). For biomedical Ti alloys corrosion is not expected to occur at temperatures under 65 °C (He et al., 2002 & Thomas et al., 2004). However, corrosion of explanted devices has been demonstrated (Figure 4.1) (Hallam et al., 2004 & Thomas et al., 2004).

Figure 4.1 Photograph of a Ti femoral stem post-implantation (2-5 yrs) indicating gross corrosion (left) and pH examinations (right) (Hallam et al., 2004)

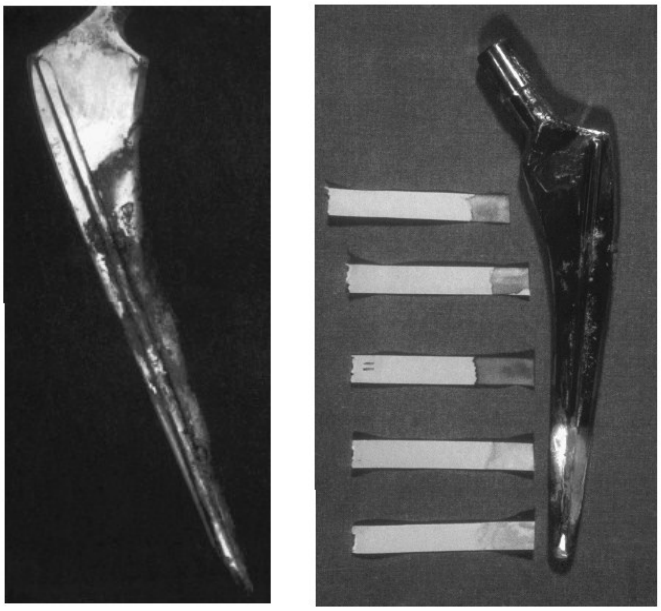

The corrosion susceptibility of Ti implant materials may be modified by organic species present particularly in inflamed tissue sites (Huang & Lee, 2005). Hypochlorous acid (HOCl) and hydrogen peroxide (H_2O_2) which are products of inflammation are known to accelerate the electrochemical reactivity of Ti (Hench, 1975 & Tengvall et al., 1989). *In-vitro* studies have documented that peroxide species can complex with Ti and the products have been shown to diffuse through cement to the bone contributing in progression of the implant inflammatory response (Tengvall et al., 1989). Furthermore, inorganic species such as sodium fluoride (NaF) found in dentifrices can also reduce the corrosion resistance of Ti and are particularly pertinent to implants in oral environments (Noguchi et al., 2008).

4.2.2 Pitting corrosion of Ti implants

Pitting corrosion of Ti implant surfaces has been documented (Dugdale & Cotton, 1964 & Beck, 1973) but such evidence has subsequently been heavily scrutinised. Pitting refers to the formation of holes or pits on the metal surface (Mudali et al., 2003) but in the context of Ti is known to result from presence of impurity inclusions (usually ferrous) or geometrical defects on the passive film (Thomas et al., 2004). True pitting corrosion is often a severe form of localised corrosion attack which contributes to extensive surface damage and release of significant amounts of metal ions (Mudali et al., 2003) and is rarely reported with Ti implant materials (Shreir et al., 1993).

4.2.3 Crevice corrosion of Ti implants

In contrast to pitting corrosion, crevice corrosion is implicated as occurring *in-vivo* and differs due to the generation of specific local chemistry which is confined spatially to within the crevice (Mudali et al., 2003). In crevices, a volume of solution can stagnate leading to local acidification and a build-up of chloride (Cl^-) and hydroxyl (OH^-) ions from the extracellular fluid gap contributing to dissolution of the metal (Thomas et al., 2004). Numerous parameters including increase in temperature, aggressive solution chemistry and a decrease in pH have been reported to influence crevice corrosion initiation of Ti in Cl, fluoride (F), halide and sulphate solutions (He et al., 2002). Nonetheless, Ti remains an electrochemically extremely passive material and studies utilising electrochemical impedance spectroscopy (EIS) and X-ray photoelectron spectroscopy have reported crevice corrosion of Ti alloys does not occur at temperatures below 65 °C (Menini et al., 2005).

4.2.4 Mechanically assisted crevice corrosion (MACC) of Ti implants

It has been theorised that crevice corrosion is unlikely to be significant for Ti implant materials (Shreir et al., 1993). However, the likelihood for crevice corrosion to occur is significantly increased by the presence of micro-motion between crevice walls which initiates surface depassivation (Hallam et al., 2004). Mechanically Assisted Crevice Corrosion (MACC) can occur on several scales – between modular implant components, between implant surfaces and cement or bone or between micron sized surface irregularities (Mudali et al., 2003).

Movement in a wide range of 1-100 μm have been identified as initiators of MACC which is also referred to as fretting corrosion within the literature (Duisabeau et al., 2004 & Geringer et al., 2005). When related to clinical outcomes MACC has been extensively attributed to orthopaedic total joint prosthesis failure (Hallab & Jacobs, 2003 & Sargeant & Goswami, 2007). Cyclic loads imposed on cemented Ti hip implants, bone-plates and screws are known to cause micro-displacements which result in disruption of the Ti oxide implant surface leading to exposure of the base metal and consequently resulting in dissolution of the metal (Duisabeau et al., 2004 & Hallam et al., 2004). The process is associated with crevice acidification and hence a corrosive medium is generated which then further accelerates the corrosive behaviour (Hallam et al., 2004).

4.2.5 Studying crevice corrosion of Ti implant materials

Artificial crevices or pits are widely used to study geometrical and chemical parameters of crevice corrosion (Isaacs, 1995). An artificial pit comprises of a metal wire or foil embedded in an inert resin and where anodic dissolution of the metal to a certain depth can be induced (Figure 4.2) (Isaacs, 1995). Build-up of high concentrations of cations within the pit leads to acidification which then induces stable pit growth (Galvele et al, 1990). The artificial pits may also provide information regarding the effect of salt films within the pits and information on the chemistry of species formed within the pit (Issacs, 1995).

Figure 4.2 Schematic diagram of an artificial pit (Issacs, 1995)

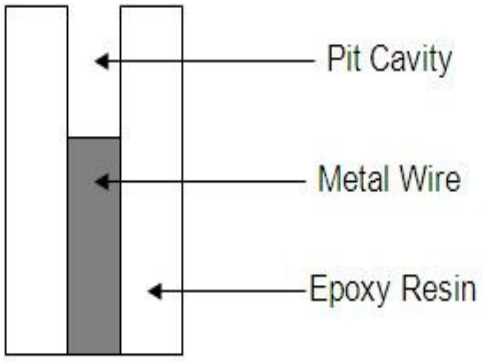

4.2.6 Understanding the Ti pit chemistry

Localised corrosion studies are difficult since they are associated with wet environments and measurements beyond basic electrochemistry are difficult to perform (Thomas et al., 2004). Therefore, experimental crevice corrosion of Ti has only been minimally reported (He et al., 2002). Ti can actively transform from an active to passive state by air, water and or other reagents to restore the metal or alloy's most common and stable oxidation state of Ti^{4+} (Menini et al., 2005). To date, investigations have attempted to mimic the physiological environment and have established Ti is susceptible to corrosion in aqueous solutions containing bromide, chloride, and iodide ions (Beck, 1973, He et al., 2002 & Noguchi et al., 2008). A preliminary investigation examined the dissolution of the passive state of Ti implant materials in physiological Ringer's solution (Souto & Burstein, 1996) and reported that at ambient temperatures, the passivity of the metal is destabilised by the presence of an aqueous chloride environment and a decrease in pH. In addition, the instability of the passive Ti oxide surface dictates the behaviour of metal dissolution products produced (Ektessabi et al., 1997). It is

therefore likely that surface roughness, crevices, complex geometries and internal line angles, and restriction of the flow of species as well as strain and stress all may contribute to corrosion which is not proportional to the surface area of the implant (Menini et al., 2005).

4.2.7 Experimental objectives

The corrosion of Ti is clearly highly complex and is influenced by a wide number of parameters (Thomas et al., 2004). The objectives of this study are therefore limited to identifying whether the same implant debris that is observed in the tissues surrounding Ti implants can be formed by (mechanically assisted) crevice corrosion simulated using an artificial pit model and measure with identical X-ray characterisation techniques. The susceptibility of Ti to modification by organic species generated during inflammation will be explored by exposing characterised Ti-oxide species to human neutrophils and measuring potential modifications (which can be hypothesised to occur in tissues) spectroscopically.

4.3 METHODS

4.3.1 Tissue excision and preparation

To study peri-implant Ti distributions in tissues associated with both CpTi and Ti-6Al-4V alloys which have also likely been exposed to different degrees of corrosion, three tissue types were obtained. Peri-implant inflamed epithelial tissue sections were obtained from consented adults (Ethical approval REC 08/H1203/128) undergoing scheduled removal or revision surgery for a failing:

(a) CpTi prostheses Grade IV. Epithelial tissue from surrounding BAHA implants in service for between 2-6 years (n=6).

(b) CpTi prostheses Grade IV. Oral mucosa from surrounding a Straumann RN SLA active dental implant in service for 6 months and 6 years (n=2).

(c) Ti-6Al-4V prostheses Grade V. Mixed connective tissue taken from adjacent to an intra-medullary stem (tibia) as part of a total knee replacement. 7 and 9 years of clinical service (n=2).

During tissue excision, metallic contamination was prevented and tissue sections were immediately orientated and snap-frozen prior to cryo-preparation. Sequential frozen sections of 4-6 μm thickness were cut with Tungsten Carbide blades and mounted on ultra-pure fused silica plates (<10 ppb Ti) (Spectrosil 2000, HeraeusQuarzglas GmbH & Co., Hanau, Germany), covered with 25 μm kapton

film (Kapton, Dupont, Wilmington, NC, USA) and sealed peripherally with epoxy resin. Alternating sections were fixed and H & E stained to provide histological reference for each experimental section. In addition, supplementary tissue sections which had not been exposed to Ti were prepared in an identical manner as control to determine if any contamination occurred during sample preparation.

4.3.2 Characterisation of Ti within peri-implant tissues

XRF mapping was performed using the micro-focus capability of I-18 beamline (Diamond Light Source, UK) in accordance with the methodology described in section 3.3.4. XANES measurements were taken at high, intermediate and low fluorescence values for Ti, identified by XRF mapping, using Si (111) crystal monochromator giving an energy range 4950 to 5050 eV with a 9 element Ge detector.

4.3.3 Ti reference standard preparation for XANES measurements

Ti standards were prepared as previously described (section 3.3.3). Further TiCl solution standards (Table 4.1) were made under inert gas and transferred into a Telfon cell under inert gas pressure for the period of the measurement. To prevent oxidation of the solution, solution standards were prepared 1 hr prior to measurements taken and both inlet and outlet tubes after transferring were immediately sealed. Spectra from the reference standards were measured simultaneously with sample spectra, where the reference standard is placed between the transmitted and third ion chamber.

Table 4.1 Ti solution standards

Compound	State	Oxidation State	Solution Composition	Environment
$TiCl_4$	Liquid	4	9 mM $TiCl_4$ in 0.55 M HCl	N_2
BSA	Liquid	4	9 mM $TiCl_4$ in 0.55 M BSA	Air
Ringers solution*	Liquid	4	9 mM $TiCl_4$ in 0.55 M Ringers Solution	Air

*Ringers solution were prepared by adding 8.5 g of NaCl, 8.5 g of KCl, 0.25 g of $CaCl_2$ and 0.22 g of $NaHCO_3$ to 1 L of distilled water. The solution was prepared 1 hr prior to electrochemical measurements or alternatively stored in 4 °C until use.

4.3.4 Setup of an electrochemical cell

3 mm wide strips of CpTi foil (50 μm thick) were cut and degreased with acetone before being sandwiched between Kapton adhesive tape with epoxy adhesive (Araldite) and attached to a polyvinyl chloride (PVC) reservoir The electrochemical cell comprised of 20 mL of 1M HCl solution and an Ag/AgCl reference electrode and a platinum wire counter electrode. Solutions with controlled additions of albumin or Ringers solution were used as an alternative electrochemical test electrolyte were employed separately (Table 4.1). All potentials reported are relative to Ag/AgCl in order to monitor the potential of crevice electrode. A potential of 11 V was provided to promote dissolution of the CpTi foil to a depth approximately 3 to 4 mm and then decreased to 7 V whilst the pit was grown under potentiostatic conditions.

4.3.5 SR-XANES measurements of artificial pits

Ti K-edge XANES was performed using the micro-focus capability of I-18 beamline (Diamond Light Source, UK). Spectra were taken prior to the corrosion of CpTi foil (50 μm thick) in fluorescence mode with a 5 x 5 μm beam footprint. An optical microscope installed on the beamline enabled identification of regions of the artificial pit for the XANES measurements enabling measurements during dissolution of the CpTi foil and evaluation of any variation in species observed with distance from the dissolving interface to the pit mouth.

4.3.6 Detection of intracellular modification of Ti nano-particles by human neutrophils

Neutrophils were isolated (Appendix I) and re-suspended at a concentration of $1x10^6$ cells/mL in PBS (Appendix I). 100 μL of the isolated cells were stimulated with 25 μL of Ti-oxide as anatase (<45 nm) at concentrations of 2000, 200, 20 and 2 ppm (section 2.2) for 1 hr at room temperature. After 1 hr the exposed cell suspension was fixed with acetone and the cells were then mounted on ultra pure silica (Spectrosil 2000, HeraeusQuarzglas GmbH & Co., Hanau, Germany) and desiccated. In addition, un-exposed cells were similarly fixed and mounted and acted as the experimental negative control.

4.4 RESULTS

4.4.1 Calibration of Ti standards

XANES spectra were acquired in transmission mode for all Ti solid (section 3.3.3) and Ti solution (Table 4.1) reference standards. Spectra were calibrated to the inflection point of Ti at 4960 eV. Ti solid reference standards as oxidized forms of rutile and anatase have three well resolved pre-edge features as described in section 3.4.2. CpTi foil (5µm) as metallic form also exhibits one well resolved pre-edge peak of higher intensity at around 4966 eV. In contrast to solid standards, the $TiCl_4$ solution reference standard exhibited a single pre-edge peak at 4971.5 eV with the intensity of the peak much higher than oxide forms (Figure 4.3).

Figure 4.3 Normalised XANES Ti K-edge spectra of Ti solid standards: 5 µm CpTi foil, rutile, mix oxide and anatase; and Ti liquid standards -$TiCl_4$

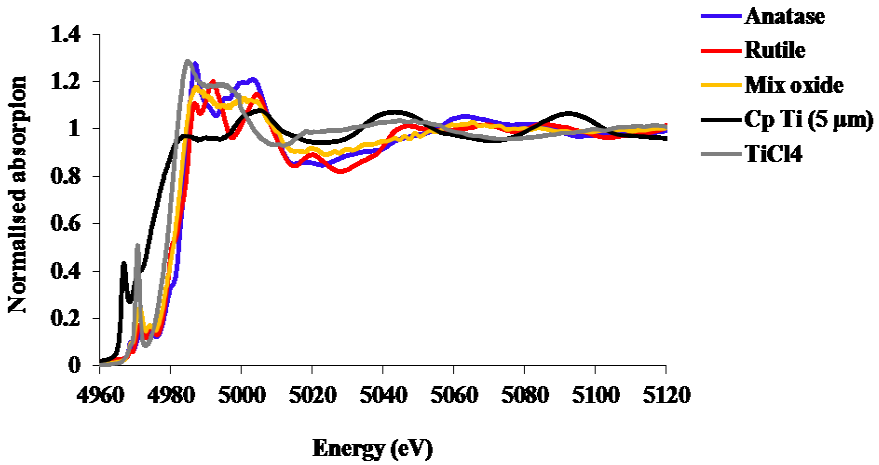

4.4.2 SR-XRF mapping of inflamed peri-implant tissues

Synchrotron X-ray fluorescence mapping of thin (4-6 μm) retrieved peri-implant tissues recovered from adjacent to percutaneous CpTi implants, to dental implants and to Ti-6Al-4V tibial stems all demonstrated Ti distributions (Figures 4.4-4.6). In oral epithelium, although Ti was detected in all of the sections studied the distribution of Ti appeared as distinct particles of <15 μm in size. In BAHA tissues as described in Chapter 3 a widespread distribution of Ti composed of different sized areas of Ti fluorescence intensity was observed. The distributions were consistently heterogeneous in all of the sections studied (11 sections from 6 patients). In orthopaedic tissues, the fluorescence intensity of Ti was the highest and the background level of Ti between "particles" was elevated suggesting Ti in ionic or nano-particulate forms.

Figure 4.4 A X-ray fluorescence map (250 × 525 µm) of the associated distribution of Ti in peri-implant skin tissues (6 µm thickness) taken from adjacent to a CpTi BAHA. Legend refers to increasing Ti fluorescence values

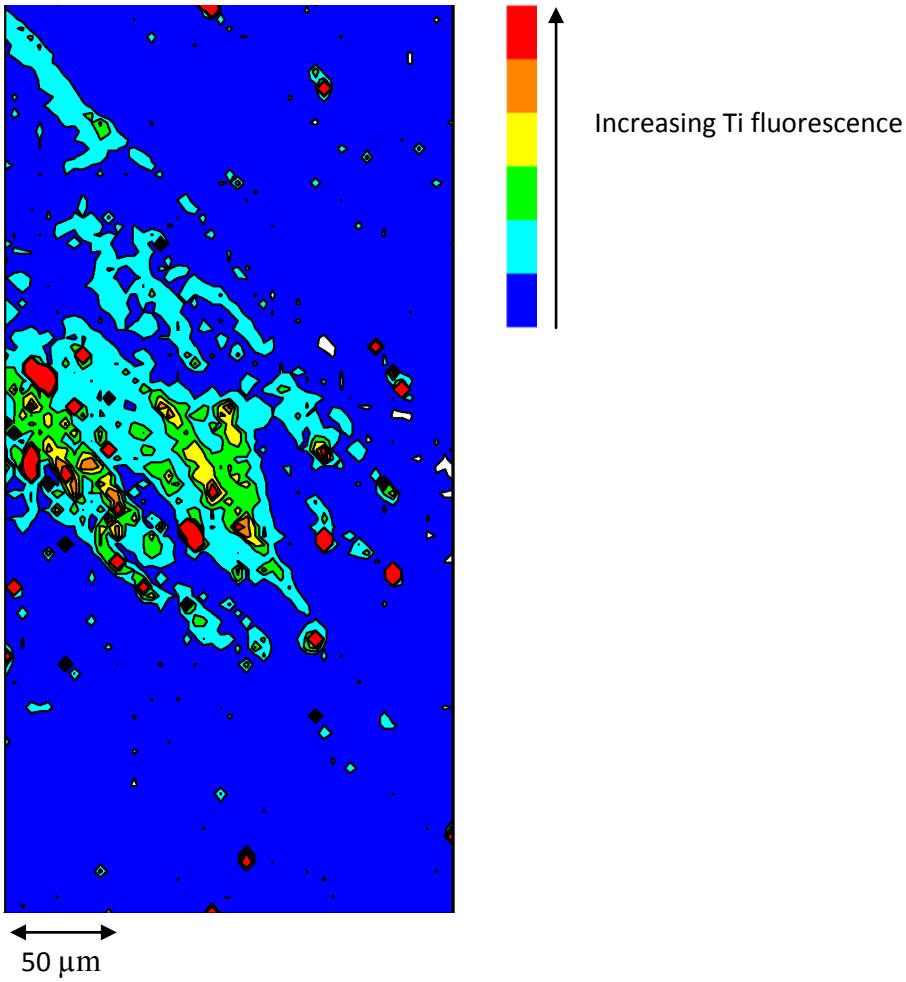

Figure 4.5 An X-ray fluorescence map (150 × 150 µm) of the associated distribution of Ti in peri-implant mixed connective tissues (6 µm thickness) taken from adjacent to a Ti-6Al-4V alloy tibial stem of a total knee replacement. Legend refers to increasing Ti fluorescence values

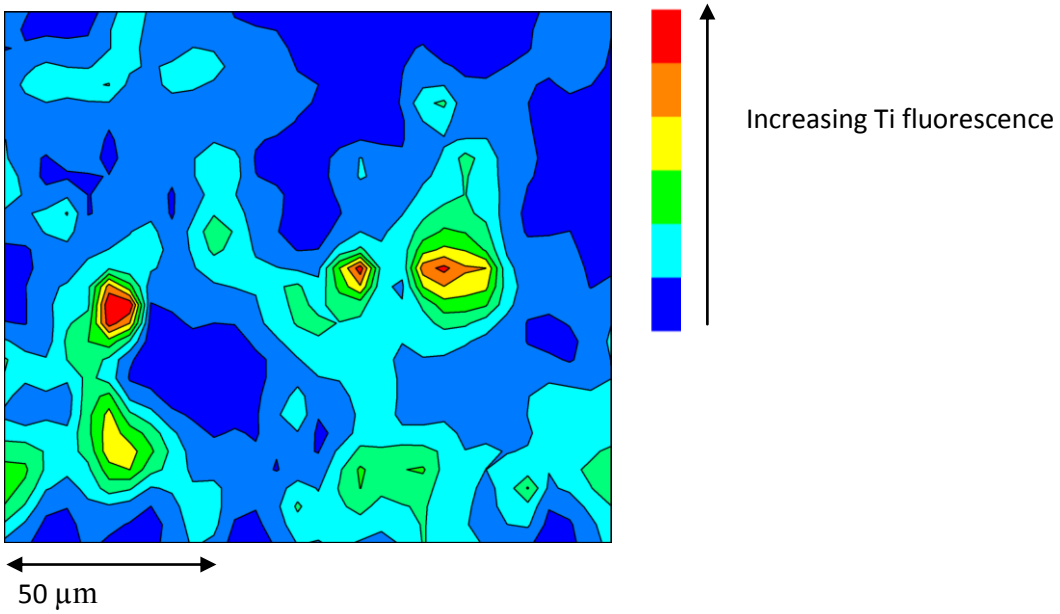

Figure 4.6 An X-ray fluorescence map (50 × 200 µm) of the associated distribution of Ti in oral epithelial tissues (6 µm thickness) taken from adjacent to a CpTi dental implant. Legend refers to increasing Ti fluorescence values

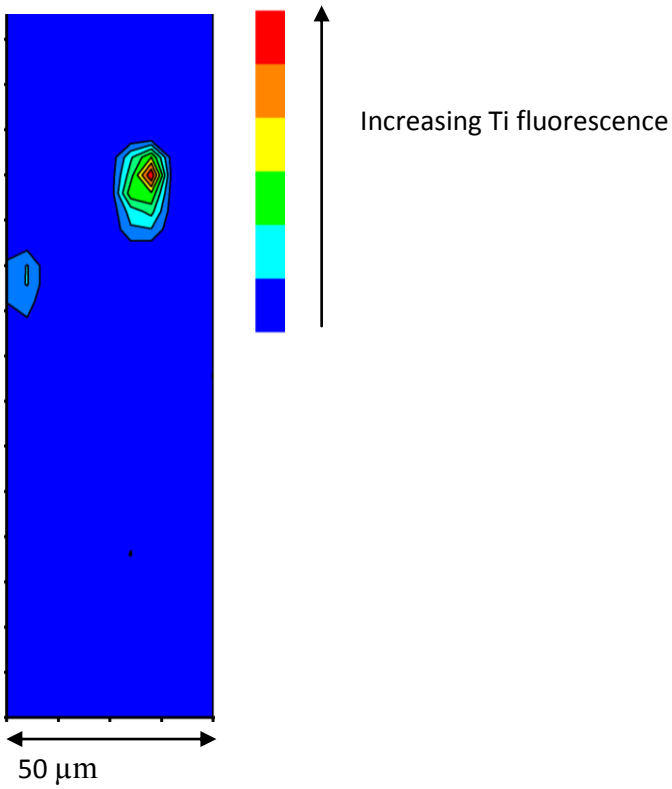

4.4.3 XANES spectra of inflamed Ti peri-implant soft tissues

XANES spectra were obtained at points of high and low concentrations of Ti identified by the Ti XRF maps (section 4.4.2). The chemical state of Ti was estimated by comparing XANES spectra to those of Ti reference standards (Figure 4.3). Where spectra appeared to be a mix of different Ti species, iterative steps of changing linear combinations of Ti standards spectra were taken to identify the dominant species component. Approximately 50 spectra could be categorised and rutile was identified to be the most predominant species localised

within the inflamed Ti implanted soft tissues from all three tissue types (Table 4.2 and Figures 4.7-4.11).

Table 4.2 Summary of the chemical state of Ti in inflamed Ti peri-implant soft tissues taken from approximately 50 spectra where peak assignment and edge energies were discernible

Tissue type	Tissue location from the implant	Chemical state of Ti (dominant species in bold)
BAHA-skin	Variable	Anatase, Peroxy and **Rutile**
BAHA-skin	Near	Metallic and **Rutile**
Oral epithelium	Variable	Anatase, Metallic and **Rutile**
Orthopaedic	Distant	Anatase, Metallic, Mix oxide and **Rutile**
Orthopaedic	Near	Anatase and **Rutile**
Orthopaedic	Contacting	Metallic

Figure 4.7 Representative normalised Ti K-edge XANES spectra pre-edge features of BAHA tissue taken from close to the implant at high fluorescence intensity compared to the Ti metallic reference standard –demonstrating well aligned pre-edge peaks

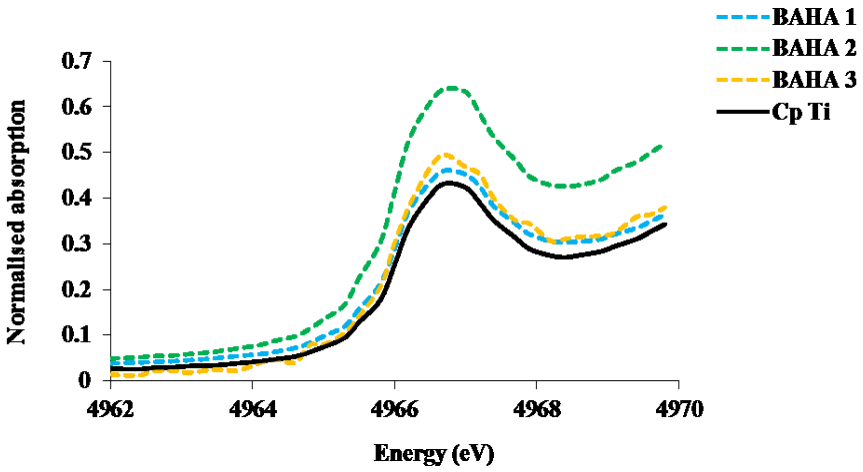

Figure 4.8 Representative normalised Ti K-edge XANES spectra of oral epithelial tissues associated with a CpTi dental implant and compared with anatase, rutile and CpTi (metallic). Experimental spectra show pre-edge oscillations consistent with oxide and although rutile was predominant linear combinations of the oxide states were likely to contribute to each spectra to some extent

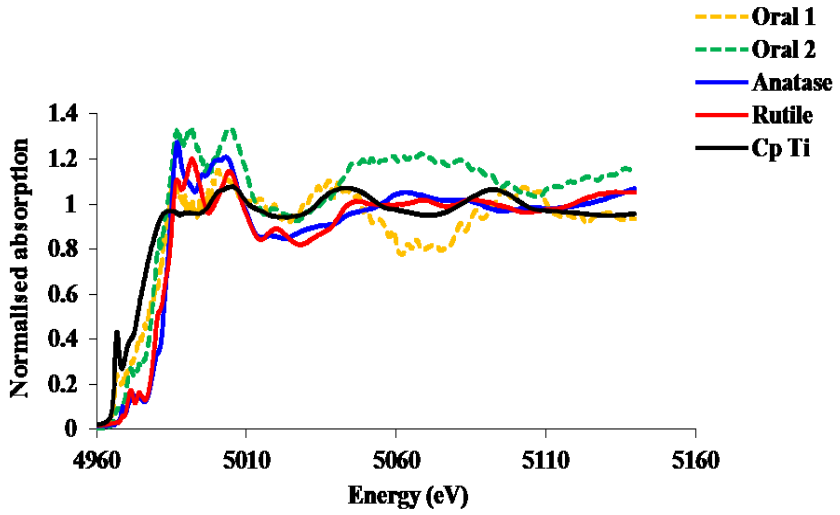

Figure 4.9 Representative normalised Ti K-edge XANES spectra of mixed connective tissue specimens taken distant from an indwelling orthopaedic Ti-6Al-4V implant and showing an extremely close resemblance to control spectra for Ti-oxide as rutile

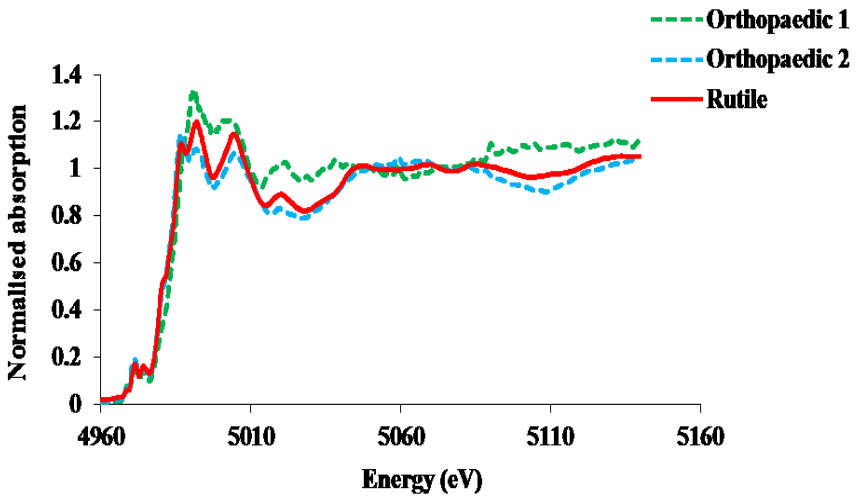

Figure 4.10 Representative normalised Ti K-edge XANES spectra of mixed connective tissue specimens in close proximity to an indwelling orthopaedic Ti-6Al-4V implant and showing resemblance to control spectra for the CpTi metallic reference standard in terms of the pre-edge features. However, the edge energy and post-edge features are more indicative of an oxide state suggesting that the area of Ti fluorescence exhibited particles of both types

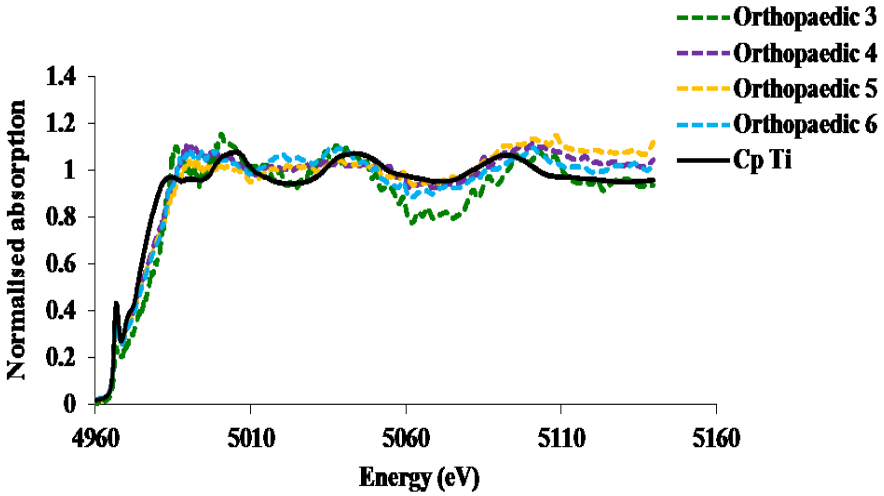

Figure 4.11 Representative normalised Ti K-edge XANES spectra of mixed connective tissue specimens taken immediately adjacent to an indwelling orthopaedic Ti-6Al-4V implant showing resemblance to the control spectra of Ti-oxide as anatase or a linear combination of anatase and rutile

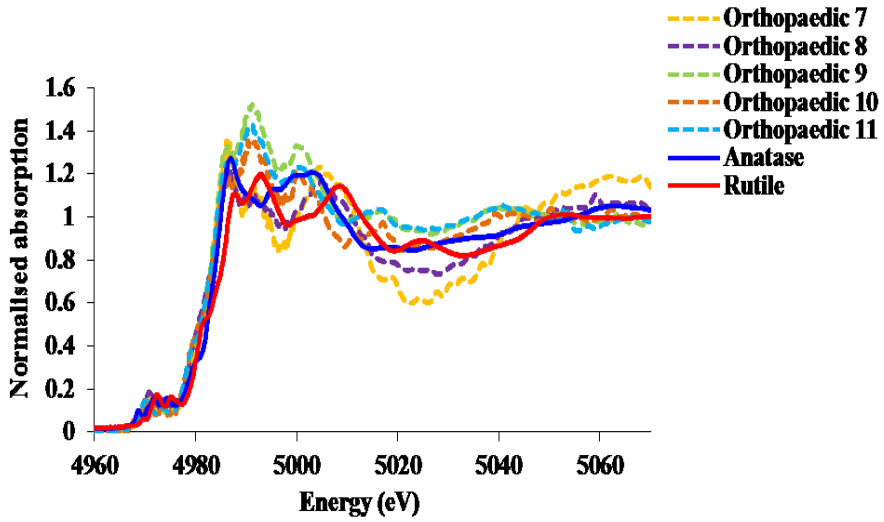

4.4.4 SR-XANES measurements of Ti speciation during simulated corrosion

Before corroding the Ti foil in the artificial pit, XANES spectra were acquired in fluorescence mode (Figure 4.12). Due to the thickness of the 50 µm foil the spectra were compressed at energies above the edge due to self-absorption effects. A 5 µm CpTi foil was therefore substituted for the reference standard and a pre-edge peak was clearly evident around 4967 eV.

Figure 4.12 Normalised XANES Ti K-edge spectra of 5 µm CpTi foil standard (measured in transmission mode) and 50 µm CpTi foil in artificial pit (measured in fluorescence mode)

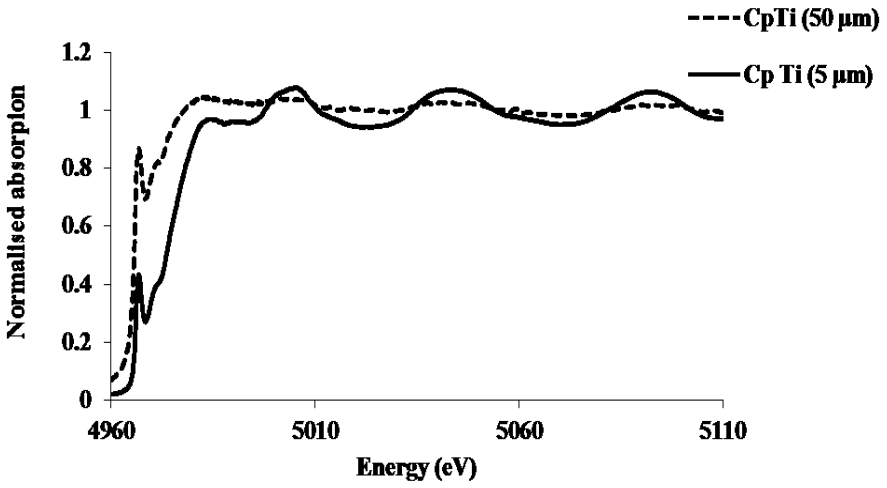

During the simulated corrosion process in various environments, the metal/solution interface was non-uniform and exhibited considerable roughness. In addition, dark and bright regions inside the pit and the formation of a salt film at the metal solution interface were visible with optical microscopy (Figure 4.13).

Figure 4.13 An optical image of the Ti artificial pit grown at 7 V (Ag/AgCl) in 1M HCl. The black solid line at the top shows the original sample edge position before dissolution and the oval shape shows characteristic bright and dark regions from which XANES measurements were taken

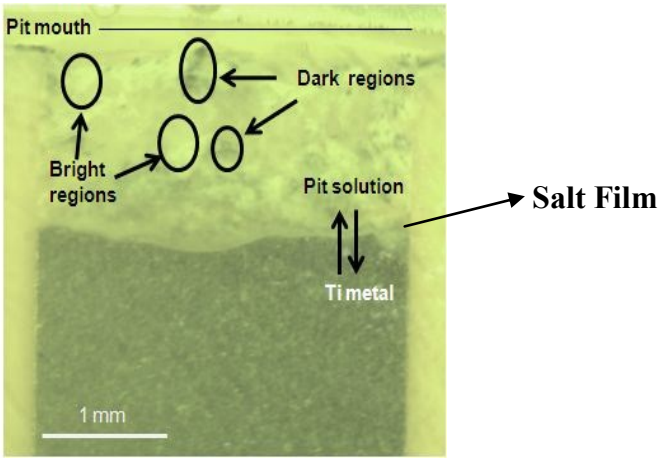

The optical imaging allowed identification of areas of interest for a series of XANES measurements inside the pit including obtaining spectra from bright and dark regions and above the pit (pit mouth) (indicated as solid line in Figure 4.13). An array of heterogeneous Ti species including $TiCl_4$, Ti as oxidized forms as anatase and rutile and as metallic forms were detected (Table 4.3 and Figures 4.14-4.18).

Table 4.3 Summary of the chemical state of Ti corrosion products in Ti artificial pit

Spot Number	Position	Areas	Chemical state of Ti
1 and 2	Inside the Pit	Bright	Metallic
3	Inside the Pit	Bright	Anatase, Rutile and $TiCl_4$
4	Inside the Pit	Bright	Metallic and $TiCl_4$
5	Inside the Pit	Bright	Anatase, Rutile and $TiCl_4$
6-8	Inside the Pit	Dark	Metallic
9	Above the Pit	Bright	Anatase, Rutile and Metallic
10 and 11	Above the Pit	Bright	Anatase, Rutile and $TiCl_4$

Figure 4.14 A normalised XANES Ti K-edge spectra of bright spots 1 and 2 inside the pit show similar pre-edge features to the 5 µm CpTi standard but post-edge features suggest a combination with oxide

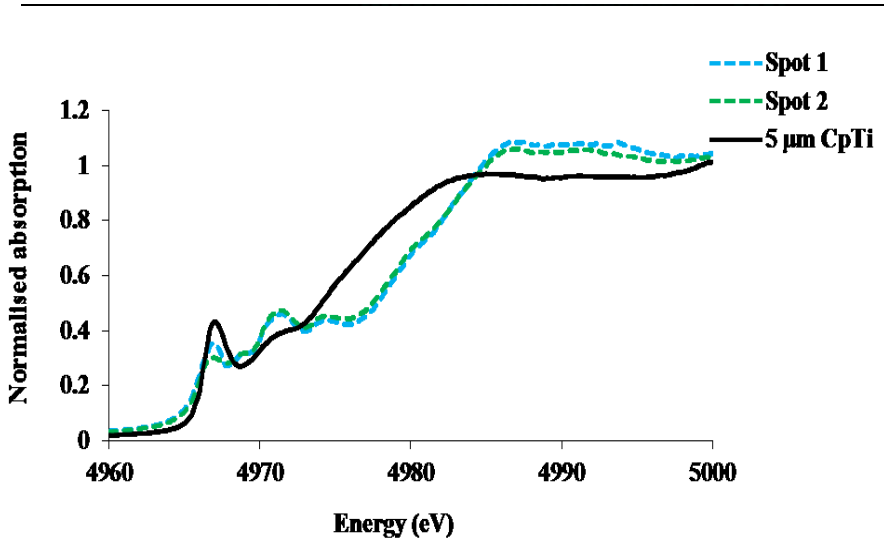

Figure 4.15 A normalised XANES Ti K-edge spectra of bright spot 3 (region inside the pit) compared with anatase, rutile, $TiCl_4$ and 5 µm CpTi standards suggests a linear combination of oxide and $TiCl_4$ forms

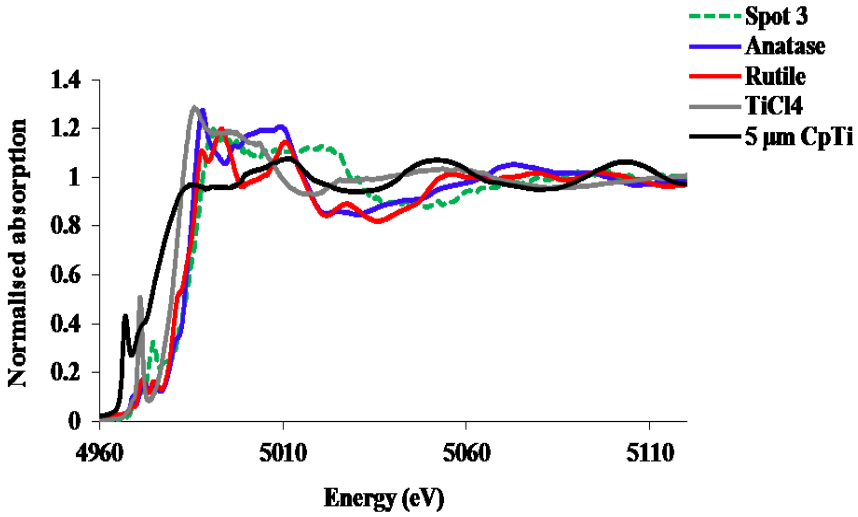

Figure 4.16 A normalised Ti K-edge spectra of spot 4 (bright region inside the pit) exhibits pre-edge and above edge features similar to the $TiCl_4$ reference standard whereas the edge area was similar to 5 µm CpTi (metallic)

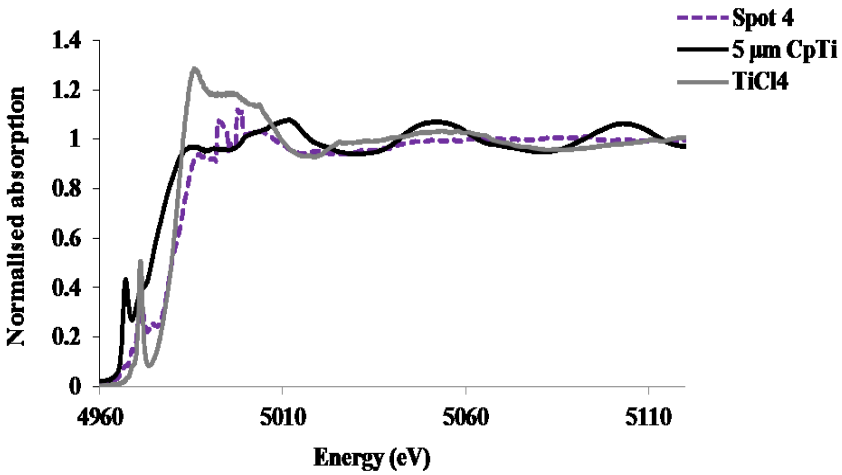

Figure 4.17 A normalised Ti K-edge spectra of spot 5 (bright region inside the pit) compared with anatase, rutile and $TiCl_4$ reference standards. The pre-edge was similar to combination of $TiCl_4$, anatase and rutile standards whereas the edge area was close representation of anatase and above edge area indicated similarity to anatase and rutile

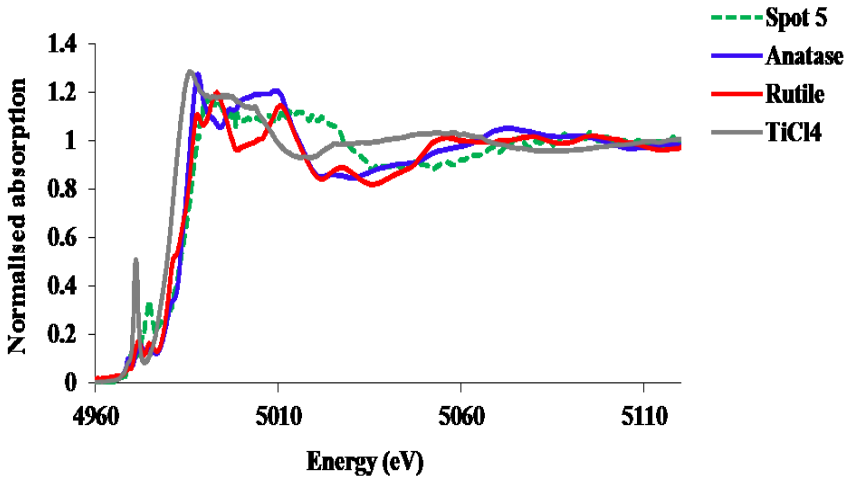

Figure 4.18 Normalised pre-edge spectra of dark regions from inside the pit compared with 5 µm CpTi (metallic). Furthermore, XANES measurements were acquired from three variable dark regions inside the pit and were similar to 5 µm CpTi. The intensity of the pre-edge peaks was higher than the metallic reference standard measured in transmission mode indicating evidence of non-linearity and for spectrum 6 especially resembled the 50 µm CpTi foil measured in fluorescence mode. These spectra are indicative of the generation of metallic particles from a corrosion process

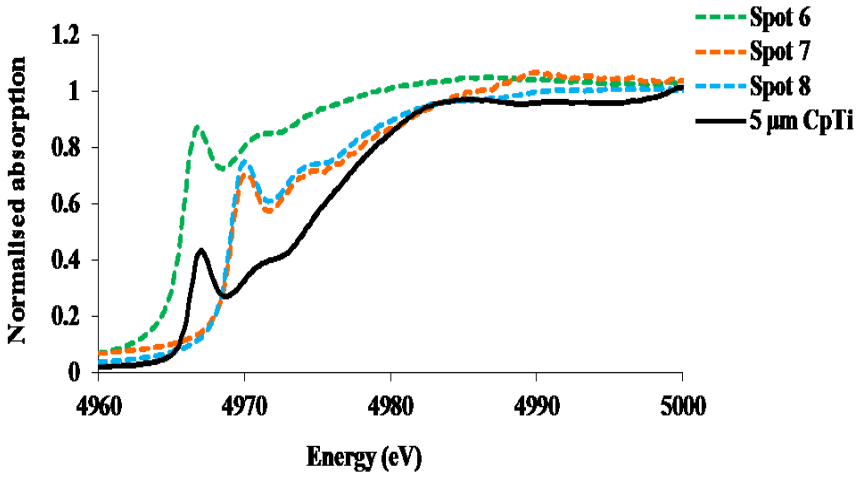

4.4.5 SR-XANES measurements of dissolution of Ti in artificial pit containing albumin (BSA)

A series of XANES measurements were acquired at two different time points whilst observing the dissolution of Ti in an electrochemical cell containing an albumin solution. Two consecutive XANES measurements represented as region 1 and 2 were acquired immediately at 7 V during the dissolution process and one XANES measurement represented as region 3 was acquired 40 mins following arresting of the corrosion process. In contrast to the previously described spectra, Ti species were found only in oxidized forms and no metallic form debris was observed (Figures 4.19 & 4.20).

Figure 4.19 Normalised XANES Ti K-edge spectra of regions 1 and 2 compared with rutile and mix oxide reference standards showing a good approximation to rutile (Ti-oxide)

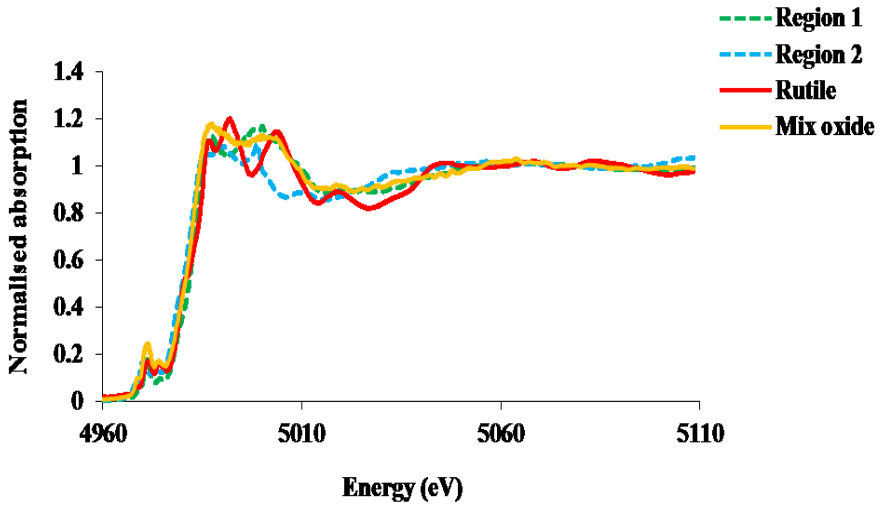

Figure 4.20 Normalised XANES Ti K-edge spectra of region 3 indicating a very close approximation to Ti-oxide as anatase

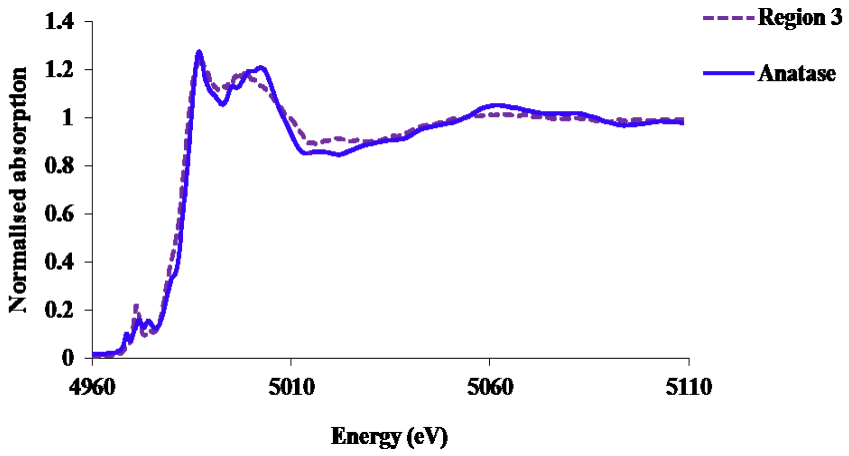

4.4.6 SR-XANES measurements of dissolution of Ti in artificial pit containing Ringers solution

A XANES spectrum was acquired whilst observing the dissolution of Ti in an electrochemical cell containing Ringers solution and is represented as region 4 (Figure 4.21). Similar to the XANES spectra of dissolution of Ti in solution containing albumin (section 4.4.5), no metallic spectra were observed with the closest approximation being a combination of oxide and solution species (mix between oxide and $TiCl_4$).

Figure 4.21 Normalised XANES Ti K-edge spectra of region 4 compared with mix oxide and $TiCl_4$ reference standards

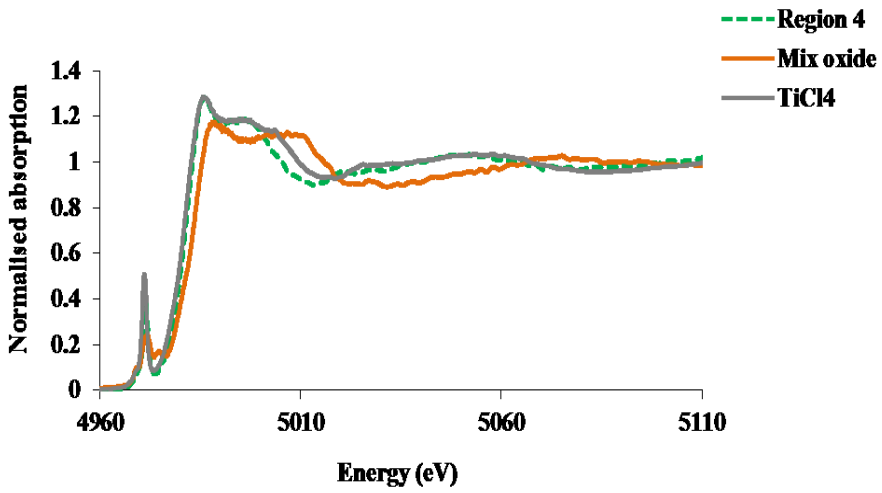

4.4.7 XANES spectra of Ti stimulated neutrophils

XANES spectra taken from single neutrophils which had been exposed to Ti oxide as anatase nanoparticles (<45nm) at 2000 and 200 ppm revealed a possible transformation of Ti co-ordination assumed to be occurring within or at the surface of the cell. The majority of spectra demonstrated a close approximation to

the anatase (Figure 4.22a). However, when a lower concentration of nanoparticles was used, spectra more consistent with a rutile state were observed (Figure 4.22b). For neutrophils exposed to anatase at 20 and 2 ppm the spectra were too noisy to be classified.

Figure 4.22 Normalised Ti K-edge XANES spectra taken from neutrophils stimulated with Ti-anatase at (a) 2000 ppm compared with anatase reference standard and (b) at 200 ppm compared with rutile reference standard. Figure 4.22b demonstrates post-edge features much more closely aligned with rutile

(a)

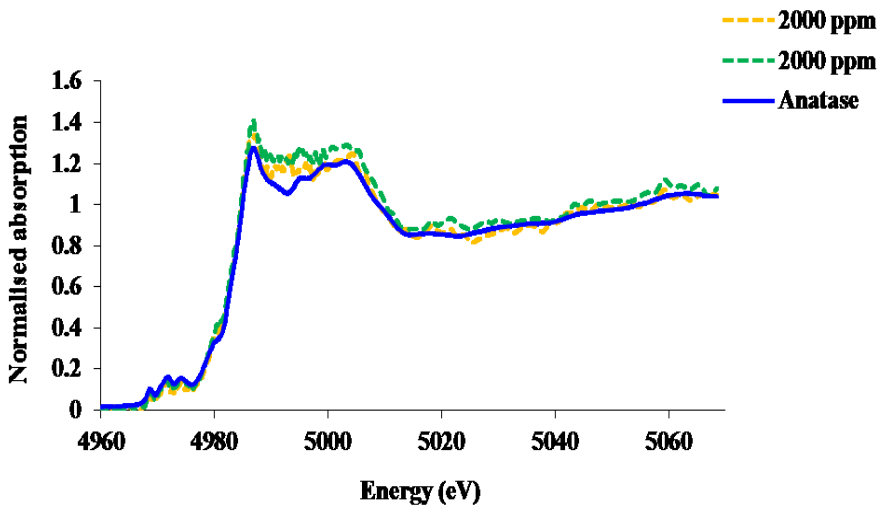

(b)

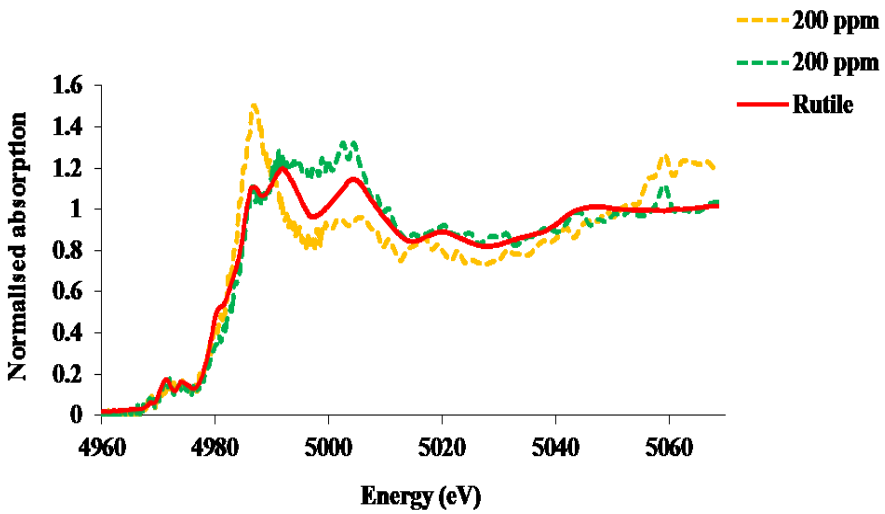

4.5 DISCUSSION

The use of Ti implants and especially transmucosal and percutaneous devices was initially associated with extremely high clinical success rates when the considered outcome measures were osseointegration capability and short term function (Ratner, 2001). It is now acknowledged that chronic problems associated with Ti implants are common and extremely difficult to manage (Ratner, 2001). Most research focuses on the impact of microbial colonisation of Ti surfaces (Fansson, 2009) and on possible dysregulation of host immune responses (Flatebø et al., 2006). However, there is increasing attention on whether Ti in free (particle and ionic) forms in the peri-implant soft tissues can modify the inflammatory response (Iavicoli et al., 2011). In Chapter 3, further evidence was provided to demonstrate the release of Ti into peri-implant soft tissues and suggested that the processes leading to the Ti release are likely to be corrosion mediated (on a micro-scale) (Thomas et al., 2004). Two alternative routes exist to the generation of the observed Ti distributions associated with the skin penetrating implants studied. Firstly, there are tribological mechanisms including 2 and 3 body wear (Budinski, 1991), however for skin penetrating implants and dental implants –wear processes that occur within the soft tissue cuff surrounding the implant are highly unlikely. A second alternative are biocorrosion mechanisms whereby cellular activity (microbial and/or eukaryotic) (Mudali et al., 2003) and extracellular contents (e.g. endotoxin, peroxide species and local acidification) mediate Ti release (Tengvall et al., 1989). It is important to note however, that biocorrosion mechanisms are chemically mediated (Mudali et al., 2003) and in common with crevice corrosion

will be exacerbated by existing disruption of the Ti oxide layer –through micromechanical routes (Menini et al., 2005).

In this Chapter, extensive Ti distributions surrounding Ti-6Al-4V tibial stems and CpTi percutaneous implants was observed (section 4.4.2). Ti-6Al-4V has a lower corrosion resistance than CpTi (section 1.1.4) (Elias et al., 2008) however, the tissues probed were taken at time of revision surgery and aseptic loosening of the intramedullary Ti component of the device had already occurred leading to associated wear processes. During wear, depassivation of the Ti surface also occurs leading to secondary chemical reactions however; metal particulate debris would be expected to have dominated. Interestingly, in these mixed connective tissues surrounding the indwelling Ti-6Al-4V implant, the majority of debris was in oxide forms (Table 4.2) demonstrating that the Ti had been in ionic form at some stage (Beck, 1973 & Vicentini et al., 1975). A high background level of Ti spread throughout the tissues further suggested that Ti may still be in non-particulate form bound to biomolecular components. The oral epithelium taken from around dental implants demonstrated a dispersed distribution of Ti (Figure 4.6) and was likely to be particles. Both oxide forms and metallic debris was identified but again the species that dominated was Ti-oxide as rutile. The higher quantities of Ti observed in percutaneous implants when compared with transmucosal are possibly related to less of the released material being lost from the soft tissue crevice around the implant when compared with the gingival crevice. The observation of XANES spectra in all three tissue types that resembled species intermediary between metallic and oxide again was suggestive

of a corrosive process leading to the release of small particles. The mixed spectra gave a possible indirect indication of size effects whereby as a particle size reduces in the nano-scale the proportion of surface atoms (co-ordinated with oxygen) to core atoms which maybe as oxide or in a metallic form increases. With nano-sized metallic particles a spectra between oxide and metallic may be expected due to the relative contributions of the surface and core atoms. The spectroscopic findings were consistent with a corrosion process and also with processes leading to the generation of particles observed on a nano-scale. To provide supporting evidence it was important to be able to demonstrate that all the species observed could be generated through corrosion and to further attempt to identify why rutile species may dominate.

A considerable advantage of synchrotron spectroscopy is the ability to undertake measurements in "wet" environments (Willmott, 2011). This in the current study allowed the chemistry of a corroding Ti crevice/pit to be studied. The high lateral resolution of the microfocus-beam of the I-18 beamline (Diamond Light Source) enabled the corrosion pit to be probed at visually distinct areas to identify regional variation of the Ti chemistry away from the corroding interface.

In accordance with previous pitting investigations reported (Beck, 1973), 1 M HCl was used as an electrolyte to initiate acidification in the potential corrosion sites. Once initiated the aggressive electrochemical conditions were reduced (reducing voltage from 11 to 7 V) to reduce the diffusion rate of escaping ions from the pit cavity. It should be highlighted that whilst the conditions appear

biologically unrealistic on a microscopic scale, the same levels of acidity will be anticipated in crevice corrosion conditions *in-vitro* (Issacs, 1995). Notably, under these conditions it was demonstrated using XANES measurements that released Ti is found as $TiCl_4$ and that with distance from the pit, Ti^{4+} becomes oxidised forming insoluble particles which can be observed to be co-ordinated as anatase or rutile or a mixture of both (Table 4.3). Furthermore, for the first time it was demonstrated that crevice corrosion of CpTi can lead to the generation/ release of Ti metallic fragments and this may further account for the occasional observation of Ti in this form in the oral epithelial and skin tissues studied in the current investigation.

Electrochemical dissolution of Ti in the presence of albumin (BSA) was undertaken in order to closely mimic the *in-vivo* environment (section 4.4.5). Proteins including albumin are a major constituent of physiological medium and albumin has been demonstrated to be one of the most prevalent proteins to bind to metal ions (Vamanu et al., 2008). The potential influences of the protein present will be its adsorption to the Ti foil surface, its modification of local acidity and possible associations with particles and ions that are released. The XANES measurements acquired differed from the Cl^- dominated medium in section 4.4.4 revealing an array of heterogeneous Ti species but only in oxidized forms as anatase and rutile and mixed speciation. No metallic traces of Ti were observed in pit containing albumin solution and no solution species were identifiable. This finding could suggest that albumin itself is mopping up some of the Ti^{4+} and in doing so modifying local acidity so that formation of oxide particles is promoted.

The findings do not however help to elucidate the seemingly preferential occurrence of Ti-oxide as rutile within the tissues.

Ti corrosion was also studied in the presence of ringers solution (section 4.4.6). Components of ringers solution have previously been reported to accelerate the dissolution process of Ti and are representative of the physiological medium *in-vivo* (Souto & Burstein, 1996). Unfortunately, due to limited experimental beam time, XANES measurements were only preliminary but demonstrated the formation of Ti-oxide species which appear intermediary between oxide states and the solution species, $TiCl_4$. These findings are consistent with previous studies studying Ti corrosion behaviour in ringers solution which have suggested that a series of depassivation followed by repassivation processes occur with time (Souto & Burstein, 1996).

These series of experiments have demonstrated the capability of crevice corrosion mechanisms to generate the range of Ti species which had been observed in a range of tissues. Importantly the heterogeneity of species observed in the pit simulation experiments (section 4.4.4) were consistent with the heterogeneity observed in the tissues (section 4.4.3) and that the Ti speciation in corroding crevices is heavily influenced by environmental variables such as the presence or absence of protein (Huang & Lee, 2005) or the different biologically relevant electrolytes found in physiological fluids (Shreir, 1993). However, what could not be explained was the predominance of Ti-oxide as rutile that was observed in the tissues. A preliminary experiment was undertaken to identify whether cellular

products or processes could potentially modify Ti once they accumulate within the tissues. Neutrophils were chosen as they are professional phagocytes (Dale et al., 2008) which have the capability of producing species such as H_2O_2 (Hampton et al., 1998) which are known to complex with Ti oxide (Tengvall et al., 1989). In Chapter 3, Ti-peroxy compounds were observed which gave further support to a hypothesis of cellular mediated modification of Ti. In the current study, high purity anatase nanoparticles were used to stimulate neutrophils (activity was monitored by enhanced chemiluminescence of controls). XANES spectra taken before and after exposures demonstrated that some of the Ti as anatase now appeared in a co-ordination more similar to rutile (section 4.4.7). As the transition temperatures from anatase to rutile have been reported to be >500°C (Czanderna et al., 1958) it is important to note that this is not an energetically favourable scenario. Possible mechanisms that could account for the observed spectra were that within the phagosome the Ti ions are generated and then re-oxidise in a rutile form. Alternatively, it may simply be that the anatase nanoparticles are small enough that their surface atoms dominate their XANES spectra. Exposure of the nanoparticles to cellular or extracellular contents e.g. proteins may lead to surface adsorption of these biomolecules and distortion of the surface Ti-O bonds leading to the spectral modification.

4.6 CONCLUSION

In this chapter it has been demonstrated that a highly chemically heterogeneous distribution of Ti exists in peri-implant tissues and through simulations it can be further shown that its generation can be accounted for by crevice corrosion mechanisms. The speciation of Ti appears to be highly sensitive to the physiological environment and there is sufficient evidence to suggest that Ti release may be further modified within the peri-implant soft tissues. These findings highlight the importance to now understand the biological consequences of such Ti products on chronic peri-implantitis.

CHAPTER 5

THE EFFECT OF TITANIUM IMPLANT DERIVATIVES ON THE NEUTROPHIL RESPIRATORY BURST

5.1 PREFACE

Enhanced chemiluminescence assays were used to determine the effect of direct stimulation of neutrophils with 'Ti implant derivatives.' Dose dependent total and extracellular Reactive Oxygen Species (ROS) production was measured following stimulation and compared against unstimulated controls. Significantly elevated ROS production from stimulated cells was observed with low concentrations of Ti implant derivatives (2 ppm). The magnitude of ROS production was influenced by Ti particle size and speciation. Neutrophil internalisation and subsequent intracellular distribution of Ti oxide nanoparticles was observed using Transmission Electron Microscopy (TEM) and Energy Dispersive X-ray (EDX) techniques. Data from neutrophil respiratory burst assays and observations of intra-cellularisation of Ti implant derivatives suggest that oxidative stress induction by such products may contribute to a pro-inflammatory state in susceptible patients and lead to the progression of the peri-implant inflammatory response.

5.2 INTRODUCTION

5.2.1 Neutrophil respiratory burst

Oxidative stress is associated with chronic inflammatory conditions (Edwards, 1994 & Nel et al., 2006) and degenerative diseases (Ames, 1993, Floyd, 1999 & Kadenbach et al., 2009) which manifest due to increased cellular production of reactive oxygen metabolites that may be released into the extracellular environment (Matthews et al., 2007). Neutrophils have been recognised to play a vital role in inducing an oxidative stress environment and have been demonstrated to be important in the progression of periodontitis (Asman et al., 1985, Chapple & Mathews, 2007 & Wright et al., 2008). In neutrophils, oxidative stress results from a process known as the respiratory burst (Babior, 1984). The respiratory burst is associated with an increased consumption of molecular oxygen which is utilised by the nicotinamide adenine dinucleotide phosphate (NADPH) oxidase enzyme complex to yield highly-reactive oxygen species (ROS) (Figure 5.1) (Battino et al., 1999 & Dahlgren et al., 2007).

Figure 5.1 Schematic representation of ROS release from neutrophils (Robinson, 2008)

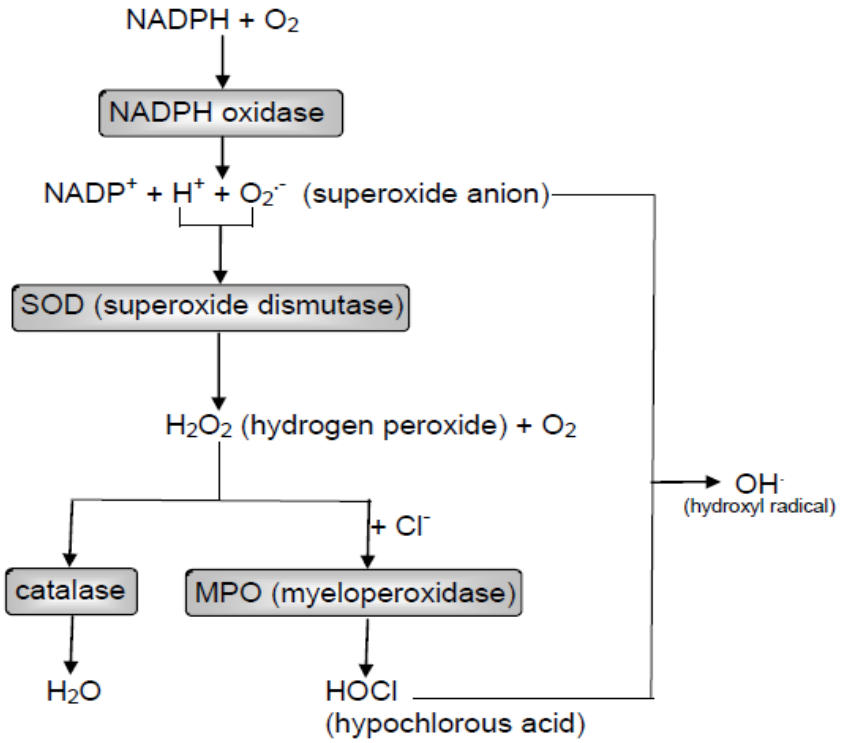

NADPH (Nicotinamide Adenine Dinucleotide Phosphate) - an enzyme complex used to reduce oxygen to superoxide and hydrogen peroxide

SOD (Superoxide Dismutase) - catalyzes the reduction of O_2^- to H_2O_2

Catalase reduces H_2O_2 to H_2O

MPO (Myeloperoxidase) - major constituent of the azurophil cytoplasmic granules which consumes H_2O_2 produced by the neutrophil to HOCL

5.2.2 The NADPH oxidase enzyme complex and its properties

The NADPH oxidase consists of one membrane bound compound (flavocytochrome b_{558} comprising of $gp91^{phox}$ and $p22^{phox}$ subunits) and four cytosolic components ($p47^{phox}$, $p40^{phox}$, $p67^{phox}$ and Rac) which are dormant in resting neutrophils. The assembly and activation of the complex is reported to occur on the plasma membrane, within the cytosol and on the membranes of specific granules (Figure 5.2) (Hampton et al., 1998 & Kobayashi et al., 1998).

Figure 5.2 Possible sites for NADPH oxidase complex assembly and activation in human neutrophils (Dahlgren & Karlsson, 1999)

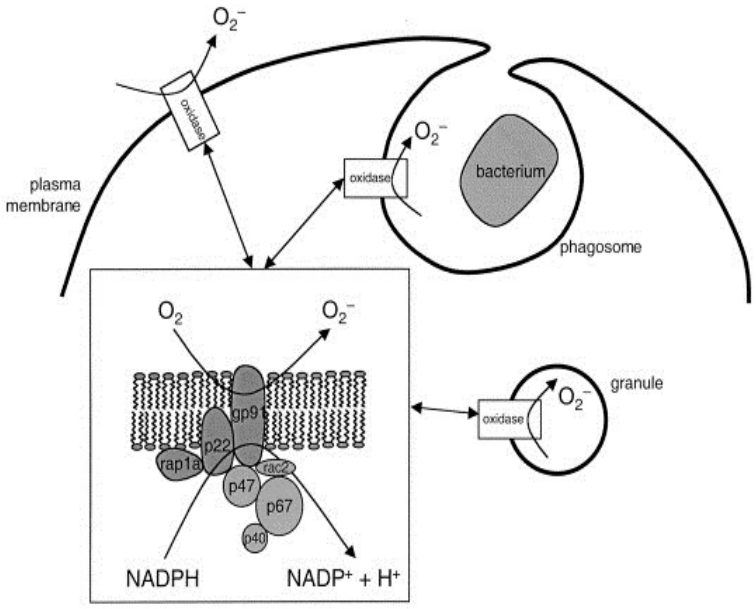

Studies have identified that through receptor dependent or independent activation in neutrophils, the cytosolic proteins become phosphorylated and through an unknown intracellular signal translocate to the membrane bound component, flavocytochrome b (Hampton et al., 1998). Association of the heterodimer flavocytochrome b protein localised in the plasma membrane and in membranes of

intracellular granules leads to oxidation of glucose in the hexose monophosphate shunt (NADPH oxidase) causing assembly and activation of the NADPH oxidase enzyme complex (Borregaard et al., 1983). The electron donor, NADPH via the flavocytochrome b subunit in the cytosol spontaneously reduces one or two electrons from oxygen (O_2) to generate superoxide anions (O_2^-) and H_2O_2 respectively in an intracellular compartment such as the phagosome (Figure 1.3) (Kobayashi et al., 1998 & Dhalgren & Karlsson, 1999) or in the extracellular *milieu* (Figure 5.2) (Babior 1999).

These primary products (O_2^- and H_2O_2) are further recognised to be reduced by other cellular systems including superoxide dismutase (SOD) which catalyzes the reduction of O_2^- to H_2O_2 and/or by catalase which reduces H_2O_2 to H_2O (Dahlgren & Karlsson, 1999). H_2O_2 produced within cells can diffuse across cell and nuclear membranes (Hancock, 1997 & Nathan, 2006) causing activation of pro-inflammatory mediators which can consequently contribute to excessive inflammation (Chapple et al, 2007).

In addition, following interactions with the cellular enzyme myeloperoxidase (MPO) (localised in the neutrophil azurophil granule) (Klebanoff, 2005), the primary products are metabolised further to form potentially toxic substances, such as hypochlorous acid (HOCl), chloramines and hydroxyl radicals ($^{\cdot}OH$) (Figure 5.1) (Dahlgren et al., 1999). The NADPH respiratory burst products are highly reactive and can be ferried to the phagosome or to the extracellular *milieu* with the aim of directly or indirectly inducing microbial death (Freitas et al.,

2009). The activated NADPH enzyme possesses a deactivation mechanism to limit ROS release in inflamed sites, however failure of inactivation leads to over production of ROS metabolites resulting in host tissue damage (Epstein & Weiss, 1989) (sections 1.5.2 & 5.2.3). It has been demonstrated that neutrophils from periodontitis patients have a deficiency in the key oxidative deactivation, due to reduced glutathianione (GSH), which appears to be a constitutive defect (Dias et al., 2013).

5.2.3 Role of ROS species in host tissue destruction

The toxicity of ROS to host tissues may occur directly or indirectly through interactions of ROS species with cellular and extracellular components (Mathews et al., 2007). Formation of free radicals beyond the normal threshold in the host is reported to exacerbate inflammatory responses (Hampton et al., 1998); induce loss of defence homeostasis (Chapple et al., 2007) and potentially induce apoptosis of other immune cells (Hildeman et al., 2003 & Park et al., 2008). Studies document that elevated oxygen radicals and inflammatory mediators including H_2O_2 and HOCl released into the extracellular environment contribute to peri-prosthetic bone loss and tissue destruction (Doorn et al., 1998). Moreover, neutrophils from periodontitis patients are hyperactive and hyper-reactive with respect to ROS release (Mathews et al., 2007) and the oxidatively stressed neutrophils direct superoxide into the extracellular sites (Dias et al., 2013).

5.2.4 The interaction of ROS with Ti implant surfaces

Superoxide, singlet oxygen, H_2O_2, HOCl, chloramines and ·OH radicals which are all derivatives of respiratory burst products (Battino et al., 1999) have been demonstrated or hypothesized to interact with Ti implant surfaces. An *in-vitro* study utilising a spin trapping technique reported Ti incubated with H_2O_2 formed a yellow coloured $Ti_{(IV)}H_2O_2$ complex (Tengavall et al., 1988 & 1989). The complex is reported to trap superoxide radicals therein which consequently form variable Ti peroxy compounds. However, the pro-inflammatory potential of such Ti peroxy compounds has yet to be studied.

Alternatively, H_2O_2 and Ti may possibly yield hydroxyl radicals (·OH) and Ti hydroxide radicals via Fenton or Haber Weiss reactions (Tengvall et al., 1989) which could induce Nuclear Factor-kappa Beta (NF-kB) and/or DNA strand breaks as hydroxylation contributes to extracellular oxidative damage (Shi et al., 1999). In addition, Ti is also reported to complex with HOCl which in the context of cemented orthopaedic devices has been reported to diffuse through cement to the bone further contributing to the progression of peri-implant inflammatory response (Thomas et al., 2004).

5.2.5 Measurement of respiratory burst release

Numerous techniques are available for the measurement of free radical release by professional phagocytes such as neutrophils (Table 5.1) (Curtin et al., 2002). Techniques for measuring the cellular production of ROS should be (a) highly

sensitive, (b) specific for a particular oxygen metabolite, (c) distinguish the cellular site of ROS release and (d) should not interfere with cellular functions, thus avoiding false quantification (Dahlgren et al., 1999). However, no single technique has been shown to be capable of satisfying all the above criteria (Dahlgren et al., 1999).

Table 5.1 Techniques used for measuring cellular production of different reactive oxygen species (ROS) (Dahlgren et al., 1999)

TECHNIQUE	MEASURING PRINCIPLE	CELLULAR LOCALSATION	SENSITVITY
Superoxide anion			
Photometry	Reduction of cytochrome c	Extracellular	Low sensitivity as H_2O_2 may interfere with the assay
Luminometry	Isoluminol chemiluminescence	Extracellular	High sensitivity as detects O_2^- despite the requirement of peroxidase
Luminometry	Lucigenin chemiluminescence	Extracellular	High sensitivity but less than isoluminol
Hydrogen peroxide			
Fluorometry	Peroxidase dependent oxidation of PHPA ± azide	Intracellular	Low sensitivity
Fluorometry	Peroxidase dependent oxidation of scopoletin ± azide	Extracellular	Low sensitivity but higher than PHPA system
Non-identified oxygen radical			
Luminometry	Luminol chemiluminescence	Intracellular and extracellular	High sensitivity
Fluorometry	Oxidation of 2, 7-dichlorofluorescein or dihydrorhodamine	Intracellular	Low sensitivity

Enhanced chemiluminescence assays are considered the most sensitive and selective accurate real-time methods for low level superoxide detection especially during the respiratory burst (Lundqvist, 1996). Chemiluminescence assays utilise a luminometer (Aggarwal et al., 2004) which measures the light emitted, expressed in relative light units (RLU) from the oxidative end products produced by an *in-vitro* reaction between ROS and the chemiluminophores employed (Yamaguchi et al., 2002). The type of luminophore used for measuring ROS is critical as the molecular species responsible for the chemiluminescence are usually unknown (Yamaguchi et al., 2002).

Luminol [5-amino-phthalazine-1,4(2H,3H)-dione] (Albrecht, 1928) is one of the most extensively used chemiluminescence probes as it can cross biological membranes thereby decreasing the detection limit substantially and making the technique very sensitive (Lundqvist, 1996). The molecular species reported for luminol chemiluminescence is dependent on the combined activity of NADPH and MPO (Stevens et al., 1978). Thus, the reagent reacts with a variety of free radicals including the superoxide anion, $^{\cdot}OH$ and H_2O_2 enabling the measurement of ROS released from the cells (extracellular activity) as well as ROS originating from unidentified subcellular compartments such as the phagosome (intracellular activity) (Briheim et al., 1984 & Dhalgren & Karlsson, 1999). HOCl is the principle ROS, detected by luminol, however currently there is limited understanding about the diffusion properties of luminol through the different membranes of the phagocyte (plasma membrane, granule membrane and phagolysosomal membrane) (Dahlgren & Karlsson, 1999).

In the reaction, luminol is oxidised by ROS products generated by neutrophils to aminodiphthalate (Gorsuch, 1969) (Figure 5.3). The aminodiphthalate produced is in an excited state which returns to its ground state accompanying with the emission of photons (*hv*) in the visible region of the spectrum (λ=425 nm) responsible for the resulting chemiluminescence (Alegria-Schaffer et al., 2009) (Figure 5.3).

Figure 5.3 Simplified representation of luminol oxidation which generates light (*hv* represents photon) (Alegria-Schaffer et al., 2009)

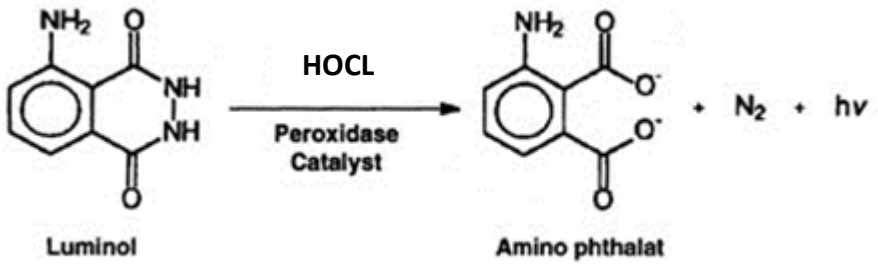

A further chemiluminophore is isoluminol (Lundqvist, 1996) which differs from luminol with respect to the position of the amino group in the phthalate ring of the molecule (Figure 5.4). The change in the position of the amino group does not change the ability of the molecule to react with ROS (Dahlgren & Karlsson, 1999).

Figure 5.4 Schematic molecular representations of luminol and isoluminol (Yamaguchi et al., 2002)

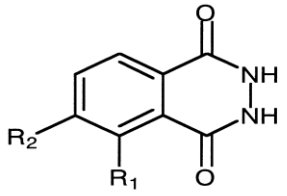

	R_1	R_2
5-Aminophthalazine-1,4(2*H*,3*H*)-dione (Luminol)	NH_2	H
6-Aminophthalazine-1,4(2*H*,3*H*)-dione (Isoluminol)	H	NH_2

Isoluminol [6-aminophthalazine-1,4-(2H,3H)-dione] follows the same light generating mechanism as luminol (Lundqvist, 1996 & Dahlgren & Karlsson, 1999). However, moving the amino group away from the first carbon atom in the aromatic ring makes the isoluminol molecule more hydrophilic and less able to transverse biological membranes, therefore predominately detecting extracellular ROS release (Figure 5.5) (Lundqvist, 1996 & Dahlgren & Karlsson, 1999). In addition, isoluminol shows 10-100 times weaker chemiluminescence than that of luminol (Yamaguchi et al., 2002) and the availability of released cellular MPO also hinders the isoluminol light generating reaction (Dahlgren & Karlsson, 1999). Accordingly, owing to the fact that isoluminol chemiluminescence signal is weaker, exogenous peroxidase such as horseradish peroxidase (HRP) is added to the measuring system to amplify the isoluminol chemiluminescence signal (Lundqvist, 1996).

Figure 5.5 Membrane permeability of luminol and isoluminol (Dahlgren & Karlsson, 1999)

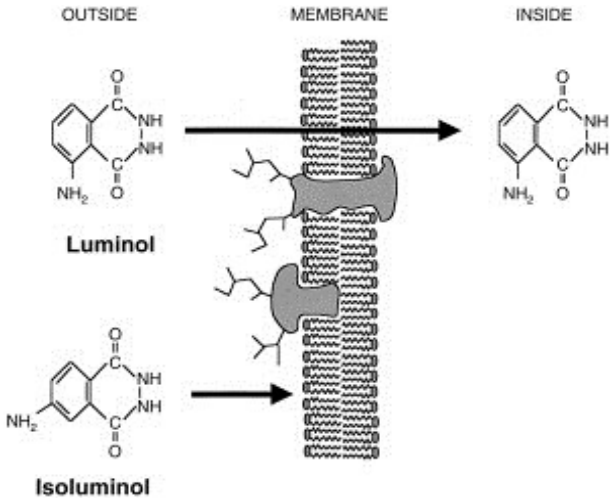

A number of studies report that Ti nanoparticles presented as oxide species cause oxidative stress in various cell types including osteoblasts (Pioletti et al., 1999 & Li et al., 2010), BEAS-2B (Park et al., 2008), fibroblasts (Bhattacharya et al., 2009) and many more (Long et al., 2007 & Jin et al., 2011) and can lead to either cell apoptosis (Wang et al., 2003, Park et al., 2008 & Kang et al., 2009) or necrosis (Tsutsui et al., 1999 & Osano et al., 2003). However, surprisingly the pro-inflammatory potential of Ti of different chemical speciation and particle sizes representative of implant derived debris on mammalian neutrophils (Kumazawa et al., 2002 & Goncalves et al., 2010) is poorly researched.

Colorimetric, fluorometric and chemiluminescence assays of cellular processes are considerably complicated by the presence of particulate stimuli which may interfere with light output through absorption and with chemical reactions involved in the light production. Despite the extensive interest in cellular

responses to particles, this significant issue is rarely considered. In the context of the current investigation, TiO_2 absorbs light in a spatial range overlapping the emission spectra of common chemiluminophores (luminol λ=425 nm and isoluminol λ=526 nm) with different observations according to speciation. Furthermore, TiO_2 may also complex with produced ROS species such as H_2O_2 and O_2^- (section 5.2.4) (Tengvall et al., 1988). As a result considerable care must be taken to account for the possible interference effects the stimulus has on the measurement.

5.2.6 Neutrophil phagocytosis

In addition to the neutrophil respiratory burst, neutrophils also display increased consumption of O_2 during phagocytosis (Baldridge & Gerard, 1933 & Sbarra & Karnovsky, 1959) of foreign material and/or inflammatory mediators (May & Machesky, 2000). Neutrophils are recognised as the main leukocytes in humans with the function of phagocytosis (Metchnikoff, 1893). Phagocytosis represents a cellular engulfment process encompassing diapedesis, pseudopod formation and endocytosis to form a phagosome, but this process may also lead to tissue injury (Hensen & Oades, 1973), if reactive species are released from the neutrophil during phagocytosis.

Numerous authors using imaging techniques such as transmission electron microscopy (TEM) have reported phagocytosis of Ti metallic wear debris in macrophages (Xing et al., 2008 & Hirayama et al., 2011), osteoblasts (Pioletti et al., 1999 & Meng & Yang, 2013), bone marrow-derived mesenchymal stem cells

(MSCs) (Wu et al., 2011) and fibroblasts (Osano et al., 2003). Ti debris as nanoparticles is proposed to be rapidly phagocytosed by cells as aggregates forming membrane bound vesicles and/or as individual particles via pinocytosis or endocytosis (Shanbhag et al., 1995 & Hallab, 2009). Moreover, investigators have demonstrated that the uptake of Ti nanoparticles into specific immune cell compartments can activate pro-inflammatory and pro-osteoclastogenic cytokines mediators including TNF-α, RANKL, M-SCF, PGE2, IL-1, IL-6 and IL-8 (Tuan et al., 2008) which could potentially influence peri-implant inflammatory responses (Pioletti et al., 1999 & Hiryama et al., 2011). Surprisingly, to date there is limited evidence for the phagocytosis of Ti nanoparticles by neutrophils and the subsequent distribution of Ti at the subcellular level (Kumazawa et al., 2002).

5.3 METHODS

5.3.1 *Ex-vivo* determination of ROS production from stimulated neutrophils

Chemiluminophores including luminol and isoluminol were employed to detect total and extracellular ROS production by stimulated neutrophils. A 30 mM stock solution was produced by dissolving 0.5 g of luminol (A8511; Sigma-Aldrich, UK) or isoluminol (A8264; Sigma-Aldrich, UK) in 94.05 mL of 1 mM NaOH prior to storage at 4 °C. The working solution was then prepared by diluting 1 mL of the stock solution of luminol/isoluminol in 9 mL of phosphate buffered saline (PBS) (Appendix I) and the pH was adjusted to 7.3 using dilute NaOH or HCl.

5.3.2 Stimuli used to induce ROS production in neutrophils

The control (Table 5.2) and experimental stimuli (Table 2.1; section 2.2) were prepared by adding high purity reagents to PBS. Table 5.2 demonstrates the working concentration of the prepared solution and stimulation concentration once added to the experimental system.

Table 5.2 Stimuli used to induce ROS production

Stimuli (Acronym)	Supplier	Working Concentration	Stimulation Concentration
Phosphate Buffer Saline (PBS)	Made in house (Appendix I)	-	-
Ops *S. Aureus* (Ops *Sa*) (non-viable)	LGC Standards, UK ATCC 9144	$6x10^8$/mL in PBS	MOI[1] 1:300
F. Nucleatum (*FN*) (non-viable)	LGC Standards, UK ATCC 10953	$6x10^8$/mL in PBS	MOI[1] 1:100

[1]MOI: Multiplicity of Infection

5.3.3 Characterisation of Ti stimuli

In order to characterise the appearance of Ti particles and to evaluate Ti dispersion behaviour, Ti stimuli (Table 2.1; section 2.2) were dispersed in distilled water at a concentration of 200 ppm which was then dripped onto 200-mesh copper TEM grids. Samples were then left overnight to air dry and then studied using TEM (JEOL 1200, Japan) at variable magnifications.

5.3.4 Blocking buffer (1% PBS-BSA)

10 g of Bovine Serum Albumin (BSA) (A4503; Sigma-Aldrich, UK) was dissolved in 1 L of PBS to yield 1% PBS-BSA. The solution was stored at -20 °C until use.

5.3.5 GPBS (Glucose supplemented PBS)

GPBS comprised 1.8 g of glucose, 0.15 g of $CaCl_2$ (S10070; Sigma-Aldrich, UK) and 1.5 mLs of $MgCl_2$ (1M; S22093; Sigma-Aldrich, UK) were added to 1 L of PBS and stored at 4 °C.

5.3.6 HRP (Horseradish peroxidase)

HRP provided in a salt free lyophilized powder form (P8375; Sigma-Aldrich, UK) was prepared in PBS of stock concentration of 1 U/µL and stored at -15 °C until further use. 75 µL of the stock was further diluted in 675 µL of PBS for it to be used at 0.1 U/µL.

5.3.7 Sensitivity of chemiluminescence assay

An experimental concern was that there may be an underestimation of the magnitude of the detected light signal as the Ti stimuli prepared as dispersions in PBS are likely to limit light transmission by light absorption where the effects will be concentration dependent. Therefore, the specific light emission of luminol/isoluminol was studied in the absence and presence of the Ti stimuli dispersed in PBS at a concentration of 2000, 200, 100, 20, 10, 2 and 1 ppm using a calibrated spectrometer (USB400, Ocean Optics, Dunedin, USA). A blank cuvette was placed in the spectrometer and intensity (Counts) against light wavelength (nm) was recorded. To the same cuvette, 2 mL of the respective Ti dispersion was added and light transmission was measured five times; between each measurement the cuvette was agitated so that the Ti particles remain

dispersed during the measurement process. The light emission spectra for luminol/isoluminol were also measured five times. Light absorbance by each stimulus condition was calculated as a function of the decrease in peak emission wavelengths of luminol (λ=425 nm) and isoluminol (λ=526 nm) respectively (Liu et al., 1996).

Since ROS species are known to react with Ti species (section 5.2.4) further calibrations were performed to identify whether the generated ROS were being consumed by non-light generating reactions. To ascertain these reactions the Ti stimuli (Table 2.1; section 2.2) prepared as dispersions in PBS at a concentration of 2000, 200, 20 and 2 ppm were suspended in luminol/isoluminol and then were reacted with H_20_2 following measurement of light output by a Tube Luminometer (Lumat^3 LB 9508, Berthold Technologies, Germany). The light output was first read for a blank tube for 15 secs and then 1.5 mL of luminol/isoluminol was transferred to the same tube and read for another 15 secs. The light measurements were paused and 500 µL of the luminol/isoluminol was replaced with 200 µL of 1% PBS-BSA, 10 µL of HRP and 75 µL of GPBS and read for consecutive 15 secs. 200 µL of the Ti stimuli were added to the same tube followed by thorough vortexing and monitored for 30 secs. The mixing was effective so that all the Ti particles remained in solution during the measurement process. 15 µL of 0.1% H_2O_2 was then added to the same tube followed by thorough vortexing and light output was monitored for the subsequent 30 secs. The assay was repeated five times and the light quenching potential of the Ti stimuli was calculated by

recording the proportional reduction in the peak luminescence of the test sample (RLU).

5.3.8 Enhanced chemiluminescence assay for the measurement of ROS production from stimulated neutrophils

Neutrophils were isolated and re-suspended at a concentration of $1x10^5$ cells/mL in PBS as previously described using a Percoll® density gradient (Appendix I). A 96-well white micro-plate (Immunolon2, Dynex, Chantilly, VA, USA) was pre-blocked with 200 µL of 1% PBS-BSA per well and stored overnight at 4 °C. The blocking buffer was removed by washing the plate five times with sterile PBS using a plate washer (Bio-Tek ELx50, Vienna). All assays were performed at 37 °C using a luminometer (LB96, Berthold UK Ltd., Milton Keynes, UK) where light output was recorded for 1 sec per well in RLU. Each well contained 45 µL of GPBS with 30 µL of luminol (3 mmol/L), or 15 µL of HRP (0.6 µg/mL) with 60 µL of isoluminol (3 mmol/L). 100 µL of isolated neutrophils were added and light output was monitored for 30 mins to set a baseline. Cells were then stimulated with 25 µL of either heat killed Ops *Sa* (MOI: 300-bacteria/neutrophil) or *FN* (MOI: 100-1) as positive controls and PBS as a negative control. Experimental stimuli included 25 µL of high purity Ti (Table 2.1; section 2.2) prepared as sonicated dispersions of 2000, 200, 20 and 2 ppm in PBS. All samples were run in replicates of five within 2 hrs of blood collection. The entire assay was conducted around 10-20 times for each Ti species, and on each occasion neutrophils were sourced from different healthy volunteers.

5.3.9 *Ex-vivo* detection of Ti nanoparticles internalised by mammalian neutrophils

Interactions between Ti nanoparticles and mammalian neutrophils were investigated using TEM (TEM; JEOL 1200, Japan). Neutrophils were extracted from healthy volunteers as previously described (Appendix I) and re-suspended at a concentration of $1x10^5$ cells/mL in PBS. 6 mL of the isolated cells suspended in PBS, were proportioned into two equal volumes of 3 mL. Cells from each group were stimulated with 500 µL of Ti oxide as anatase (≤45 nm) (248576; Sigma-Aldrich, UK) dispersed in PBS (Table 2.1; section 2.2) at a concentration of 2000 ppm. In addition, one group of the Ti stimulated cells was also exposed to 250 µL of cytochalasin B (cytoB; extracted from *Drechslera dematioidea*) at a concentration of 10 µg/mL in PBS which is a known phagocytosis inhibitor (C6762; Sigma-Aldrich, UK). Stimulated cells were left at room temperature for 1 hr and then repeatedly washed in PBS (x10) (centrifuged between each wash step). Both suspensions were then fixed with 2.5% glutaraldehyde followed by 1% osmium tetroxide for 1 hr. Samples were then dehydrated using graded ethanol dilutions prepared in distilled water ranging from 50, 60, 70, 80, 90 to 100% for 10 mins each. After ethanol treatment, cells were embedded in a propylene oxide resin. Ultra-thin sections (~100 nm) were cut with a diamond knife microtome (UC6, Leica Ltd. Co, Germany) and then transferred onto 200-mesh copper TEM grids, stained with 3% uranyl acetate and lead nitrate. Sections were examined at variable magnifications using TEM-JEOL 1200 (JEOL 1200, Japan). In addition, Energy Dispersive X-ray (EDX) spectroscopy analysis (JEOL 2100, Japan) was conducted to locate Ti nanoparticles within the acquired images. The experiment

was conducted twice employing the same Ti stimuli as anatase (oxide) (≤45 nm at 2000 ppm), with neutrophils sourced from different healthy volunteers.

5.3.10 Statistical analysis

Statistics were performed using SPSS 20 software. The data were initially explored for normality using a Shapiro-Wilk test at a 95% significance level. Comparison between groups was made using Wilcoxon Sign Rank tests at a 95% significance level.

5.4 RESULTS

5.4.1 Dispersion of Ti particles

TEM images of the Ti stimuli of oxide and metallic species of varying particle size dispersed in distilled water (200 ppm), revealed levels of agglomeration (Figure 5.6) consistent with those reported in previous literature (Tamura et al., 2002, Wang et al., 2009 & Jin et al., 2011). For all nano sized Ti stimuli, a mixture of agglomerated particles (Figure 5.6; Left) and mono- dispersed nanoparticles (Figure 5.6; Right) were observed. Agglomerated particles remained below 1 μm in diameter however there was inherent variability in the size and morphology observed (Figure 5.6). For metallic particles sourced in high purity forms, but separated by sieve sizes variation in size was also observed (Figure 5.6) up to the maximum diameter reported by the manufactures (Table 2.1; section 2.2).

Figure 5.6 TEM images acquired at variable magnifications revealing surface properties of Ti stimuli dispersed in distilled water at a concentration of 200 ppm as agglomerates (Left) and individual particles (Right)

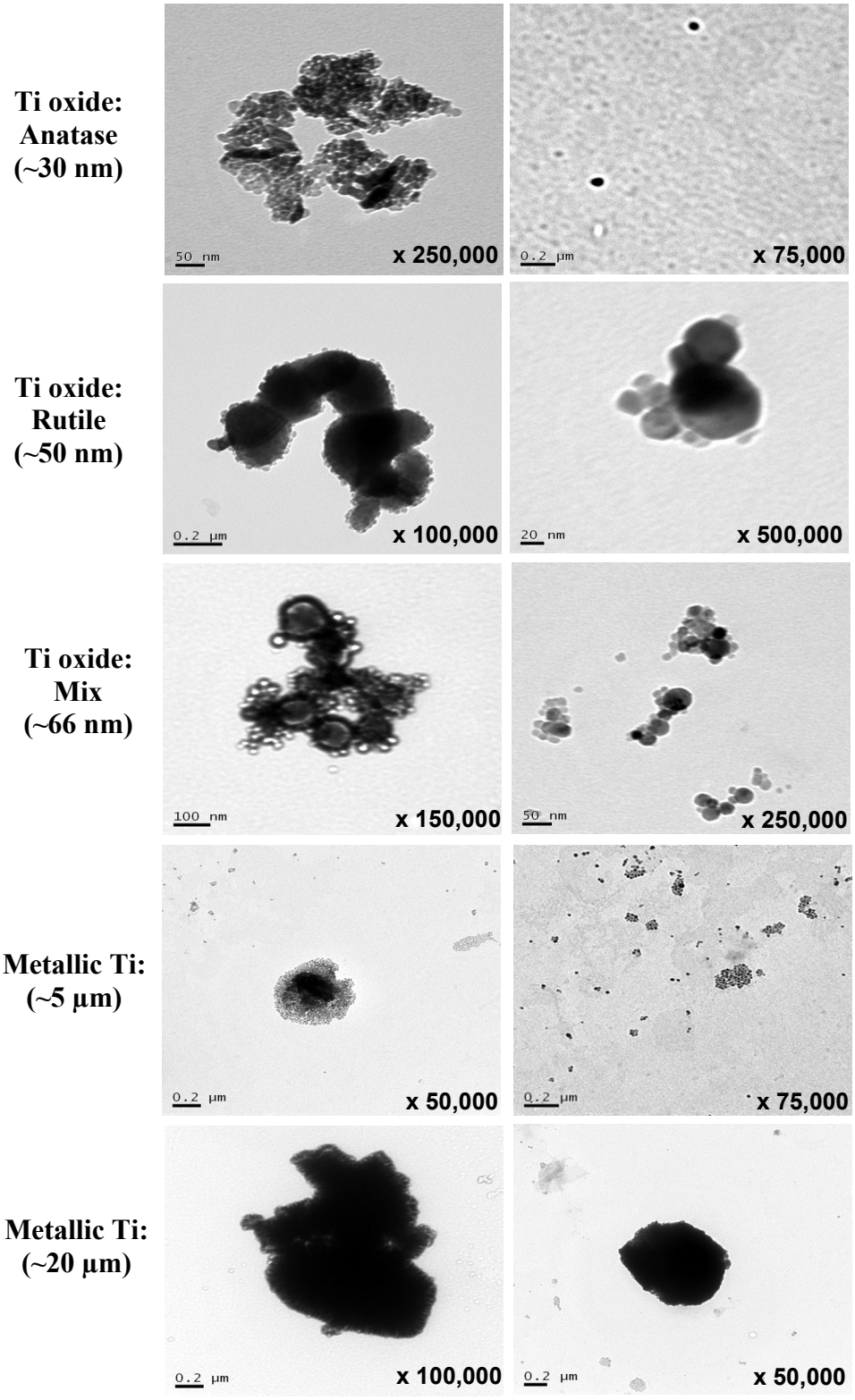

5.4.2 Sensitivity of chemiluminescence ROS quantification

Spectroscopic measurements were used to estimate the attenuation of the light signal by the Ti stimuli used (Table 2.1; section 2.2) (Lappalainen et al., 2001). In these methods each sample acts as a reference for itself. The effect of light absorption at wavelengths (λ) corresponding to the peak emission wavelengths of luminol (λ=425 nm) and isoluminol (λ=562 nm) by Ti stimuli is reported in Table 5.3 and Table 5.4 respectively.

Table 5.3 Percentage attenuation of light output at emission maxima of luminol (λ=425 nm) following interaction with Ti stimuli at concentrations of 2000, 200, 20, 10, 2 and 1 ppm

	Attenuation of light output (%) following interaction with Ti stimuli					
Ti (ppm)	**Anatase (~30 nm)**	**Rutile (~50 nm)**	**Oxide Mix (~66 nm)**	**Metallic (~5 µm)**	**Metallic (~20 µm)**	**Peroxy (size unknown)**
2000	88	88	89	63	88	84
200	87	74	87	42	85	53
20	49	50	51	22	37	31
10	24	21	27	8	11	15
2	11	10	11	7	7	8
1	7	7	7	1	2	2

Table 5.4 Percentage attenuation of light output at emission maxima of isoluminol (λ=562 nm) following interaction with Ti stimuli at concentrations of 2000, 200, 20, 10, 2 and 1 ppm

	Attenuation of light output (%) following interaction with Ti stimuli					
Ti (ppm)	**Anatase (~30 nm)**	**Rutile (~50 nm)**	**Oxide Mix (~66 nm)**	**Metallic (~5 µm)**	**Metallic (~20 µm)**	**Peroxy (size unknown)**
2000	91	91	92	67	91	88
200	90	77	91	47	90	58
20	53	53	55	25	41	34
10	27	24	27	9	14	16
2	11	12	11	7	7	8
1	7	7	7	1	2	4

For all tested Ti species a reduction in the light signal was observed and was concentration dependent (Tables 5.3 & 5.4). The light signal in the presence of Ti as oxide nanoparticles or micron-sized metallic particles at a concentration of 2000 and 200 ppm interacting with luminol and isoluminol, was reduced by >80% (Table 5.3) and >90% (Table 5.4) respectively. Ti as oxide nanoparticles attenuated to a greater extent than micron-sized metallic particles (Tables 5.3 & 5.4). Increasing metallic particle size resulted in increased light attenuation (Tables 5.3 & 5.4). Ti peroxy compound also inhibited light output; but to a lesser extent (Tables 5.3 & 5.4).

In addition to spectroscopy, tube luminometer measurements were used to estimate the reduction in chemiluminescence due to potential reaction of Ti stimuli with ROS species (in addition to photo-activation) (section 5.2.4) (Tengvall et al., 1988). For all conditions a log-linear reduction of light output was observed with increasing concentrations of Ti stimuli (Figure 5.7).

Figure 5.7 Log plots of light absorbance (RLU) in (a) luminol and (b) isoluminol containing Ti as oxide nanoparticles or micron sized metallic particles dispersed in PBS at concentrations of 2000, 200, 20 and 2 ppm following stimulation with 0.1% H_20_2

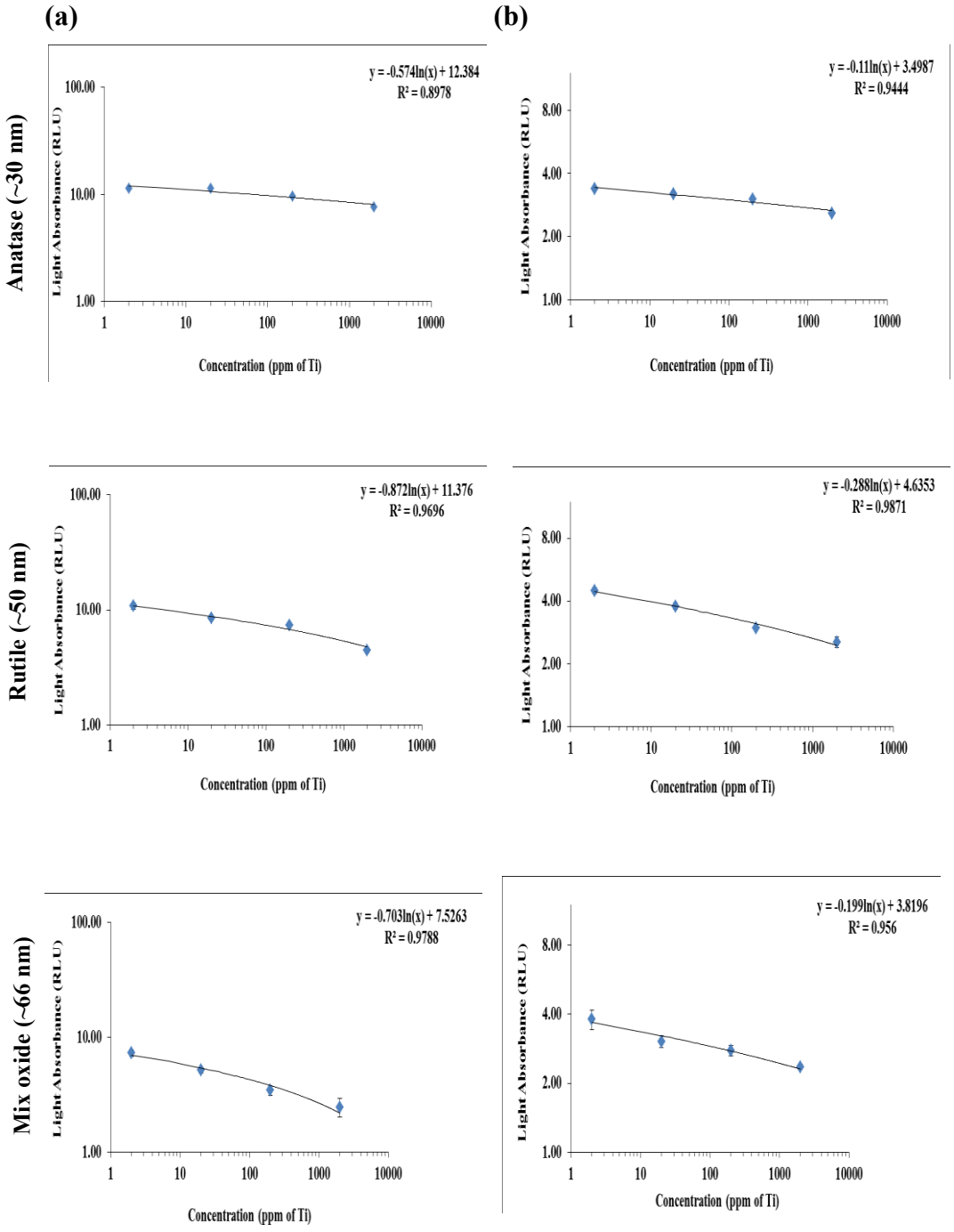

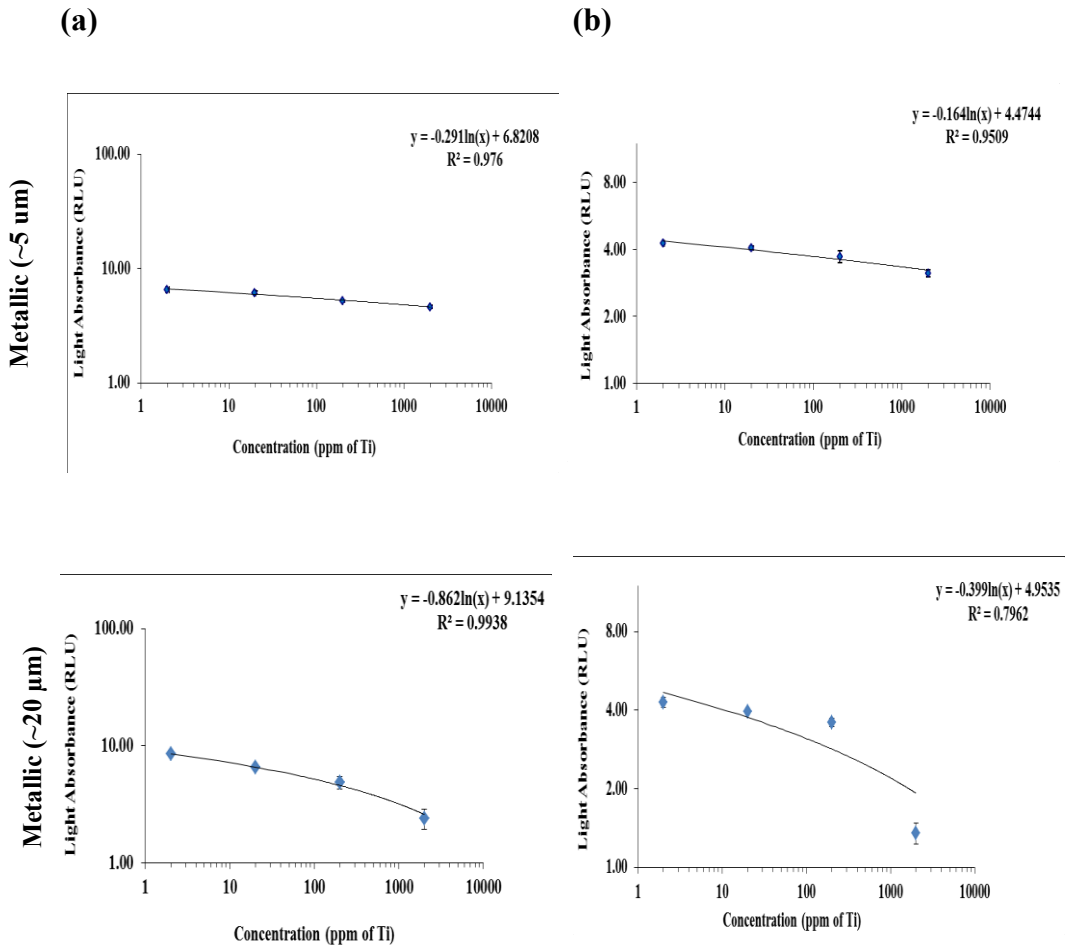

Inhibition of light output by Ti measured by the tube luminometer (Figure 5.7) is similar to the percentage attenuation of light signal calculated by the spectrometer (Tables 5.3 & 5.4). The magnitude of the detected light signal measured for luminol and isoluminol excitation was quenched to a greater extent by Ti as oxide nanoparticles in comparison with micron-sized metallic particles (Figure 5.7). The magnitude of the light output was reduced with increasing Ti concentrations in a log-linear relationship (Figure 5.7).

5.4.3 *Ex-vivo* chemiluminescence quantification of neutrophil ROS release

Chemiluminescence measurements of the respiratory burst of neutrophils at 2 hr post stimulation sourced from 10-20 different volunteers is presented in the form of Box/Whisker plots indicating median, inter-quartile range, 10^{th} and 90^{th} percentiles and outliers (Figures 5.8-5.11). The plots demonstrate the maximum RLU at 2 hrs against stimulus employed. Significant differences between groups are marked by asterisk(s) (Figures 5.8-5.11).

Stimulation of cells from 20 different volunteers with Ops *Sa* and *FN* (positive controls) resulted in significantly increased total and extracellular ROS production in comparison with PBS (negative control) stimulated cells ($P<0.005$ for each comparison) (Figure 5.8). Insignificant differences in total ROS release were observed between Ops *Sa* and *FN* stimulated cells ($P=0.333$). However, for extracellular ROS release a significantly higher magnitude of light output was measured for *FN* exposed neutrophils in comparison to Ops *Sa* ($P=0.003$) (Figure 5.8b).

Figure 5.8 Box/Whisker plots demonstrating (a) total (luminol dependent) and (b) extracellular (isoluminol dependent) ROS production following stimulation with Ops *Sa* and *FN* (positive controls) in comparison with PBS (negative control)

(a) **(b)**

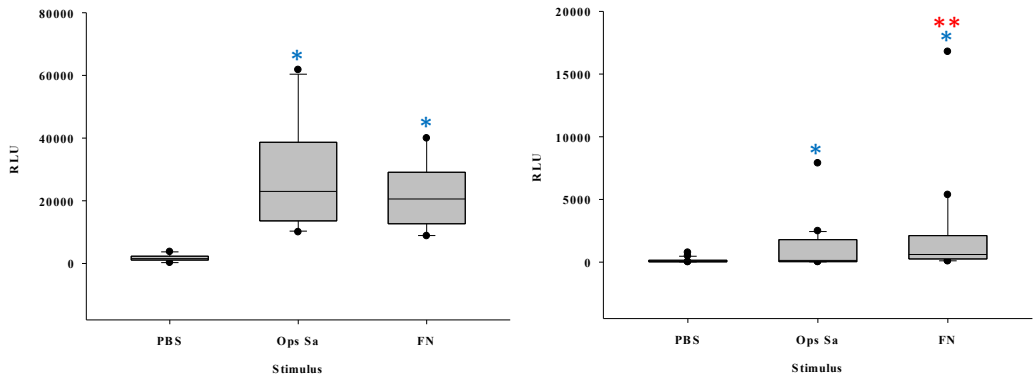

Significant different from PBS*
Significant different from Ops *Sa***

Significantly increased and dose-dependent total and extracellular ROS release resulted from neutrophil stimulation with the Ti implant derivatives employed at concentrations of 2000, 200, 20 and 2 ppm when compared with the PBS stimulated cells ($P<0.05$ for each comparison) (Figures 5.9 & 5.10). However, the exception to the above was for extracellular ROS production in response to stimulation with Ti oxide as anatase (~30 nm) at 2 ppm ($P=0.937$) (Figure 5.9). Data is representative of neutrophils sourced from 10-20 different volunteers.

Figure 5.9 Box/Whisker plots of (a) total (luminol dependent) and (b) extracellular (isoluminol dependent) ROS production following stimulation with nano sized Ti oxides as anatase (~30 nm), rutile (~50 nm) and mix oxide (~66 nm) dispersed in PBS of 2000, 200, 20 and 2 ppm

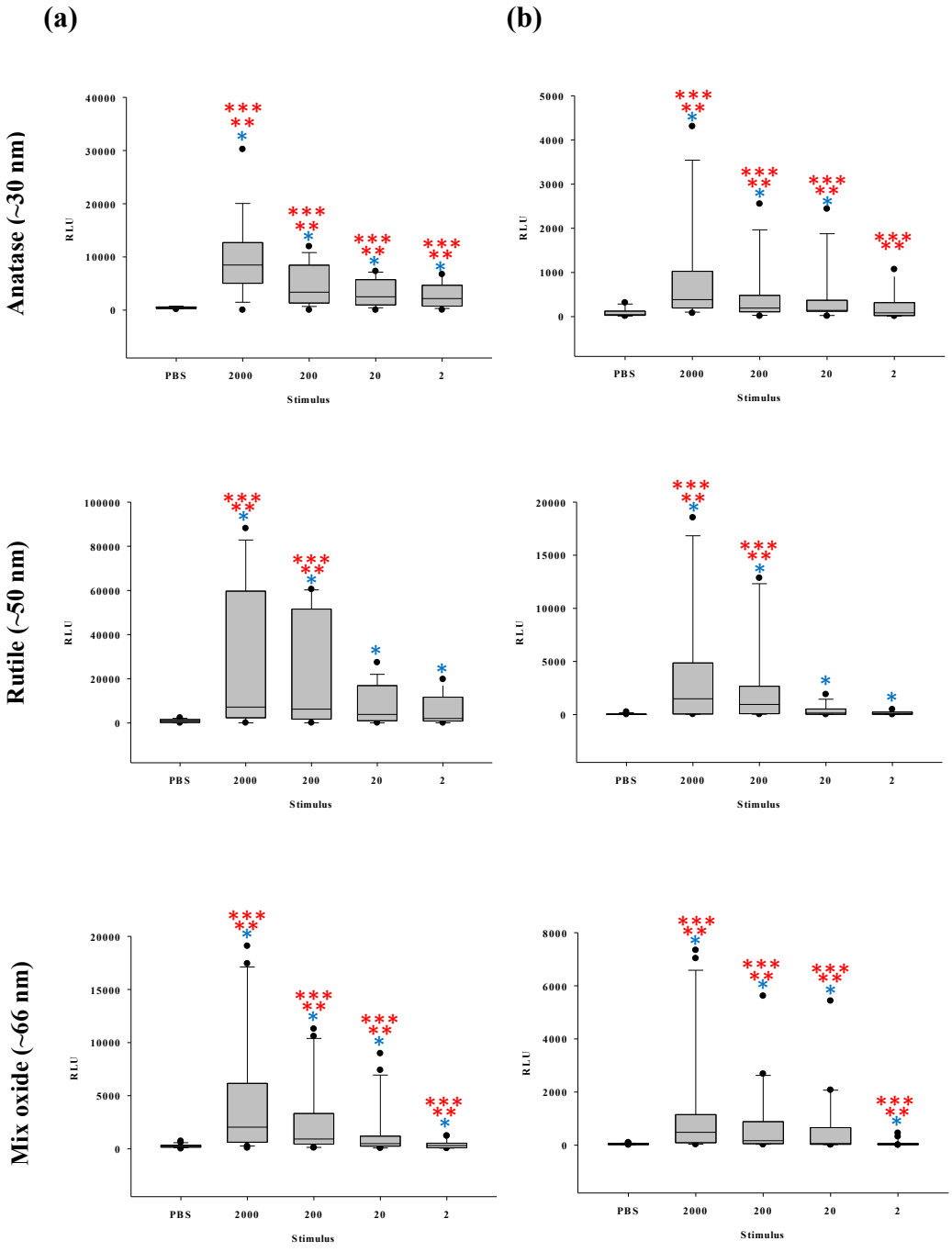

Significant different from PBS*
Significant different from Ops *Sa***
Significant different from *FN**

Stimulation of cells sourced from 15 different volunteers with Ti oxide as anatase (~30 nm) at all tested concentrations resulted in significantly lower total and extracellular ROS production when compared with Ops *Sa* ($P<0.002$) and *FN* ($P<0.001$) exposed cells (Figure 5.9). However, Ti oxide as rutile (~50 nm) at 2000 and 200 ppm resulted in significantly increased total and extracellular ROS production when compared with Ops *Sa* ($P<0.001$) and *FN* ($P<0.001$) stimulated cells (Figure 5.9). In common with anatase (~30 nm) stimulated neutrophils, responses to mix oxide (~66 nm) at all tested concentrations resulted in significantly decreased total and extracellular ROS release when compared with Ops *Sa* ($P<0.01$) and *FN* ($P<0.01$) stimulated cells (Figure 5.9).

Stimulation of cells sourced from 12 different volunteers with Ti as metallic species (~5 & ~20 µm) produced lower total and extracellular ROS production when compared with Ops *Sa* and *FN* exposed cells and no significant difference in ROS production was observed between the two metallic sized Ti species (P>0.333) (Figure 5.10). Ti as micron sized metallic species at tested concentrations of 2000 and 200 ppm showed significantly reduced total and extracellular ROS release when compared with Ti oxides as nanoparticles (P<0.008 for 2000 and 200 ppm tested concentrations).

Figure 5.10 Box/Whisker plots of (a) total (luminol dependent) and (b) extracellular (isoluminol dependent) ROS production following stimulation with metallic Ti as ~5 and ~20 µm sized dispersed in PBS at concentrations of 2000 and 200 ppm

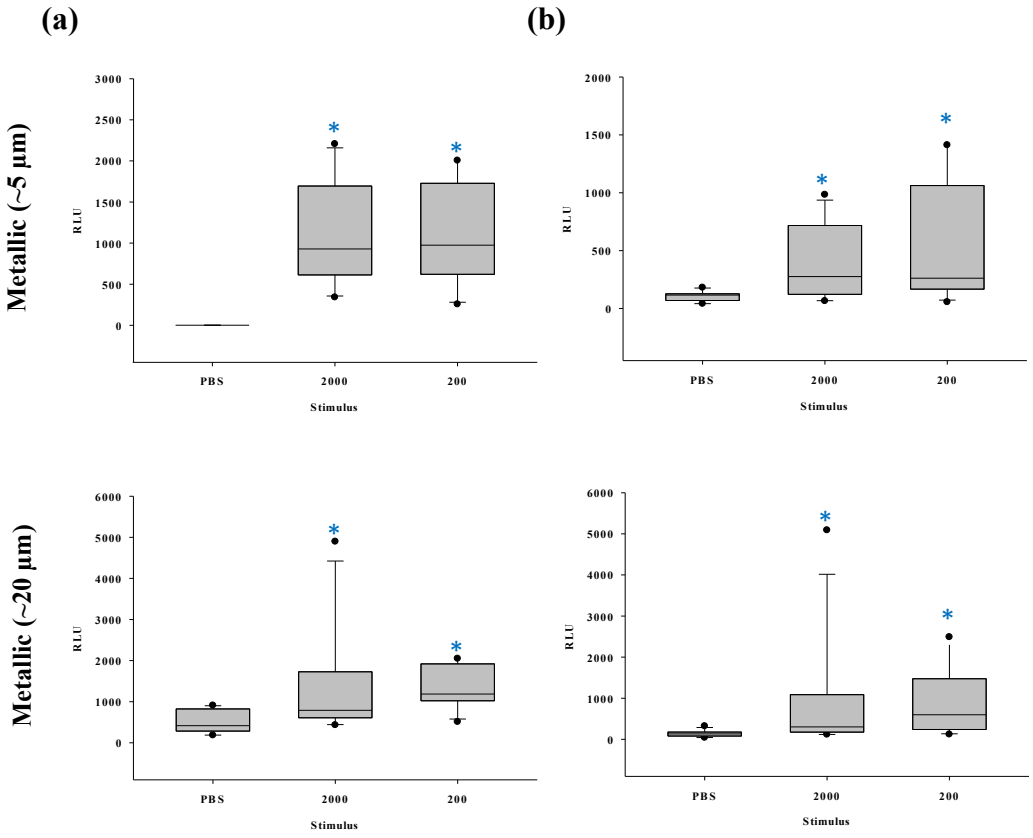

Stimulation of cells sourced from 10 different volunteers with Ti peroxy (size unknown) species revealed a significant increased dose dependent total ($P<0.008$) and extracellular ROS production ($P<0.003$) at all tested concentrations in comparison with PBS stimulated cells (Figure 5.11). The magnitude of total and extracellular ROS production was reduced in comparison with Ops *Sa* ($P<0.005$) and *FN* ($P<0.005$) stimulated cells (Figure 5.11) but similar to stimulation with Ti oxide species as rutile (~50 nm) ($P=0.285$) and anatase (~30 nm) ($P=0.372$) for all tested concentrations. Significantly increased ROS production resulted following stimulation with Ti peroxy (size unknown) species at all tested concentrations when compared with Ti as mixed oxide (~66 nm) ($P<0.005$) and metallic species (~5 & 20 µm) ($P<0.003$).

Figure 5.11 Box/Whisker plots of (a) total (luminol dependent) and (b) extracellular (isoluminol dependent) ROS production following stimulation with Ti peroxy species dispersed in PBS at concentrations of 2000, 200, 20 and 2 ppm

(a) **(b)**

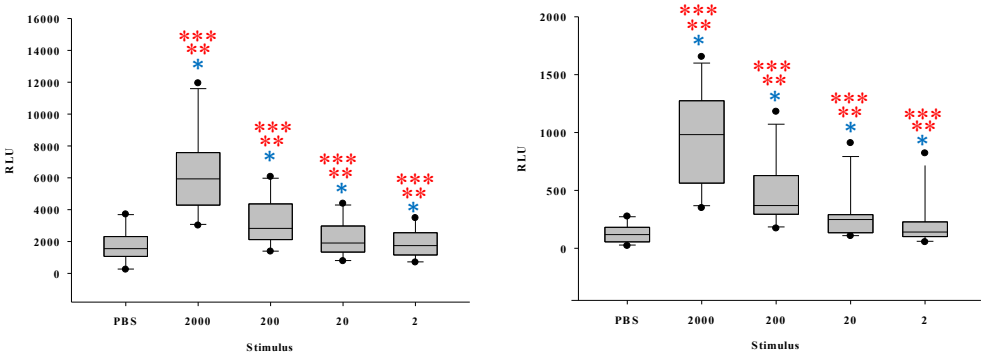

Significant different from PBS*
Significant different from Ops *Sa***
Significant different from *FN*****

5.4.4 Ti size and species specific magnitude of ROS production

Median values of light output from chemiluminescence assays of the neutrophil respiratory burst in response to Ti implant derivatives of varying particle size and species are displayed in Figure 5.12. The plots demonstrate total (luminol) (Figure 5.12; Left) and extracellular (isoluminol) (Figure 5.12; Right) chemiluminescence (RLU) against particle size (nm) respectively.

Total ROS production measured at all tested concentrations was significantly increased for Ti oxide as rutile speciation with ~50 nm a particle size in comparison with all other tested Ti species (Figure 5.12). Extracellular ROS production was also higher for Ti oxide as rutile (~50 nm) measured at 2000 and 200 ppm when compared with all other tested Ti species (Figure 5.12). However, stimulation with Ti oxides as anatase (~30 nm) and mixed oxide (~66 nm) species, similar magnitudes of total and extracellular ROS production was observed (Figure 5.12). Metallic species of ~5 μm and ~20 μm sizes resulted in the lowest magnitude of total and extracellular ROS production at tested concentrations of 2000 and 200 ppm (Figure 5.12).

Figure 5.12 Median plots presented on a log scale of (a) total (luminol) and (b) extracellular (isoluminol) ROS production expressed in RLU of Ti oxides as anatase (~30 nm), rutile (~50 nm) and mix oxide (~66 nm); and metallic species of ~5 µm and ~20 µm sized stimulated cells at concentrations of 2000, 200, 20 and 2 ppm compared to particle size in nanometers (nm)

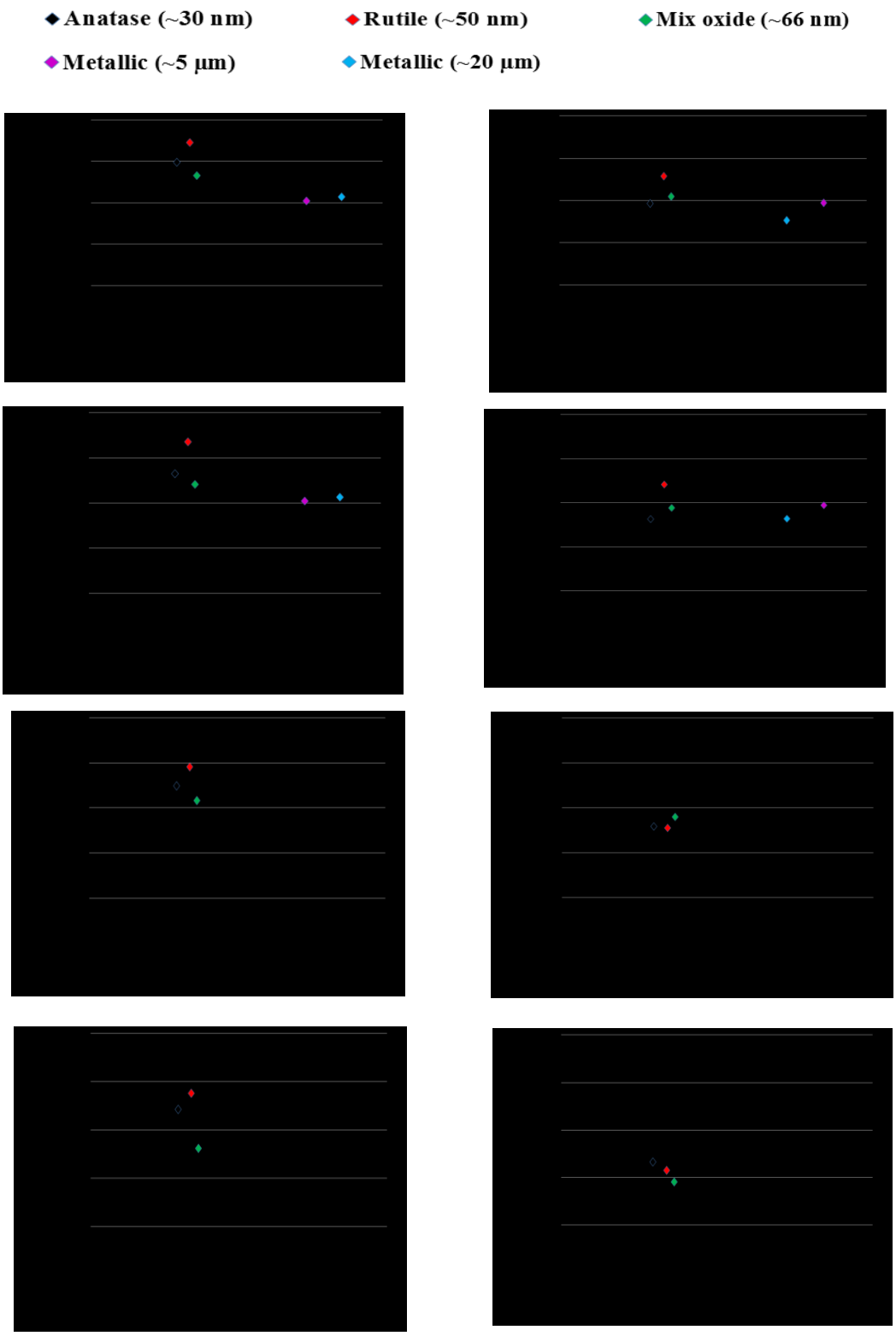

5.4.5 Kinetics of ROS production from stimulated neutrophils

The onset of the respiratory burst and the production of ROS over time were observed following stimulation with Ti oxide as nanoparticles and micron sized metallic particles (Figure 5.13). Stimulation of the respiratory burst with Ti oxide nanoparticles at a concentration of 2000 ppm was rapid with peak light emission observed almost immediately following stimulation (Figure 5.13). The maximum luminol/isoluminol chemiluminescence signal for Ti oxide nanoparticle stimulated neutrophils at a concentration of 2000 ppm was observed at ~2000 secs (stimuli added at 1800 secs) followed by a rapid decay in the signal at ~3000 secs (Figure 5.13). In contrast, the generation of ROS species for Ti oxide nanoparticles stimulated cells at concentrations of 200 and 20 ppm was slower with the maximum luminol/isoluminol light output observed from ~2500 secs onwards followed by a more gradual decay (Figure 5.13).

In comparison to the kinetics of the neutrophil respiratory burst by Ti oxide nanoparticles, the kinetics of ROS release following stimulation with Ti as metallic micron sized particles at a concentration of 2000 and 200 ppm was similar to Ops *Sa* and *FN* exposed cells (Figure 5.13). Although the magnitude of luminol/isoluminol chemiluminescence signal was decreased for metallic micron sized particles stimulated cells at a concentration of 2000 and 200 ppm, the onset time to peak in light output and decay in light signal followed the same pattern (Figure 5.13). A maximum onset of luminol/isoluminol chemiluminescence signal for metallic stimulated cells was observed at ~3000 secs followed by gradual decay in the signal until ~6000 secs (Figure 5.13).

Figure 5.13 Kinetics of ROS production of neutrophils following stimulation with Ti implant derivatives as oxide nanoparticles or micron sized metallic particles, Ops *Sa* and *FN*. Response is calibrated as chemiluminescence (RLU) vs. time (secs). Typical curves are displayed for each condition and scales are not common for graphs displayed

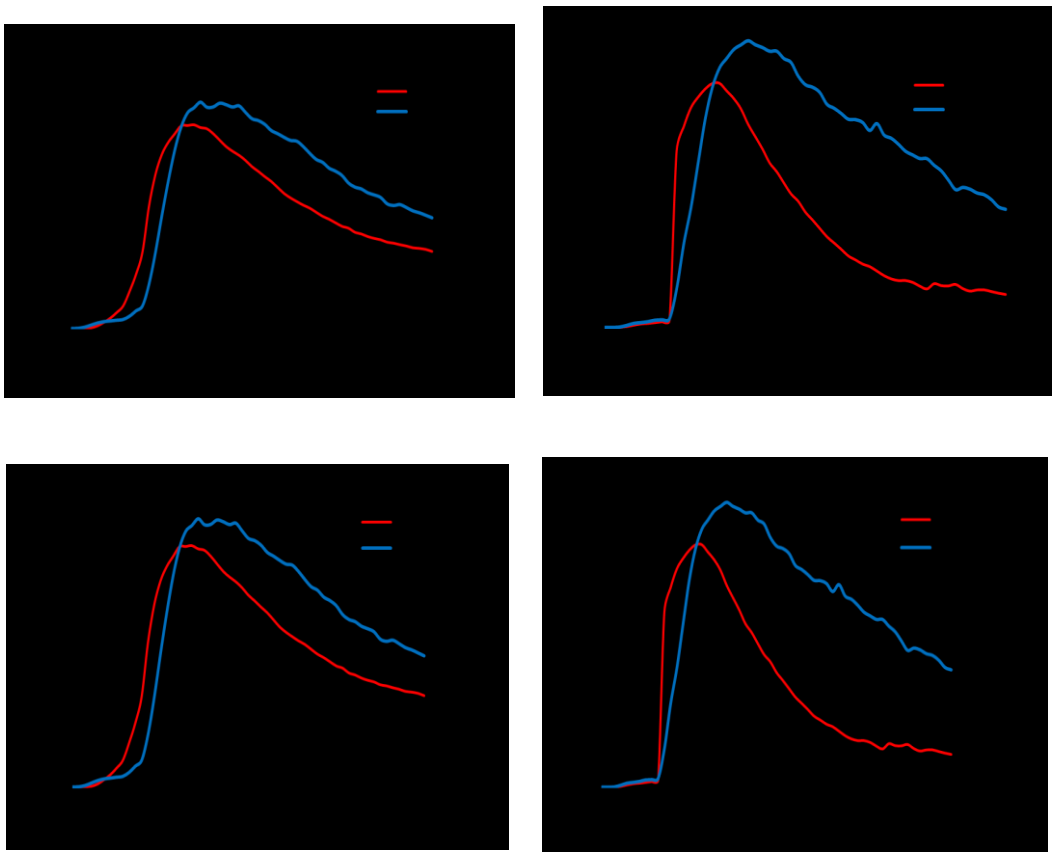

5.4.6 *Ex-vivo* phagocytosis of Ti implant derivatives by mammalian neutrophils

The phagocytosis of Ti oxide as anatase nanoparticles (≤45 nm) at a concentration of 2000 ppm by neutrophils was demonstrated using TEM (Figures 5.14-5.16). The TEM images acquired after 1 hour Ti exposure indicated cell surface interaction with particles (black and white features marked in Figure 5.14) and cellular uptake of Ti nanoparticles as agglomerates (Figure 5.14). Membrane bound uptake of Ti nanoparticles was also visualised within the neutrophil (Figure 5.14).

Figure 5.14 TEM image (JEOL 1200, Japan) acquired at 10,000 magnification of isolated neutrophil post 1 hr stimulation with Ti oxide as anatase (≤45 nm) dispersed in PBS at a concentration of 2000 ppm

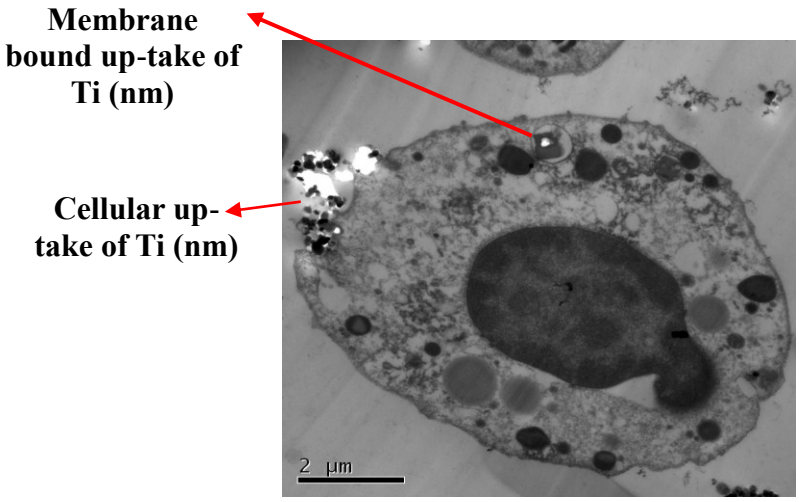

In addition, higher magnification images of Ti stimulated neutrophils revealed modifications of the cell membrane demonstrating the classical appearance of pseudopods (encircled in red) forming around agglomerations of Ti nanoparticles (Figure 5.15).

Figure 5.15 Enlarged TEM images (JEOL 1200, Japan) acquired at 10,000 magnification of isolated neutrophils post 1 hr stimulation with Ti oxide as anatase (≤45 nm) dispersed in PBS at a concentration of 2000 ppm

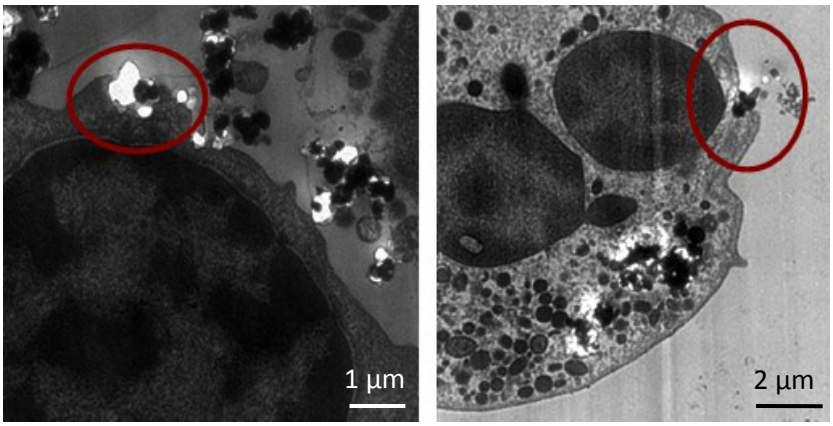

Agglomeration of Ti nanoparticles in the cytoplasm of the neutrophil was observed (Figures 5.16). The presence of Ti nanoparticles as aggregates within the neutrophil membranes was fluorescently confirmed by EDX (Figures 5.16).

Figure 5.16 TEM image (JEOL 2100, Japan) (Left) and EDX (Right) in fluorescence mode acquired at 10,000 magnification of an isolated neutrophil post 1 hr exposed to Ti oxide as anatase (≤45 nm) dispersed in PBS at 2000 ppm identifying distribution of Ti nanoparticles as aggregates on the neutrophil surface

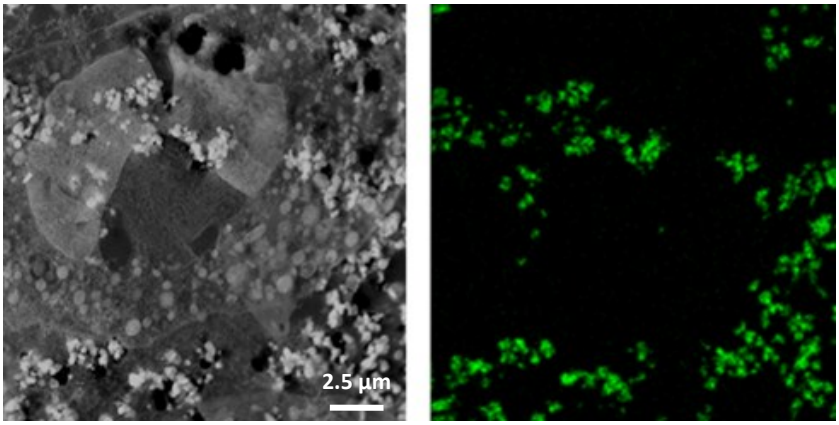

In contrast pre-exposure to the actin inhibitor cytoB (10 µg/mL) followed by stimulation with Ti oxide as anatase (≤45 nm) at a concentration of 2000 ppm dispersed in PBS revealed no presence of membrane bound and/or cellular uptake of Ti nanoparticles into the neutrophil (Figure 5.17).

Figure 5.17 TEM images of isolated neutrophils post 1 hr co-stimulation with Ti oxide as anatase (≤45 nm) dispersed in PBS at a concentration of 2000 ppm and phagocytosis inhibitor cyto B (10 µg/mL)

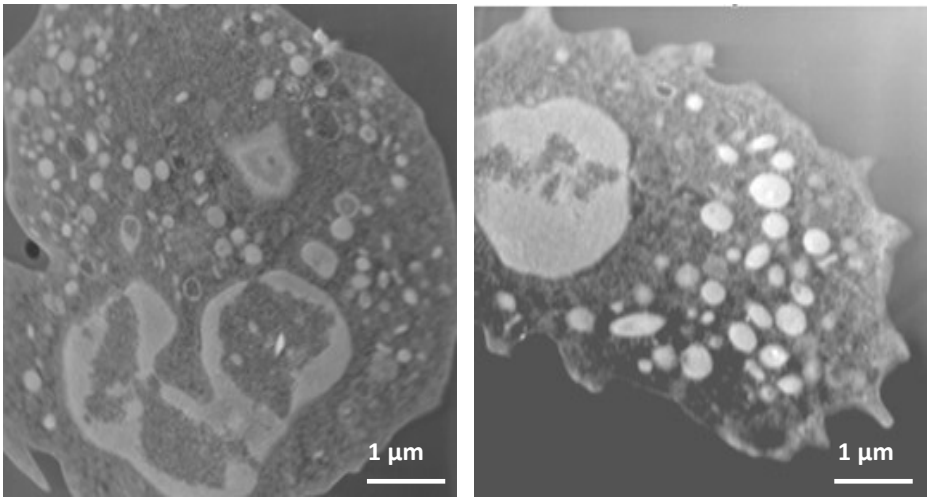

5.5 DISCUSSION

Neutrophils are sensitive immune cells but not responsive to all biochemical stimuli (Edwards, 1994). Measurement of ROS generation and consequent oxidative stress are considered to be strong indicators of a toxic effect of particles on such cells (Jin et al., 2011). Previous studies have demonstrated that Ti as fine metallic particles of up to 3 μm (Tamura et al., 2002) can stimulate oxidative burst reactions in healthy neutrophils (Kumazawa et al., 2002). In the current study, it was confirmed that Ti implant derivatives representative of those forms in tissues as oxide nanoparticles and micron sized metallic particles and Ti peroxy species, all stimulated neutrophil ROS release in a concentration dependent manner (Figures 5.9-5.11) and that the particle size and speciation (Figure 5.12) of the Ti stimuli were important parameters for determining the magnitude of the response. These *ex-vivo* observations demonstrate the capacity of Ti to modify inflammatory responses *in-vivo* as the Ti stimuli of varying concentrations and speciation employed were representative of the heterogeneity of the Ti debris observed in inflamed tissues surrounding percutaneous implants (Chapters 3 & 4).

Significant stimulation of total and extracellular ROS release was observed from all Ti challenged neutrophils at concentrations as low as 2 ppm (Figures 5.9-5.11). Large variations in the magnitude of ROS release were observed as a consequence of individual (neutrophil donor) responses which are likely to vary on a day to day basis. These enhanced responses (in magnitude of ROS production) suggest increased sensitivity of certain individuals; however this was not systemically evaluated. Moreover, ROS measurements were significantly underestimated due

to interactions of the Ti stimuli with the ROS themselves (Tengvall et al., 1988) or by photo-absorption of the chemiluminescence light signal (Kaida et al., 2004 & Zhang et al., 2004). This suggests a significantly increased potency of Ti as a ROS stimulator and that lower concentrations of Ti will also result in ROS generation.

Previous studies have documented that Ti particles can alter cell function and phenotype with differential effects regulated by particle size (Choi et al., 2005, Liu & Webster, 2006, Long et al., 2007 & Lovern & Klaper, 2006). In the current study, it was demonstrated that Ti as oxides including anatase (~30 nm), rutile (~50 nm) and mix oxide (~66 nm) species all stimulated increased levels of ROS release in comparison with metallic particles of ~5 μm and ~20 μm sizes (Figures 5.9 & 5.10). In addition, Ti peroxy complexes (unknown size) also resulted in increased ROS production when compared with metallic micron sized species (Figures 5.10 & 5.11). Ti peroxy species are of interest as they are a potential product of chemical reactions between TiO_2 and H_2O_2 (Tengvall et al., 1988), a ROS product of the neutrophil respiratory burst (Figure 5.1) (Hampton et al., 1998). These have been identified in tissues and their capacity to stimulate ROS production is important as it demonstrates a continuation of pro-inflammatory potential of Ti, following the initial interaction of TiO_2 with the neutrophil (section 5.2.4). The dependency of the observed magnitude of ROS release on Ti particle size may be a consequence of differences in particle interactions with cell membranes; the capacity for cell internalisation; and surface interactions with biomolecules (Kumazawa et al., 2002 & Tamura et al., 2002). Cellular effects

have been shown to be more pronounced when Ti particles are smaller than the cell (neutrophil cell size ranges from 5-10 μm) (Kumazawa et al., 2002) enabling cellular internalisation of the particles via pathways including pinocytosis, endocytosis and/or phagocytosis with the specific pathway being dependent upon particle size (Tamura et al., 2002, Long et al., 2007 & Pierre, 2010). In addition to cellular uptake, membrane interactions of nanoparticles are likely to be more significant when compared with micron sized particles due to the increased surface area for contact and the increased surface energy of the particles (Long et al., 2007 & Lundqvist, 1996). It is known that the surface area of particles is a major determinant of cellular toxicity (Jin et al., 2011). Ti oxides as nanoparticles have a larger surface area and different physicochemical properties including higher surface energies (Long et al., 2006) than micron sized particles. It is proposed that in the current study, cell activation by nanoparticles is likely to have occurred through different pathways when compared with the larger metallic species. This is supported by observations of a rapid onset of the respiratory burst in Ti nanoparticle stimulated neutrophils when compared with cells stimulated with the larger particles (Figure 5.13) in combination with the observed magnitude of ROS release.

Despite Ti oxides of similar nanoparticle sizes being employed, significant differences in total and extracellular ROS production were observed for rutile speciation (~50 nm) when compared with anatase (~30 nm) and mixed oxide (~66 nm) species (Figure 5.9). TEM imaging demonstrated similar aggregation of the nanoparticles in terms of their size however there was inevitable heterogeneity in

the aggregate morphology (Figure 5.6). It may be postulated that rutile *in-vivo* significantly contributes to increased extracellular damage as it is one of the predominant Ti implant derivatives observed within inflamed tissues (Chapter 4). However, further studies are required to determine whether this is indeed a biological effect of Ti-O bond co-ordination or simply a morphological sensitivity.

Exposure to Ti oxide as nanoparticles resulted in a more rapid activation of the respiratory burst by comparison with all other tested stimuli (Figure 5.13). Cellular internalisation with Ops *Sa* and *FN* is associated with Fc-γ and TLR-4 receptor mediated activation respectively, leading to activation of secondary messengers, Protein kinase C (PKC) and NADPH oxidase assembly, and ultimately ROS production following phagocytosis (Huizinga et al., 1989 & Kawai & Akira, 2009). Particulate debris has been shown to interact with cell surface receptors (Dobrovolskaia & McNeil, 2007); however these interactions are likely to be highly variable. Furthermore, nano sized particles have been shown to be both phagocytosed and/or endocytosed passing directly through the cell membrane (section 5.4.6). The consequence of receptor mediated uptake (Pierre, 2010) leading to accumulation within phagosomes of the neutrophil is consistent with the observed rapid and increased ROS production (Figure 5.13). However, at increased concentrations of Ti, the particles may induce phagosomal destabilisation (Hussain et al., 2010). Nanoparticles endocytosed have been shown to have a strong binding affinity for phosphorylated proteins (Larsson et al., 2003) which may also account for the rapid and excessive ROS release (Goncalves &

Girard, 2011). In contrast, the kinetics of the respiratory burst at 200 and 20 ppm for oxide nanoparticles was slower and did not reduce rapidly (Figure 5.13). This may suggest at higher concentrations the effects on cell viability may be responsible for the loss of the light signal rapidly within the assay. At lower concentrations cell viability is improved leading to more prolonged ROS release (Figure 5.13). As these conditions are more likely to be observed *in-vivo*, one notable manifestation would be excessive tissue damage via a prolonged extracellular ROS release (Bergamini et al., 2004).

In contrast, the kinetics of the neutrophil respiratory burst by micron sized metallic particle stimulated cells (Figure 5.13) was suggested to be independent of particulate uptake. It is likely that cells stimulated with micron sized particles may have attempted and re-attempted to perform phagocytosis but due to the size limitation the cells are often incapable in many cases due to complexity of the particle to be internalised. A negative effect of such cellular interactions has been reported as receptor clustering (Pierre, 2010) which may inhibit cell responses to critical stimuli in the extracellular environments.

There is limited data on the uptake of Ti nanoparticles as agglomerates and their distribution within the compartments of the neutrophil (Kumazawa et al., 2002). TEM images acquired within this study distinguished the distribution of Ti nanoparticles in single cells with a detection sensitivity and resolution well suited to explore subcellular interactions (section 5.4.6). The findings revealed neutrophils extending membrane derived pseudopods to phagocytize aggregated

particles of the Ti oxide anatase (≤45 nm) (Figure 5.15). Furthermore, the nanoparticles were observed to penetrate the plasma membrane (non-membrane bound) and be located in the cytosol including in the region of nuclear membranes (Figure 5.16). The underlying mechanism of Ti nanoparticle distribution within the neutrophil cell compartments may be as a result of binding to proteins within the cell, mediated by its electrostatic properties, thus becoming entrapped (Jovanovic et al., 2011). Co-stimulation of neutrophils with Ti oxide in the form of anatase (≤45 nm) and following exposure to cyto B (phagocytosis inhibitor) (Honeycutt & Niedel, 1986) resulted in no cellular uptake of any Ti particles (Figure 5.17). Cyto B is an actin inhibitor (Honeycutt & Niedel, 1986 & Hensen & Oades, 1973) and accordingly the lack of observed phagosomes containing Ti particles was not surprising, however no uptake of Ti was observed at all (Figure 5.17). The lack of endocytosis may be as a consequence of further effects of cytoB (beyond the actin cytoskeleton inhibition but was not definitively demonstrated in this study) (O'Flaherty et al., 1978).

5.6 CONCLUSION

The present findings suggest that Ti implant derivatives in the form of oxide nanoparticles and micron-sized metallic particles, and peroxy species can be potent inducers of the neutrophil respiratory burst. However, responses to Ti as oxide nanoparticles compared with micron sized metallic species suggest increased complexity of the cellular and subcellular interactions which have implications for the progression of the peri-implant inflammatory response.

CHAPTER 6

THE IMPACT OF TITANIUM IMPLANT DERIVATIVES EXPOSURE ON NEUTROPHIL EXTRACELLULAR TRAP (NET) RELEASE FROM HUMAN NEUTROPHILS

6.1 PREFACE

This chapter investigates the potential of 'Ti implant derivatives' accumulated within peri-implant tissues to stimulate the release of Neutrophil Extracellular Traps (NETs) which may influence resolution of peri-implant infection and/or the progression of peri-implant inflammation. A MNase assay was employed for *ex-vivo* fluorometric quantification of NET release from neutrophils challenged with nano and micron sized Ti species at concentrations of 2000 and 200 ppm and compared with control conditions. Fluorescence microscopy was used to visualise NET release and the morphology of NET structures from challenged neutrophils. Finally, the capacity for NET structures to adhere to Ti implant surfaces was studied in the presence and absence of a physiologically representative protein adsorbed layer.

6.2 INTRODUCTION

6.2.1 Neutrophil Extracellular Traps (NETs)

The first evidence describing the capacity of neutrophils to extrude web-like strands of processed chromatin fibres and granule protein complexes into the extracellular environment was reported in 2004 (Brinkmann et al., 2004). The structures were described as Neutrophil Extracellular Traps (NETs) and their formation represents a unique form of programmed cell death which is non-exclusively regulated by NADPH oxidase generation of Reactive Oxygen Species (ROS) (Palmer et al., 2012). The entire process of NET formation has been termed as NETosis (Fuchs et al., 2007).

The point at which NETs are released by the neutrophil is important as it ends the capacity of the cell to perform vital functions such as phagocytosis (Fuchs et al., 2007) and the recruitment of immune cells (Bartneck et al., 2010). The sequence of events involved in NET release begins with the generation of ROS via receptor ligand interactions or activation of the NADPH oxidase complex via mitochondrial ROS generation (Fuchs et al., 2007). Subsequently, long strands of DNA migrate from the nucleus to the cytoplasm and mix with granular and some selected cytoplasmic proteins before being actively released through the plasma membrane into the extracellular space (Brinkmann et al., 2004 & Fuchs et al., 2007). Following the release of NET structures, the plasma membrane ruptures completely (Brinkmann et al., 2004) and the cell dies (Brinkmann & Zychlinsky, 2012).

6.2.2 NET morphology

The composition of NETs has been characterised using a variety of methods including mass spectrometry (MS) (Saffarzadeh et al., 2012), proteomics (Knight, 2012) and immunofluorescence (Bergamo, 2012). DNA has been identified as the major structural component and forms complexes with proteins derived from all three neutrophil granule types (Brinkmann & Zychlinsky, 2012). To date, proteins including neutrophil elastase (NE), cathepsin G and myeloperoxidase (MPO) (derived from azurophil granules); lactoferrin (secondary granules) and gelatinase (tertiary granules) have been associated with NETs (Papayannopoulos et al., 2010 & Hakkim et al., 2011). In contrast, certain proteins such as CD63, actin and tubulin have been shown to be excluded (Hakkim et al., 2011). Visualisation of NETs using scanning electron microscopy (SEM) has identified that the DNA based structures have an average diameter of 15-17 nm with globular protein domains of approximately 25 nm (Brinkmann & Zychlinsky, 2012). However, these can also aggregate into larger threads with a diameter of ~50 nm (Brinkmann & Zychlinsky, 2012) forming netted structures of hundreds of nm in length and width (Clark et al., 2007).

6.2.3 The function of NETs

The exact function of NETs is still not fully understood, however, NETs have been described as contributing to both anti-inflammatory (Clark et al., 2007, Kessenbrock et al., 2009, Papayannopoulos & Zychlinsky, 2010 & Hakkim et al., 2010) and pro-inflammatory processes (Brinkmann et al., 2004 & Gupta et al.,

2005). The physiological or pathological impact of NETs is proposed to be dependent upon the magnitude of release and the specific NET composition which may consist of high or low concentrations of granular proteins (Urban et al., 2009).

6.2.3.1 Anti-infectious role of NETs

The contribution of NETs to the host defence system has been identified in a number of pathological conditions including necrotizing fasciitis (Buchananan et al., 2006) and pneumonia (Beiter et al., 2006). Neutrophils have been shown to release NETs with antimicrobial functionality into the extracellular environment and form 'traps' that serve as a physical barrier for microorganisms (Remijsen et al., 2011 & Riyapa et al., 2012); preventing their spread and limiting the extent of damage to healthy tissues (Esmon et al., 2011). Trapping microbes prevents their dissemination and inactivates virulence factors (Hampton et al., 2008). So far NETs have been demonstrated to trap bacteria, pathogenic parasites, fungi and yeasts (Brinkmann and Zychlinsky, 2012). The ability of NETs to kill microbes is hypothesised to be due to the local effects of NET associated proteins which exert antimicrobial activity localised in proximity to the pathogen even at low concentrations (Riyapa et al., 2012). These include enzymes (lysozyme & proteases), antimicrobial peptides (defensins), ion chelators (calgranulin) and histones (Brinkmann et al., 2004). These components which are present on NETs may be present in combination or in isolation (Bergamo et al., 2012 & Riyapa et al., 2012). Increased concentrations of these components found on NETs are associated with increased antimicrobial activity (Bergamo et al., 2012).

6.2.3.2 Pro-inflammatory role of NETs

In contrast, NET release has also been shown or proposed to exacerbate pathological conditions such as periodontitis (Delbosc et al., 2011), streptococcal infections (Molloy, 2006), appendicitis (Fuchs et al., 2007), shigellosis (Brinkmann et al., 2004), cystic fibrosis (CF), ischemia (Brinkmann et al., 2012), pre-eclampsia (Gupta et al., 2005) autoimmune and thrombotic disorders (Farquharson et al., 2011) and contribute to the overall inflammatory *milieu* (Remijsen et al., 2011). It has been proposed that the formation of NETs can prolong inflammation by concentrating antimicrobial proteins (AMPs) (Brinkmann et al., 2012) and serine proteases such as elastase and cathepsin G within tissues and therefore increase the risk of tissue damage (Forsyth et al., 1994). The DNA component of NETs in the extracellular matrix has also been suggested to be immunogenic (Lande et al., 2007) and investigators have shown initiation and maturation of antigen presenting cells (APCs) such as bone marrow and dendritic cells (DCs) by up-regulating the expression of MHC-II, CD40 and CD54 (Ishii et al., 2001). In addition, extracellular DNA elicits TLR-9 signalling in DCs (Garcia-Romo et al., 2011) and monocytes (Tillack et al., 2012) which stimulate the production of interferons (IFNs), thus exacerbating adaptive and autoimmune responses (Brinkman et al., 2012). This has been proposed as a driver of a type-1 IFN gene expression signature in blood neutrophils from periodontitis patients (Wright et al., 2008).

The pro-inflammatory activity of NETs has been observed in the mucolytic therapy for CF patients (Manzenreiter et al., 2012) who were treated with

recombinant DNases to disintegrate NETs (Segal et al., 2005) with the aim of liquefying sputum, reducing its viscosity and facilitating mucus clearance (Buchanan et al., 2006). However, this therapeutic approach proved to be problematic as disintegrated NETs released neutrophil elastase which further processed core histones contributing to tissue damage (Buchanan et al., 2006 & Papayannopoulos et al., 2011). Notably studies currently document that histones induce a number of pathological effects including collateral damage via toll-like receptors (TLR-2/4) (Gupta et al., 2010), kill endothelial cells (Saffarzadeh et al., 2012) and are implicated in the pathogenesis of sepsis (Xu et al., 2009) and systemic lupus erythematosus (SLE) (Garcia-Romo et al., 2011) .

6.2.4 Inducers of NET release

Several inducers of NET release have been identified including bacteria (Fuchs et al., 2007), parasites (Guimaraes-Costa et al., 2009), fungi (Brinkmann et al., 2012), yeast (Urban et al., 2006b), cytokines (Brinkmann et al., 2004), antibody-antigen complexes (Garcia-Romo et al., 2011 & Lande et al., 2011), microbial components such as lipophosphoglycans (Oehmcke et al., 2009) and bacterial endotoxins (Brinkmann et al., 2004). Interestingly, antibodies in concentrated/aggregated forms e.g. IgG coated beads are also capable of inducing NETs, however IgG in free solution does not (Fuchs et al., 2007 & Kessenbrock et al., 2009).

The most dominant NET triggers reported are ROS including hydrogen peroxide (H_2O_2) (Fuchs et al., 2007) and hypochlorous acid (HOCl) (Palmer et al., 2012).

In-vitro studies have also identified phorbol myristate acetate (PMA) (Guimaraes-Costa et al., 2009) and lipopolysaccharide (LPS) (Neeli et al., 2009 & Lim et al., 2011) to be enhancers of NET release. It is clear that, NET release is variable according to the nature of the stimulus employed and the processes involved in NETosis involve multiple pathways (Fuchs et al., 2007). A whole live bacterium has been shown to induce NETs more efficiently than a single TLR-4 activator such as LPS (component of outer membrane of gram negative bacteria) alone (Clark et al., 2007 & Fuchs et al., 2007).

6.2.5 Mechanism(s) of NET release

Neutrophils are short lived (2-4 days) and therefore current knowledge regarding the molecular mechanism(s) by which NETs are produced is limited. One of the first reports describing the process of NETosis was identified by employing PMA as a stimulus. In this early report, PMA was identified to cause rapid NET release (Takei et al., 2006). PMA is lipophilic and therefore able to cross the cell membrane quickly bypassing any cell surface receptor interactions (Seligmann et al., 1980). PMA in neutrophils is a potent activator of the NADPH oxidase (Teufelhofer et al., 2003) and evokes NET release in a relatively prolonged activation of protein kinase C (PKC) by replacing the role of the physiological activator diacylglycerol (DAG) (Newton, 1995 & Ermert et al., 2009). In addition, subsequent *in-vitro* studies also recognised that PMA enhanced NET release by 53% in neutrophils in response to the parasite *L. amazonensis* (Guimaraes-Costa et al., 2009) and also up-regulated responses to *y*east *Candida albicans* (Urban et al., 2006b) and to *Aspergillus nidulans* (Bianchi et al., 2009). Findings from the

three studies propose that activation upstream of NADPH oxidase complex (also known as phagocytic oxidase PHOX/NOX2) and downstream of PKC culminates in a NET release cascade involving the Raf-MEK-ERK kinase pathway (Hakim et al., 2011) and Rac2 (Neeli et al., 2009 & Lim et al., 2011).

In chapter 5 the traditional role of the NADPH oxidase was described in the context of production of ROS species to eliminate pathogens (Sequchi & Kobayashi, 2002). However, the oxidase also displays a number of less well known roles in neutrophil physiology such as regulation of NET release (Amulic et al., 2012). Evidence for this has been observed in chronic granulomatous disease (CGD) patients whose NADPH oxidase enzyme complex is compromised (Bakri et al., 2009) and therefore fails to elicit NET release when neutrophils are stimulated with potent inducers such as PMA or bacteria (Dinauer 2005, Brinkmann & Zychlinsky, 2012 & Palmer et al., 2012). However, interestingly when the CGD neutrophils were treated with H_2O_2, a product of dismutation of O_2^- during ROS release (section 5.2.2), the cells resulted in NET release (Bergamo, 2012). The same was observed for HOCl treated CGD neutrophils (Palmer et al., 2012), HOCl derived from MPO. These findings indicate that exogenous H_2O_2 targets the same molecule as endogenously produced H_2O_2 suggesting that overall NET release is regulated by the downstream signaling of NADPH oxidase at the HOCl level, even though the NADPH oxidase complex itself is not functional (Fuchs et al., 2007). Further evidence that ROS and specifically H_2O_2 regulate NET formation has been reported (Fuchs et al., 2007). When neutrophils were exposed to low concentrations of diphenyl- eneiodonium

(DPI) (oxidase inhibitor) and catalase (degrades H_2O_2 to molecular O_2 and water during ROS formation), ROS and NET release were inhibited in response to potent PHOX inducers namely PMA and *S. aureus* (Fuchs et al., 2007). Conversely upon employing the catalase inhibitor, 3-amino-1,2,4 triazole (3-AT), both ROS and NET release were evoked (Fuchs et al., 2007). However, the precise mechanism(s) underpinning both processes is yet unclear. Furthermore, conflicting to the above report, it was recently demonstrated that NET release was decreased following 3-AT stimulation (Palmer et al., 2012). Thus it may be concluded that ROS species formation (section 5.2.2) contributes to microbe killing via two strategies (a) intra-phagosomal killing in live neutrophils and/or (b) act as secondary messengers for stimulating NET mediated killing post NETosis (Amulic et al., 2012). It is also now known that NET formation is not solely dependant on ROS production but specifically HOCl which can directly stimulate NET release (Palmer et al., 2012).

The overall process of NET formation is incomplete without chromatin de-condensation and the association of AMPs (Papayannopoulos et al., 2010 & Remijsen et al., 2011). Studies have generalized that MPO and neutrophil elastase found on NETs and stored in the azurophilic granules regulate the process (Papayannopoulos et al., 2010). It is proposed that upon NADPH oxidase activation, both MPO and NE are released through an unknown mechanism (Papayanopoulos et al., 2010) and that MPO independent of its enzymatic activity acts synergistically with NE causing degradation of the linker histones H1 (Papayannopoulos et al., 2010). In addition to the above proposed model,

experimental evidence has confirmed that both NE and MPO are required for chromatin de-condensation (Papayannopoulos et al., 2010 & Parker et al., 2012). For example, NE deficient mice fail to secrete NETs (Papayannopoulos et al., 2010). The role of MPO which yields HOCl during ROS formation was investigated by employing HOCl as a stimulus to CGD neutrophils (Palmer et al., 2012). Studies revealed that when HOCl is directly added to CGD neutrophils, NET release was stimulated (Palmer et al., 2012). This observation confirms that ROS are essential for NET formation and further substantiates the involvement of MPO and MPO derived HOCl displays a regulatory role in NET release (Palmer et al., 2012). In addition, Palmer et al., (2012) employed the specific MPO inhibitor 4-aminobenzoic acid hydrazide (4-ABAH) which resulted in inhibition of NETs confirming data from Papayannopoulos et al., (2010). The current evidence supports the fact that superoxides, ROS and the by-products of the respiratory burst such as MPO contribute to the activation of NETosis and overall the process may be NADPH oxidase dependent (Fuchs et al., 2007) or independent (Pilsczek et al., 2010).

6.2.6 NETosis distinct to apoptosis and necrosis

NETosis is distinct to cellular apoptosis (Fadeel, 2009) and necrosis (Fuchs et al., 2007). Preliminary evidence reports that NETs may form in as little as 10 minutes after cell stimulation, a process more rapid than apoptosis (Brinkmann et al., 2004). During NET formation, the neutrophils flatten, remaining motile and phagocytic (Brinkmann et al 2004). Their nuclei lose their characteristic lobular morphology and fill the majority of the intracellular cytoplasmic space (Fuchs et

al., 2007). Concomitantly, the chromatin begins to decondense so the distinction between eu- and hetero-chromatin is lost (Brinkmann et al., 2004). Lastly, both the nuclear and granular components homogenise and form web-like structures called NETs which are ejected into the extracellular environment (Fuchs et al., 2007). This indicates that NETs are formed by a controlled extrusion, rather than by the random spilling of granule and nuclear contents into the extracellular space (Fuchs et al., 2007).

In contrast, during cell necrosis the nuclear membrane remains intact; there is no loss of differentiation between eu- and hetero-chromatin and extracellular DNA release does not occur (Fuchs et al., 2007). Similarly, during apoptosis there is no DNA fragmentation; chromatin is strongly exhibited and is separated into several membrane bound apoptotic bodies and no cell contents are released into the extracellular space (Fuchs et al., 2007). Apart from the morphological distinctions mentioned above, both NETosis and apoptosis are highly regulated processes but apoptosis requires proteases known as caspases which are regarded as 'executioners of apoptosis' (Chang & Yang, 2000). In contrast, NETosis process is currently understood to be independent of such compounds (Fuchs et al., 2007).

6.2.7 NETs detection and quantification

A number of methods have been adopted to visualise and quantify NET release (Grinberg et al., 2008). To date, microscopy (Brinkmann et al., 2004, Hakkim et al., 2010, Papayannopoulos et al., 2010 & Metzler et al., 2011), immuno-staining (Oklu et al., 2013) and SEM (Brinkmann et al., 2004, Krautgartner & Vitkov,

2008 & 2009, Urban et al., 2009 & Manzenreiter et al., 2012) have been employed to visualise NET release and NET structures. Previously antibodies to detect histone and/or granule components were utilised to detect NET release (Fuchs et al., 2007). However, more sensitive immuno-fluorescence visualisation techniques involving SYTOX® Green (Martinelli et al., 2004) have been developed (Grinberg et al., 2008). SYTOX® Green is a DNA intercalating dye which fluoresces upon binding to DNA (Grinberg et al., 2008). The application of SYTOX® Green previously has been claimed to possibly inhibit NET formation (Brinkmann et al., 2004). However as demonstrated by its application in subsequent publications, this was not the case (Ermert et al., 2009) and it now is regarded as the 'gold standard' to determine NET release (Grinberg et al., 2008).

NET release may also be quantified fluorometrically which is helpful in order to make comparisons regarding the potency of stimuli (Meijer, 2012). Initial studies involving quantification of NET release were based on images. These included counting the number of discrete areas of DNA larger in size than a neutrophil (Buchanan et al., 2006) or the number of neutrophil forming NETs as a percentage of total cell count (Grinberg et al., 2008). Such attempts however were ruled out over time as these techniques were highly biased and unreliable when individual cells could not be distinguished. Another limitation of quantifying NET release this way was that capturing images was dependent on the entire field being visualised (Buchanan et al., 2006 & Grinberg et al., 2008). Subsequent studies, successfully developed a robust fluorometric method for quantification of extracellular NET-DNA release using SYTOX® Green dye to stain the

extracellular NET-DNA (Alghamdi et al., 2005 & Ermert et al., 2009). However, this method also presented some limitations in the fluorometric measurement of extracellular NET-DNA release. The complicating factor involved was the staining of intracellular DNA of dead cells (von Köckritz-Blickwede, 2008). This was resolved by the introduction of the MNase assay which is now deemed the most appropriate method for the fluorometric quantification of extracellular NET-DNA release (Fuchs et al., 2007, Ramos-Kichik et al., 2009 & Wang et al., 2009).

Initially, before considering MNase, mammalian DNase was employed but later studies demonstrated its capacity to bind to actin causing depolymerisation and preventing polymerisation which interferes with the NET release mechanism (Hitchcock, 1980). As a consequence MNase has been demonstrated to be suitable for the digestion of extracellular genomic DNA as it is a DNase secreted by *S. aureus* (Buchanan et al., 2006) which acts as an endo- and exo-nuclease to yield 3'mono- or di-nucleotides (Heins et al., 1967). It is relatively non-specific in terms of base sequence preference, although preferentially cleaves chromatin at the linker region between nucleosomes (Noll, 1974). Another key methodological finding has been that following prolonged incubation times such as >4 hrs for human neutrophils stimulated with microbes, toxins or drugs the DNA release may be caused by other mechanisms in addition to NETosis (Brinkmann & Zychlinsky, 2012). Therefore, studies quantifying NET release are reported to be conducted within the 4 hr incubation time to avoid false NET-DNA experimental readouts (Brinkmann & Zychlinsky, 2012).

Chapter 5 demonstrated that Ti nano and micron sized particles can be phagocytosed by the human neutrophil and induce dose-dependent ROS release (through oxidative burst reactions) (Kumazawa et al., 2002 & Goncalves et al., 2011). NET release is closely related to the process of respiratory burst and ROS production appears to be a crucial process involved in inducing NET release (Fuchs et al., 2007 & Papayannopoulos & Zychlinsky, 2009). Therefore, the effect of Ti stimulation of neutrophils on NET production is relevant to the overall understanding of the inflammatory response.

6.3 METHODS

6.3.1 *Ex-vivo* determination of NET production

The fluorescent DNA stain, SYTOX® Green was supplied at a concentration of 5 mM in DMSO (S7020; Invitrogen, Paisley, UK) and has a fluorescence excitation/emission maxima of 504/523 nm respectively. SYTOX® Green is a high affinity DNA staining dye and used to visualise NETs and to allow fluorometric quantification of the magnitude of extracellular NET-DNA release from stimulated neutrophils. 1 µL of the stock was further diluted in 999 µL of PBS (Appendix I) for it to be used at 10 µM and stored at -20 °C until further use.

6.3.2 Stimuli used to induce NET production in neutrophils

The control (Table 6.1) and experimental stimuli (Table 2.1; section 2.2) were prepared by adding high purity reagents to RPMI-1640. Table 6.1 demonstrates the working concentration of the prepared solution and stimulation concentration once added to the experimental system.

Table 6.1 Stimuli used to induce NET formation

Stimuli (Acronym)	Supplier Cat No.	Working Concentration	Stimulation Concentration
RPMI-1640 supplemented with glutamine (RPMI)	Sigma-Aldrich R2405	-	-
Hypochlorous acid (HOCl)	Sigma-Aldrich 425044	1%	0.57%
Phorbol 12-myristate 13-acetate (PMA)	Sigma-Aldrich P8139	405 nM in RPMI-1640	50 nM
Ops S. Aureus (Ops Sa) (non-viable)	LGC Standards ATCC 9144	$6x10^8$/mL RPMI-1640	MOI[1] 1:300
F. Nucleatum (FN) (non-viable)	LGC Standards ATCC 10953	$6x10^8$/mL RPMI-1640	MOI[1] 1:100

[1]MOI Multiplicity of Infection (number of bacteria per neutrophil).

6.3.3 Visualisation of NET release

Neutrophils were extracted (Appendix I) and re-suspended at a concentration of $1x10^5$ cells/mL in RPMI-1640 media supplemented with 1 U/mL of glutamine (Sigma-Aldrich, UK). 300 µL of the cell suspension were added to each well of a transparent 24-well sterile plate (CLS3527; Corning Costar, Dorset, UK) which had been pre-blocked with 500 µL of 1% PBS-BSA per well and stored overnight at 4 °C. The blocking buffer was removed by pipetting prior to cell addition. Cells were incubated for 30 mins at 30 °C and subsequently stimulated with 75 µL of the stimuli summarized in Table 6.1 and Table 2.1 (section 2.2). Overall, two replicates for each stimulus were conducted and the entire experiment was repeated four times.

6.3.4 Image capturing and processing

NET formation was visualised using an epi-fluorescence microscope (Nikon Eclipse TE300, Japan) with a 472 nm fluorescent excitation filter and a 520 nm emission filter (BrightLine® GFP-3035B, Semrock). 25 µL of 10 µM SYTOX® Green in PBS (S7020; Invitrogen, Paisley, UK) was added to the suspended cells and images were acquired at 0, 1, 2, 3 and 4 hrs following stimulation, using a digital camera (Nikon Coolpix 990, Japan) with a x20 microscope objective lens.

6.3.5 Sensitivity of fluorometric quantification of DNA

NET derived nuclear DNA complexes with different protein components which exhibit variability in dye binding and subsequent fluorescence (Saffarzadeh et al., 2012). In addition, previous work quantifying NETs by fluorescence techniques have been reported using white micro-well plates or black micro-well plates (Bruns et al., 2010), which introduces further variability to the measured fluorescence. Therefore, the sensitivity range for fluorescence detection of extracellular NET-DNA release following SYTOX staining was investigated in both black (3915; Corning, Lowell, MA, USA) and white micro-well plates (Immunolon2, Chantilly, VA, USA) by calibrating the assay with known concentrations of calf thymus DNA. The calf thymus DNA (S89370; Sigma-Aldrich, UK) stock solution was prepared at 1 mg/mL using molecular biology grade water and thorough vortexing prior to storage at -20 °C. To calibrate the measurement of fluorescence, the stock of calf thymus DNA was diluted further to produce concentrations ranging from 0 to 1 µg/mL. 10 µL of the known

concentrations of calf thymus DNA with an additional 175 µL of RPMI-1640 media supplemented with 1 U/mL of glutamine (Sigma-Aldrich, UK) were stained with 15 µL of 10 µM SYTOX® Green (S7020; Invitrogen, Paisley, UK) in black and white micro-well plates for 10 mins at room temperature allowing the DNA to bind. Each DNA standard was performed in triplicate and calibrated three times. Readings were obtained in arbitrary fluorescence units (AFU) using a fluorometer (Twinkle LB970, Berthold Technologies, Germany) with excitation and emission filter wavelengths of 485 and 525 nm, respectively.

6.3.6 Micrococcal nuclease (MNase) assay of NET release

Further neutrophils were prepared (Appendix I) and re-suspended at a concentration of $1x10^5$ cells/mL. 100 µL of the cell suspension, with an additional 75 µL of RPMI-1640 supplemented with 1 U/mL of glutamine (Sigma-Aldrich, UK), was added to each well of a sterile 96-well white plate (Immunolon2, Dynex, Chantilly, VA, USA) which had been pre-blocked with 200 µL of 1% PBS-BSA per well and stored overnight at 4 °C. The blocking buffer was removed prior to cell addition. Cells were incubated at 30 °C for 30 mins and then stimulated with 25 µL of the control or experimental stimuli (Table 6.1 & Table 2.1; section 2.2). All stimuli were run in quadruplicate and cells were incubated for an additional 3 hrs at 30 °C. Following incubation, to separate extruded NET-DNA from the cellular debris, 15 µL of MNase (LS004797; Worthington Biochemical Corporation, Lakewood, NJ, USA) was added to each well and left at room temperature for 20 mins. The plate contents were then centrifuged at 1800 rcf for 10 mins and 150 µL of the supernatant containing the separated

extracellular NET-DNA was then transferred to a 96-well black micro-plate (3915; Corning, Lowell, MA, USA) containing 15 µL of 10 µM SYTOX® Green in PBS (S7020; Invitrogen, Paisley, UK) per well. Over a period of 5 mins fluorometric measurements were acquired five times for each well in order to quantify the NET-DNA release. The total fluorescence from each well was measured at 37 °C and recorded in arbitrary fluorescence units (AFU) using a Twinkle LB970 (Berthold Technologies, Germany) with excitation and emission filter wavelengths of 485 and 525 nm, respectively. To investigate the effect of well colour on fluorescence measurements NET-DNA release was quantified from stimulated neutrophils with the separated supernatant in 96-well white micro-plates (Immunolon2, Chantilly, VA, USA) (parallel study run simultaneously with the black wells using the same neutrophils for each well "pair") also containing 15 µL of 10 µM SYTOX® Green in PBS (S7020; Invitrogen, Paisley, UK). The experiment was repeated twelve times for black wells (during which eight times white wells were also used in parallel using the same neutrophil source).

6.3.7 *Ex-vivo* detection of NET adherence on Ti implant surfaces

Ti discs Grade IV (Commercially pure; Cp) and Grade V (Ti-6Al-4V) (12 mm diameter, 1 mm thickness, Titanium Products Ltd, Birmingham, UK) were used as model substrates to investigate the adherence of NETs to Ti implant surfaces in the presence and absence of a protein adsorbed layer.

6.3.7.1 Ti discs-Ti implant substrate models preparation

Ti discs were prepared by sequential polishing on a grinding and polishing machine (DAP-7, Struers, Rotherham, UK) with waterproof silicon carbide grit papers (Struers, Solihull, UK) from P220 through P320, P500, P800, P1000, P1200, P2400 up to P4000 with distilled water as a lubricant. Twelve Ti discs of grade IV and V each were manufactured for each surface finish determined by the final SiC abrasive grade. Mirror-like surfaces were created by further polishing the P4000 surfaces on a MD chem disc (Struers, Solihull, UK) with colloidal silica particles of 0.04 μm using water as a lubricant (Struers, Solihull, UK). To create a consistent surface all polished specimens were sonicated for 10 mins each in acetone followed by ethanol and distilled water. The samples were then autoclaved at 121 °C for 1 hr (Prestige Medical, Minworth, UK) to sterilise them prior to use.

6.3.7.2 Fluorometric quantification of NET-DNA release on Ti implant discs-Ti implant model substrates

NET interaction with Ti implant surfaces in the presence and absence of a protein adsorbed layer were investigated. To allow protein adsorption on Ti discs, six Grade IV and V discs each were immersed in a sterile 24 well transparent plate (CLS3527; Corning Costar, Dorset, UK) containing 500 μL of 1% PBS-BSA per well and stored at room temperature for 2 hrs prior to cell addition. A further six Grade IV and V Ti discs each were also placed in an additional 24 sterile well transparent plate containing none 1% PBS-BSA. Neutrophils were extracted (Appendix I) and re-suspended at a concentration of $1x10^5$ cells/mL. 600 μL of the

cell suspension were added to each well containing the Ti disc. The 1% PBS-BSA buffer was removed prior to cell addition (section 6.3.3). Wells containing Ti discs with cells were incubated at 30 °C for 30 mins and then stimulated with 150 µL of either PMA, HOCl or RPMI. Each stimulus was run in duplicate and the cell suspensions with the Ti discs were further incubated at 30 °C for 2 hrs. Extracellular NET-DNA release was quantified fluorometrically as detailed in section 6.3.6 after the 2 hr incubation period by transferring 400 µL of the cell suspension from the 24 well transparent plate (CLS3527; Corning Costar, Dorset, UK) to 96-well black micro-plates (3915; Corning, Lowell, MA, USA) containing 15 µL of 10 µM SYTOX® Green in PBS (S7020; Invitrogen, Paisley, UK) per well. The entire experiment was conducted four times and on each occasion neutrophils were sourced from different healthy volunteers.

6.3.7.3 Visualisation of NETs adherence on Ti discs-Ti implant model substrates

Following NET-DNA quantification in the liquid compartment of wells containing Ti discs, the discs were washed with RPMI three times, fixed in 2.5% glutaraldehyde fixative for 30 mins and then dehydrated through graded solutions of ethanol diluted in distilled water from 10, 20, 30, 40, 50, 60, 70, 80, 90, to 100% for 10 mins each. Samples were then dried using a critical point drier (Bio-Rad E3000, Sussex, UK). Samples were initially placed into the critical point drier chamber immersed in 100% ethanol. The ethanol was then replaced with CO_2 in a purging chamber five times. The chamber was then slowly heated to 32 °C, the critical point of CO_2, in order to evaporate all the remaining moisture. The

dried sample was then mounted onto 25 mm aluminium stubs and SEM images were acquired using a JEOL JSM-840 (JEOL, Japan) at an accelerating voltage of 20 KeV, at high vacuum.

6.3.8 Statistical analysis

Statistics were performed using SPSS 20 software. The data were initially explored for normality using a Shapiro-Wilk test at a 95% significance level. A Kruskal-Wallis test was then used to determine significant differences between group means at a 95% significance level. Comparisons between individual group means were determined by Mann-Whitney tests at a 95% significance level.

6.4 RESULTS

6.4.1 *Ex-vivo* time course fluorescence visualisation of NET release

Fluorescence microscopy of stimulated neutrophils was conducted to identify NET release over different time periods following stimulation. HOCl (Palmer, 2012), PMA (Gupta et al., 2005 & Ermert et al., 2009), periodontal bacteria including non-viable Ops *Sa* (Fc-γ mediated) (Huzinga et al., 1989) and *FN* (TLR-4/2 mediated) (Remer et al., 2003) are well characterised inducers of NET release and were employed within this study as positive controls. RPMI-1640 was used as the negative control stimulus. NET production was visually characterised at hourly intervals up to 4 hours. Experimental simulation with Ti oxide as nanoparticles and micron sized metallic species dispersed in RPMI-1640 at concentrations of 2000 and 200 ppm was also performed (Table 2.1; section 2.2).

Figures 6.1-6.3 are representative fluorescence images taken from four repeat experiments and presented on a standardised scale. These images are further correlated with the fluorometric quantification of NET-DNA production measurements (section 6.4.3).

Figure 6.1 Images of NET fluorescence captured at 0, 1, 2, 3 and 4 hours of neutrophils stimulated with RPMI, HOCl, PMA, Ops *Sa* and *FN*

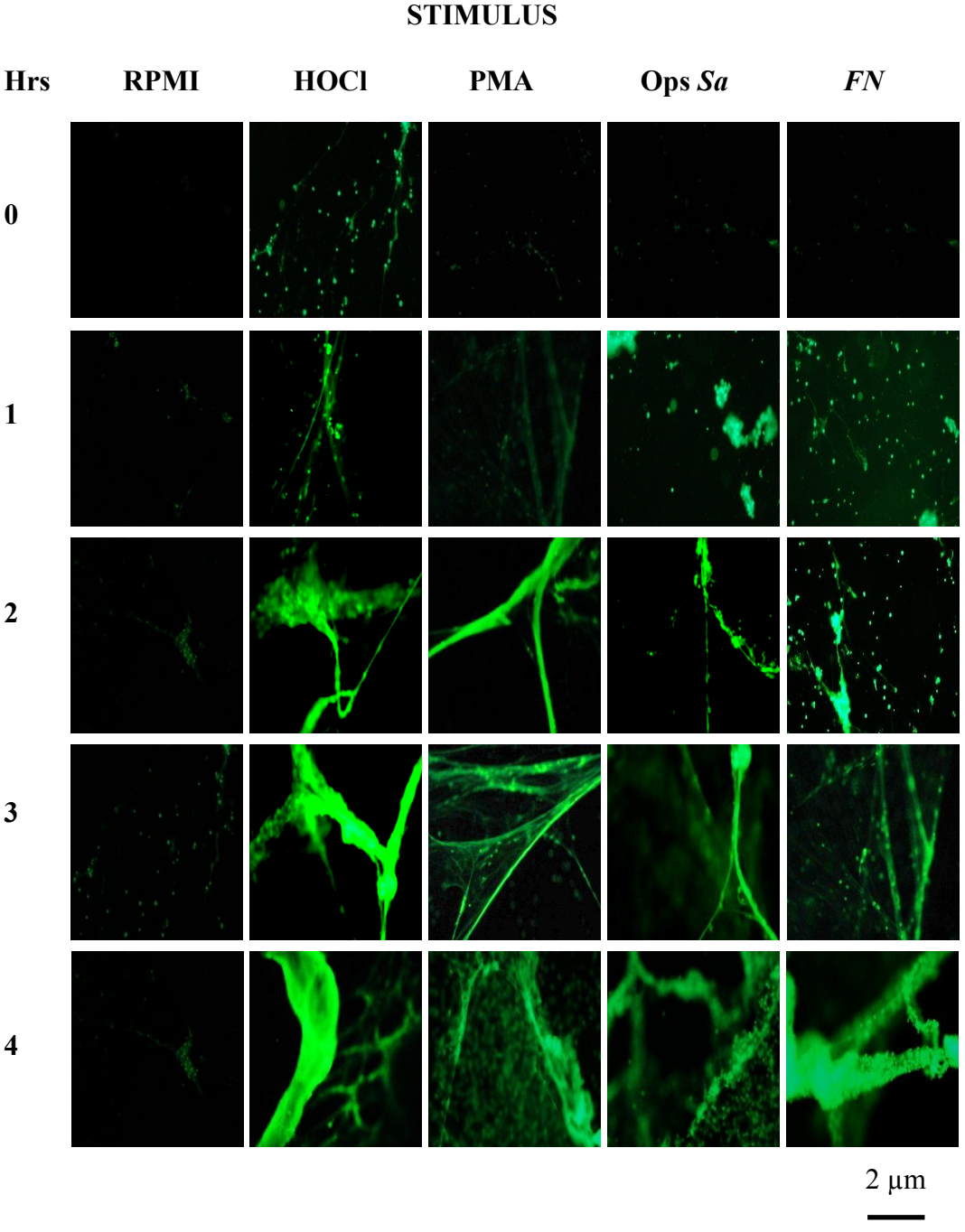

Figure 6.2 Images of NET fluorescence of neutrophils stimulated with Ti oxide as nanoparticles and micron sized metallic particles dispersed in RPMI at a concentration of 2000 ppm

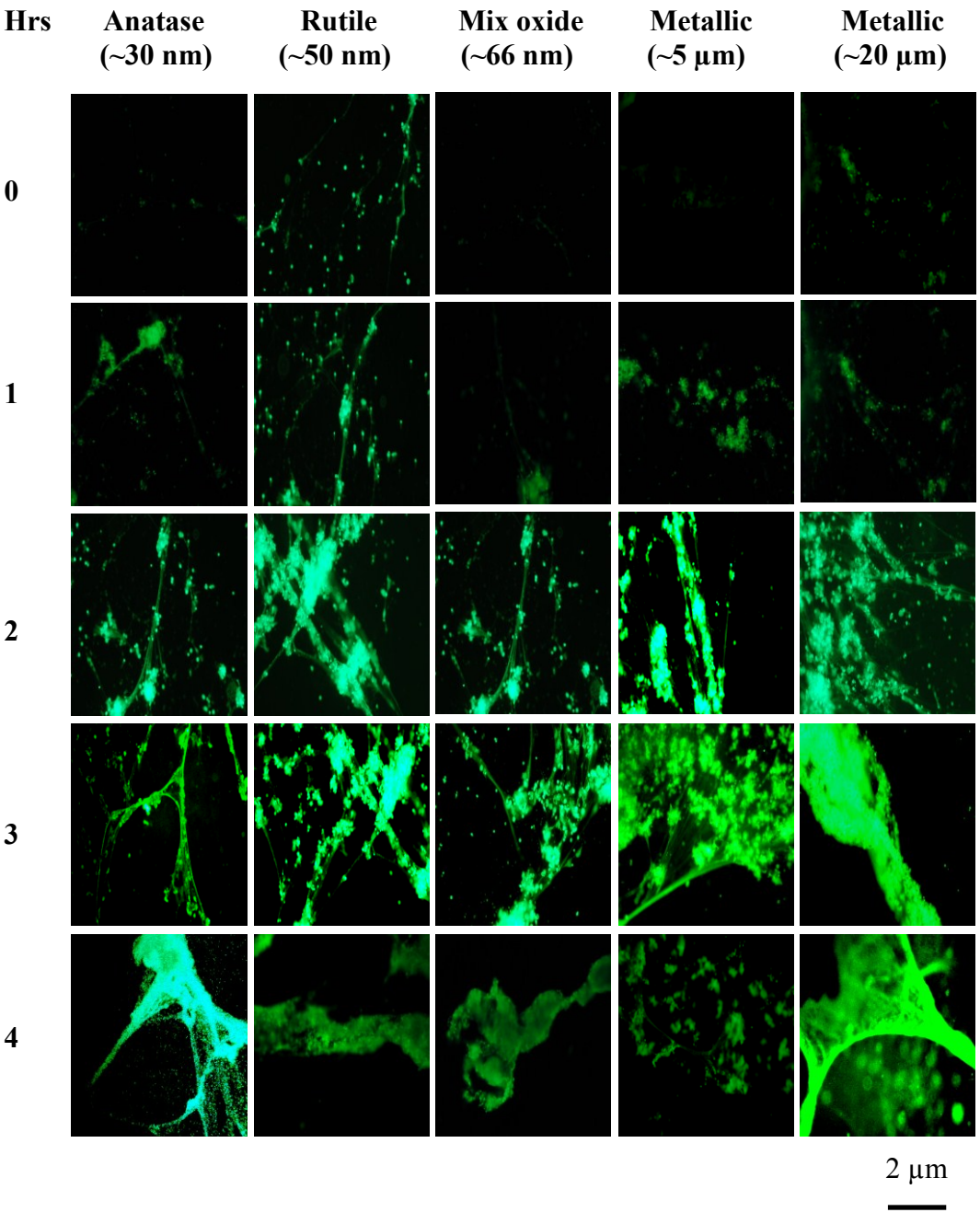

Figure 6.3 Images of NET fluorescence of neutrophils stimulated with Ti oxide as nanoparticles and micron sized metallic particles dispersed in RPMI at a concentration of 200 ppm

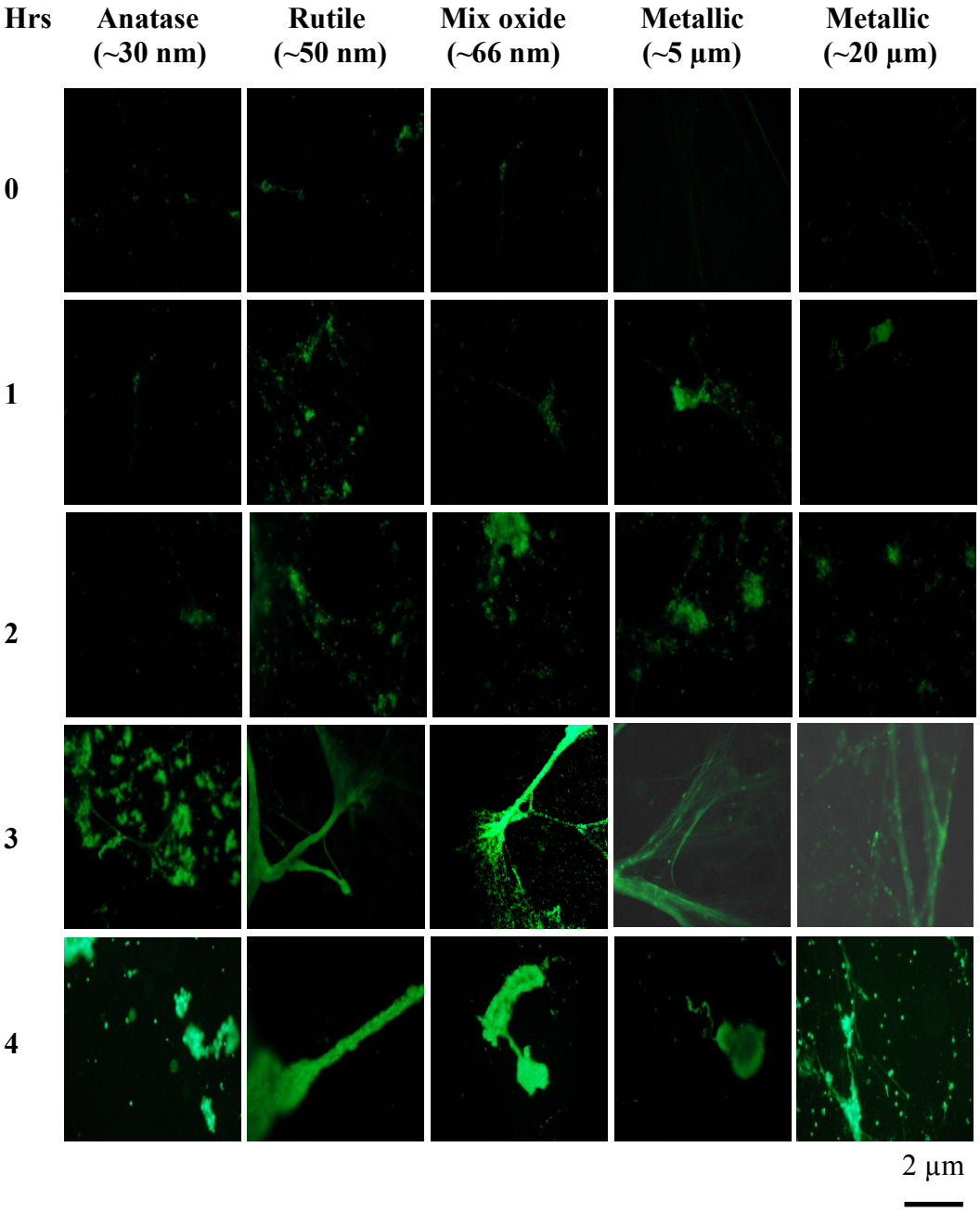

Prior to stimulation and at 1 hr post stimulation with positive controls and Ti stimuli, low levels of fluorescence were detected (Figures 6.1-6.3) for all conditions, except when cells were stimulated with HOCl where a NET-like morphology was observed. After 2 hrs stimulation NET like structures began to be observed for all stimulation conditions (Figures 6.1-6.3). After 3 hrs, fluorescence was further increased and structures resembled the more typical strand like NET morphology (Figures 6.1-6.3) as described by Brinkmann et al., (2004) & Behrendt et al., (2010). At 4 hrs post stimulation, fluorescence levels were further increased, however, NET morphology was observed to resemble denser web-like strands which were not as distinctive to those observed at 3 hrs. Therefore, 3 hrs was chosen as the optimal time point (provided adequate fluorescence intensity and NET morphology) for the NET-DNA quantification assay.

6.4.2 Sensitivity of fluorometric quantification of DNA

The sensitivity range for fluorometric detection of extracellular NET-DNA release following SYTOX staining and the comparison of the effect of micro-well colour on the fluorescence detected (measured in AFU) was calibrated using known concentrations of calf thymus DNA. Results are presented as a logarithmic standard calibrated curve of the mean of fluorescence in AFU against known concentrations of calf thymus DNA in µg/mL (Figure 6.4). Increased fluorescence levels were observed in white wells when compared with black wells (Figure 6.4) and this was confirmed upon reading blank white wells without SYTOX® Green which produced an excessive baseline reading of 6000 AFU, compared to 10 AFU for blank black wells without SYTOX® Green.

Figure 6.4 Fluorometric detection of SYTOX stained calf thymus DNA

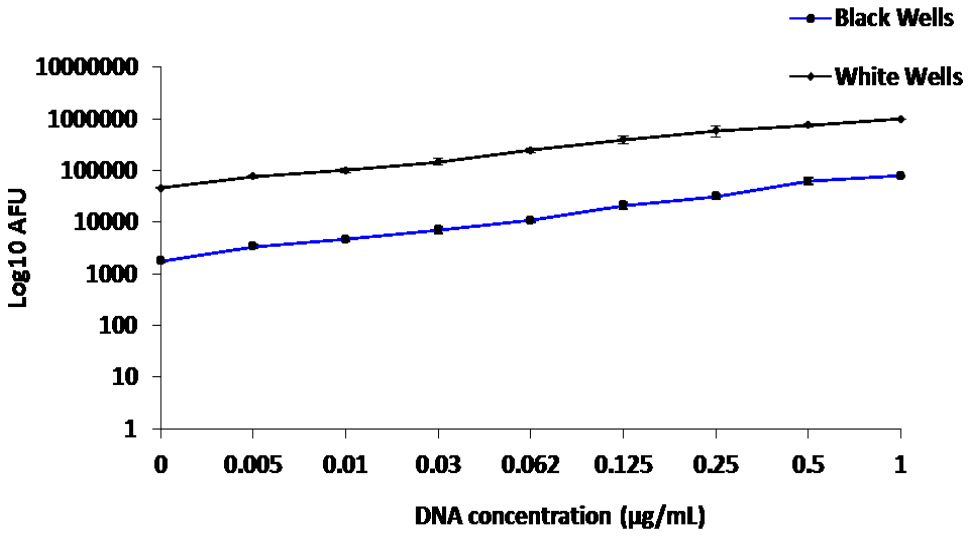

Fluorometric quantification of a known concentration of calf thymus DNA was employed to determine the percentage of neutrophils producing NETs. Studies have demonstrated that on average human neutrophils contain 5 pg of DNA (Mee & Adelstein, 1981). The total DNA content for 10^5 neutrophils, used in each well for this study, therefore equates to a total DNA content of 0.5 µg. The standard curve was used to determine the percentage of stimulated neutrophils in each well producing NETs. For example, HOCl employed as a dominant NET inducer (Palmer et al., 2012) produced fluorescence values of 25000 AFU in black wells. According to the standard curve (Figure 6.5) this corresponds with approximately 0.25 µg of DNA (indicated by dashed line in Figure 6.5) and it may be concluded that [(0.25 µg/0.5 µg)*100] = 50% of the 10^5 neutrophils in each well are producing NETs when stimulated with HOCl. Accordingly, for each stimulated condition, the percentage of neutrophils producing NETs quantified in black wells is estimated (Table 6.2).

Figure 6.5 Ascertaining the percentage of HOCl stimulated neutrophils at a concentration of 1x10^5 cells/mL producing NETs quantified in black wells

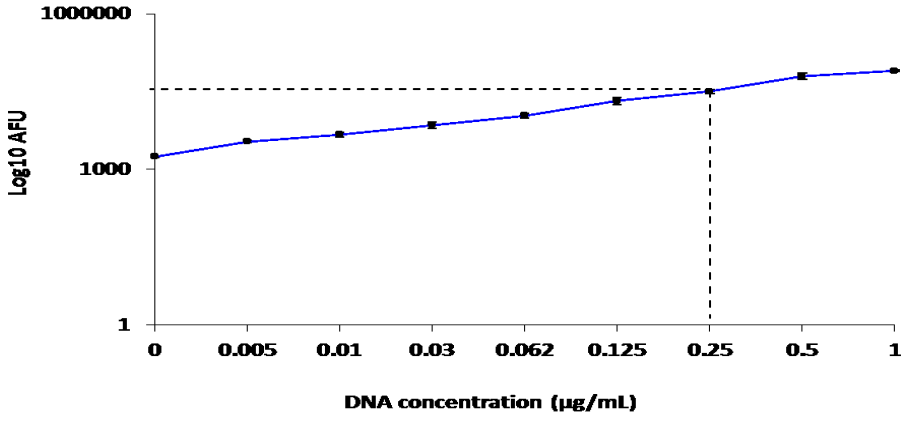

Table 6.2 Estimated percentage of cells at a concentration of $1x10^5$ cells/mL producing NETs quantified in black wells

Stimuli	Average NET-DNA release (AFU)	Conc. Of DNA (µg/mL)	Estimated percentage of neutrophils producing NETs (%)
RPMI	**728**	-	-
HOCl	**25000**	0.25	50
PMA	**13519**	0.18	36
Ops *Sa*	**10100**	0.16	32
FN	**9259**	0.16	32
Anatase 2000 ppm	**5207**	0.13	26
Anatase 200 ppm	**4124**	0.12	24
Rutile 2000 ppm	**20558**	0.22	44
Rutile 200 ppm	**13438**	0.18	36
Mix oxide 2000 ppm	**8937**	0.15	30
Mix oxide 200 ppm	**5422**	0.13	26
Metallic (~5 µm) 2000 ppm	**9024**	0.16	32
Metallic (~5 µm) 200 ppm	**7198**	0.14	28
Metallic (~20 µm) 2000 ppm	**6968**	0.13	26
Metallic (~20 µm) 200 ppm	**6321**	0.13	26

6.4.3 *Ex-vivo* fluorometric quantification of extracellular NET-DNA release

Extracellular NET-DNA release in the supernatant of stimulated neutrophils of 12 independent experiments after a 3 hr incubation period in black wells was quantified in AFU (Figures 6.6 & 6.8). Extracellular NET-DNA release in the supernatant of stimulated neutrophils of 8 independent experiments after a 3 hr incubation period in white wells was also quantified in AFU (Figures 6.7 & 6.9). Fluorometric measurements are presented in the form of Box/Whisker plots (median, inter-quartile range, 10^{th} and 90^{th} percentiles and outliers) (Figures 6.6-6.9). Significant differences between groups are marked by asterisk(s) (Figures 6.6-6.9).

The extracellular NET-DNA release quantified in black wells (Figures 6.6 & 6.8) was explored using a Shapiro-Wilk test at a 95% significance level, which identified the data to be not normally distributed. A Kruskal-Wallis test demonstrated significant differences between the magnitude of NET formation following neutrophil stimulation with positive and negative control stimuli ($P<0.001$). Pair-wise comparisons using Mann-Whitney tests demonstrated that all positive control stimuli resulted in significantly increased NET formation when compared to the negative control RPMI ($P<0.001$) (Figure 6.6).

Figure 6.6 Box/Whisker plot of extracellular NET-DNA release quantified in black wells of 3 hr control stimulated neutrophils including RPMI, HOCl, PMA, Ops *Sa* and *FN*

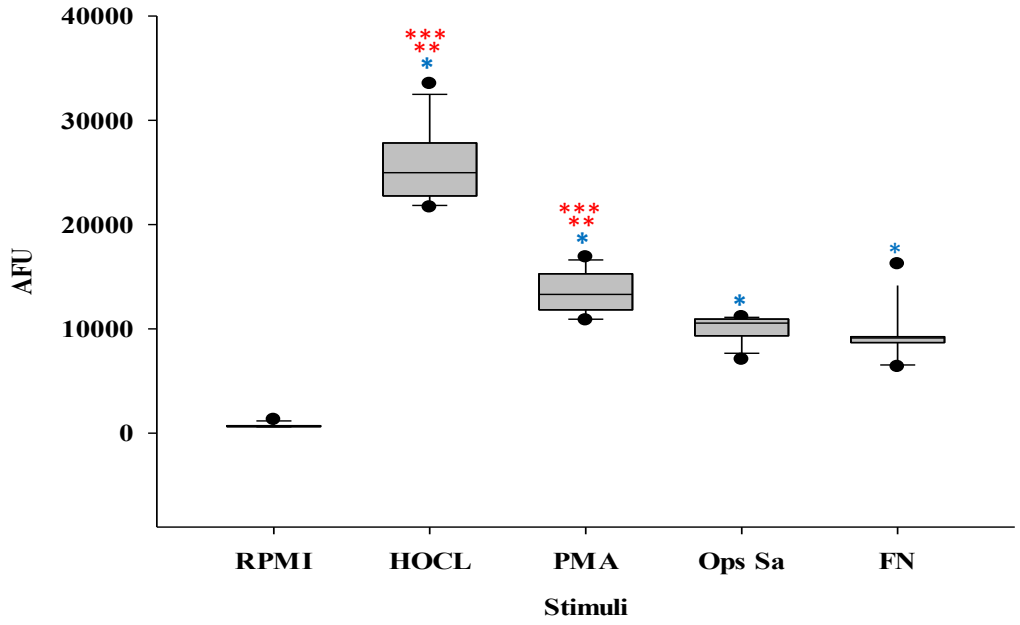

Significant different from RPMI*
Significant different from Ops *Sa***
Significant different from *FN*****

The extracellular NET-DNA release quantified in white wells (Figures 6.7 & 6.9) was explored using a Shapiro-Wilk test at a 95% significance level, which identified the data to be not normally distributed. A Kruskal-Wallis test demonstrated significant differences between the magnitude of NET formation following neutrophil stimulation with positive and negative control stimuli ($P<0.001$). Pair-wise comparisons using Mann-Whitney tests demonstrated that all positive control stimuli ($P<0.002$) except *FN* ($P=0.074$) resulted in significantly increased NET formation when compared to the negative control of RPMI (Figure 6.7).

Figure 6.7 Box/Whisker plot of extracellular NET-DNA release quantified in white wells of 3 hr control stimulated neutrophils including RPMI, HOCl, PMA, Ops *Sa* and *FN*

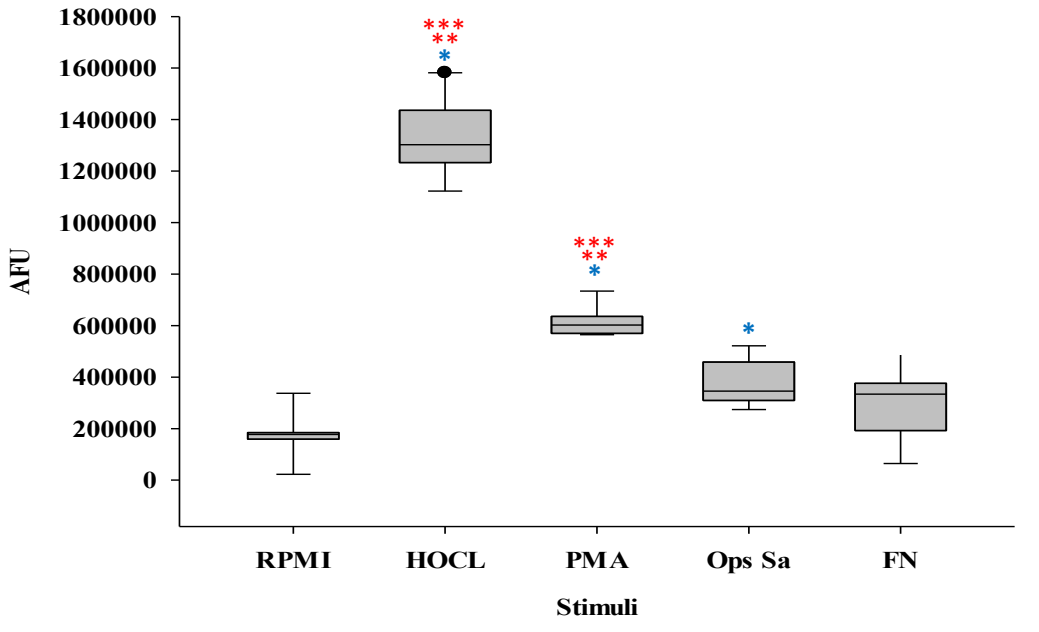

Significant different from RPMI*
Significant different from Ops *Sa***
Significant different from *FN*****

Extracellular NET-DNA release in response to the positive control stimulated neutrophils in both black (Figure 6.6) and white wells (Figure 6.7) was significantly highest from HOCl stimulated neutrophils ($P<0.001$) followed by PMA, Ops *Sa* and *FN* exposures.

The magnitude of DNA fluorescence quantified in black wells from neutrophils stimulated with Ti oxide as nanoparticles and with micron sized metallic species at 2000 and 200 ppm was concentration dependent (Figure 6.8). Pair-wise comparisons using Mann-Witney tests demonstrated that all Ti species at 2000 ppm and 200 ppm resulted in significantly increased extracellular NET-DNA release when compared with the negative control RPMI ($P<0.001$). Exposure to Ti oxide as rutile (~50 nm) at 2000 and 200 ppm resulted in significantly increased NET-DNA release when compared with all other Ti stimuli ($P<0.001$) (Figure 6.8). No significant differences in the magnitude of NET formation were found between mixed oxide (~66 nm) and ~20 μm sized metallic species of 2000 ppm ($P=0.82$) (Figure 6.8a), mix oxide and ~5 μm sized metallic species of 2000 and 200 ppm ($P=0.25$) (Figure 6.8) and between ~20 μm and ~5 μm sized metallic species of 2000 and 200 ppm ($P=0.25$ & 0.30) (Figure 6.8).

Figure 6.8 Box/Whisker plots of extracellular NET-DNA release quantified in black wells of 3 hr stimulated neutrophils with Ti oxide as nanoparticles and micron sized metallic species dispersed in RPMI at a concentration of (a) 2000 ppm and (b) 200 ppm

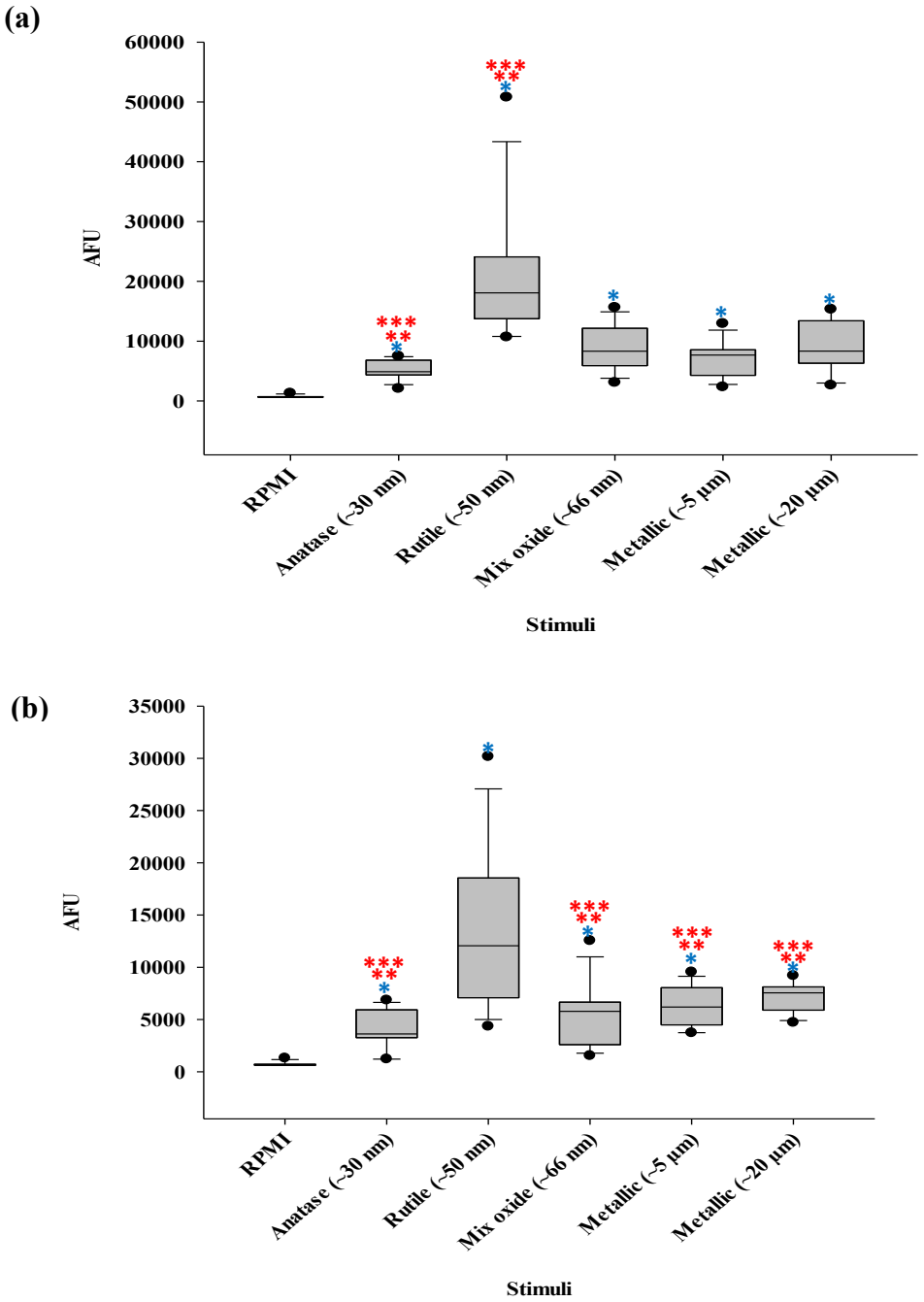

Significant different from RPMI*
Significant different from Ops *Sa***
Significant different from *FN*****

Similar to experiments in black wells, a dose-dependent extracellular NET-DNA release was observed in white wells from neutrophils stimulated with Ti oxide as nanoparticles and micron sized metallic species at concentrations of 2000 and 200 ppm (Figure 6.9). Pair-wise comparisons using Mann-Witney test demonstrated that all Ti oxides at 2000 ppm and 200 ppm ($P<0.002$) except Ti oxide as anatase (~30 nm) ($P=0.06$) resulted in significantly increased extracellular NET-DNA release when compared with the negative control RPMI (Figure 6.9).

Figure 6.9 Box/Whisker plots of extracellular NET-DNA release quantified in white wells of 3 hr stimulated neutrophils with Ti oxide as nanoparticles and micron sized metallic species dispersed in RPMI at a concentration of (a) 2000 ppm and (b) 200 ppm

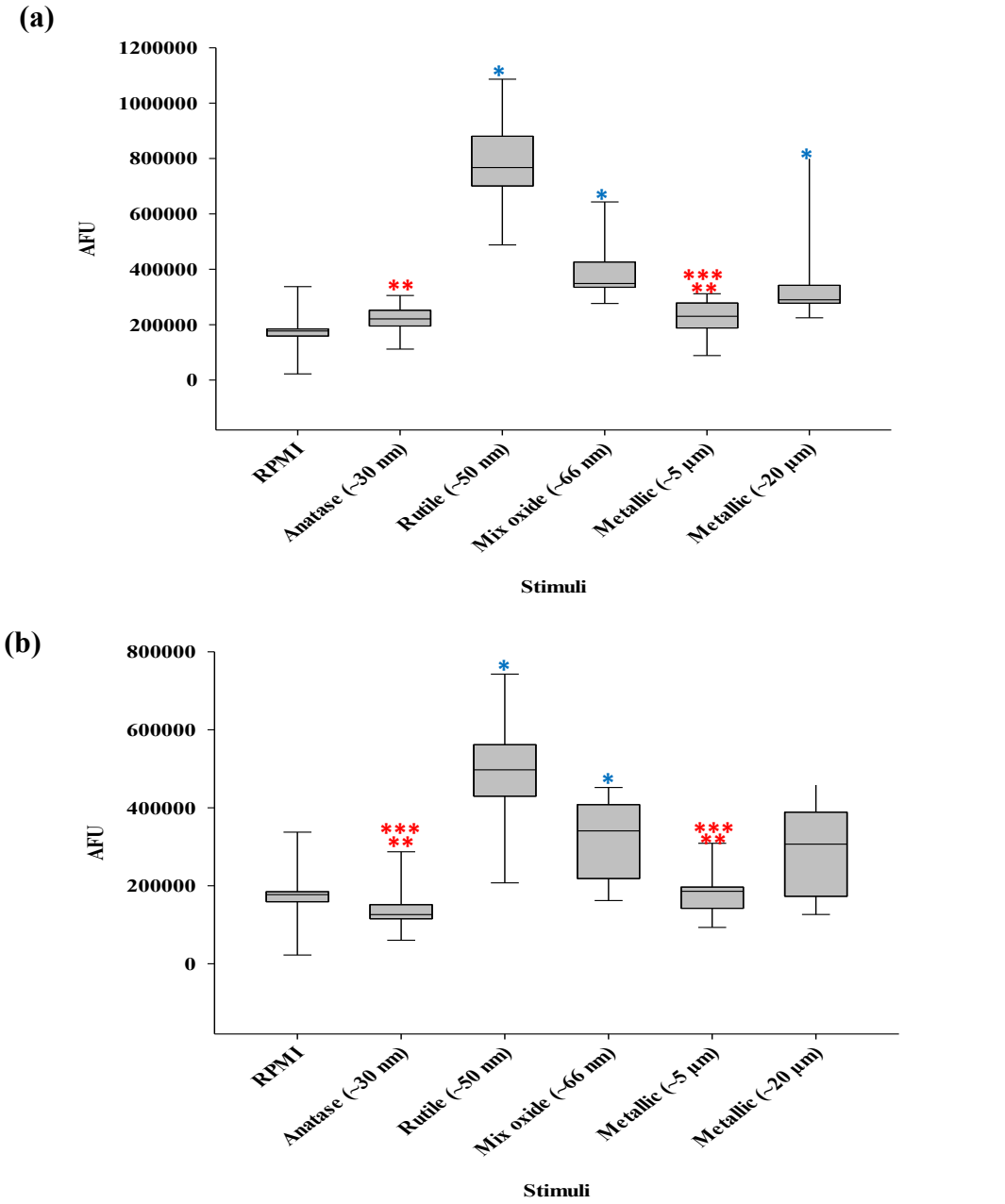

Significant different from RPMI*
Significant different from Ops *Sa***
Significant different from *FN*****

6.4.4 *Ex-vivo* visualisation of NET adherence to Ti implant surfaces

SEM of stimulated neutrophils co-incubated with Ti discs was used to detect NET adherence to Ti implant surfaces in the presence and absence of a protein adsorbed layer (Figure 6.10). HOCl (Palmer et al., 2012) and PMA (Gupta et al., 2005, Ermert et al., 2009) were employed as positive NET inducers and RPMI-1640 was used as the negative control stimulus. NETs were observed to adhere to Ti implant surfaces in the presence and absence of a protein layer, however increased NET adhesion was observed when proteins were present on the Ti surface (representative of the clinical situation) (Figure 6.10).

Figure 6.10 Images of NET adherence to protein adsorbed Ti implant surfaces (top) vs. non-protein adsorbed Ti implant surfaces (bottom)

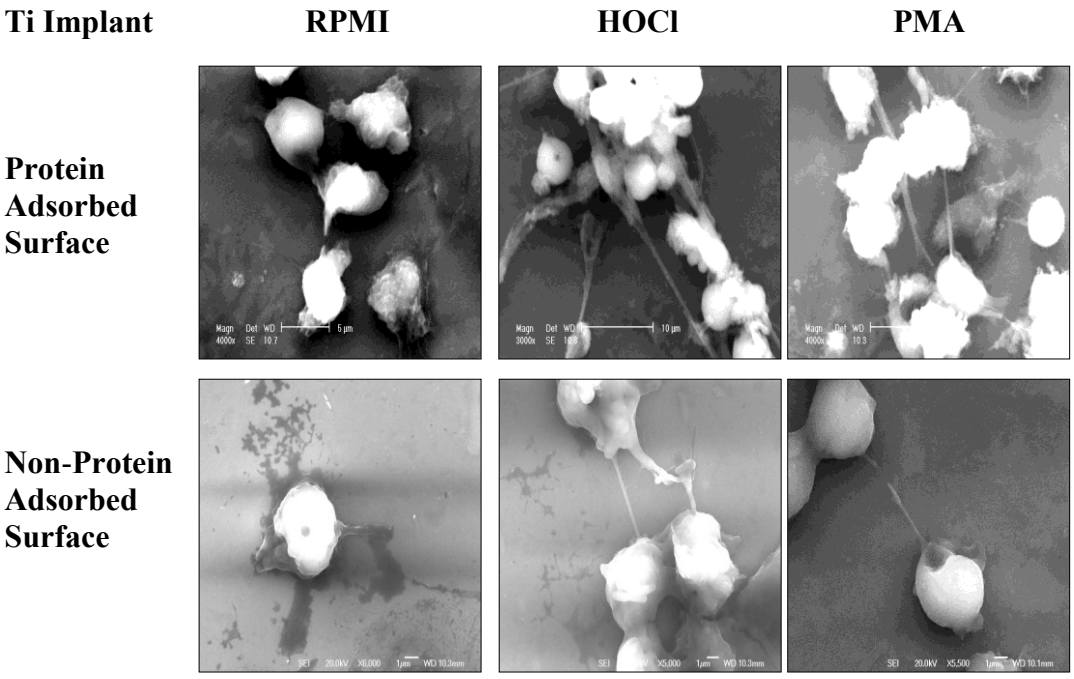

6.4.5 *Ex-vivo* quantification of NET-DNA release of stimulated neutrophils on Ti implant surfaces

In addition to direct visualisation of NET adherence to Ti implant surfaces, NET-DNA release was also quantified following neutrophil stimulation in the presence of a Ti implant surface with and without a protein adsorbed layer (Figure 6.11). Data represents four individual experiments quantifying NET-DNA release in black wells using the MNase assay (section 6.3.7.2).

The data demonstrates stimulated neutrophils in presence of a protein adsorbed layer exhibited statistically increased levels of NET-DNA release (Figure 6.11a) relative to a non-protein adsorbed layer (Figure 6.11b) ($P<0.005$). However, for both negative ($P<0.001$ for RPMI) and positive ($P<0.001$ for HOCl and PMA) stimuli, measurements were proportionally increased by a similar factor suggesting that the observed effect attributable to the protein layer may be negligible.

Figure 6.11 Box/Whisker plot of *ex-vivo* NET-DNA quantification of stimulated neutrophils on Ti implant surfaces (a) in presence of a protein adsorbed layer and (b) in absence of a protein adsorbed layer

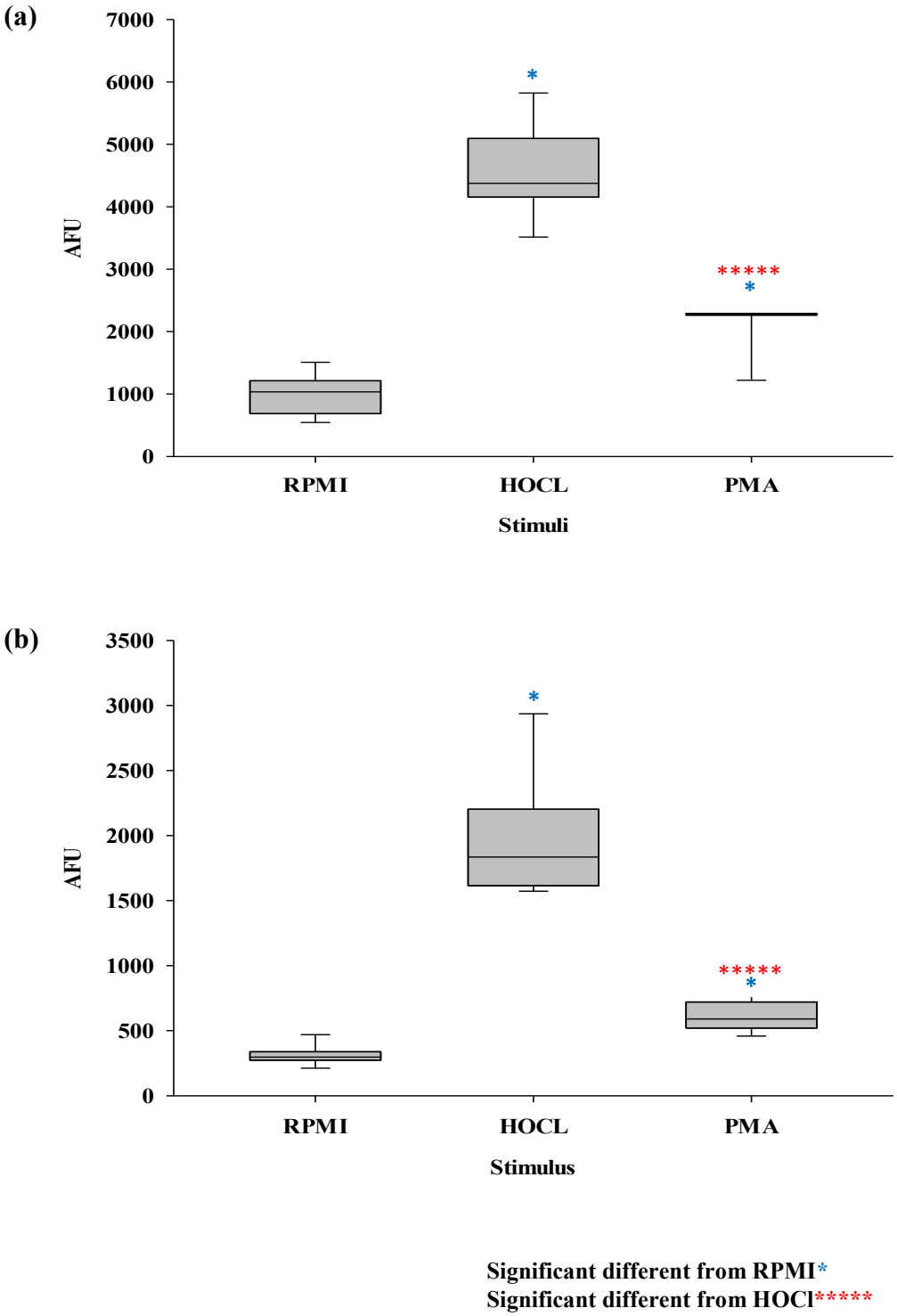

6.5 DISCUSSION

Currently only one study has identified NET release from neutrophils following stimulation with Ti. The study reported responses of fish neutrophils, *Pimpehales promelas* (Jovanovic et al., 2011b) to Ti oxide nanoparticles at levels representative of environmental exposure. The authors demonstrated that 0.1 ppm of Ti oxide as nanoparticles (speciation not defined) was sufficient to stimulate NET release (Jovanovic et al., 2011b). However, the underlying functional mechanism by which Ti can modulate NET release is not known. In Chapter 5, it was demonstrated that Ti implant derivatives representative of debris found *in-vivo* as oxide nanoparticles and micron sized metallic species stimulated dose dependent and Ti oxide species specific ROS production from human neutrophils. It is understood that activation of the respiratory burst in neutrophils may cause the cell to either trigger apoptosis or NETosis (Amulic et al., 2012) and the generation of reactive oxygen species is known to be important in the induction of NET formation (Amulic et al., 2012). Therefore, in the current study, the same Ti implant derivatives were used to stimulate neutrophils before *ex-vivo* fluorometric visualisation of NET structures (section 6.4.1) and quantification of extracellular NET-DNA release (section 6.4.3).

Observations of Ti (oxide or metallic) stimulated cells after 1 and 2 hrs of stimulation demonstrated relatively low levels of fluorescence (Figures 6.1-6.3). This suggests that only a small number of non-viable cells were present and NET release was minimal at this stage. This was consistent with the positive control stimuli with the exception of 0.57% HOCl stimulated neutrophils which exhibited

increased fluorescence levels after 1 hr stimulation and clear NET like structures were seen to form consistent with Palmer et al., (2012). The remaining control and Ti stimulated neutrophils were subsequently observed to produce NETs only after 3 hrs of stimulation and the resultant morphologies were consistent with previous descriptions of NET release appearing as discrete DNA strands (Brinkman et al., 2004/2007, Urban et al., 2009 & Behrendt et al., 2010). Interestingly, for Ti stimulated neutrophils at 3 hrs, the NET-DNA strands were abundant but appeared to be aggregated and associated with agglomerates of Ti particles. The capacity of the Ti particles to strongly stimulate NETosis may be a consequence of the internalised Ti which cannot be digested by neutrophil components remaining within the phagosomal compartments and thus chronically stimulating the NADPH oxidase (Segal, 2005). Chronic stimulation of the respiratory burst had been shown to be associated with a decrease in pH and a flow of K^+ and Cl^- ions into the phagosomes which may further contribute to release of elastase and cathepsin G (antimicrobial proteins found on NETs) (Segal, 2005) (Figure 6.12).

Figure 6.12 Schematic representation of NET signalling pathway of Ti oxide as nanoparticles or micron sized metallic particle stimulated neutrophils

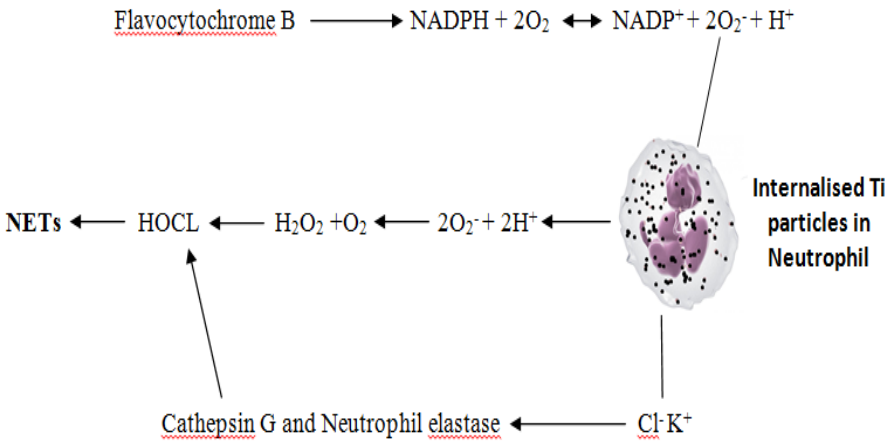

It is proposed that chronic activation of the NADPH oxidase (respiratory burst) by internalised particles may lead to its prolongation which consequently ruptures the cell (Papayannopoulos et al., 2010). Moreover, it is known that Ti particles possess strong binding affinity towards proteins (Vamanu et al., 2008) and therefore when cell rupture occurs the internalised particles possibly complex with AMPs which may then be ejected back into the physiological environment and continue to contribute to the progression of extracellular damage (Jovanovic, 2011). The strong binding affinity of the particles to NETs was demonstrated in the current study, however, it could not be explicitly determined whether this was an association with previously internalised particles or free extracellular particles in the medium.

In contrast, micron sized metallic particles which cannot be easily phagocytosed by mammalian neutrophils (often larger in size than the cell) (Chapter 5) also stimulated NETs. It has been proposed that the neutrophil may attempt and re-attempt to phagocytose the particle leading to the activation of the oxidase. This induced hyperactivity of the neutrophils may also cause the cells to eventually enter NETosis. In contrast to the nanoparticles the resulting NETs observed were not seen to be associated with the micron sized Ti particles and this difference from the nanoparticles may be accounted for by their reduced surface energies (Thorek & Tsourkas, 2008).

Visualisation of NET structures at 4 hrs after stimulation with both positive controls and Ti stimuli revealed that although the fluorescence levels were

increased, the NETs were denser in morphology (less NET-like). Therefore, 3 hrs was chosen as an optimal time for extracellular NET-DNA quantification (to avoid false NET-DNA experimental readouts). Fluorometric quantification of extracellular NET-DNA in both black and white wells was performed to determine the effect of well colour and allow correlation with previously reported findings. Fluorescence levels measured in AFU for stimulated neutrophils in white wells were around 1000 times higher than quantified in black wells, however scaling between the measures differed and the white wells were considered to be less sensitive. Black wells were therefore used for quantification of NET-DNA release in further assays.

The NET quantification data was identified to be not normally distributed varied considerably with individual (neutrophil donor) responses, which were assumed to vary on a day to day basis. Enhanced responses (in magnitude of NET production) suggest increased sensitivity of certain individuals; however this was not systemically evaluated. The data coincided with previous findings that HOCl is a dominant ROS trigger for NET formation (Palmer et al., 2012) in comparison to the other inducers of NET release employed including PMA, Ops *Sa* and *FN*. Stimulation with Ti oxide as nanoparticles resulted in statistically higher orders of dose-dependent extracellular NET-DNA release when compared with micron sized metallic particles at the same concentrations and was consistent with the fluorescence microscopy.

The differences in the biological activity of Ti as nanoparticles and as micron sized particles have been attributed primarily to the ability or inability of the neutrophil to firstly internalise the particle and secondly attempt to digest the particle within the phagosome. However, it is now clear that considerable differences in the mechanisms of nanoparticle uptake by neutrophils occur including pathways of pinocytosis, endocytosis and/or phagocytosis (Tamura et al., 2002, Long et al., 2007 & Pierre, 2010) when compared with larger particles. The high surface to volume ratio of nanoparticles and higher surface energies not only modify intra-cellularisation potential (Thorek & Tsourkas, 2008), but also their subsequent interactions in intra-cellular compartments or within the cytosol. Although specific mechanisms cannot be derived from the findings of this study, the variability in cell responses to nanoparticles of different size and speciation suggests the existence of multiple pathways. Moreover, determining the mechanisms underpinning the inconsistencies in the dose-dependent magnitude of extracellular NET-DNA release observed is further complicated by inherent variability in particulate agglomeration-associated with dispersing different concentrations of particles in solution (Tirado-Miranda et al., 2003). Particle agglomeration may determine whether the nanoparticles become phagocytosed leading to higher orders of respiratory burst and for NET release (Thorek & Tsourkas, 2008).

NET release also appeared sensitive to the speciation of the Ti oxide nanoparticles with the greatest response observed to Ti oxide as rutile (~50 nm). In comparison with other experimental stimuli, these particles were larger than anatase (~30 nm)

and smaller than the mix oxide (~66 nm). This observation was not surprising as a similar pattern in the magnitude of ROS production was observed (Chapter 5). The finding is consistent with the previous reports regarding the dependency of NET formation on a ROS-dependent pathway (Fuchs et al., 2007 & Amulic et al., 2012). However, the correlation between the increased ROS production observed for rutile and NET formation (Figures 5.9 & 6.8) cannot be explicitly linked, because the molecular mechanism(s) of both ROS and NET release pathways to Ti exposures were not considered within the current study. An alternative hypothesis whereby there was a morphological sensitivity to rutile itself, or to aggregation effects, or responses to surface associated biomolecules cannot be excluded (Tirado-Miranda et al., 2003).

In the *in-vivo* environment, it is known that Ti oxide nanoparticles readily bind to combinations of human serum proteins including fibrinogen and immunoglobulin (Lundqvist, 1996), and albumin (Vamanu et al., 2008). In the context of the progression of inflammation, understanding the role of particulate-protein associations is necessary in order to identify the mechanisms determining cell entry and cellular activation (Park et al., 2008, Wang et al., 2008 & Jin et al., 2011). Protein association with Ti particles may further modify agglomeration effects through attractive and/or repulsive forces modifying surface energy (Tirado-Miranda et al., 2003). The association of particles with NETs is previously unreported and may indeed modify their functional activity.

The study also demonstrated the adherence of NETs to a model of a Ti implant surface in the presence and absence of a protein adsorbed layer (section 6.4.4). NET adherence to Ti discs was observed to be increased in the presence of surface adsorbed proteins which were representative of the *in-vivo* conditions. Fluorometric quantification of extracellular NET-DNA release of PMA and HOCl-stimulated neutrophils incubated on protein adsorbed Ti implant surfaces resulted in significantly increased NET release in comparison to PMA and HOCl stimulated neutrophils incubated on Ti implant surfaces in absence of a protein adsorbed layer. The retention of NET like structures on biomaterial surfaces is interesting particularly if anti-microbial activity is retained as they may interact with surface pathogens. The retention of NETs in a site of inflammation has also been proposed to be pro-inflammatory (Remijsen et al., 2011) and further studies are required to ascertain their functionality and impact on peri-implant inflammation.

6.6 CONCLUSION

The findings demonstrate that Ti implant derivatives as oxide nanoparticles and micron sized metallic particles, both representative of products observed in peri-implant tissues, can be potent stimulators of NETs. It is suggested that there is a strong correlation with ROS production; however, further mechanisms sensitive to particle size and speciation also appear to be active. NETs have been demonstrated for the first time to bind to Ti surfaces and may impact on the peri-implant inflammatory response. Further studies are required to determine the dependency of NET formation upon the pathways of particle internalisation and on the subsequent distribution of the particles within the neutrophil.

CHAPTER 7

THE EFFECT OF NEUTROPHIL PRIMING WITH TITANIUM IMPLANT DERIVATIVES UPON SUBSEQUENT MICROBIAL STIMULATION

7.1 PREFACE

It is possible that neutrophils may be primed by Ti implant derivatives within peri-implant tissues, which may then alter neutrophil responses to bacterial challenge. Therefore, enhanced chemiluminescence and Micrococcal Nuclease (MNase) assays were used to determine the impact of priming selected Ti derivatives (oxide or metallic) upon NADPH oxidase stimulation and Neutrophil Extracellular Trap (NET) formation by neutrophils. Responses following priming with Ti derivatives to peri-implant pathogens including opsonised *S. aureus* (Ops *Sa*) (Fc-γ receptor mediated) and *F. nucleatum* (*FN*) (TLR-4 receptor mediated); and/or physiological agonists such as phorbol myristate acetate (PMA) were investigated. The Ti species were representative of products of mechanically assisted crevice corrosion (Ti oxide as nanoparticles) or larger debris generated through tribiological processes (micron sized metallic Ti). Neutrophils primed with Ti at minimal stimulatory concentrations (50 ppm) produced a significant decrease in the release of ROS and NETs in response to Ops *Sa* exposure (Fc-γ receptor mediated), but the response to *FN* (TLR-4 receptor mediated) was unaffected. In contrast, Ti primed neutrophils (at 50 ppm) exposed to PMA exhibited increased NET release.

7.2 INTRODUCTION

7.2.1 Neutrophil priming

Priming of neutrophils arises *in-vivo* at sites of inflammation (Edwards, 1994 & Brown et al., 2004) and has been shown to significantly affect the nature of the cell response (Dias et al., 2010). The induction of a state of pre-activation of neutrophils by agents such as eicosanoids and/or cytokines (e.g. IL-6, IL-8 & TNF-α) (Gainet et al., 1999) at low concentrations, followed by subsequent stimulation with physiological agonists resulting in the generation of a more powerful inflammatory response (Smith, 1994 & Hatanaka et al., 2003) is known as priming. A variety of neutrophil priming agents have been recognised (Table 7.1), with variable efficiencies and kinetics.

Table 7.1 Priming agents (Shalaby et al., 1987, Koenderman et al., 1989 & Edwards, 1994)

Primer Type	Priming Agent
Cytokines	IL-1β, IL-6, IL-8, IL-18, TNF-α, GM-CSF, GCSF and IFN-α/γ
Lipids	PAF, PMA, lysophosphatidylcholine, arachinoid acid, leukotrienes (LTB1) and ceramide (C2 and C6)
Bacterial	LPS and opsonised zymosan
Others	Angiotensin II, homocysteine, C5a, Ca^{2+} and immune complexes

Neutrophil priming with such agents may enhance respiratory burst reactions and effect phagocytosis and bacterial killing processes (Edwards, 1994). In contrast, priming agents have also been shown to cause inhibition of the respiratory burst (Guichard et al., 2005) and/or fail to induce superoxide production in neutrophils

(Koenderman et al., 1989). These functional changes in the neutrophil are typically observed within 15-60 mins following exposure to the priming agent and are caused by mobilisation of intracellular granules which form pre-formed receptors on the plasma membrane (Edwards, 1994). Priming can affect the number and the binding affinity of the receptors to their ligand (Edwards, 1994) which is independent of down-stream effects.

Among the prominent neutrophil priming agents are inteferons (IFNs) (IFN-α/γ) (2-50 U/mL) (Berton et al., 1986 & Atzeni et al., 2002) which are reported to be produced during infection (Koyama et al., 2008). These are released by helper T-cells during cell activation and by natural killer cells in response to species such as IL-2 and H_2O_2 (Wright et al., 2008). The importance of IFN-α and its influence on the hyperactivity and hyper-reactivity of neutrophils in periodontitis patients has been acknowledged (Wright et al., 2008 & Dias et al., 2010). Studies indicate that IFN-α causes inhibition of neutrophil apoptosis through Phosphatidylinositide 3-Kinases (PI3K), Protein Kinase C-δ (PKC-δ), Nuclear Factor-kB (NF-kB) and Signal Transducers and Activators of Transcription (STAT) signalling pathways (Wang et al., 2003 & Sakamoto et al., 2005). In addition, previous priming studies with IFN-α suggest prolongation of the neutrophil lifespan (Wright et al., 2008) and are reported to enhance respiratory burst reactions upon exposure to secondary stimuli (Gyllenhammar et al., 1988 & Little et al., 1994).

Therefore, priming agents in combination with secondary stimuli have been shown to affect the assembly and activation of the NADPH oxidase (NOX)

complex and influence the magnitude of the immunological response (Guichard et al., 2005). However, the priming agent is not directly involved in the activation of the NOX complex itself (Edwards, 1994). In contrast, priming agents can manifest their impact through modulation of the activation of different receptors and therefore may influence more than one signalling pathway (Edwards, 1994).

7.2.2 Receptor expression in neutrophils for recognition of foreign material

Initial recognition of foreign material and/or pathogens and pathogen associated molecular patterns (PAMPs) (Mogensen, 2009) involves activation of pattern recognition receptors (PRRs) which induce an inflammatory response (Medzhitov, 2001). Neutrophils express toll-like receptors (TLRs) which are a major class of PRRs that recognise a variety of specific PAMPs including bacterial lipopolysaccharides (LPS), peptidoglycans (PGNs), lipoteichoic acids from gram positive bacteria and viral nucleic acids (Madianos et al., 2005). Activation of such receptors enables identification and enables transduction of signals to various intracellular adaptor molecules that elicit the pathogen-specific destruction (Witko-Sarsat, 2000).

In addition to TLR, Fc-γ receptors (Fc-γR) are another class of specific receptor which are extensively expressed in neutrophils (100,000-200,000 receptors per cell) and are important in neutrophil mediated damage (Pierre, 2010). There are three different Fc-γR classes recognised in neutrophils including Fc-γRI (CD64), Fc-γRII (CD32) and Fc-γRIII (CD16) with different binding affinity to IgG and different functionality (Quayle et al., 1997). Fc-γRI is a high-affinity IgG receptor

that binds to monomeric IgG (Quayle et al., 1997) which is induced by activated neutrophils in the presence of cytokines such as IFNs (Wright et al., 2010). In contrast, Fc-γRII is constitutively expressed in neutrophils in two isoforms including Fc-γRIIa and Fc-γRIIb which also bind to monomeric IgG however with low affinity; yet display higher affinity towards dimers or aggregates of IgG (Quayle et al., 1997). Both isoforms of Fc-γRII initiate different functional responses in neutrophils (Wright et al., 2010) where Fc-γRIIa is an activating receptor (Belostocki et al., 2005) and Fc-γRIIb generates an inhibitory signal (Radstake et al., 2006). Evidence suggests that neutrophils challenged with opsonised bacteria initiate chemotaxis, phagocytosis and killing via Fc-γRIIa (Belostocki et al., 2005). However, Fc-γRIII which binds complexes of IgG with low affinity displays a pivotal role in ROS secretion in response to immune complexes (Fossati et al., 2002). Moreover, priming causes intracellular stores of Fc-γRIII to be mobilized to maintain expression (Fossati et al., 2002).

7.2.3 Neutrophil phagocytosis

Priming of cells also confers morphological changes and cytoskeletal alterations (Edwards, 1994) which are remodelling phenomena most prominently observed when cells undergo phagocytosis (Metchnikoff, 1893). The understanding of the underlying mechanism(s) by which professional phagocytes e.g. neutrophils serve to internalise and/or remove particulate material from the extracellular space is of immense value (Pierre, 2010).

Phagocytosis which is a specialised actin dependent process is known to be mediated through different signalling pathways (Kwiatkowska & Sobota, 1999). The phagocytic route which has been suggested for Ti particulate uptake involves Fc-γR engagement and activation (Dobrovolskaia and McNeil, 2007). Fc-γR mediated internalisation is characterised by dramatic extension of the plasma membrane around the particle (May & Machesky, 1997) and is associated with activation of superoxide production and/or the release of pro-inflammatory cytokines (Roitt, 1994). Activation of Fc-γR in response to particles coated with Igs (mainly IgG) (Yokota et al., 1992) which act as opsonins has been shown to render the particle more susceptible to phagocytosis (May & Machesky, 1997). In contrast, other studies have proposed that nanoparticles are internalised by neutrophils via caveolae-mediated endocytosis; clathrin mediated endocytosis (da Rosa, 2013) and/or receptor mediated phagocytosis including the mannose receptor, complement receptor, and scavenger receptor (Pierre, 2010).

The impact of direct exposure of Ti implant derivatives on neutrophil morphology and activation (ROS and NET release) has been demonstrated (Chapters 5 & 6). However, the potential of Ti oxide as nanoparticles and micron sized metallic particles to interfere or perturb responses (ROS and NET release) to a bacterial challenge and/or to exogenous agents has not been established. Moreover, the understanding and morphological characteristics of neutrophil phagocytosis of Ti nanoparticles via Fc-γR (IgG opsonised) route is limited. Investigation of these effects will enable better understanding regarding the potential mechanism(s) by

which Ti implant derivatives contribute to the progression of the peri-implant inflammatory response.

7.3 METHODS

7.3.1 *Ex-vivo* determination of Ti implant derivatives capacity to perturb neutrophil responses

Neutrophil priming was performed to determine the capacity of Ti implant derivatives to perturb neutrophil ROS release and NET formation responses to either peri-implant pathogens including Ops *Sa* and *FN*; and/or a physiological agonist-PMA. Enhanced chemiluminescence assays and MNase assays were employed to quantify ROS and NET production respectively, from primed neutrophils.

7.3.2 Preparation of primers to perturb neutrophil ROS and NET responses

Control and experimental primers were prepared by adding high purity reagents to PBS (Appendix I) for enhanced chemiluminescence assays and to RPMI-1640 for MNase assays. Table 7.2 demonstrates the working concentration of the prepared solution and the stimulation concentration once added to the experimental system.

Table 7.2 Primers employed to perturb neutrophil ROS and NET responses

Primer	Supplier Cat Number	Working Concentration	Stimulation Concentration
Inteferon-alpha (IFN-α)	R & D Systems 11200-2	250 U/mL	2.5 U/mL
Ti-anatase (~30 nm)	Alfa-Aesar 039953	100 ppm	50 ppm
Ti-rutile (~50 nm)	Sigma-Aldrich 1317802	100 ppm	50 ppm
Ti-metallic (~5 μm)	Produced in house (section 2.2.2)	100 ppm	50 ppm

7.3.3 *Ex-vivo* enhanced chemiluminescence assay quantifying ROS release from primed and/or unprimed neutrophils

A 96-well white plate (Immunolon2, Dynex, Chantilly, VA, USA) was pre-blocked with 200 µL of 1% PBS-BSA per well and stored overnight at 4 °C. All assays were performed at 37 °C using a Berthold microplate luminometer (LB96, EG and G Berthold UK Ltd., Milton Keynes, Bucks, UK) where light output was recorded for 1 sec per well in relative light per units (RLU). Each well contained 45 µL of glucose supplemented PBS (GPBS) (section 5.3.5) with 30 µL of luminol (3 mmol/L) (section 5.3.1), or 60 µL of isoluminol (3 mmol/L) (section 5.3.1) with 15 µL horseradish peroxidise (HRP) (section 5.3.6). 100 µL of isolated cells (Appendix I) at a concentration of $1x10^5$ cells/mL suspended in PBS were added per well and light output was monitored for 30 mins to establish baseline signal. At 30 mins, selected cells were primed with 10 µL of either IFN-α (positive control primer) or Ti oxide nanoparticles as anatase (~30 nm) or rutile (~50 nm) (experimental primers) (Table 7.2) and light output was monitored again for a further 30 mins. At 1 hr, primed and unprimed cells were stimulated with 25 µL of either PBS (negative control), opsonised *S. aureus* (Ops *Sa*) (MOI: 300-bacteria/neutrophil) or *F. nucleatum* (*FN*) (MOI: 100-1) (Appendix II) and light output was monitored for a further 2 hrs. All samples were run in quadruplicate. The assay was performed twelve times with neutrophils sourced from different healthy volunteers.

7.3.4 Quantification of ROS release from neutrophils co-stimulated with Ti and Ops *Sa* (IgG opsonised) with primed or unprimed neutrophils

To identify whether Ti implant derivatives mediate an Fc-γR mediated pathway, a further set of isolated cells (Appendix I) at a concentration of $1x10^5$ cells/mL were re-suspended in PBS. The assay was performed as detailed in section 7.3.2 where 100 μL of suspended cells in PBS were added per well and light output was monitored for 30 min to establish a baseline signal. At 30 min, selected cells were primed with 10 μL of either IFN-α (control primer) or Ti oxide nanoparticles as rutile (~50 nm) or ~5 μm sized metallic particles (experimental primers) and light output was monitored for a further 30 mins. At 1 hr, primed cells were subsequently stimulated with 25 μL of Ops *Sa,* whereas selected unprimed cells were either (a) co-stimulated with 25 μL of Ti oxide nanoparticles as rutile (~50 nm) or ~5 μm sized metallic particles with Ops *Sa* (Fc-γR mediated) or alternatively (b) stimulated with 25 μL of either PBS, Ops *Sa, FN* or Ti oxide nanoparticles as rutile (~50 nm) or ~5 μm sized metallic particles (controls), following which light output was monitored for a further 2 hrs. All samples were run in quadruplicate. The assay was performed thirteen times with neutrophils sourced from different healthy volunteers.

7.3.5 Micrococcal nuclease (MNase) assay quantifying NET release from primed and/or unprimed neutrophils

Isolated neutrophils at a concentration of $1x10^5$ cells/mL were re-suspended in RPMI-1640 supplemented with 1 U/mL of glutamine (Sigma-Aldrich, UK) (section 6.3.6). 100 μL of the cell suspension with an additional 65 μL of RPMI

was added to each well of a sterile 96-well white plate (Immunolon2, Dynex, Chantilly, VA, USA) which had been pre-blocked with 200 μL of 1% PBS-BSA per well and stored overnight at 4 °C. The blocking buffer was removed by pipetting prior to cell addition. Cells were incubated at 30 °C for 30 mins and then selected cells were primed with either 10 μL of control primer (IFN-α) or experimental primer (Ti oxide as nanoparticles or micron sized metallic particles) (Table 7.2). At 1hr, incubated primed and unprimed cells were subsequently stimulated with 25 μL of either RPMI, Ops *Sa, FN* or PMA (Appendix II). All samples were run in quadruplicate and cells were incubated for an additional 2 hrs at 30 °C. Following incubation (pre-primed, primed and after stimulation period), to separate extruded NET-DNA from the cellular debris, 15 μL of MNase (LS004797 Worthington Biochemical Corporation, Lakewood, NJ, USA) was added to each well and left at room temperature for 20 mins. The plate was then centrifuged at 1800 rcf for 10 mins and 150 μL of the supernatant containing the separated extracellular NET-DNA was then transferred to 96-well black micro-plates (3915; Corning, Lowell, MA, USA) containing 15 μL of 10 μM SYTOX® Green in PBS (S7020; Invitrogen, Paisley, UK) per well. Over a period of 5 mins fluorometric measurements were acquired five times for each well in order to quantify the NET-DNA release. The total fluorescence from each well was measured at 37 °C and recorded in arbitrary fluorescent units (AFU) using a Twinkle LB970 (Berthold Technologies, Germany) with excitation/emission filter wavelengths of 485/525 nm, respectively. The experiment was repeated twelve times with neutrophils sourced from different healthy volunteers.

7.3.6 *Ex-vivo* imaging of cellular interactions of neutrophils co-stimulated with Ti nanoparticles and Ops *Sa* (IgG opsonised)

To investigate the cellular interactions of Ti species with Ops *Sa* (Fc-γR mediated), 700 µL of isolated neutrophils at a concentration of $1x10^5$ cells/mL were re-suspended in 175 µL of Ti oxide as rutile (~50 nm) dispersed in PBS at a concentration of 200 ppm (Table 2.1; section 2.2). The suspended cells in Ti rutile (~50 nm) were immediately stimulated with 175 µL of Ops *Sa* (IgG opsonised) and then incubated for 1hr at 37 °C. At 1 hr the co-stimulated cells were repeatedly (x10) centrifuged and washed in PBS. The suspension was immediately fixed with 2.5% glutaraldehyde (1hr) and then 1% osmium tetroxide (1hr). Post-fixation samples were dehydrated through a series of alcohol solutions (50-100%). After ethanol treatment, cells were embedded in propylene oxide resin. Thin sections were cut with a diamond knife-microtome and stained with 3% uranyl acetate and lead citrate. The sections were examined using a JEOL 1200 TEM.

7.3.7 Statistical analysis

Statistics were performed using SPSS 20 software. The data were initially explored for normality using a Shapiro-Wilk test at a 95% significance level. Comparison between individual group means was performed using Wilcoxon Sign Rank tests at a 95% significance level.

7.4 RESULTS

7.4.1 *Ex-vivo* chemiluminescence quantification of ROS release from primed and/or unprimed neutrophils

Chemiluminescence measurements of ROS release from unprimed and primed neutrophils sourced from 12 different healthy volunteers at 2 hrs following stimulation with periodontal pathogens (Ops *Sa* and *FN*) is presented in the form of Box/Whisker plots (median, inter-quartile range, 10^{th} and 90^{th} percentiles and outliers) (Figure 7.1). The plots demonstrate the maximum RLU at 2 hrs against the condition (unprimed and/or primed) and stimulus employed.

The chemiluminescence data was explored using the Shapiro-Wilk test at a 95% significance level where the data was identified to be not normally distributed (Figure 7.1). Pair-wise comparisons using Wilcoxon Sign rank tests demonstrated that all unprimed and/or primed cells exposed to periodontal pathogens resulted in significantly increased total and extracellular ROS release in comparison with cells exposed to the negative control stimulus (PBS) ($P<0.005$ for each comparison) (Figure 7.1).

No significant difference in the magnitude of total and extracellular ROS production was observed between unprimed cells exposed to either Ops *Sa* or *FN* (positive controls) ($P=0.94$) (Figure 7.1). Similarly, no significant difference in the magnitude of total and extracellular ROS production was observed between IFN-α primed cells exposed to Ops *Sa* or *FN* (control primer) ($P>0.05$) (Figure 7.1). A significantly increased magnitude in total ROS production was observed

when IFN-α primed cells exposed to Ops *Sa* when compared with unprimed cells exposed to the same stimulus (P=0.01) (Figure 7.1a). In contrast, no significant difference in extracellular ROS production was observed when IFN-α primed cells exposed to Ops *Sa* when compared with unprimed cells exposed to the same stimulus (P=0.07) (Figure 7.1b). However, IFN-α primed cells exposed to *FN* exhibited no significant change in total or extracellular ROS release when compared with unprimed cells (P>0.05) (Figure 7.1).

Cells primed with anatase (~30 nm) or rutile (~50 nm) resulted in significantly decreased total and extracellular ROS production when compared with IFN-α primed cells and unprimed cells when stimulated with Ops *Sa* (P<0.05) (Figure 7.1). In contrast, no significant difference in ROS production was observed between anatase (~30 nm) or rutile (~50 nm) primed cells when compared with IFN-α primed cells and unprimed cells exposed to *FN* (P>0.05) (Figure 7.1).

Figure 7.1 Box/Whisker plots demonstrating (a) total (luminol dependent) and (b) extracellular (isoluminol dependent) ROS production of unprimed and/or primed neutrophils. Scales are not common for plots displayed

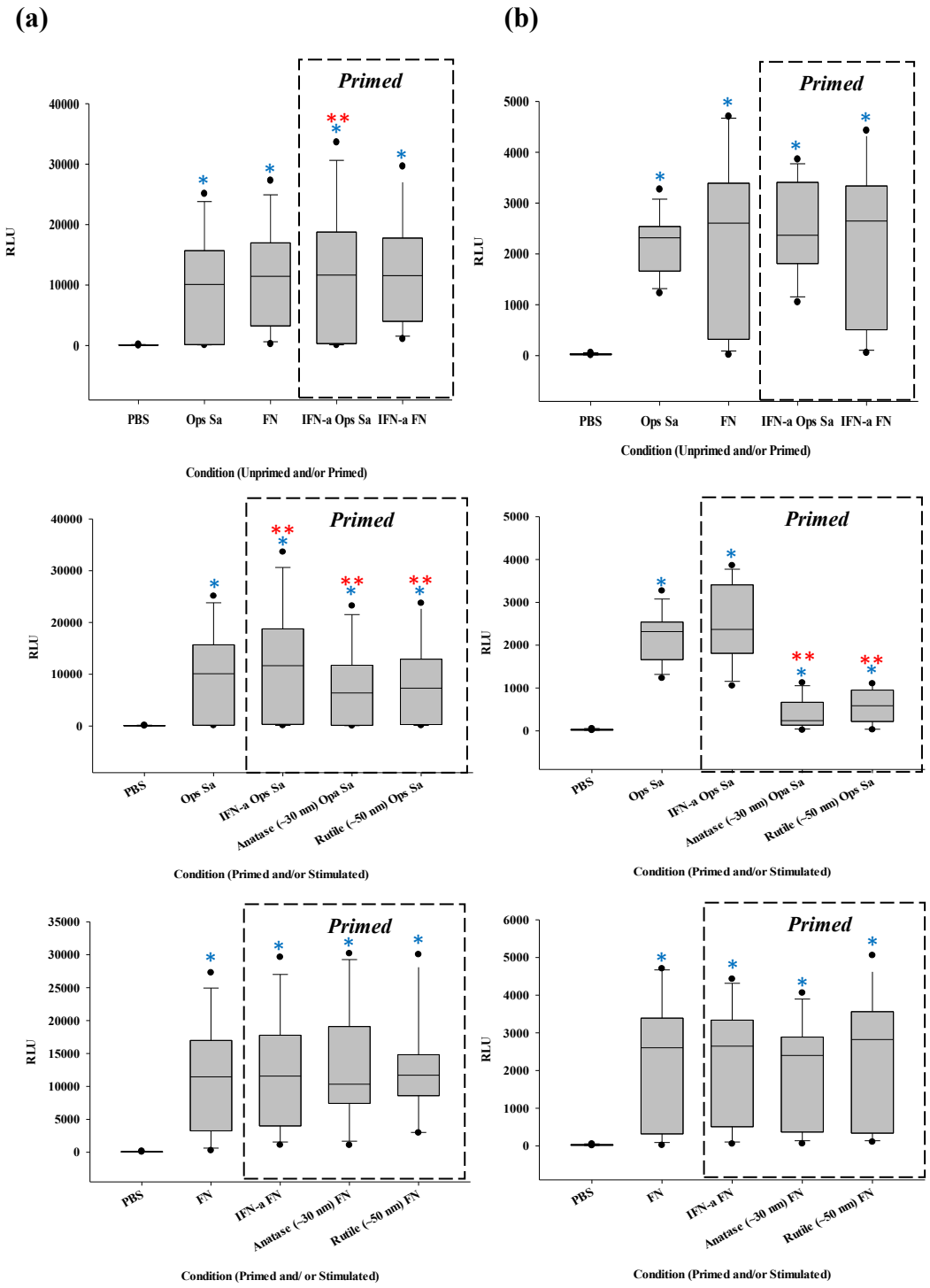

7.4.2 Quantification of ROS release from neutrophils co-stimulated with Ti and Ops *Sa* (IgG opsonised) with unprimed or primed neutrophils

To further help determine whether Ti implant derivatives mediate an Fc-γR mediated pathway, neutrophil ROS release was measured from 13 different healthy volunteers where selected cells have been either (i) unprimed but exposed to either PBS, Ops *Sa*, *FN* or Ti (rutile and metallic) (controls) (ii) primed with Ti (rutile or metallic) or IFN-α then stimulated with Ops *Sa* and/or (iii) co-stimulated with Ti (rutile or metallic) and Ops *Sa* (IgG opsonised) together. Data is presented in the form of Box/Whisker plots demonstrating maximum RLU at 2 hrs against condition (unprimed, primed and/or co-stimulated) employed (Figure 7.2).

The chemiluminescence data was explored using the Shapiro-Wilk test at a 95% significance level where the data was identified to be not normally distributed (Figure 7.2). Pair-wise comparisons using Wilcoxon Sign rank tests demonstrated that all tested conditions (co-stimulated, primed and/or unprimed cells) resulted in significantly increased total and extracellular ROS release in comparison with unprimed cells exposed to PBS ($P<0.002$ for each comparison) (Figure 7.2).

A similar pattern of total and extracellular ROS production was observed for cells unprimed and primed with either IFN-α or Ti oxide as rutile (~50 nm) as detailed in sections 5.4.3 and 7.4.1 respectively. In addition, cells primed with metallic Ti (~5 μm) then stimulated with Ops *Sa* resulted in a significantly lower magnitude of ROS production when compared with IFN-α primed cells and unprimed cells exposed to the same stimulus ($P<0.002$ for each comparison) (Figure 7.2).

The highest magnitude of ROS production was observed from cells co-stimulated with Ti oxide nanoparticles as rutile (~50 nm) and Ops *Sa* (IgG opsonised) together when compared to all other tested unprimed and primed cell conditions ($P<0.05$) (Figure 7.2). In contrast, ROS production from metallic Ti (~5 μm) and Ops *Sa* (IgG opsonised) co-stimulated cells were significantly reduced when compared with IFN-α primed and unprimed cells exposed to Ops *Sa* ($P<0.02$ for each comparison) (Figure 7.2). However, metallic Ti (~5 μm) and Ops *Sa* (IgG opsonised) co-stimulated cells resulted in significantly increased ROS release when compared with responses from unprimed cells exposed to metallic Ti (~5 μm) species and metallic Ti (~5 μm) primed cells exposed to Ops *Sa* ($P<0.004$) (Figure 7.2).

Figure 7.2 Box/Whisker plots demonstrating (a) total (luminol dependent) and (b) extracellular (isoluminol dependent) ROS production from neutrophils co-stimulated with Ti (rutile or metallic) and Ops *Sa* (IgG opsonised) together with unprimed or primed neutrophils. Scales are not common for plots displayed

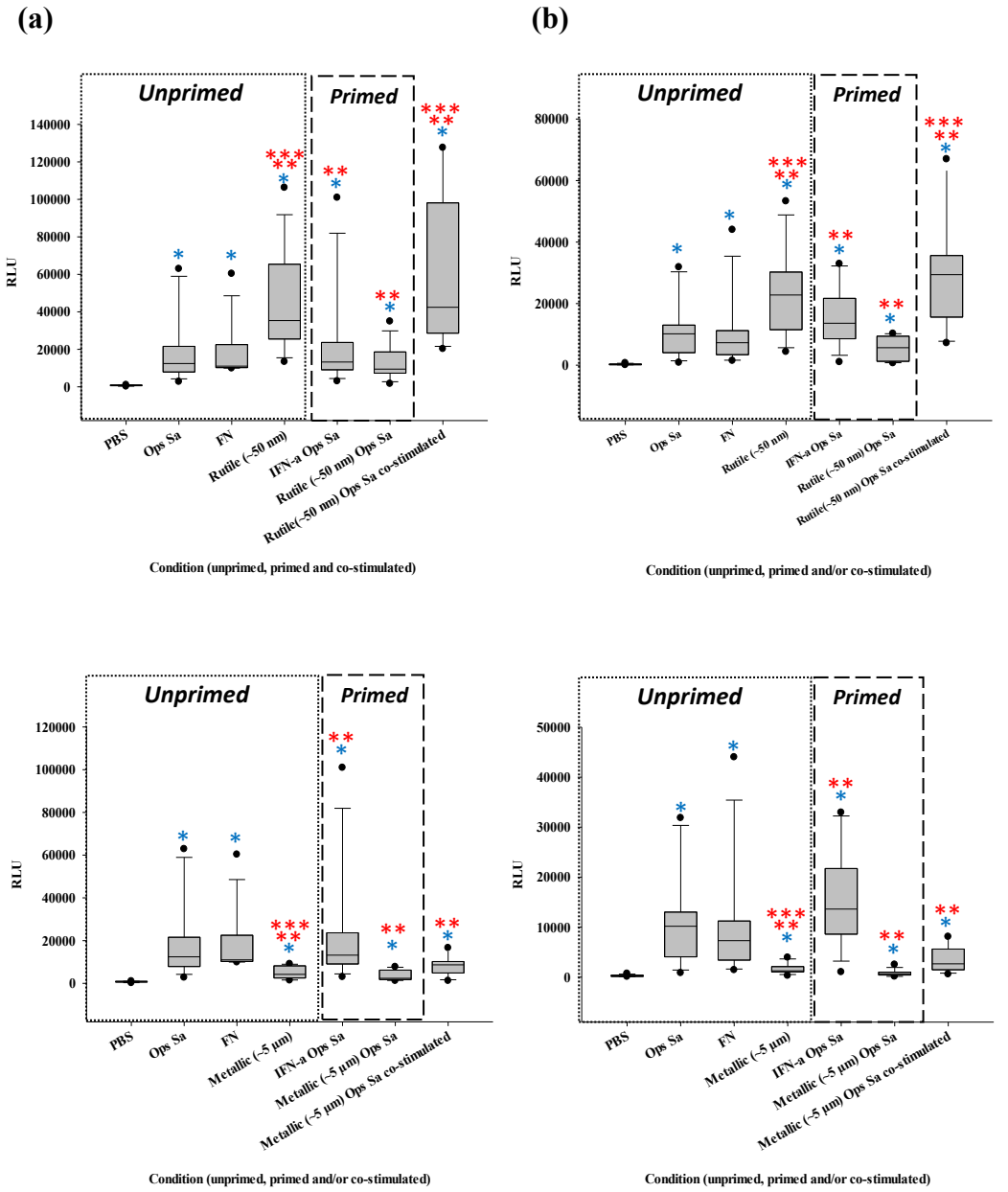

7.4.3 *Ex-vivo* fluorometric quantification of NET release from unprimed and primed neutrophils

Fluorometric measurements of extracellular NET-DNA release in the supernatant of unprimed and primed neutrophils sourced from 12 different volunteers exposed to periodontal pathogens (Ops *Sa* or *FN*) and physiological agonists (PMA) after a 3 hr incubation period in black wells was quantified in AFU (Figure 7.3). The fluorometric measurements are presented in the form of Box/Whisker plots demonstrating maximum AFU quantified against condition (unprimed and/or primed) employed.

The extracellular NET-DNA release data was explored using a Shapiro-Wilk test at a 95% significance level, which identified the data to be not normally distributed (Figure 7.3). Pair-wise comparisons using Wilcoxon-Sign Rank test demonstrated that all tested conditions (unprimed and primed) resulted in significantly increased NET formation when compared to the negative control RPMI ($P<0.004$ for each comparison) (Figures 7.3).

No significant difference in extracellular NET-DNA release was observed between unprimed cells exposed to Ops *Sa* or *FN* (positive controls) ($P=0.11$) and/or between IFN-α primed cells exposed to Ops *Sa* or *FN* (control primer) ($P=0.51$). In contrast, significantly increased NET release was observed for unprimed and IFN-α primed cells exposed to PMA when compared with unprimed and IFN-α primed cells exposed to Ops *Sa* or *FN* ($P=0.005$ for each comparison) (Figure 7.3).

Figure 7.3 Box/Whisker plots of extracellular NET-DNA release quantified in black wells after 3 hr incubation period for unprimed and primed neutrophils. Scales are not common for the plots displayed

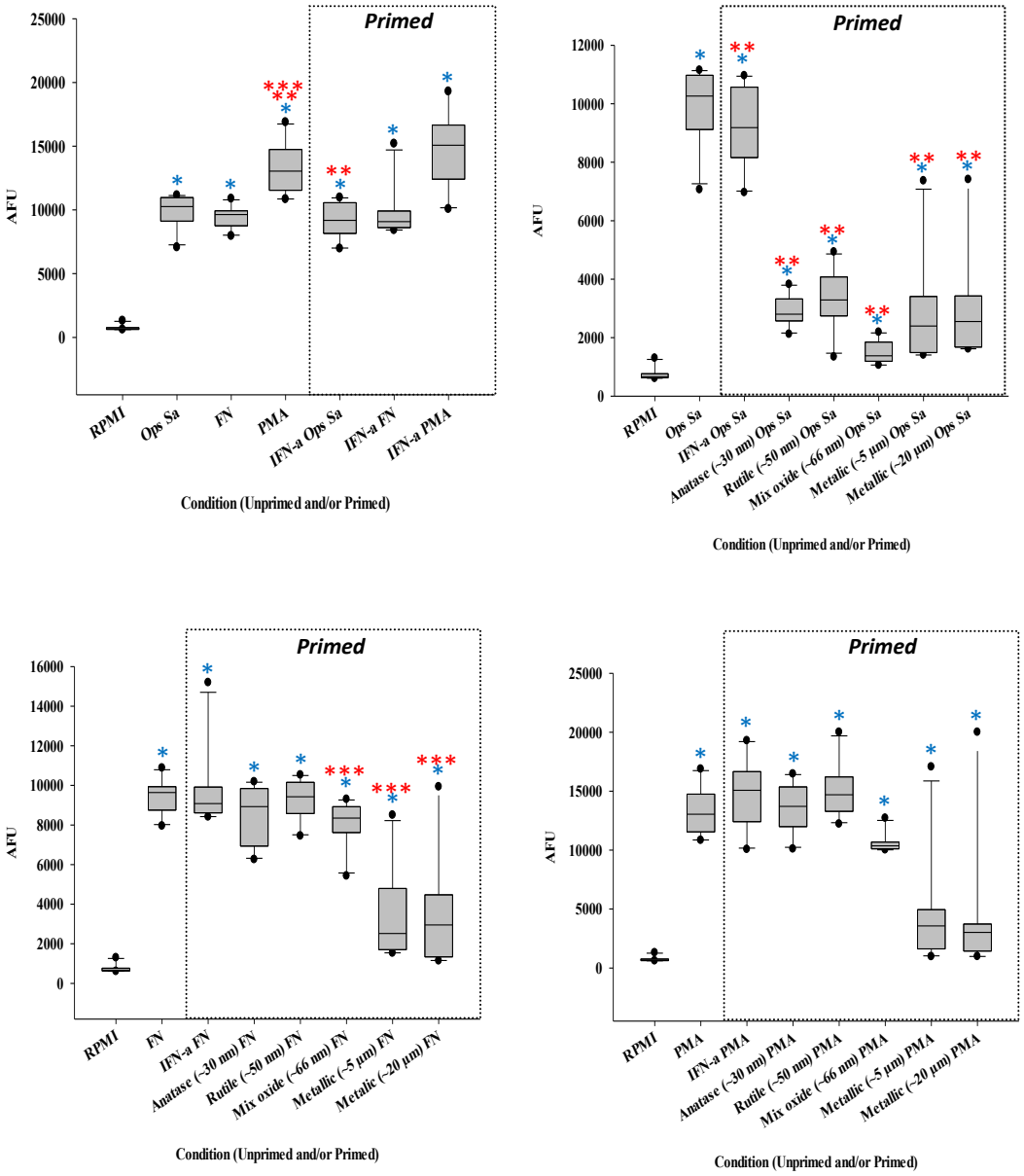

Significant different from PBS*
Significant different from OPS *Sa***
Significant different from *FN*****

IFN-α primed cells resulted in significantly decreased NET release when compared with unprimed cells when exposed to Ops *Sa* (P=0.007) (Figure 7.3). When cells were primed with Ti oxide as nanoparticles or micron sized metallic particles a significantly decreased extracellular NET-DNA release was observed when compared with unprimed and/or IFN-α primed cells exposed to Ops *Sa* (P=0.007 for each comparison) (Figure 7.3).

In contrast, no significant difference in NET production was observed between IFN-α primed cells and unprimed cells exposed to *FN* (P=0.88). In addition, no significant difference in NET production was observed between Ti oxide as nanoparticles primed cells when compared with unprimed and/or IFN-α primed cells exposed to *FN* (P>0.05). In contrast, Ti as micron sized metallic (~5 & 20 μm) primed cells resulted in significantly reduced NET release when compared with unprimed and/or IFN-α primed cells exposed to *FN* (P<0.007) (Figure 7.3).

The highest magnitude of extracellular NET-DNA release was observed from unprimed and primed cells exposed to PMA when compared to all other tested unprimed and primed cell conditions exposed to either Ops *Sa* or *FN* (Figure 7.3). However, no significant differences in NET release were observed between IFN-α primed cells when compared with unprimed cells exposed to PMA (P=0.05). In addition, no significant difference in NET production was observed between anatase (~30 nm) or rutile (~50 nm) primed cells exposed to PMA when compared with unprimed and/or IFN-α primed cells exposed to PMA (P>0.05). However, significant differences in NET production were observed for mix oxide

(~66 nm) and micron sized metallic (~5 & ~20 μm) primed cells exposed to PMA with compared with unprimed and/or IFN-α primed cells exposed to PMA ($P<0.009$ for each comparison) (Figure 7.3).

7.4.4 *Ex-vivo* imaging of cellular interactions of neutrophils co-stimulated with Ti nanoparticles and Ops *Sa* (IgG opsonised)

TEM was performed on neutrophils which had been co-stimulated for 1 hr with rutile (~50 nm) at a concentration of 200 ppm and Ops *Sa* (IgG opsonised) (Figure 7.4). The TEM images indicated cellular uptake of large numbers of *Sa*. The surface of the phagocytosed *Sa* were themselves associated with nanoparticles as agglomerates (black and white features) (Figure 7.4).

Figure 7.4 TEM image (JEOL 1200, Japan) acquired at 10,000 magnification of an isolated neutrophil post 1 hr co-stimulation with Ti oxide as rutile (~50 nm) dispersed in PBS at a concentration of 200 ppm and Ops *Sa* (IgG opsonised)

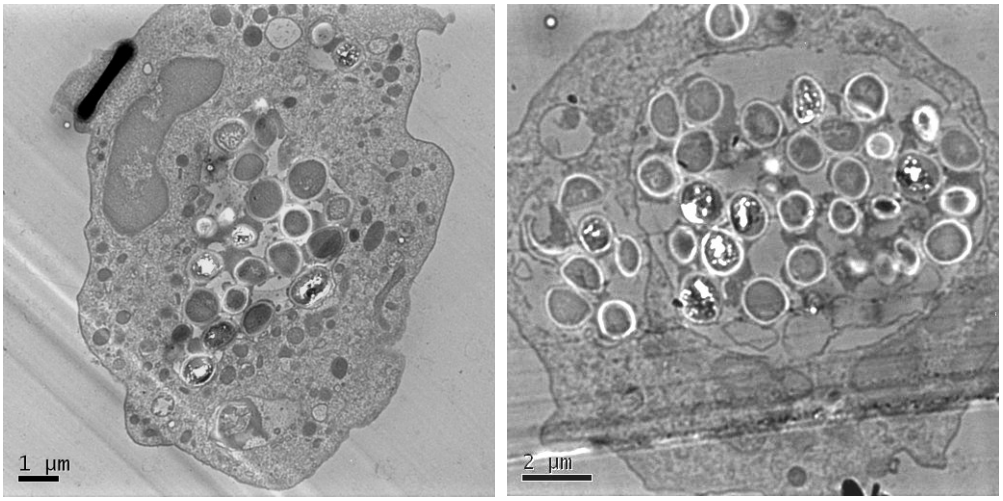

7.5 DISCUSSION

The capacity of Ti as oxide nanoparticles or micron sized metallic particles to modify neutrophil ROS and NET responses to periodontal pathogens has not been previously investigated. In peri-implant disease bacterial colonisation of the implant surface by pathogens including Ops *Sa* (gram positive) and *FN* (gram negative) are known to contribute to peri-implant inflammation (Remer et al., 2001 & Huzinga et al., 1997). The phagocytosis of Ops *Sa* and *FN* by human neutrophils involves Fc-γR and TLR-4 activation respectively and these pathways are well characterised. In the current study, findings were compared with a PMA stimulus which is a non-physiological diester responsible for enhancing inflammatory reactions (ROS and NET) via activation of Protein Kinase C (PKC). Previous studies on the priming of neutrophils have used IFN-α as control primer which has been shown to enhance ROS responses to periodontal pathogens (Ops *Sa* or *FN*).

Interestingly, Ti oxide primed neutrophils reduced ROS release when the cells were exposed to Ops *Sa* but did not affect responses to *FN*. Similarly, metallic Ti primed cells also reduced ROS release when the cells were exposed to Ops *Sa*. Differential inhibition of neutrophil ROS activity in Ti (oxide or metallic) primed neutrophils suggests specific effects on Fc-γR pathways whereas TLR-4 activation appeared to be unaffected. The inhibition of ROS activity may possibly result from Ti implant derivatives becoming associated with blocking Fc-γR sites which reduce the concentration of Fc-γR ligand interactions. The ROS activity was less inhibited when neutrophils were primed with the ~5 μm sized metallic Ti

particles when compared with oxide nanoparticles and the latter have been shown to have greater affinity for the cell surface membrane. The consequences of such modulation of ROS release will be a failure to induce an adequate inflammatory response to the pathogen. Decreased activity and reactivity of Ti (oxide or metallic) primed neutrophils to further respond to other inflammatory mediators needs further evaluation.

To further identify whether Ti implant derivatives modify ROS activity through Fc-γR activity, neutrophils were co-stimulated with Ti implant derivatives (oxide or metallic) and Ops *Sa*. The data demonstrated that co-stimulated cells exhibited the highest magnitude of ROS release which is contradictory to previous observations that Ti priming reduces the response to Ops *Sa*. This observation is possibly a consequence of exposing neutrophils with a stimulatory concentration of both Ops *Sa* and the Ti nanoparticles, in contrast to exposing the neutrophils to priming concentrations. Moreover, imaging of Ti and Ops *Sa* co-stimulated cells demonstrated a strong surface interaction of the *Sa* with the Ti nanoparticles and high levels of phagocytosis (Figure 7.4). The Ti surface association with Ops *Sa* may also cause masking or blocking of the surface opsonins and therefore a decrease in neutrophil activation but this was not observed.

A higher magnitude of ROS release was observed for metallic Ti (~5 μm) and Ops *Sa* co-stimulated cells when compared with ~5 μm metallic Ti primed cells exposed to Ops *Sa* and/or unprimed cells stimulated with ~5 μm metallic Ti conditions. However, the magnitude of ROS release was still observed to be less

than IFN-α primed and unprimed cells exposed to Ops *Sa* (Figure 7.2). This suggests that the effects are mediated by particle size. Differential responses are possibly a consequence of neutrophils co-activated by Ti implant derivatives and *Sa* behaving differently when compared with pre-activated cells exposed with Ti implant derivatives following subsequent exposure to Ops *Sa*. This suggests neutrophils exposed to Ti are activated and thus possess enhanced ROS release, in contrast to inactivated cells exposed to Ti. This observation was supported, in chapter 5 where phagocytosis and subsequent ROS production processes by neutrophils exposed to micron sized metallic Ti particles was demonstrated to be lower than nanoparticles.

As discussed in Chapter 6, the mechanism of NET release is dependent on the ROS release pathway. Therefore, the capacity of Ti implant derivatives (oxide or metallic) to possibly modify NET production in response to Ops *Sa* and *FN* was also investigated. Similar to the inhibition of ROS activity by Ti (oxide or metallic) primed neutrophils that was observed following exposure to Ops *Sa*, inhibition of NET release was also demonstrated upon exposure to the same stimuli. However, in contrast to the effects of priming on ROS release, priming with micron sized metallic Ti particles also reduced the magnitude of NET release to *FN*. This down regulation of NET release may possibly be attributed to cell death or decreased stimulatory activity which is consistent with the ROS release data.

In contrast, Ti (oxide or metallic) primed neutrophils exposed to PMA exhibited the highest orders of NET release. This enhanced activity of the cell is possibly as a consequence of the hydrophilic nature of PMA which by-passes cell surface membranes and therefore readily interacts with the cell which has already entered into a pre-activated state due to the exposure to Ti implant derivatives. Therefore, it may be concluded that the capacity of Ti (oxide or metallic) primed neutrophils to inhibit NET responses to periodontal pathogens or to enhance NET responses to PMA is dependent upon the Ti implant derivatives interaction with the surface receptors and the magnitude of the response is governed by the nature of the Ti stimulus.

7.6 CONCLUSION

These findings suggest that Ti (oxide or metallic) implant derivatives can modify the response of neutrophils to periodontal pathogens and pro-inflammatory molecules (PMA). The modification of the response involves to some extent the Fc-γR pathway which was differentially down-regulated by exposure to low levels of Ti (either as oxide or metallic particles). The consequence of the observations would be an inadequate response to certain periodontal pathogens, leading to their persistence in the tissues and inducing a perpetuation of the chronic inflammation.

CHAPTER 8

THE EFFECT OF TITANIUM IMPLANT DERIVATIVES ON NEUTROPHIL CHEMOTAXIS

8.1 PREFACE

This chapter explores the effect(s) of the exposure of selected Ti implant derivatives (oxide or metallic) on the chemotactic response of neutrophils using the Insall bridge chamber. To date, there are no studies which demonstrate whether Ti implant derivatives act as chemoattractants promoting neutrophil migration into the peri-implant tissues. Furthermore, it is currently not known whether neutrophil exposure to Ti implant derivatives modifies the cell's chemotactic behaviour. The chemotactic responses to Ti derivatives presented as oxide (rutile) (~50 nm) and as metallic (~5 μm) species were initially studied. The species were representative of products of mechanically assisted crevice corrosion (Ti as oxide nanoparticles) or larger debris generated through tribiological processes (micron sized metallic Ti). Subsequently, the chemotactic response of neutrophils previously exposed to Ti as rutile (~50 nm) and metallic (~5 μm) species to physiological chemoattractants fMLP (strong chemoattractant) and IL-8 (moderate chemoattractant) was investigated.

8.2 INTRODUCTION

8.2.1 Neutrophil motility

The migration of neutrophils into peri-implant tissues (Van Dyke, 1985) and their subsequent accumulation is a histological characteristic of peri-implant disease (Itakura et al., 2011 & Tong et al., 2012). Neutrophils have been demonstrated to migrate into pathological sites at speeds of up to 20 μm min^{-1} following chemoattractant gradient(s) which may include bacterial derived peptides such as N-Formyl-Methionyl-Leucyl-Phenylalanine (fMLP) (Witko-Sarsat et al., 2000); proteolytic fragments of the extracellular matrix (Senior et al., 1980) and chemokines such as Interleukin-8 (IL-8) (Leonard & Yoshimura, 1990).

Cell motility may be defined as chemotaxis or chemokinesis (Pfeffer, 1884). Chemotaxis is the directional migration of cells along a chemical concentration gradient (Zachariae, 1993 & Insall, 2010) which contributes to cell accumulation at specific sites (Devreotes and Zigmond, 1988). In contrast, chemokinesis is the random movement of cells (Wells, 2000) in response to an extracellular signal (Lippincott Schwartz, 2005 & Insall, 2010). Cell motility itself is governed by a complex series of cellular processes including cell protrusion/pseudopod formation, adhesion, de-adhesion and contraction of the cell (Muinonen-Martin et al., 2012). In neutrophils, motility is controlled by cell surface receptor activation which leads to the re-organisation of the actin cytoskeleton framework (Glogauer et al., 2000 & Ciccheti, 2002). Activated neutrophils undergo a sequence of structural changes (Zigmond, 1977 & Seveau et al., 2001) resulting in a polarised

morphology with a distinct actin rich front lamella and tail-like uropod at the dorsal end which forms an axis that is orientated in the field of the chemoattractant (Benard et al., 1999 & Larmonier et al., 2011). Chemoattractants induce F-actin polymerisation of the leading edge of the cell causing it to move directionally within the concentration gradient of the chemoattractant species (Larmonier et al., 2012).

8.2.2 Role of chemoattractants in cell motility

The speed, frequency and directionality of cell migration are influenced by the chemoattractant species (Lippincott-Schwartz, 2005). Neutrophils are understood to have multiple receptors for the recognition of chemoattractants (Wagner & Roth, 2000). One of the predominant chemotactic receptors expressed on the plasma membrane of a neutrophil (Edwards, 1994) is the 32-kDa heterotrimeric G-protein-coupled, pertussis-toxin-sensitive fMLP receptor (~50,000/cell) (Williams et al., 1977). This receptor recognises bacterial and mitochondrial proteins that are formylated at their amino terminal (De Nardin et al., 1991 & Ciccheti, 2002). Activation of the fMLP receptor stimulates multiple processes including degranulation, oxidative burst, cytoskeletal changes, priming for enhanced response to other activators in addition to chemotaxis (Wagner & Roth, 2000); fMLP being a potent chemoattractant. The most comprehensively studied neutrophil receptors are the chemokine receptors (mainly CXCR1 & CXCR2) for IL-8 (Premack & Schall, 1996). Chemokines are a group of approximately forty small proteins (6-15 KDa) (Nickel et al., 1999) with similar cysteinyl containing structures (Wagner & Roth, 2000). IL-8 also known as the neutrophil attractant

protein-1 (NAP-1) (Edwards, 1994) is an 8 KDa protein (Nickel et al., 1999) which is a moderately potent activator for neutrophils inducing chemotaxis (Wagner & Roth, 2000), exocytosis (Baggiolini & Clark-Lewis, 1992) and the respiratory burst (Guichard et al., 2005). It is expressed in neutrophils in response to lipopolysaccharides (LPS) (Edwards, 1994), inflammatory cytokines (e.g. TNF-α & IL-1) (Deforge et al., 1992) and after exposure to priming agents such as granulocyte macrophage colony-stimulating factor (GM-CSF) (Witko-Sarsat, 2000).

8.2.3 Parameters influencing the outcome of the chemotactic response and its implications for inflammation

In the absence of inflammation, neutrophils are partitioned in the bloodstream (Witko-Sarsat, 2000). However, at sites of tissue inflammation and infection, an array of inflammatory mediators (e.g. IL-8, IFN-α, TNF-α) behave as either attractants or repellents and act to regulate neutrophil chemotaxis (Herlihy et al., 2013). The cell's *speed* (a measure of random movement in any direction), *velocity* (speed in a consistent direction towards or away from the inflammatory mediator) and the *chemotactic index* (the accuracy of migration measured as the angled movement in the direction of the chemoattractant) are three important parameters involved in predicting the outcome of the chemotactic response to the inflammatory mediator (Sapey et al., 2011). Moreover, the ability of the cell to migrate and the *speed* of migration are dependent upon the availability of cell surface receptors and their attachment to the chemoattractant (Lippincott-Schwartz, 2005). This in turn depends on the concentration of the ligand, the

concentration of the ligand receptor and the ligand receptor binding affinity (Palecek et al., 1997).

In certain cases, the magnitude of the chemotactic response of the cell may be slow and/or repulsive (restricted or away) to a specific inflammatory mediator which consequently inhibits cell migration and accumulation in the tissues (Herlihy et al., 2013). The inhibition of the neutrophil chemotactic response at inflamed tissue sites by chemorepellents promotes pathological tissue damage and delays the inflammatory resolution processes (Brubaker et al., 2013). Likewise, an excessively increased and/or directed cell movement towards the inflammatory mediator may also contribute to the perpetuation of the inflammatory response. This may lead to tissue destruction via oxidative damage and the release of proteases (Larmonier et al., 2011) due to the disproportionate accumulation of neutrophils at the inflamed site. Therefore, it is useful to measure the magnitude of a cell's chemotactic response (*speed*, *velocity* and *chemotactic index*) to determine potential implications for inflammation. This functional assay would provide greater insights into the expected impacts from the stimulation of the NADPH oxidase complex by Ti implant derivatives.

8.2.4 Cell motility assays

In-vivo techniques for direct observation of cell locomotion in humans and animals have been reported, however these sophisticated microscopy techniques are technically challenging, expensive and often lack reproducibility (Condeelis & Segall, 2003, Cavanagh & Weninger, 2008 & Tong et al., 2012). As a result, a

number of *in-vitro* cell motility assays have been developed to investigate biological cell migration mechanism(s). The Insall chamber (Insall, 2010) is a novel but well characterised method developed for direct and real-time visualisation of both population scale and single cell chemotaxis behaviour at a high resolution (Muinonen-Martin et al., 2012 & Tong et al., 2012). The device is simple, inexpensive to fabricate and allows reproducible measurements. Most importantly, these bridge shaped chambers allow chemotaxis to be accurately distinguished from (random) chemokinesis behaviour (Muinonen-Martin et al., 2012).

8.2.5 The Insall bridge chamber geometrical design and assay principle

The Insall chamber (Insall, 2010) consists of a square closed central chamber separated from a square outer chamber by two bridges on opposite sides (Figure 8.1). The outer chamber is utilised as a chemoattractant reservoir where direct administration of the chemoattractant is conducted (indicated by red arrows on Figure 8.1) (Muinonen-Martin et al., 2012 & Tong et al., 2012). The bridges measure 3 mm in length with widths of 0.5 mm and 1 mm respectively. The narrow and wide bridges produce two different gradients of the chemoattractant within the one assay system (Figure 8.1) (Muinonen-Martin et al., 2012).

Figure 8.1 Schematic representation of Insall bridge chamber

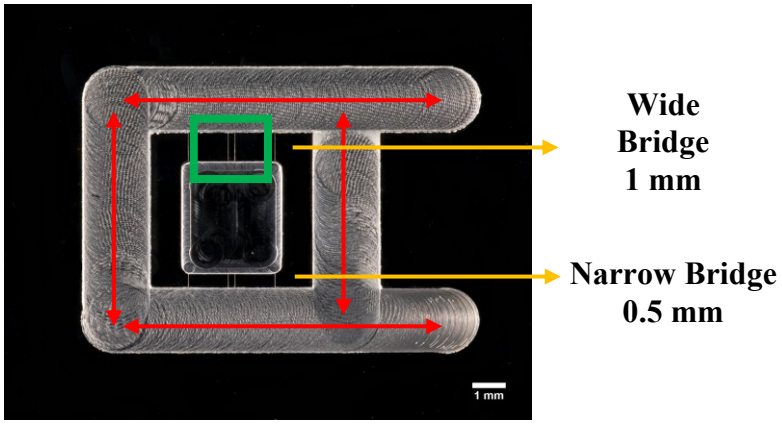

Cells are plated onto a glass cover slip which is then inverted over the central chamber leaving a small gap of 20-30 µm between the bridge and the cover slip (Insall, 2010). The gap is too small for fluid movement to occur, but large enough to allow diffusion of the chemoattractant (Figure 8.1) (Muinonen-Martin et al., 2012 & Tong et al., 2012). Cells centrally located on the wide bridge, between the outer and inner square chambers are then observed using an inverted time lapse microscope (indicated by green box on Figure 8.1) (Zigmond et al., 1998, Muinonen-Martin et al., 2012 & Tong et al., 2012) recording multiple image frames over the time course of the experiment.

8.3 METHODS

8.3.1 Preparation of neutrophils for chemotaxis assay

The chemotaxis assay was conducted within four hrs of neutrophil isolation (Appendix I). Isolated cells at a concentration of $1x10^6$ cells/mL were re-suspended in RPMI-1640 media and incubated at 37 °C and 5% CO_2 in a humidified atmosphere until use.

8.3.2 Cover slip preparation

22 mm x 22 mm (0.16-0.18 mm thick) cover slips were washed in 0.1 M HCl for 1 min followed by further washing with distilled water twice for 1 min each. The cover slips were then coated with 500 µL of 7.5% BSA for 2 min. Excess coating was carefully tipped off and replaced with 300 µL of the prepared cell suspension at 37 °C for 20 mins allowing cells to adhere to the cover slip.

8.3.3 Chemoattractant preparation

Control and experimental chemoattractants were prepared by adding high purity reagents to RPMI-1640. Table 8.1 demonstrates the working concentration of the prepared solution and final stimulation concentration once added to the experimental system.

Table 8.1 Chemoattractants used to induce chemotaxis

Chemoattractant	Supplier/Cat No.	Working Concentration	Stimulation Concentration
RPMI-1640	Sigma-Aldrich R0883	-	-
N-Formyl-Met-Leu-Phe (fMLP)	Sigma-Aldrich F3506	400 µg/mL	4 ng/mL
Interleukin-8 (IL-8)	Sigma-Aldrich SRP3098	200 ng/mL	10 ng/mL
Ti oxide-rutile (~50 nm)	Sigma-Aldrich 1317802	100 ppm	50 ppm
Metallic-Ti (~5 µm)	Prepared in house (section 2.2.2)	100 ppm	50 ppm

8.3.4 Insall chamber preparation

The inner and outer wells of the Insall chamber (Beatson Institute, Glasgow, UK) were washed three times with RPMI-1640 buffer followed by leaving a droplet of the buffer in the inner well to entirely cover the surface (Figure 8.1). The prepared cover slip with adherent cells was then inverted onto the prepared chamber so that cells were overlying the inner chamber and bridge areas avoiding air bubbles. Excess buffer was subsequently blotted from the edges of the cover slip taking care to avoid movement of the cover slip, which could result in shearing of the cells over the bridge. Fluid that had been displaced into the outer well was carefully removed using absorbent filter paper. 70 µL of a specified chemoattractant was then pipetted into the chemotactic reservoir (outer chamber) (Figure 8.1) developing a gradient across the bridge. The entire Insall chamber was then inverted and mounted onto a slide holder prior to time lapse microscopy. All measurements were conducted at 22 ± 1 °C. The assay was repeated three

times for each chemoattractant where neutrophils were sourced from different donors each time.

8.3.5 Time lapse microscopy

A Nikon TE2000-E (TE2000-E, Japan) inverted time lapse microscope was used to capture images. The microscope was configured with an auto-focus to ensure the quality of the image. Overlapping images across an area at the mid-point of the width of the bridge were captured using an x20 objective. Images were acquired every 10 secs for up to 20 mins.

8.3.6 Preparation of Ti pre-treated neutrophils for chemotaxis assay

To determine if Ti implant derivatives modify neutrophil 'chemotactic behaviour', a further set of 600 µL of isolated cells (Appendix I) at a concentration of $1x10^6$ cells/mL suspended in RPMI-1640 were pre-treated with 150 µL of Ti as oxide-rutile (~50 nm) or metallic (~5 µm) species at a concentration of 50 ppm. The pre-treated cells were incubated at 37 ^oC and 5% CO_2 in a humidified atmosphere for 20 mins prior to exposure to known chemoattractants including RPMI (negative control), fMLP and IL-8 (section 8.3.3) using the Insall chamber. The experiment was repeated three times with neutrophils isolated from different healthy donors. Cell from each donor were used for all aspects of the experiment i.e. were exposed to all three chemoattractants.

8.3.7 Cell tracking and quantitative data analysis

The manual tracking plug-in for Image J was used to track 15 individual cells migrating on the wider bridge of the chamber within the overlapping fields of view created by the time-lapse images. In addition, the chemotaxis plug-in was quantified using MATLAB (MathWorks, Natick, MA, USA) to analyse cell behaviour. The magnitude of a cell's chemotactic response including *speed*, *velocity* and *chemotactic index* (Table 8.2) were calculated as a measure of shift in the cosine θ angle (Figure 8.2) of a migrating cell.

Table 8.2 Dynamic parameters calculated

Chemotaxis Parameter	Measure of	Formula	Units
***Speed* (Chemokinesis)**	$\frac{\text{total movement distance}}{\text{Time}}$	$\frac{\delta}{\text{Time}}$	$\mu m.min^{-1}$
***Velocity* (Chemotaxis)**	$\frac{\text{distance moved in the direction of the chemoattractant}}{\text{Time}}$	$\frac{\Delta\cos\theta}{\text{Time}}$	$\mu m.min^{-1}$
***Chemotactic Index* (Chemotactic accuracy)**	Extent of migration in the direction of the chemoattractant	$\Delta\cos\theta$	μm

Figure 8.2 The direction of neutrophil migration calculated as a measure of shift in the angle θ

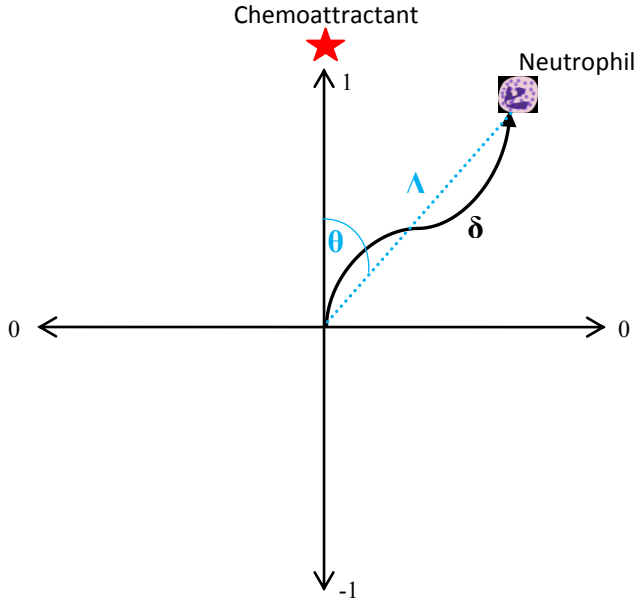

8.3.8 Statistical analysis

Wilcoxon Sign Rank test was conducted to determine whether the circular distribution of 45 tracked cells was random or non-random. Subsequently, a one-way analysis of variance (ANOVA) followed by post-hoc Tukey test were used to compare group means of *speed*, *velocity* and *chemotactic index* at a 95%

significance level. Statistics were performed using Graphpad Prism version 3.02 statistical software.

8.4 RESULTS

8.4.1 Change of neutrophil morphology in response to chemoattractants

Neutrophils go through a sequence of morphological changes following activation (Zigmond & Sullivan, 1979). Time lapse images taken every 10 secs for 20 mins were assessed at 10 mins to define the morphology of the cells. Positive control chemoattractants included fMLP (strong) and IL-8 (moderate) and a negative control chemoattractant as RPMI-1640. Experimental chemoattractants employed were Ti as rutile (oxide; ~50 nm) and metallic (~5 μm) species prepared as dispersions in RPMI-1640 at a concentration of 50 ppm.

RPMI exposed cells were round and spherical indicating the cells were not activated (Figure 8.3). In contrast, fMLP, IL-8 and Ti (oxide or metallic) species exposed cells acquired the morphology of a stimulated cell with the cell periphery becoming irregular exhibiting small membrane protrusions and retractions (Figure 8.3).

Figure 8.3 Morphology of human neutrophils at 10 mins post exposure to RPMI (negative control chemoattractant), fMLP or IL-8 (positive control chemoattractants) and Ti implant derivatives (experimental chemoattractants)

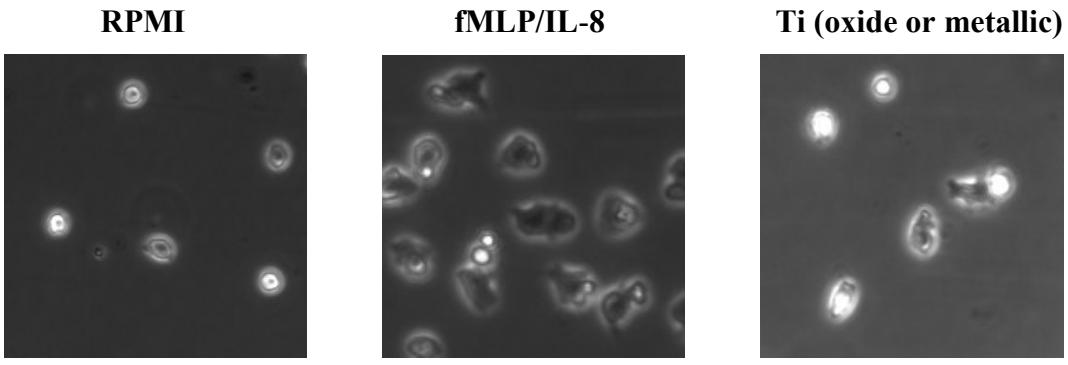

8.4.2 Modulation of induced neutrophil direction of movement in response to the chemoattractants

Cell tracks of 15 individual cells migrating on the central area of the wider (1.0 mm) bridge of the chamber (indicated by green box on Figure 8.1) were assessed to determine the directional migration of neutrophils to the chemoattractants employed (section 8.3.4). Data is presented in the form of spider plots which indicate the paths of 15 individual cells (Figure 8.4).

The spider plot of RPMI (negative control chemoattractant) exposed cells indicated none or minimal migration (Figure 8.4). In contrast, spider plots of cells exposed to fMLP and IL-8 (positive control chemoattractants) exhibited directional (upwards) movement towards the chemoattractant gradient (Figure 8.4). Notably, cells migrating to fMLP chemoattractant exhibited increased movement when compared with IL-8 moving a distance of between 80 and 100 μm (towards the chemoattractant gradient) for fMLP within the 20 min measured assay time compared with <80 μm for IL-8 (Figure 8.4).

Spider plot of cells exposed to Ti as rutile (oxide; ~50 nm) and metallic (~5μm) species (experimental chemoattractants) at a concentration of 50 ppm exhibited no significant directional migration (Figure 8.4). Ti implant derivatives (oxide or metallic) exhibited none or limited chemoattractant properties.

Figure 8.4 Spider plots indicating individual cell paths to chemoattractants including RPMI, fMLP, IL-8 and Ti oxide as rutile (~50 nm) and metallic (~5 µm) species at concentration of 50 ppm dispersed in RPMI-1640

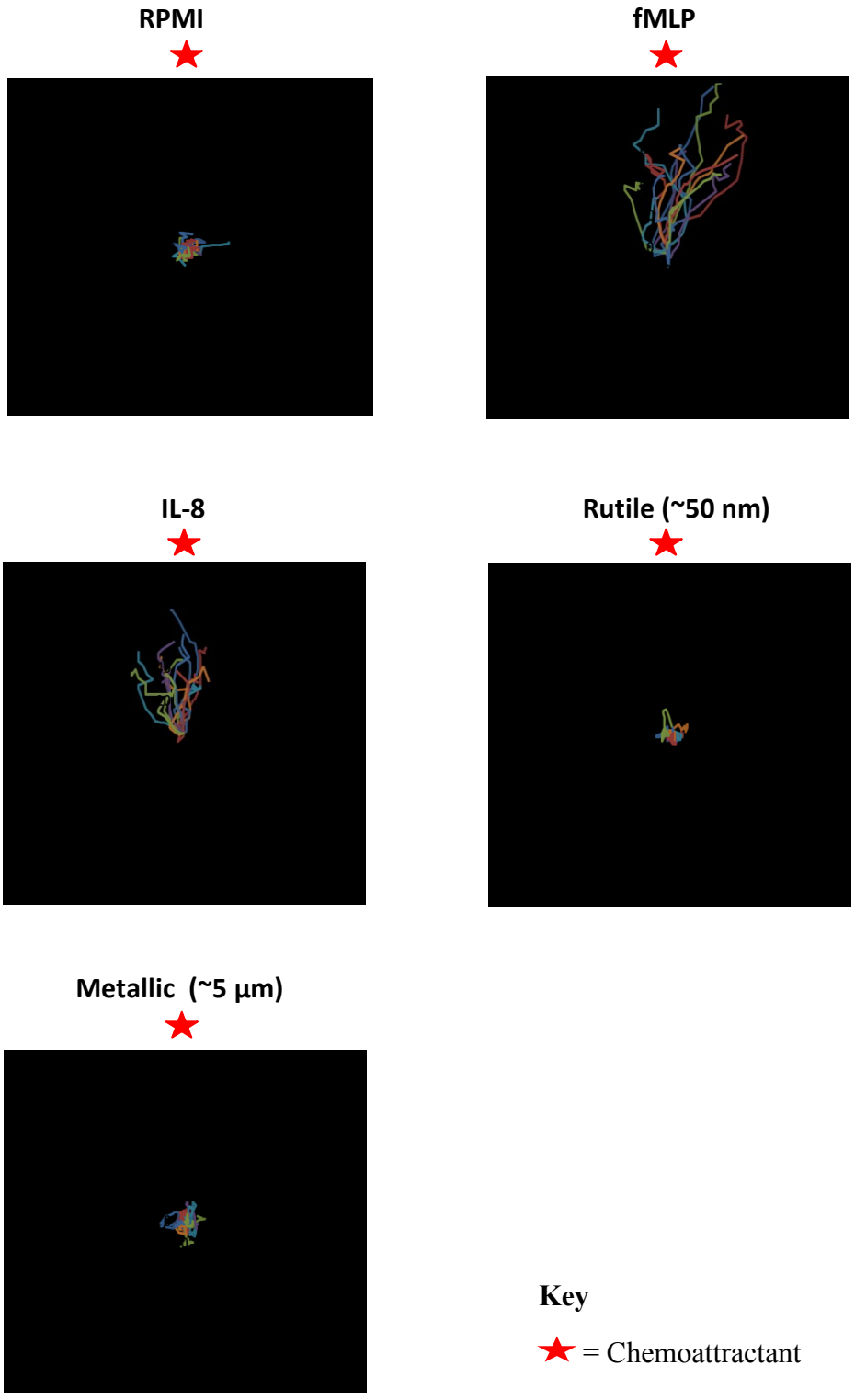

8.4.3 Modulation of the direction and magnitude of the chemotactic response induced by neutrophils in response to the chemoattractants

Quantification of the chemotactic response was performed and displayed as rose plots (Figures 8.5 & 8.6). Rose plots use end point data to plot points on a unit circle showing a red line indicating the direction and magnitude of the mean resultant vector (Figure 8.5 & 8.6; Left) and angular histograms associated with the trajectories (Figure 8.5 & 8.6; Right). Circles dotted on the edge of the circle represent the 45 individual cells tracked (Figures 8.5 & 8.6; Left). The dotted blue lines from the centre of the circle represent the confidence intervals (Figures 8.5 & 8.6; Left).

The mean resultant vector length of cells exposed to RPMI was of a low magnitude (0.2556) with wide 95% confidence intervals consistent with the random movement of cells (Figure 8.5; Left). The evidence for non-directed migration was further supported by a Wilcoxon Sign Rank test for non-random movement ($P>0.05$) (Figure 8.5). In comparison to RPMI exposed cells, the mean resultant vector length for fMLP and IL-8 was increased to 0.8988 and 0.9183, respectively with corresponding narrow 95% confidence intervals in the direction of the chemoattractants (Figure 8.5). The evidence for directed migration of cells to fMLP and IL-8 chemoattractants was supported by a significant Wilcoxon Sign Rank test ($P=0.001$) respectively, demonstrating cell chemotaxis (directed migration) towards the chemoattractant gradient (Figure 8.5).

Figure 8.5 Rose plots quantifying the neutrophil chemotactic response to chemoattractants including RPMI, fMLP and IL-8

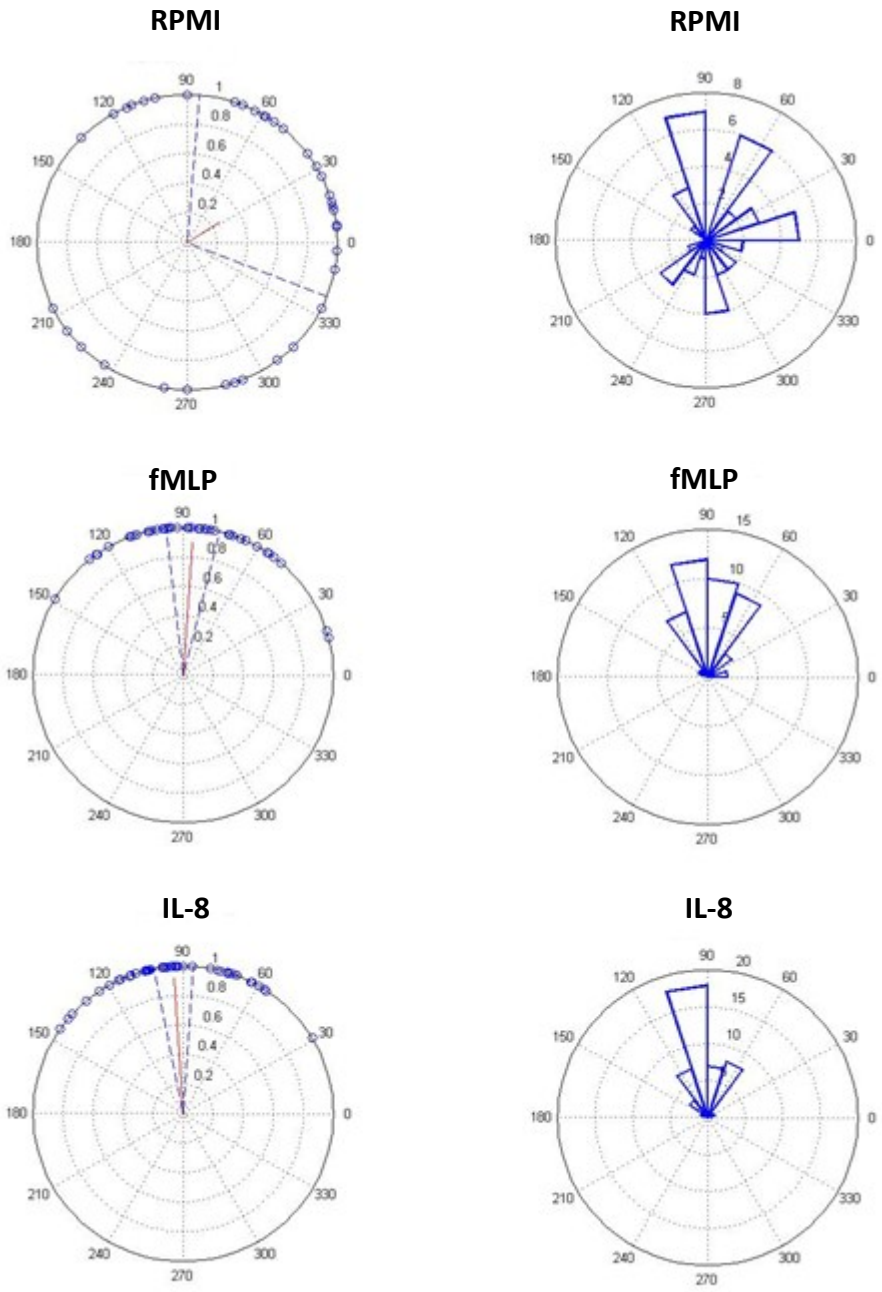

Chemoattractant was situated at 90^{o}, uppermost point in the rose plots.

When Ti oxide as rutile (~50 nm) and metallic (~5 μm) species at a concentration of 50 ppm were used as experimental chemoattractants, the mean resultant vector lengths were 0.2263 and 0.2481 respectively (Figure 8.6). The magnitude of the mean resultant vector length for Ti (oxide or metallic) species was significantly decreased when compared with fMLP and IL-8 (positive control chemoattractants) ($P<0.05$) (Figure 8.5) but similar to RPMI (negative control chemoattractant). The rose plot of rutile (~50 nm) as a chemoattractant indicated wide 95% confidence intervals and the predominant direction was in the opposite direction of the chemoattractant gradient (Figure 8.6). The apparent repulsive behaviour exhibited by cells when Ti-rutile (~50 nm) was used as a chemoattractant was supported by a significant Wilcoxon Sign Rank test ($P=0.0091$) (Figure 8.6). The rose plot for the metallic (~5 μm) stimulus indicated a similar wide 95% confidence interval. No evidence for directed migration of cells to metallic (~5 μm) species was observed, confirmed by an insignificant Wilcoxon Sign Rank test ($P=0.07$) and resulting chemokinesis (from the uniform angular distribution of cells) (Figure 8.6).

Figure 8.6 Rose plots quantifying the neutrophil chemotactic response to Ti oxide as rutile (~50 nm) and metallic (~5 µm) species at concentration of 50 ppm dispersed in RPMI-1640

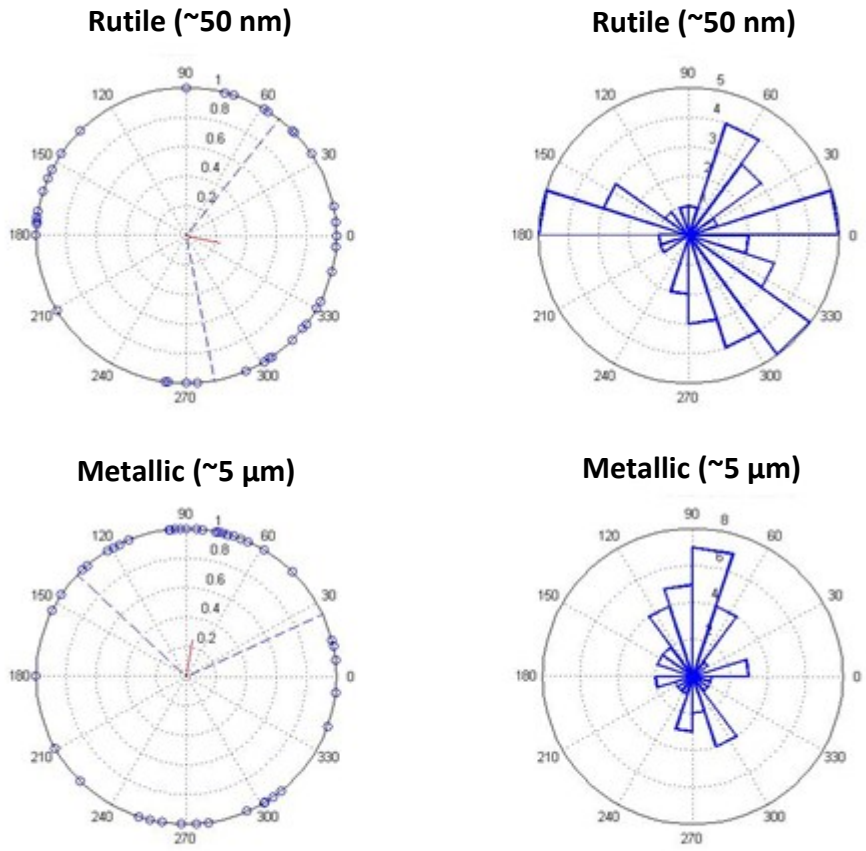

Chemoattractant was situated at 90^{o}, uppermost point in the rose plots.

8.4.4 Modulation of direction induced by Ti pre-treated neutrophils in response to known chemoattractants

The chemotactic response of neutrophils pre-exposed to Ti as rutile (~50 nm) and metallic (~5 μm) species at a concentration of 50 ppm to known chemoattractants RPMI, fMLP and IL-8 was also investigated. Spider plots indicated minimal directional migration for Ti (rutile or metallic) pre-treated neutrophils toward the negative control chemoattractant gradient RPMI (Figure 8.7). However, directional migration was observed for Ti (rutile or metallic) pre-treated cells towards the chemoattractant gradients fMLP and IL-8 (Figure 8.7). Notably, Ti as rutile (~50 nm) and metallic (~5 μm) pre-treated cells travelled distances up to 100 μm and 200 μm, respectively towards the fMLP chemoattractant gradient (Figure 8.7) and this was significantly increased when compared to the untreated cells (Figure 8.4) ($P<0.005$). However, Ti as rutile (~50 nm) and metallic (~5 μm) pre-treated cells travelled <60 μm towards the IL-8 chemoattractant gradient (Figure 8.7) which was significantly less than untreated cells (Figure 8.4).

Figure 8.7 Spider plots indicating individual cell paths of pre-treated cells with Ti as rutile (~50 nm) and metallic (~5 µm) species at a concentration of 50 ppm dispersed in RPMI-1640 to known chemoattractants RPMI, fMLP and IL-8. Scales are not common between chemoattractants used

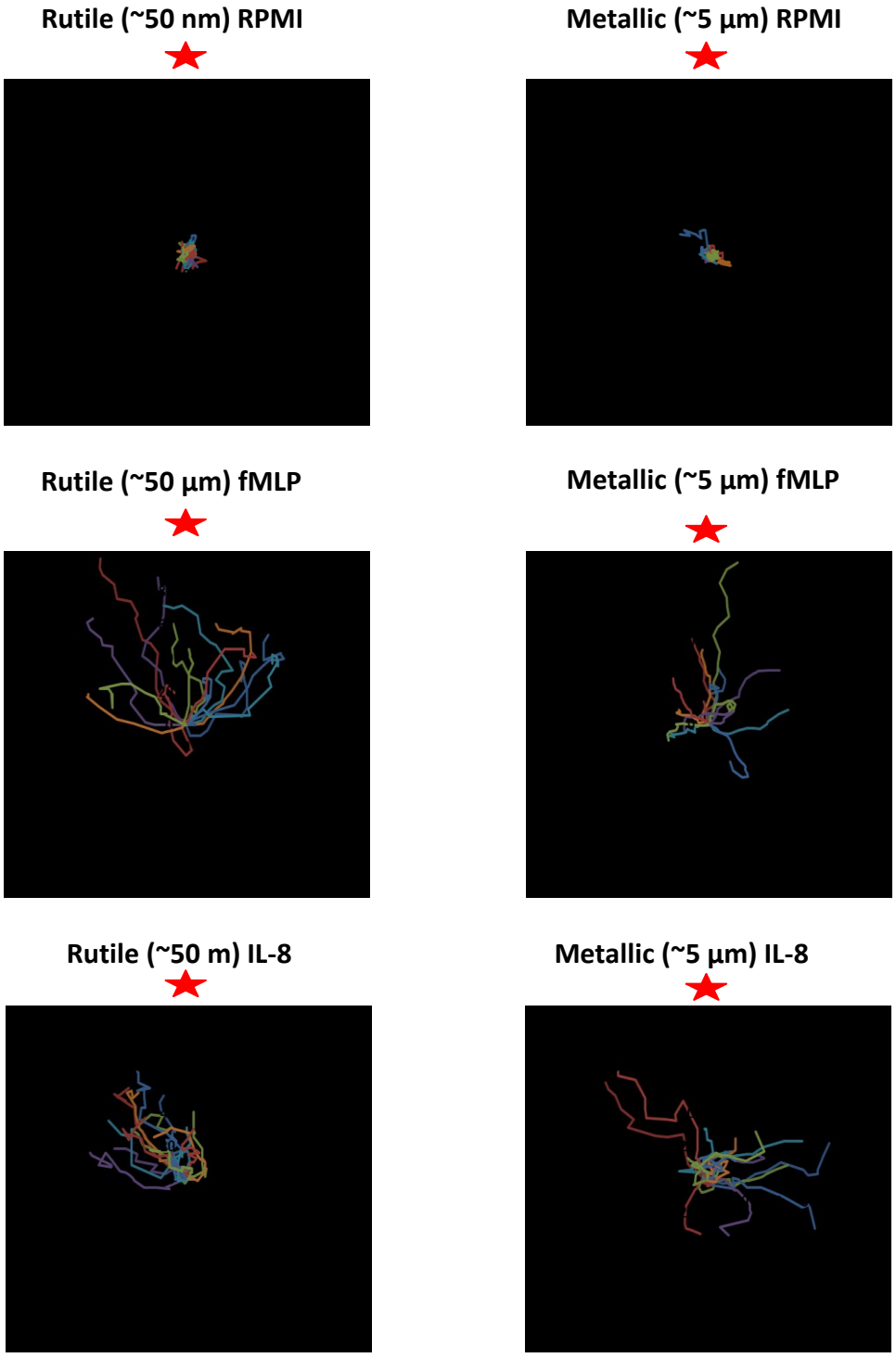

8.4.5 Modulation of the direction and magnitude of the chemotactic response induced by Ti pre-treated neutrophils in response to known chemoattractants

Analysis of chemotaxis using rose plots demonstrated that Ti (rutile or metallic) pre-exposed neutrophils were unaffected in their response to RPMI (Figure 8.8). Random movement was observed with a mean resultant vector length of 0.2790 (rutile; ~50 nm) and 0.2364 (metallic; ~5 µm) with wide 95% confidence intervals and little directionality towards the RPMI chemoattractant was shown (Figure 8.8).

Figure 8.8 Rose plots quantifying the chemotactic response of Ti oxide as rutile (~50 nm) and metallic (~5 µm) species of 50 ppm pre-treated cells in response RPMI chemoattractant

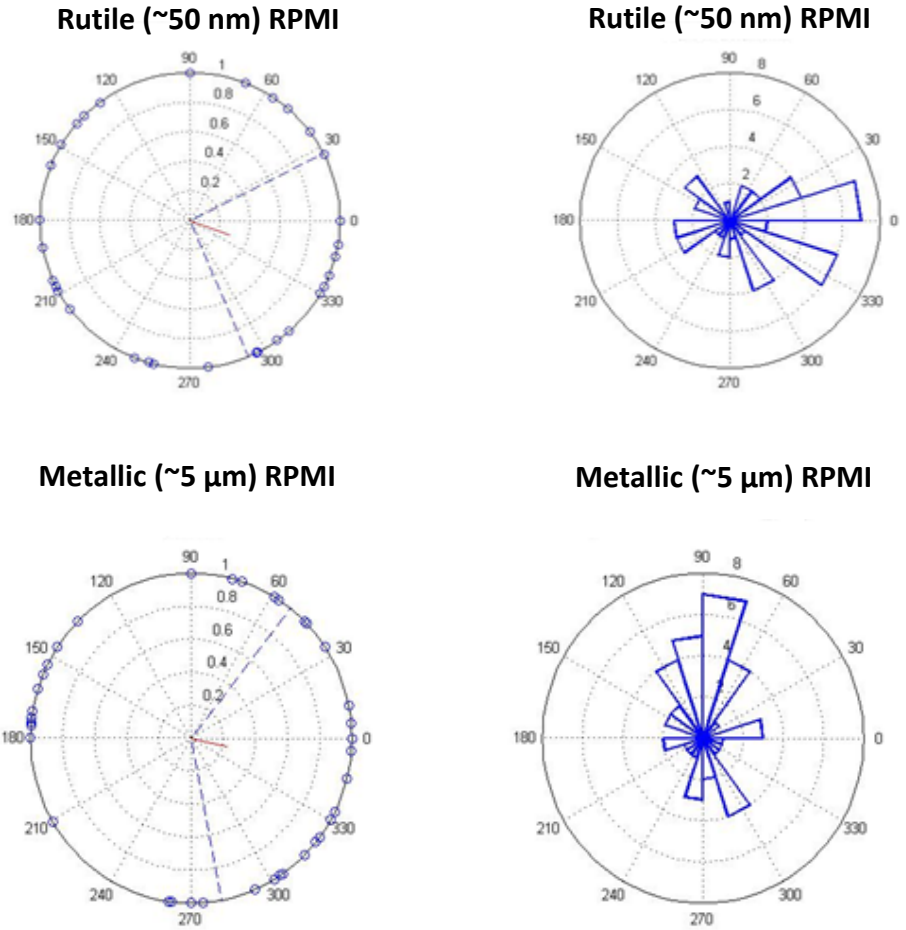

For cells pre-treated with rutile (~50 nm) at a concentration of 50 ppm and then exposed to chemoattractants fMLP and IL-8 (Figure 8.9), the magnitude of the mean resultant vector length of fMLP treated cells (0.6810) was reduced in comparison with IL-8 treated cells (0.7180) with a narrow 95% confidence interval in the direction of the chemoattractant gradient (Figure 8.9). Wilcoxon Sign Rank test demonstrated a significant chemotaxis behaviour for both fMLP and IL-8 chemoattractant ($P<0.001$).

Figure 8.9 Rose plots quantifying the chemotactic response of Ti oxide as rutile (~50 nm) of 50 ppm pre-treated cells in response to fMLP and IL-8 chemoattractants

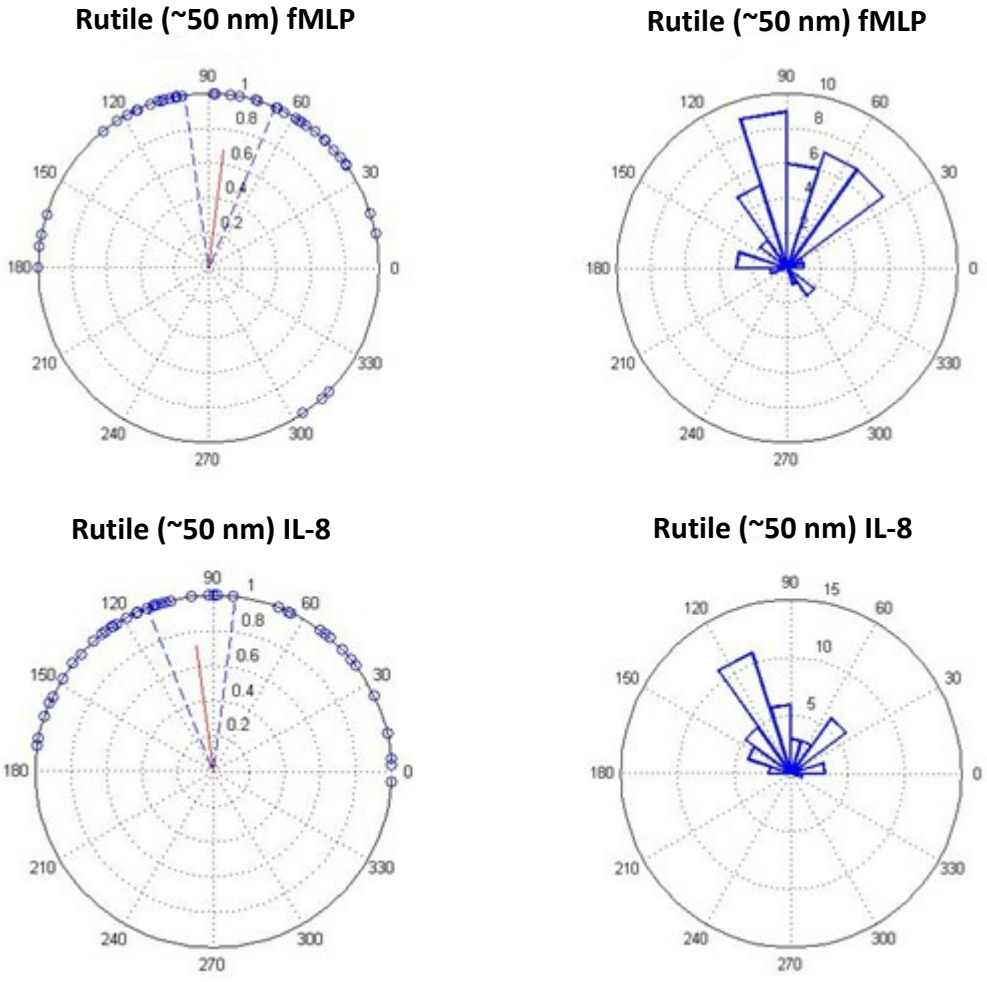

Rose plots for cells pre-treated with Ti-metallic (~5 μm) at a concentration of 50 ppm exposed to chemoattractants fMLP and IL-8 demonstrated modified behaviour (Figure 8.10). The magnitude of the mean resultant vector length of metallic fMLP treated cells (0.6593) was significantly increased in comparison with metallic IL-8 treated cells (0.3697) ($P<0.005$) (Figure 8.10). However, Ti-metallic fMLP treated cells exhibited a narrower 95% confidence interval in the direction of the fMLP chemoattractant when compared with Ti-metallic IL-8 (Figure 8.10). The evidence for Ti-metallic (~5 μm) pre-treated cells exhibiting chemotaxis (directed migration) to chemoattractants fMLP and IL-8 was supported by a significant Wilcoxon Sign Rank test ($P<0.002$).

Figure 8.10 Rose plots quantifying the chemotactic response of Ti-metallic (~5 µm) at 50 ppm pre-treated cells in response to fMLP and IL-8 chemoattractants

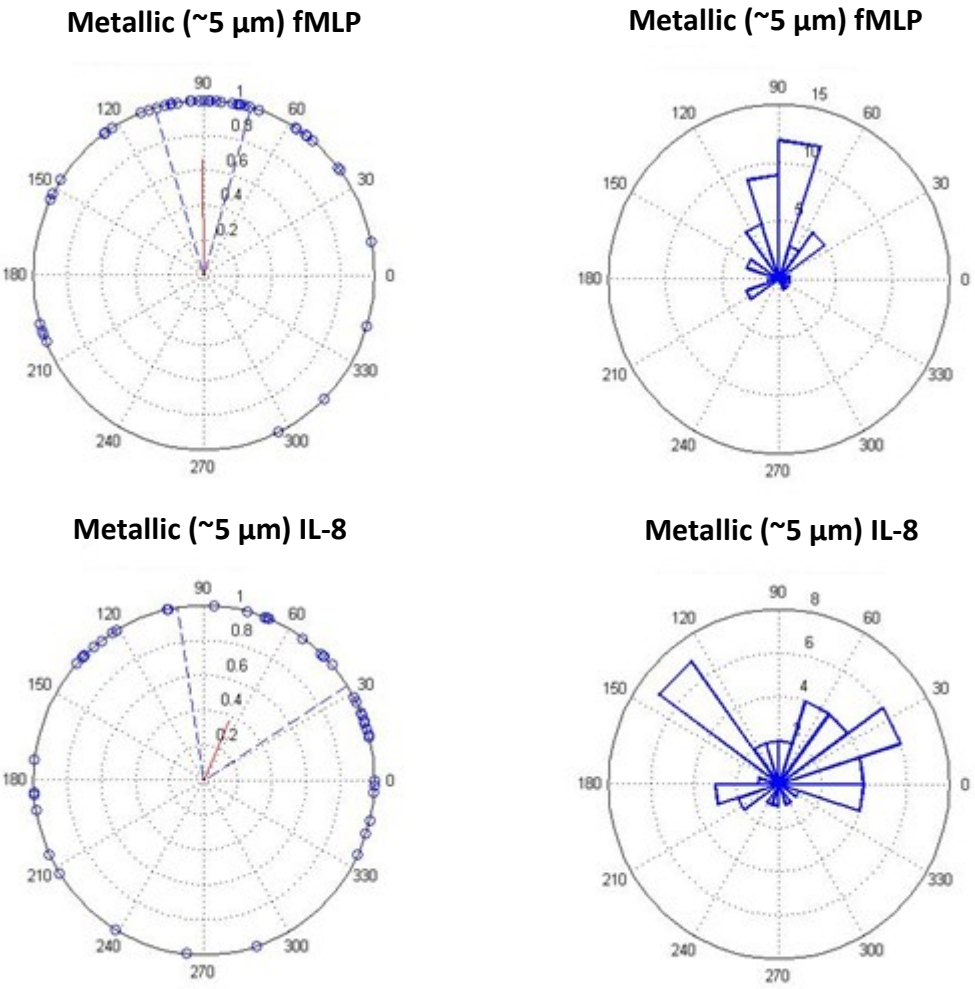

Chemoattractant was situated at 90^{o}, uppermost point in the rose plots.

8.4.6 Parameters including *speed*, *velocity* and *chemotactic index* influencing the outcome of the chemotactic response

The *speed* (Figure 8.11), *velocity* (Figure 8.12) and *chemotactic index* (Figure 8.13) are measurements of a cell's chemotactic response to the chemoattractants employed (Table 8.1). Data is presented in the form of box plots identifying the magnitude of the cells' chemotactic response on the y-axis vs. the chemoattractants employed on the x-axis [mean ± standard deviation (S.D) and full data range] (Figures 8.11-8.13).

The cell *speed* was significantly lowest following exposure to RPMI (negative control chemoattractant) for both untreated and Ti pre-treated cells ($P<0.05$) (Figure 8.11). For all other tested conditions including Ti (rutile; ~50 nm or metallic; ~5 µm) as the chemoattractant; fMLP & IL-8 (positive control chemoattractants) and Ti (rutile; ~50 nm or metallic; ~5 µm) pre-treated cells exposed to fMLP and IL-8, a significantly increased magnitude of cell *speed* was observed ($P<0.05$) (Figure 8.11). However, no significant difference in the magnitude of cell *speed* was observed between all tested conditions other than Ti-metallic pre-treated cells exposed to fMLP and IL-8 chemoattractants ($P<0.05$) (Figure 8.11). Pre-treatment of neutrophils with metallic particles (~5 µm) significantly increased *speed* in response to a positive chemoattractant when compared with all other stimulations.

Figure 8.11 Measure of cells' *speed*

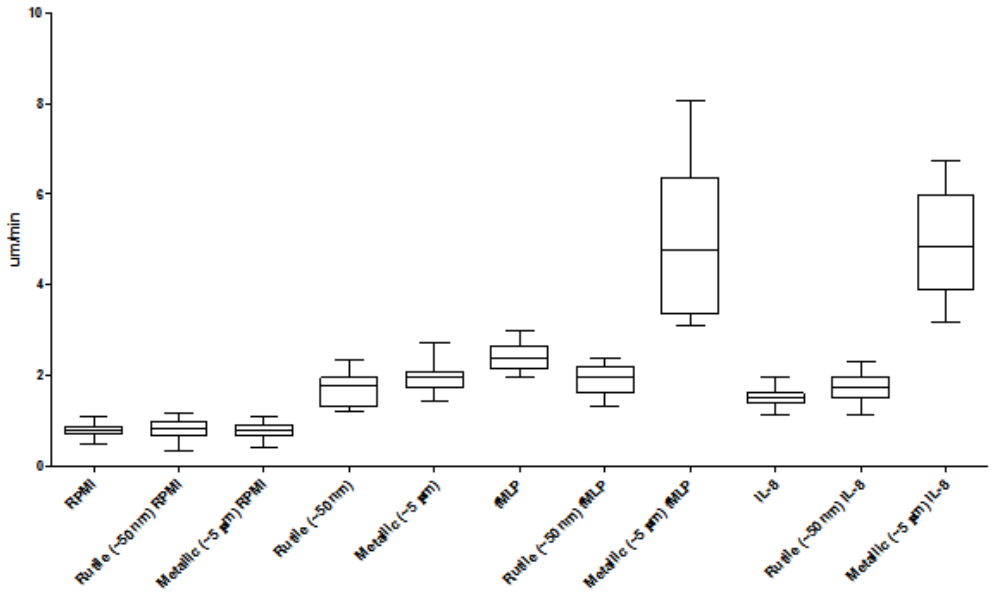

The *velocity* of cell movement (in the direction of the chemoattractant) was significantly lowest for cells exposed to RPMI (negative control chemoattractant) for both untreated and Ti pre-treated cells ($P<0.05$) (Figure 8.12); and for cells when Ti (rutile; ~50 nm or metallic; ~5 µm) was used as an experimental chemoattractant ($P<0.05$) (Figure 8.12). Significantly increased *velocities* were observed for cells exposed to fMLP and IL-8 (positive control chemoattractants) for both untreated and Ti pre-treated cells when compared to all other tested conditions ($P<0.005$) (Figure 8.12). However, cell *velocity* was significantly reduced for Ti-rutile (~50 nm) pre-treated cells when compared with untreated cells exposed to the same chemoattractants ($P<0.005$) (Figure 8.12). In contrast, cell *velocity* significantly increased for Ti-metallic (~5 µm) pre-treated cells exposed to both fMLP and IL-8 chemoattractants ($P<0.05$) (Figure 8.12).

Figure 8.12 Measure of cells' *velocity*

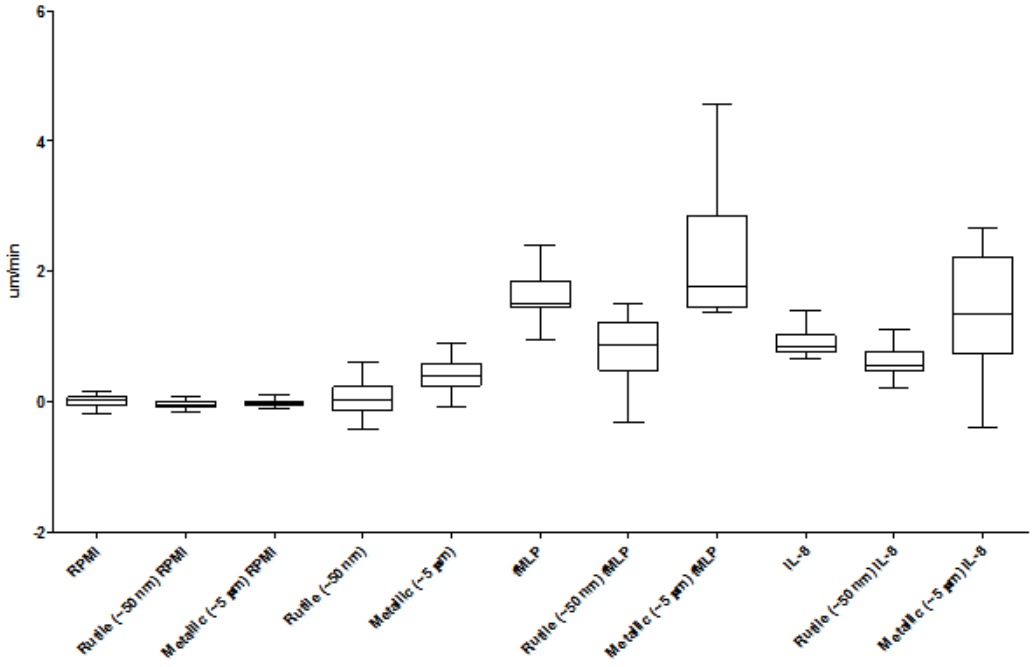

The *chemotactic index* when RPMI was used as the negative control chemoattractant for both untreated and Ti pre-treated cells was significantly lower than all other tested conditions ($P<0.05$), however an exception were rutile (~50 nm) RPMI treated cells ($P=0.12$) (Figure 8.13). The magnitude of the *chemotactic index* was significantly increased for fMLP as a chemoattractant when compared with IL-8 ($P<0.05$) (Figure 8.13). A significant decrease in the magnitude of the *chemotactic index* was observed for Ti (rutile; ~50 nm and metallic; ~5 µm) pre-treated cells exposed to both fMLP and IL-8 chemoattractants ($P<0.05$) (Figure 8.13).

Figure 8.13 Measure of cells' *chemotactic index*

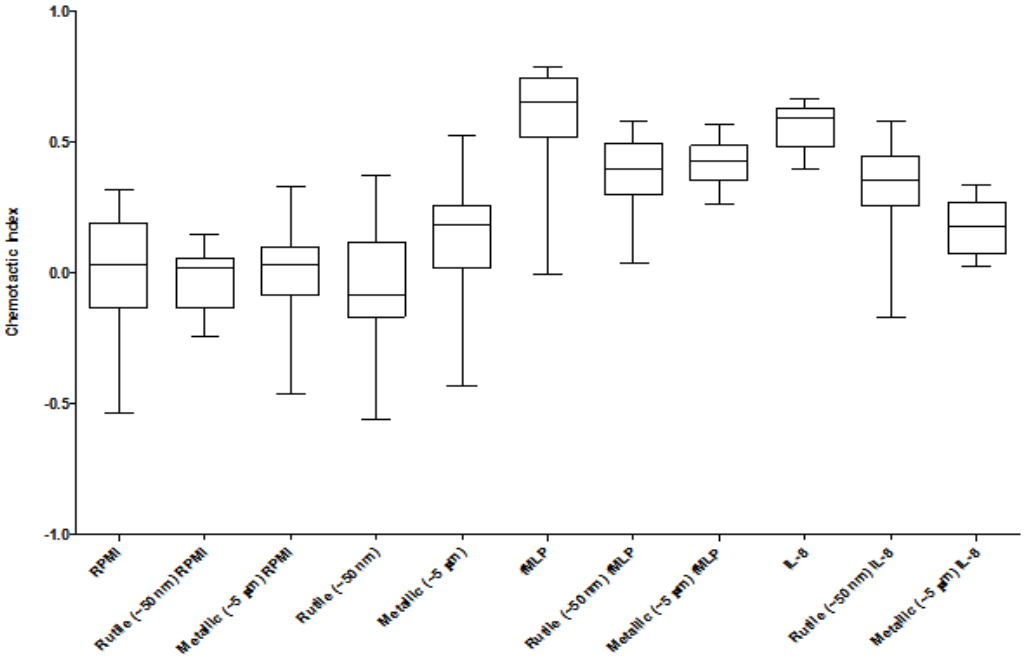

8.5 DISCUSSION

The current study used the Insall chamber (a novel *in-vitro* system) for the first time to observe chemotaxis of neutrophil populations exposed to Ti implant derivatives (oxide nanoparticles or micron sized metallic particles) at a single cell resolution. The assay was designed to determine if selected Ti implant derivatives such as rutile (~50 nm) or metallic (~5 μm) act as neutrophil chemoattractants and if cells exposed to Ti (oxide or metallic) subsequently modify chemotactic responses to known chemoattractants (fMLP and IL-8).

The findings of this study demonstrated that Ti as both oxide nanoparticles and micron sized metallic particles forms do not directly act as chemoattractants (Figures 8.4 & 8.6). This is unsurprising given the chemical stability of both forms of Ti in the pseudophysiological conditions of the Insall chamber. Analysis of cell movement parameters (*speed*, *velocity* and *chemotactic index*) of neutrophils when Ti was used as the experimental stimulus suggested some chemokinesis properties (Figures 8.11-8.13). Due to the insolubility of TiO_2 (as particles or as the passive surface of metallic particles) no concentration gradient of Ti can be established. However, when rutile (~50 nm) nanoparticles were used as a chemoattractant, minimal but significant directional movement away from the stimulus was observed (Figure 8.6). Although, this may be an experimental artefact, it may also be explained by the adsorption of components e.g. proteins (BSA) from the liquid media in the Insall chamber onto the surfaces of the nanoparticles creating small localised (negative) gradients within the experimental setup.

The exposure of neutrophils to Ti (as either oxide-rutile nanoparticles or micron sized metallic particles) resulted in modified chemotactic behaviour to known chemoattractants (fMLP and IL-8) (Figures 8.7, 8.9 & 8.10). However, the effects on chemotaxis are best considered as discrete components, *speed*, *velocity* and *chemotactic index* which differed significantly with the type of Ti exposure and the type of chemoattractant (Figures 8.11-8.13).

Pre-exposure to rutile (~50 nm) nanoparticles significantly reduced the *speed* of neutrophils whereas pre-exposure to metallic (~5 μm) particles, dramatically increased cell *speed* (Figure 8.11). An increase in cell *speed* may be associated with cell activation following e.g. phagocytosis or attempted phagocytosis of the particulate debris. Although internalisation of oxide nanoparticles has been demonstrated in this study, it has also been observed that nanoparticles accumulate on the cell membrane. This may act to inhibit cell motility (through interruption or modification of the actin cytoskeleton framework) or by possibly blocking the active site for F-actin polymerisation (Larmonier et al., 2011) on the neutrophil surface. The nanoparticles may also act to block (mask) surface receptors to the chemoattractants. In the current study exposure to oxide nanoparticles also resulted in a decrease in cell *velocity* (Figure 8.12) and *chemotactic index* (Figure 8.13) indicating that not only do cells move less but the directionality towards the chemoattractants is disturbed. It is hypothesized that cell surface interactions of nanoparticles masking receptor sites may lead to a modification in the chemical gradient that the cell can sense leading to disorientated movement. However, for cells pre-exposed to larger particles which

are not observed to aggregate at the cell membrane, both a significant increase in cell movement and a reduction in the *chemotactic index* was observed and is possibly accounted for by the cells unsuccessful attempts to phagocytose the associated particle (Figure 8.13). Of particular note was a significant decreased *chemotactic index* associated with IL-8 as a chemoattractant when compared with fMLP (Figure 8.13). This interesting finding may be explained by the likely production of IL-8 (or other chemoattractants) by the active neutrophils (via the NF-kB and MAPK mediated pathway) (Ryu et al., 2004) in response to larger particles which leads to modification of the chemoattractant gradient in the local environment and hence a modification of cell movement.

The recruitment and activation of neutrophils to sites of peri-implantation may be driven by responses to microbial stimuli (e.g. LPS) (Edwards, 1994). However, the current study demonstrates that Ti debris (in forms encountered in the tissues) (Chapters 3 & 4) may significantly modify neutrophil chemotaxis within the tissues, reducing chemotactic accuracy and *velocity* potentially leading to the progression of peri-implant inflammation. The results suggest that Ti may influence the existing chemical concentration gradient, reducing or significantly increasing cell *speed* depending on the nature of the Ti stimulus and reducing the *chemotactic index* in the presence of inflammatory mediators (Figures 8.11 & 8.13). The mechanisms underlying the process appear complex but seemingly are sensitive to cell membrane association with particles and cell activation (likely through phagocytosis) (Pierre, 2010). The data suggests that in the presence of significant quantities of Ti implant derivatives neutrophils are more likely to

cause host tissue damage due to their disrupted movement through the inflamed tissue and simulataneously activation of ROS and NET release.

8.6 CONCLUSION

Neutrophils are key mediators of inflammation and their recruitment, activation and migration is regulated by range of chemoattractants at inflammatory sites (Witko-Sarsat, 2000). Results indicate that although Ti implant derivatives do not act as chemoattractants, following previous exposure to Ti the cells chemotactic response to e.g. inflammatory cytokines may be significantly modified. This may result in an inability for the neutrophil to adequately migrate to sites of bacterial invasion or may result in the cells persistence in areas of non-inflamed tissue contributing to host tissue damage.

CHAPTER 9

GENERAL DISCUSSION

9.1 Discussion

In the current thesis it was demonstrated using synchrotron X-ray micro-focus spectroscopy that a scattered and heterogeneous (concentration, size and chemical species) distribution of Ti can be present in inflamed peri-implant soft tissues adjacent to both indwelling and skin/mucosal penetrating Ti implants (Chapters 3 & 4). For mixed connective tissues associated with indwelling orthopaedic implants where wear and/or loading processes are a major factor for the deterioration of the implanted device, the presence of large quantities of Ti were not surprising. However, the accumulation of significant levels of Ti in thin sections (6 μm thick) of tissues excised from adjacent to skin penetrating Ti implants cannot be explained by the action of macroscopic wear processes. Findings suggest that previous investigations have lacked the pre-requisite detection sensitivity to identify Ti in such tissues and that Ti debris may indeed play some vital role in determining the clinical outcomes of these devices.

Using XANES the Ti distribution identified in the inflamed skin penetrating peri-implant tissues was characterised to exist in a variety of Ti co-ordinations including oxide, metallic and peroxy-complexes and Ti soluble products ranged in size (Chapter 4). The heterogeneity of the Ti debris and the predominance of oxide species are unlikely to be accounted for debris resulting from implant insertion (where metallic particles would be unexpected). In contrast, the findings

suggested that the Ti implant derivatives accumulated within skin penetrating peri-implant tissues result from mechanically assisted crevice corrosion (MACC) processes occurring *in-vivo* (Adya et al., 2005 & Addison et al., 2012). These findings are of significant concern and suggest that the passive oxide layer on Ti implants responsible for maintaining the biocompatibility of the biomaterial is transiently disrupted in service (Adya et al., 2005). To confirm the hypothesis electrochemical studies were performed in which an artificial pit of Ti was corroded at pitting potential of 7 V. XANES analysis of the Ti corrosion products formed within the artificial pit (Chapter 4) identified the same Ti species that were previously shown to be accumulated within peri-implant inflamed tissues (Chapters 3 & 4). The findings are strongly indicative that passive Ti medical device surfaces are subjected to MACC processes *in-vivo*. MACC of Ti surfaces results in the release of Ti ions which subsequently oxidise forming insoluble particles from nano-scale to micron sized or complex with biomolecules in the peri-implant environment (Thomas et al., 2004 & Vamanu et al., 2004).

Within the tissues where XRF mapping confirmed Ti distributions, neutrophils were observed. This is unsurprising given that these cells are the predominant acute inflammatory cells in the peri-implant site (Chapter 3). Neutrophils are known to be having a significant impact on the progression of periodontal disease (Kantarci et al., 2003 & Nussbaum et al., 2011) and are thought to similarly influence the progression of peri-implantitis (Klinge et al., 2005 & Berglundh et al., 2011). The role of a pathogenic biofilm in the failure of skin and mucosal penetrating Ti implants is increasingly studied (Gitto et al., 1994 & Ahmed et al.,

2012). However, there is almost no research on the role of Ti, and its potential to influence inflammatory outcomes despite the known importance in aseptic Ti prosthesis failure in an orthopaedic context (Ratner, 2001). Therefore, a range of neutrophil responses including phagocytosis, respiratory burst, NET release, priming, cytokine release and chemotaxis were studied to determine the potential impact of Ti implant derivatives on neutrophil function (Chapters 5-8 & Appendix IV). Ti species representative of crevice corrosion products as identified within peri-implant tissues were studied and neutrophil responses were correlated to particle size, speciation and concentration.

The current investigation demonstrated that the Ti implant derivatives in all forms observed in tissues (either oxide nanoparticles or micron sized metallic particles) *in-vivo* do not act as chemoattractants for neutrophil chemotaxis (Chapter 8) into inflamed peri-implant tissue sites. This suggests that in the absence of other chemoattractants (microbial products or cellular signalling molecules) the presence of Ti in the peri-implant tissues from a neutrophil response perspective is largely unimportant. However, in the presence of another stressor the prior accumulation of Ti can become important if it modifies neutrophil activity at the site (Chapters 7 & 8).

In this study it was demonstrated that Ti particles are readily internalised by the neutrophil dependent on particle size. Large particle > 3 μm were less readily internalised (Kumazawa et al., 2001, Tamura et al., 2002, Jovanović et al., 2011) and the smallest particle size were suggested to enter the cell by a combination of

phagocytosis and endocytosis mechanisms (Pierre, 2010). The strong association of nanoparticles with cell membranes is particularly interesting given their apparent interactions with cell surface receptors (Tamura et al., 2002). This was highlighted by the differential priming effects observed on neutrophils and the subsequent effects on pathways involving Fc-γR and TLR receptors (Chapter 7). Importantly, all Ti species were demonstrated to be inducers of ROS and NET release but with a dependence on particle size, species and dose (Chapters 5 & 6). Moreover, simulation of oxidative burst in neutrophils exposed to nano and micron sized Ti species was consistent with NET release in neutrophils exposed to similar assay conditions. This observation further supports the growing evidence that NETosis is closely related to the process of respiratory burst and ROS production appears to be crucial signal in initiating NET release (Bruns et al., 2010 & Remijsen et al., 2011).

The differential magnitude of ROS and NET release observed between Ti oxide nanoparticles (of different size and speciation) and micron sized metallic particles is difficult to interpret. However, the results demonstrate that Ti oxide nanoparticles have greater pro-inflammatory potential and this has been attributed to their increased surface energies (Nel et al., 2006 & Hussain et al., 2009) and intra-cellularisation mechanisms (Kumazawa et al., 2001, Tamura et al., 2002 & Pierre, 2010). Phagocytosis of Ti oxide nanoparticles was demonstrated to be more feasible in comparison with larger particulate debris. However presence of non-membrane bound particles in the cytosol demonstrates non-phagocytosis mechanisms do occur. Nanoparticles were shown to have strong affinity to cell

membranes (Chapter 5) and were suggested to effect cell motility, cell chemotaxis (Chapter 8) and activation of cell surface receptors (Chapter 7).

Inhibition of ROS and NET release was demonstrated to periodontal pathogens Ops *Sa* and it was proposed that Ti implant derivatives may block or mask Fc-γR sites which then fail to recognise exogenous pathogens (Chapter 7). This observation is of significant concern as demonstrates pre-exposed cell may modify the peri-implant inflammatory response in sites of infection. Similarly, inhibition of the normal chemotactic response by Ti pre-exposed cells stimulated to known chemoattractants including fMLP and IL-8 was observed (Chapter 8).

CHAPTER 10

CONCLUSIONS AND FUTURE WORK

10.1 Conclusions

Chronic inflammation associated with Ti implants leads to bone loss and ultimately failure of the device (Cobelli et al., 2011). The current study developed from evidence generated in an orthopaedic context that metal ions and particles released from an implant can be pro-inflammatory and/or modify inflammatory pathways (Chapter 4). In the context of mucosa penetrating (dental), or skin penetrating (craniofacial) implants chronic inflammatory peri-implant disease till date has been attributed to characteristics of the surface biofilm (Klinge et al., 2005 & Berglundh et al., 2011) and to the host response (Flatebø et al., 2006). This study has demonstrated for the first time that extensive distributions of Ti particles (likely nano in scale) are found within the peri-implant tissues (Chapters 3 & 4) and Ti in ionic forms bound to biomolecules is likely. The study further demonstrated that mechanically assisted crevice corrosion (MACC) can account for the Ti species observed in tissues (Chapter 4). It is noted however that 'free-Ti' is likely to be further modified by interaction with cellular and extracellular components of the tissues (Lange et al., 2002 & Neumann et al., 2003). Neutrophils are highly significant in periodontal disease (Kantarci et al., 2003 & Nussbaum et al., 2011) and are found in high numbers in percutaenous and transmucosal implant sites (Chapter 3) (Klinge et al., 2005 & Berglundh et al., 2011). It was therefore assumed that these professional phagocytes will interact with Ti in the tissues. A series of experiments demonstrated that Ti-oxide,

metallic Ti and Ti-peroxy compounds all demonstrated a dose related ability to stimulate the release of ROS from human neutrophils and the magnitude of ROS release was sensitive to Ti-species and particle size (Chapter 5). In addition to ROS stimulation Ti debris was a potent stimulator of NETosis and the pattern of the stimulatory magnitude was highly consistent with the stimulation of respiratory burst (Chapter 5 & 6). Differences between responses were identified to be related to particle size but at the nano-scale Ti-O co-ordination also appeared to be important in determining cell-entry routes and membrane interactions. In addition, to the direct pro-inflammatory activity of the Ti debris, Ti exposure also resulted in modified responses of neutrophils to periodontal pathogens (Chapter 7) which may reduce the effectiveness of neutrophils to clear pathogens at the peri-implant site. These findings in combination with observations of modification of neutrophil chemotaxis behaviour suggest that that Ti implant derivatives will modify the progression of inflammation within peri-implant tissues.

10.2 Future work

The current study raises a large number of questions which yet have not been addressed within the current study and will contribute to enhancing our understanding of the underlying role of Ti corrosion products in tissues *in-vivo*:

- Evaluate the potential of Ti corrosion products to cause activation of NLRP3 inflammasome and provide insights regarding its significance which is known to cause further release of inflammatory cytokines such as IL-1 contributing to the inflammation present.

- Study the gene expression following Ti corrosion products exposure upon neutrophils which differentiates between (a) the possible receptor pathways such as PKC and inflammatory cytokines released (b) the positive or negative expression levels between the PHOX and PAD4 subunits of the NADPH complex responsible for the release of ROS and NET release mechanisms and (c) differentiate the expression levels between the three FC-γR classes.

- Investigate the impact on neutrophil chemotaxis and/or ROS responses of exposure of Ti products which have been associated with endotoxin LPS in direct stimulatory and priming assays.

- Identify the components comprised within NET structures released from neutrophils challenged with Ti implant derivatives. This will contribute in the understanding of possible interaction of Ti implant derivatives with neutrophil granular components and provide further insights regarding the functionality of the NET structures in the peri-implant environment.

- Investigate further neutrophil pathways which are possibly up-regulated or down-regulated for the induction of respiratory burst and NET release from Ti stimulated neutrophils by Ti exposure of different sizes.

- Investigate the effects on the release of pro-inflammatory cytokines and cell motility from neutrophils challenged with Ti implant derivatives which are blocked by SOD (ROS release inhibitor).

- Investigate interactions of Ti derivatives with the actin and cytoskeleton proteins which form the cytoplasmic framework of neutrophils influencing neutrophil chemotaxis and phagocytosis processes.

- Investigate the cellular effects of Ti peroxy compounds on neutrophil NET release and chemotaxis. Ti peroxy compounds are potential product of previous Ti interactions with neutrophils and hence their continued functionality is of great significance.

- Investigate the potential impact of neutrophils challenged with Ti implant derivatives on the activity of caspase 1 which is crucially involved in cell apoptosis. This investigation will provide insights regarding the induction of apoptosis by neutrophils challenged with Ti particles and compared to cell NETosis.

- Due to the interference of Ti nanoparticles in various assays, it would be interesting to investigate the biological responses to neutrophils via non-colourimetic/ fluorimetric methods e.g through gene expression or proteomic studies.

- It has been proposed that pre-activated cells with Ti oxide derivatives inhibit release of pro-inflammatory cytokine IL-1β. Therefore, it would be interesting to compare the cellular effects of IL-1β release from neutrophils stimulated with Ti implant derivatives that are producing ROS and from those that are not.

- To study whether the response of neutrophils to Ti products is influenced by an existing state of hyper-reactivity and hyper-activity as seen in chronic periodontitis.

REFERENCES

Addison, O., Davenport, A., Newport, R., Kalra, S., Monir, M., Mosselmans, J., Proops, D and Martin, R. (2012). Do 'passive' medical titanium surfaces deteriorate in the absence of wear? *Journal of Royal Society Interface,* 9(76): 3161-4.

Agarwal, A., Allamaneni, S and Said, T. M. (2004). Chemiluminescence Technique For Measuring Reactive Oxygen Species. *Reproductive BioMedicine Online*, *9*(4): 466-468.

Agins, J., Alcock, W., Bansal, M., Salvati, E. A., Wilson, D., Pellicci, M and Bullough, G. (1988). Metallic wear in failed titanium-alloy total hip replacements. A histological and quantitative analysis. *Journal of Bone Joint Surgery,* 70(3): 347-56.

Albrecht, D. (1928). Luminol-enhanced chemiluminescence induced in peripheral blood-derived human phagocytes: obligatory requirement of myeloperoxidase exocytosis by monocytes. *Journal of Leukocyte Biology,* 54(4): 300-6.

Albrektsson, T., Brånemark, I., Hansson, A and Lindström, J. (1981). Osseointegrated titanium implants. Requirements for ensuring a long lasting, direct bone-to-bone implant anchorage in man. *Acta Orthopaedica Scandinavica,* 52(2): 155-70.

Albrektsson, T., Brånemark, P., Hansson, H., Kasemo, B., Larsson, K and Lundström, I. (1983). The interface zone of inorganic implants *in-vivo*: Titanium implants in bone. *Annals of Biomedical Engineering*, 11(1): 1-27.

Albretktsson, T and Isidor, F. (1994). *Consensus report of session IV. Proceedings of the 1st European workshop on Periodontology.* Berlin: Quintessence.

Alegria-Schaffer, A., Lodge, A and Vattem K. (2009) Performing and optimizing Western blots with an emphasis on chemiluminescent detection. *Methods Enzymolology*, 463: 573-99.

Alghamdi, S and Foster, N. (2005). Seminal DNase frees spermatozoa entangled in Neutrophil Extracellular Traps. *Biology of Reproduction,* 73(6): 1174-1181.

Amano, A. (2003). Molecular interaction of *Porphyromonas gingivalis* with host cells: Implication for the microbial pathogenesis of periodontal disease. *Journal of Periodontoogyl,* 74(1): 90-96.

Ames, B. N. (1993). Oxidants, antioxidants and the degenerative diseases of aging. *Proceedings of the National Academy of Sciences*, 90(17): 7915-7922.

Amulic, B., Cazalet, G., Hayes, K., Metzler, K and Zychlinsky, A. (2012). Neutrophil function: from mechanisms to disease. *Annual Review of Immunology*, 30: 459-89.

Asman, B., Bergstrom, K., Wijkander, P and Lockowandt, B. (1985). Influence of plasma components on luminol-enhanced chemiluminescence from peripheral granulocytes in juvenile Periodontitis. *Journal of Clinical Periodontology*, 13(9): 850-855.

Atzeni, F., Schena, M., Ongari, M., Carrabba, M., Bonara, P., Minonzio, F and Capsoni, F. (2002). Induction of CD69 activation molecule on human neutrophils by GM-CSF, IFN-gamma, and IFN-alpha. *Cell Immunol*ogy, 220(1): 20-9.

Babior, B. M. (1984). The respiratory burst of phagocytes. *Journal of Clinical Investigation*, 73(3): 599-601.

Babior, B. (1999). NADPH oxidase: an update. *Blood*, 93(5): 1464-76.

Bacquart, T., Devès, G., Carmona, A., Tucoulou, R., Bohic, S and Ortega, R. (2007). Subcellular speciation analysis of trace element oxidation states using synchrotron radiation micro-X-ray Absorption Near-Edge Structure. *Analytical Chemistry*, 79(19): 7353-7359.

Bakri, G., Martel, C., Khuri-Bulos, N., Mahafzah, A., El-Khateeb, S., Al-Wahadneh, M., Hayajneh, A., Hamamy, A., Maquet, E., Molin, M., Stasia, J. (2009). First report of clinical, functional, and molecular investigation of chronic granulomatous disease in nine Jordanian families. *Journal of Clinical Immunology,* 29(2): 215-30.

Baldrige, W and Gerard, W. (1933). The extra respiration of phagocytosis. *Journal of Physiology*, 103: 235-236.

Baldwin, L and Hunt, J. (2006). Host inflammatory response to NiCr, CoCr, and Ti in a soft tissue implantation model. *Journal of Biomedical Materials Research Part A*, 79A(3): 574-581.

Bartneck, M., Keul, A., Zwadlo-Klarwasser, G and Groll, J. (2010). Phagocytosis independent extracellular nanoparticle clearance by human immune cells. *Nano Letters*, 10(1): 59-63.

Battino, M., Bullon, P., Wilson, M and Newman, H. (1999). Oxidative injury and inflammatory periodontal diseases: The challenge of anti-oxidants to free radicals and reactive oxygen species. *Critical Reviews in Oral Biology & Medicine*, 10(4): 458-476.

Beck, T. R. (1973). Pitting of Titanium. *Journal of The Electrochemical Society*, 120(10): 1310.

Becker, W., Becker, B. E., Newman, M. G and Nyman, S. (1990). Clinical and microbiologic findings that may contribute to dental implant failure. *International Journal of Oral and Maxillofacial Implants,* 5: 31-38.

Behrendt, H., Ruiz, A., Zahner, H., Taubert, A and Hermosilla, C. (2010). Neutrophil extracellular trap formation as innate immune reactions against the apicomplexan parasite Eimeria bovis. *Veterinary Immunology and Immunopathology,* 133(1): 1-8.

Beiter, K., Wartha, F., Albiger, B., Normark, S., Zychlinsky, A and Henriques-Normark, B. (2006). An endonuclease allows *Streptococcus pneumoniae* to escape from Neutrophil Extracellular Traps. *Current Biology,* 16(4): 401-407.

Bergamini, C. M., Gambetti, S., Dondi, A and Cervellati, C. (2004). Oxygen, Reactive Oxygen Species and tissue damage. *Current Pharmaceutical Design*, 10(14): 1611-1626.

Berglundh, T., Lindhe, J., Marinell, C., Ericsson, I and Liljenberg, B. (1992). Soft tissue reaction to *de novo* plaque formation on implants and teeth. An experimental study in the dog. *Clinical Oral Implants Research*, 3(1): 1-8.

Berton, G., Zeni, L., Cassatella, A and Rossi, F. (1986). Gamma interferon is able to enhance the oxidative metabolism of human neutrophils. *Biochemical Biophysics Research Community,* 138(3): 1276-82.

Bhattacharya, K., Davoren, M., Boertz, J., Schins, R. P., Hoffmann, E. and Dopp, E. (2009). Titanium dioxide nanoparticles induce oxidative stress and DNA-adduct formation but not DNA-breakage in human lung cells. *Particle and Fibre Toxicology*, 6(1): 175.

Bianchi, M., Hakkim, A., Brinkmann, V., Siler, U., Segar, R and Zychlinsky, A. (2009). Restoration of NET formation by gene therapy in CGD controls aspergillosis. *Blood*, 114(13): 2619-22.

Bianco, P., Ducheyne, P. and Cuckler, J. (1996). Titanium serum and urine levels in rabbits with a Titanium implant in the absence of wear. *Biomaterials*, 17(20): 1937-1942.

Biffi, L, Moore, E., Moore, A., Barnett, C., Carl, S and Peterson, M. (1996). Interleukin-6 delays neutrophil apoptosis. *Archives of Surgery*, 131(1): 24-30.

Black, J., Sherk, H., Bonini, J., Rostoker, R., Schajowicz, F and Galante, O. (1990). Metallosis associated with a stable titanium-alloy femoral component in total hip replacement. A case report. *Journal of Bone Joint Surgery*, 72(1): 126-30.

Bölükbaş, N., Mercan, S., Tekkesin, M and Bölükbaş, M. (2013). Determination of Titanium particles around a failed implant. *International Journal of Dental Case Reports*, 3(1): 83-88.

Borregaard, N., Heiple, M, Simons, R and Clark, A. (1983). Subcellular localization of the b-cytochrome component of the human neutrophil microbicidal oxidase: translocation during activation. *Journal of Cell Biology,* 97: 52-61.

Borregaard, N and Cowland, J. (1997). Granules of the human neutrophil polymorphonuclear leukocyte. *Blood,* 89(1): 3503-3521.

Brånemark, I., Hansson, O., Adell, R., Breine, U., Lindström, J., Hallén, O and Ohman, A. (1977). Osseointegrated implants in the treatment of the edentulous jaw. Experience from a 10-year period. *Scandinavian Journal of Plastic and Reconstructive Surgery Supplementum,* 16(1): 1-132.

Brånemark, P. (1985). *Tissue-integrated prostheses: osseointegration in clinical dentistry*. Chicago: Quintessence.

Briheim, G., Stendahl, O and Dahlgren, C. (1984). Intra- and extracellular events in luminol-dependent chemiluminescence of polymorphonuclear leukocytes. Infection and Immunity, 45(1): 1-5.

Brinkmann, V., Reichard, U., Goosmann, C., Fauler, B., Uhlemann, Y., Weiss, S., Weinrauch, Y and Zychlinsky, A. (2004). Neutrophil Extracellular Traps kill bacteria. *Science,* 303(5663): 1532-1535.

Brinkmann, V and Zychlinsky, A. (2007). Beneficial suicide: why neutrophils die to make NETs. *Nature Reviews Microbiology,* 5(8): 577-582.

Brinkmann, V and Zychlinsky, A. (2013). Neutrophil extracellular traps: Is immunity the second function of chromatin?. *The Journal of General Physiology*, 198(5): 773-783.

Broggini, N., McManus, L., Hermann, J., Medina, R., Schenk, R and Buser, D. (2006). Peri-implant inflammation defined by the implant-abutment interface. *Journal of Dental Research*, *85*(5), 473-478.

Brown, E., Stewart, Q., Bissonnette, A., Elia, A., Wilker, E and Yaffe, B. (2004). Distinct ligand-dependent roles for p38 MAPK in priming and activation of the neutrophil NADPH oxidase. *Journal of Biological Chemistry,* 279(26): 27059-68.

Brunette, M. (2001). *Titanium in medicine: material science, surface science, engineering, biological responses, and medical applications*. Berlin: Springer.

Bruns, S., Kniemeyer, O., Hasenberg, M., Aimanianda, V and Nietzsche, S. (2010). Production of extracellular traps against *Aspergillus fumigatus in vitro* and in infected lung tissue is dependent on invading neutrophils and influenced by hydrophobin RodA. *PLoS* Pathology, 6(4): 1371-1383.

Buchanan, T., Simpson, J., Aziz, K., Liu, Y., Kristian, A., Kotb, M., Feramisco, J and Nizet, V. (2006). DNase expression allows the pathogen group A *Streptococcus* to escape killing in Neutrophil Extracellular Traps. *Current Biology*, 16(4): 396-400.

Budinski, K. (1991). Tribological properties of Titanium alloys. *Wear*, 151(2): 203-217.

Bundy, J., Butler, F and Hochman, F. (1980). An investigation of the bacteriostatic properties of pure metals. *Journal of Biomedical Materials Research*, 14(5): 653-663.

Cadosch, D., Chan, E., Gautschi, P., Meagher, J., Zellweger, R and Filgueira, L. (2009). Titanium IV ions induced human osteoclast differentiation and enhanced bone resorption *in vitro***.** *Journal of Biomedical Materials Research,* 91(1): 29-36.

Carvalho, M., Magaes, T., Becker, M and Bohlen, A. (2007). Trace elements in human cancerous and healthy tissues: A comparative study by EDXRF, TXRF, synchrotron radiation and PIXE. *Spectrochimica Acta Part B: Atomic Spectroscopy*, 62(9): 1004-1011.

Cassatella, M. (1995). The production of cytokines by polymorphonuclear neutrophils. *Immunology today,* 16(1): 21-26.

Chan, E., Amir, M., Peta, C., Martin, S and Luis, F. (2009). Effects of titanium$_{(iv)}$ ions on human monocyte-derived dendritic cells. *Metallomics,* 1: 166-174.

Chang, Y and Yang, X. (2000). Proteases for cell suicide: functions and regulation of caspases. *Microbiology Molecular Biology Review,* 64(4): 821-46.

Chapple, L., Brock, G., Milward, M., Ling, N and Matthews, J. (2007). Compromised GCF total antioxidant capacity in periodontitis: cause or effect? *Journal of Clinical Periodontology,* 34(2): 103-110.

Chapple, L and Matthews, J. (2007). The role of reactive oxygen and antioxidant species in periodontal tissue destruction. *Periodontology,* 2000, 43: 160-232.

Chen, X., Rajh, W., Jager, J., Nedeljkovic, W and Thurnauer, C. (1999). X-ray absorption reveals surface structure of Titanium dioxide nanoparticles. Journal of Synchrotron Radiation, 7(3): 109-121.

Choi, G., Koh, S., Kluess, D., O'Connor, D., Mathur, A., Truskey, A., Rubin, J., Zhou, D and Sung, P. (2005). Effects of Titanium particle size on osteoblast functions *in-vitro* and *in-vivo*. *Proceedings of the National Academy of Sciences of the United States of America*, 102(12): 4578-4583.

Cicchetti, G., Allen, G and Glogauer, M. (2002). Chemotactic signaling pathways in neutrophils: From receptor to actin assembly. *Critical Reviews in Oral Biology & Medicine*, 13(3): 220-228.

Clark, R., Green, H., Kelly, M., Goodarzi, Z., McDonald, B and Tavener, A. (2007). Platelet TLR4 activates Neutrophil Extracellular Traps to ensnare bacteria in septic blood. *Nature Medicine*, 13(4): 463-469.

Cobelli, N., Scharf, B., Crisi, M., Hardin, J and Santambrogio, L. (2011). Mediators of the inflammatory response to joint replacement devices. *Nature Reviews Rheumatology*, 7(1): 600-608.

Coen, N., Khadhim, M., Wright, E., Case, C and Mothersill, C. (2003). Particulate debris from a titanium metal prosthesis induces genomic instability in primary human fibroblast cells. *British Journal of Cancer*, *88*(4): 548–552.

Cook, D., Thomas, A., Kay, F and Jarcho, M. (1988). Hydroxyapatite-coated titanium for orthopaedic implant applications. *Journal of Clinical Orthopaedic Research,* 232: 225-43.

Curtin, F., Donovan, M and Cotter, T. G. (2002). Regulation and measurement of oxidative stress in apoptosis. *Journal of Immunological Methods*, 265(1-2): 49-72.

Czanderna, W., Rao, N and Honig, M. (1958). The anatase-rutile transition. Part 1. Kinetics of the transformation of pure anatase. *Transactions of the Faraday Society*, 54: 1069.

Dahlgren, C and Karlsson, A. (1999). Respiratory burst in human neutrophils. *Journal of Immunological Methods*, *232*(1-2): 3-14.

Dahlgren, C., Karlsson, A and Bylund, J. (2007). Measurement of respiratory burst products generated by professional phagocytes. *Methods in Molecular Biology*, *412*: 349-63.

Dale, C., Boxer, L and Liles, C. (2008). The phagocytes: neutrophils and monocytes. *Blood*, 112(4): 935-45.

Da Rosa, L. (2013). Kinetic effects of TiO2 fine particles and nanoparticles aggregates on the nanomechanical properties of human neutrophils assessed by force spectroscopy. *BMC Biophys,* 19, 6(1): 11.

Dinauer, C. (2005). Chronic Granulomatous Disease and other disorders of phagocyte function. *Hematology: The American Society of Hematology Education Program,* 1: 89-95.

Di Vigilio and Reigosa, M. (2010). Response of UMR 106 cells exposed to titanium oxide and aluminium oxide nanoparticles. Journal of Biomedical Materials Research, 92(1): 80-87.

Dias, H., Matthews, B., Chapple, I., Wright, H., Dunston, R and Griffiths, H. (2010). Activation of the neutrophil respiratory burst by plasma from Periodontitis patients is mediated by pro-inflammatory cytokines. *Journal of Clinical Periodontology*, *1*, 1-7.

Dias, I., Chapple, I., Milward, M., Grant, M and Hill, E. (2013) Sulforaphane restores cellular glutathione levels and reduces chronic periodontitis Neutrophil hyperactivity *in vitro*. *PLoS Immunology*, 8(6): 664-672.

Dobrovolskaia, A and McNeil, E. (2007). Immunological properties of engineered nanomaterials. *Nature Nanotechnology*, *2*(8): 469-478.

Dodd, N and Jha, A (2009). Titanium dioxide induced cell damage: A proposed role of the carboxyl radical. *Mutation Research/Fundamental and Molecular Mechanisms of Mutagenesis*, 660(1-2): 79-82.

Doorn, F., Campbell, A., Worrall, J., Benya, D., McKellop, A and Amstutz, C. (1998). Metal wear particle characterization from metal on metal total hip replacements: Transmission electron microscopy study of peri-prosthetic tissues and isolated particles. *Journal of Biomedical Materials Research*, *42*(1): 103-111.

Driscoll, E., Deyo, C., Carter, M., Howard, W., Hassenbein, J and Bertram, A. (1997). Effects of particle exposure and particle-elicited inflammatory cells on mutation in rat alveolar epithelial cells. *Carcinogenesis,* 18: 423-30.

Duan, Y., Wang, X., Liu, C., Zheng, L., Wang, J., Zheng, L., Liu, C., Wang, X., Zhao, X., Yan, J., Wang, S., Zhang, X and Hong, F. (2010). Toxicological characteristics of nanoparticulate anatase titanium dioxide in mice. *Biomaterials*, *31*(5): 894-899.

Dugdale, I and Cotton, J. (1964). The anodic polarization of titanium in halide solutions. *Corrosion Science*, *4*(1-4): 397-411.

Duisabeau, L., Combrade, P and Forest B. (2004). Environmental effect on fretting of metallic materials for orthopaedic implants. *Wear*, 256: 805-816.

Edwards, S. W. (1994). *Biochemistry and physiology of the neutrophil*. Cambridge [England: Cambridge University Press.]

Effah, A., Bianco, D and Ducheyne, P. (1995). Crystal structure of the surface oxide layer on titanium and its changes arising from immersion. *Journal of Biomedical Materials Research*, 29(1): 73-80.

Ektessabi, A., Otsuka, T., Yokoyama, K., Albrektsson, T., Sennerby, L and Johansson, C. (1994). Application of micro beam PIXE to detect titanium ion release from dental and orthopaedic implants. *International Journal of PIXE*, 4(81): 81-91.

Ektessabi, A., Mouhyi, J., Louvette, P and Sennerby, L. (1997). Investigation of corrosion and ion release from titanium dental implants. *International Journal of PIXE*, 7(179): 179-199.

Ektessabi, A. (1998). Fluorescence and XAFS spectroscopy of ion release from metal implants in human tissues. *Journal of Synchrotron Radiation*, *5*(1): 65-66.

Elias, N., Lima, C., Valie, R and Meyers, A. (2008). Biomedical applications of titanium and its alloys. *Biological Materials Science,* 60(3): 46-49.

Epstein, H and Weiss, J. (1989). Tissue destruction by neutrophils. *New England Journal of Medicine*, 320(6): 365-376.

Ermert, D., Urban, F., Laube, B., Goosmann, C., Zychlinsky, A and Brinkmann, V. (2009). Mouse Neutrophil Extracellular Traps in microbial infections. *Journal of Innate Immunity*, 1(3): 181-193.

Esmon, C., Xu, J and Lupu, F. (2011). "Innate immunity and coagulation." *Journal of Thrombosis and Haemostatsis,* 9: 182-8.

Fadeel, B. (2009). Babies Born Without Safety NET. *Blood*, *113*(25): 6270-6271.

Falck, G., Lindberg, H., Suhonen, S., Vippola, M., Vanhala, E and Catalan, J. (2009). Genotoxic effects of nanosized and fine TiO_2. *Human and Experimental Toxicology*, 28(6-7): 339-352.

Farges, F., Brown, E and Rehr, J. (1996). Coordination chemistry of Ti(IV) in silicate glasses and melts: XAFS study of titanium coordination in oxide mode1 compounds. *Acta*. 60: 3023.

Faurschou, M and Borregaard, N. (2003). Neutrophil granules and secretory vesicles in inflammation. *Microbes and Infection*, 5(14): 1317-1327.

Ferguson, A., Laing, P and Hodge, E. (1960). The ionization of metal implants in living tissues. *The Journal of Bone and Joint Surgery,* 42:77-90.

Fielding, A., McLoughlin, M., McLeod, L., Colmont, S., Najdovska, M., Grail, D., Ernst, M., Jones, A., Topley, N and Jenkins, J. (2008). IL-6 regulates neutrophil trafficking during acute inflammation via STAT3. *Journal of Immunology*, 181(3): 2189-95.

Flatebø, S., Johannessen, C., Grønningsæter, G., Bøe, E., Gjerdet, R., Grung, B and Leknes, N. (2006). Host response to titanium dental implant placement evaluated in a human oral model. *Journal of Periodontology*, *77*(7): 1201-1210.

Floyd, A. (1999). Antioxidants, oxidative stress and degenerative neurological disorders. *Proceedings of The Society for Experimental Biology and Medicine*, 222(3): 236-245.

Forsyth, D., Talbot, V. and Beckman, I. (1994). Endothelial serpins-Protectors of the vasculature. *Clinical and Experimental Immunology*, 95(2): 277-282.

Fossati, G., Bucknall, C and Edwards, W. (2002). Insoluble and soluble immune complexes activate neutrophils by distinct activation mechanisms: changes in functional responses induced by priming with cytokines. *Annual Rheumatology Discussion,* 61(1): 13-9.

Fransson, C. (2009). *Prevalence, extent and severity of peri-implantitis*. Göteborg: Department of Periodontology, Institute of Odontology, Sahlgrenska Academy, University of Gothenburg.

Fransson, C., Wennström, J., Tomasi, C and Berglundh, T. (2009). Extent of peri-implantitis associated bone loss. *Journal of Clinical Periodontology*, 36(4): 357-363.

Freitas, M., Lima, L and Fernandes, E. (2009). Optical probes for detection and quantification of neutrophils oxidative burst. A Review. *Analytical Chimica Acta*, 649(1): 8-23.

Fuchs, A., Abed, U., Goosmann, C., Hurwitz, R., Schulze, I., Wahn, R, Volker, W., Weinrauch, Y, Volker, B and Zychlinsky, A. (2007). Novel cell death program leads to Neutrophil Extracellular Traps. *The Journal of Cell Biology*, 176(2): 231-241.

Gainet, J., Dang, C., Chollet-Martin, S., Brion, M., Sixou, M., Hakim, J and Elbim, C. (1999). Neutrophil dysfunctions, IL-8 and soluble L-selectin plasma levels in rapidly progressive versus adult and localised juvenile periodontitis: variations according to disease severity and microbial flora. *Journal of Immunology,* 163(9): 5013-9.

Galvele, J., Torresi, R and Carranza, R. (1990). Passivity breakdown, its relation to pitting and stress-corrosion-cracking processes. *Corrosion Science*, 31: 563-571.

Garcia-Garcia, E. (2005). *Molecular mechanisms of phagocytosis*. Georgetown, Texas, Landes Bioscience.

Garcia-Romo, S., Banchereau, J., Vega, B., Caielli, S., Pascual, V and Barrat, J. (2011). Netting neutrophils are major inducers of type I IFN production in pediatric Systemic Lupus Erythematosus. *Science Translational Medicine*, 3(73): 7320-7325.

Garrett, R., Boyce, F., Oreffo, O., Bonewald, L., Poser, J and Mundy, R. (1990). Oxygen derived free radicals stimulate osteoclastic bone-resorption in rodent bone *in-vitro* and *in-vivo*. *Journal of Clinical Investigation,* 85(3): 632-639.

Gemelli, E., Scariot, A and Camargo, N. H. (2007). Thermal characterization of Commercially Pure titanium for dental applications. *Materials Research*, 10(3): 241-246.

George, K., Zafiropoulos, K., Murat, Y., Hubertus, S and Nisengard, J. (1995). Clinical and microbiological status of osseointegrated implants. *Implant Dentistry*, *4*(2): 132.

Geringer, J., Forest, B and Combrade, P. (2005). Fretting-corrosion of materials used as orthopaedic implants. *Wear*, *259*(7-12): 943-951.

Goncalves, D., Chiasson, S and Girard, D. (2009). Activation of human neutrophils by titanium dioxide nanoparticles. *Toxicology*, 11, 1877-1885.

Goncalves, D and Girard, D. (2011). Titanium dioxide (TiO2) nanoparticles induce neutrophil influx and local production of several pro-inflammatory mediators *in vivo*. *International Journal of Immunopharmacology,* 11(8):1109-15.

Gorsuch, D. (1969). Studies on the chemiluminescence of Luminol. *Photochemistry and Photobiology*, 15(6): 567-583.

Grant, M., Monksfield, P., Proops, D., Brine, M., Addison, O., Sammons, R., Matthews, J., Reid, A and Chapple, I. (2010). Fluid exudates from inflamed bone-anchored hearing aids demonstrate elevated levels of cytokines and biomarkers of tissue and bone metabolism. *Otology and Neurotology,* 31(3): 433-439.

Griess, C. (1968). Crevice corrosion of titanium in aqueous salt solutions. *Corrosion,* 24: 96-109.

Griffin, M and Schnitzer, E. (2011). Overcoming key technological challenges in using mass spectrometry for mapping cell surfaces in tissues. *Molecular Cell Proteomics,* 10(2):300-21.

Griffiths, H and Lunec, J. (1988). Effect of polymorph derived oxidants on IgG in relation to rheumatoid factor binding. *Scandinavian Journal of Rheumatology Supplement,* 75: 148-56.

Grinberg, N., Rosenshine, I and Shpigel, N. (2008). Beta-hydroxybutyrate abrogates formation of bovine neutrophil extracellular traps and bactericidal activity against mammary pathogenic Escherichia coli. *Infection and immunity*, 76(6): 2802-7.

Guimaraes-Costa, B., Nascimento, T., Froment, S., Soares, P., Morgado, N and Conceicao-Silva, F. (2009). *Leishmania amazonensis* are killed by Neutrophil Extracellular Traps. *Proceedings of the National Academy of Sciences*, 106(16): 6748-6753.

Gupta, K., Hasler, P., Holzgreve, W., Gebhardt, S andHahn, S. (2005). Induction of Neutrophil Extracellular DNA lattices by placental microparticles and IL-8 and their presence in preeclampsia. *Human Immunology*, 66(11): 1146-1154.

Gupta, K., Joshi, B., Philippova, M., Erne, P., Hasler, P and Hahn, S. (2010). Activated endothelial cells induce Neutrophil Extracellular Traps and are susceptible to NETosis-mediated cell death. *FEBS Letters*, 584(14): 3193-3197.

Gurr, J., Wang, A., Chen, C and Jan, K. (2005). Ultrafine titanium dioxide particles in the absence of photoactivation can induce oxidative damage to human bronchial epithelial cells. *Toxicology*, 213(1-2): 66-73.

Gustafsson, Å., Lindstedt, E., Elfsmark, S and Bucht, A. (2011). Lung exposure of titanium dioxide nanoparticles induces innate immune activation and long-lasting lymphocyte response in the Dark Agouti rat. *Journal of Immunotoxicology,* 8(2):111-21.

Haffajee, D., Socransky, S., Patel, R and Song, X. (2008). Microbial complexes in supragingival plaque. *Oral Microbiol Immunol,* 23(3): 196-205.

Hakkim, A., Furnrohr, G., Amann, K., Laube, B., Abed, A and Brinkmann, V. (2010). Impairment of Neutrophil Extracellular Trap degradation is associated with Lupus Nephritis. *Proceedings of the National Academy of Sciences*, 107(21): 9813-9818.

Hakkim, A., Fuchs, T., Martinez, N., Hess, S., Prinz, H and Zychlinsky, A. (2011). Activation of the Raf-MEK-ERK pathway is required for neutrophil extracellular trap formation. *Nature chemical biology*, *7*: 75–77.

Hallab, J., Anderson, S., Caicedo, M., Brasher, A., Mikecz, K and Jacobs, J. (2004). Effects of soluble metals on human peri-implant cells. *Journal of Biomedical Materials Research,* 74(1): 124-40.

Hallab, J and Jacobs, J. (2009). Biologic effects of implant debris. *NYU Hospital for Joint Diseases*, 67(2): 182-8.

Hallam, P., Haddad, F and Cobb, J. (2004). Pain in the well fixed, aseptic titanium hip replacement. The role of corrosion. *The Journal of Bone & Joint Surgery,* 86(1): 27-30.

Hamilton, F., Wu, N., Porter, D., Buford, M., Wolfarth, M and Holian, A. (2009). Particle length-dependent titanium dioxide nanomaterials toxicity and bioactivity. *Particle and Fibre Toxicology*, 6(1): 35.

Hampton, B., Kettle, J and Winterbourn, C. (1998). Inside the neutrophil phagosome: oxidants, myeloperoxidase and bacterial killing. *Blood,* 92(9): 3007-17.

Hancock, J. (1997). Superoxide, hydrogen peroxide and nitric oxide as signalling molecules: their production and role in disease. *British Journal of Biomedical Science*, 54(1): 38-46.

Hanlon, J., Ozuna, S., Shortkroff, C., Sledge B., Thornhill, T and Spector, M. (1992). "Analysis of metallic wear debris retrieved at revision arthoplasty." *Implant Retrieval Symposium of the Society for Biomaterials,* St Charles. Illinois.

Hansen, D. (2008). Metal corrosion in the human body: The ultimate bio-corrosion Scenario. *The Electrochemical Society Interface*, *1*: 31-34.

Hart, J., Quinn, D., Sampson, B., Sandison, A., Atkinson, A and Skinner, A. (2010). The chemical form of metallic debris in tissues surrounding metal-on-metal hips with unexplained failure. *Acta Biomaterialia*, 6(11): 4439-4446.

Hart, A., Quinn, P and Mosselmans, J. (2012). Microfocus X-ray spectroscopy helps solve mystery over poor human biocompatibility of hip replacements *Spectrocopy village* Beamline I18

Hatanka, E., Monteagudo, P., Marrocos, M and Campa, A. (2006). Neutrophils and monocytes as potentially important sources of pro-inflammatory cytokines in diabetes. *Clinical and Experimental Immunology,* 146: 443-447.

He, X., Noël, J and Shoesmith, W. (2002). Temperature dependence of crevice corrosion initiation on titanium grade-2. *Journal of The Electrochemical Society*, 149(9): 440

Hedenborg, M. (1988). Titanium dioxide induced chemiluminescence of human polymorphonuclear leukocytes. *International Archives of Occupational Environmental Health,* 61(1-2): 1-6.

Heins, N., Suriano, R., Taniuchi, H and Anfinsen, B. (1967). Characterization of a nuclease produced by *Staphylococcus aureus*. *Journal of Biological Chemistry,*242(5): 1016-20.

Hench, L. (1975). Prosthetic implant materials. *Annual Review of Materials Science*, 5(1): 279-300.

Henson, P and Oades, Z. (1973). Enhancement of immunologically induced granule exocytosis from neutrophils by Cytochalasin B. *The Journal of Immunology*, *110*: 290-293.

Herlihy, S., Pilling, D., Maharjan, A and Gomer, R. (2013). Dipeptidyl peptidase IC is a human and m urine neutrophil chemoattractant. *The Journal of Immunology,* 190: 1-10.

Hettige, S and Norris, S. (2012). Moratality after local allergic response to titanum cranioplasty. *Acta Neurochir*, 154(9): 1725-6.

Hildeman, D., Mitchell, T., Kappler, J and Marrack, P. (2003). T cell apoptosis and reactive oxygen species. *The Journal of Clinical Investigation*, 111(5): 575–581.

Hirayama, T., Tamaki, Y., Takakubo, Y., Iwazaki, K., Sasaki, K., Ogino, T., Goodman, B., Konttinen, T and Takagi, M. (2011). Toll-like receptors and their adaptors are regulated in macrophages after phagocytosis of lipopolysaccharide-coated titanium particles. *Journal of Orthopaedic Research,* 29(7): 984-92.

Hitchcock, E. (1980). Actin deoxyroboncuclease I interaction. Depolymerization and nucleotide exchange. *Journal of Biological Chemistry,* 255(12): 5668-5673.

Holgers, M. (2000). Characteristics of the inflammatory process around skin penetrating Titanium implants for aural rehabilitation. *Audiology,* 39(5): 253-259.

Honeycutt, P and Niedel, J. (1986). Cytochalasin B enhancement of the diacylglycerol response in formyl peptide-stimulated neutrophils. *The Journal Of Biological Chemistry*, 261(34): 15900-15.

Huang, H and Lee, T. (2005). Electrochemical impedance spectroscopy study of Ti–6Al–4V alloy in artificial saliva with fluoride and/or bovine albumin. *Dental Materials*, 21(8): 749-755.

Huizinga, W., Van Kemenade, F., Koenderman, L and Dolman, M. (1989). The 40-kDa Fc gamma receptor (FcRII) on human neutrophils is essential for the IgG-induced respiratory burst and IgG-induced phagocytosis. *Journal of Immunology,* 142(7): 2365-9.

Hussain, S., Moisan, F., Fleury-Feith, J., Billon-Galland, A., Martens, A and Thomassen, C. (2009). Oxidative stress and proinflammatory effects of carbon

black and titanium dioxide nanoparticles: Role of particle surface area and internalized amount. *Toxicology*, 260(1-3): 142-149.

Hussain, S., Thomassen, C., Ferecatu, I., Borot, C., Andreau, K., Martens, A and Marano F. (2010). Carbon black and titanium dioxide nanoparticles elicit distinct apoptotic pathways in bronchial epithelial cells. *Fibre Toxicology,* 16(7): 1012.

Iavicoli, I., Leso, V., Fontana, L and Bergamaschi, A. (2011). Toxicological effects of titanium dioxide nanoparticles: a review of *in-vitro* mammalian studies. *European review for medical and pharmacological sciences*, 15(5): 481-508.

Ichinose, S., Muneta, T., Sekiya, I., Itoh, S., Aoki, H and Tagami, M. (2003). The study of metal ion release and cytotoxicity in Co-Cr-Mo and Ti-Al-V alloy in total knee prosthesis - scanning electron microscopic observation. *Journal of Material Science* 14(1): 79-86.

Ingham, E and Fisher, J. (2000). Biological reactions to wear debris in total joint replacement. *Proceedings of the Institution of Mechanical Engineers, Part H: Journal of Engineering in Medicine*, 214(1): 21-37.

Isaacs, H. S. (1995). In situ X-ray microprobe study of salt layers during anodic dissolution of stainless steel in chloride solution. *Journal of The Electrochemical Society*, 142(4): 1111.

Ishii, J., Suzuki, K., Coban, C., Takeshita, F., Itoh, Y., Matoba, H., Kohn, D and Klinman, M. (2001). Genomic DNA released by dying cells induces the maturation of APCs. *Journal of Immunology,* 167(5): 2602-2607.

Itakura, A., Verbout, N., Phillips, K., Insall, R., Gailani, D., Tucker, E., Gruber, A and McCarty, O. (2011). Activated factor XI inhibits chemotaxis of polymorphonucleasr leukocytes. *Journal of Leukocyte Biology,* 90(1): 923-927.

Jacobs, J., Gilbert, J and Urban, R. (2011). Current concepts review - Corrosion of metal orthopaedic implants. *The Journal Of Bone And Joint Surgery*, 80A(2): 421-430.

Jin, C., Zhu, B., Wang, X and Lu, Q. (2008). Cytotoxicity of titanium dioxide nanoparticles in mouse fibroblast cells. *Chemical research in toxicology*, 21(9): 1871-1877.

Jin, C., Tang, Y., Yang, F., Li, X., Xu, S., Huang, y., et al. (2011). Cellular toxicity of TiO2 nanoparticles in anatase and rutile crystal phase. *Biological Trace Element Research*, 141(1-3): 3-15.

Johansson, H., Wennerberg, A and Albrektsson, T. (1998). Quantitative and qualitative investigations of surface enlarged titanum and titanium alloy implants. *Clinical Oral Implant Research*, 9: 1-10.

Jolivet, J., Cassaignon, S., Chanéac, C., Chiche, D., Durupthy, O and Liu, H. (2006). Nanomedicine for implants: a review of studies and necessary experimental tools. *Biomaterials,* 28: 354-69.

Jolivet, J., Cassaignon, S., Chanéac, C., Chiche, D., Durupthy, O and Portehault, D. (2010). Design of metal oxide nanoparticles: Control of size, shape, crystalline structure and functionalization by aqueous chemistry. *Comptes Rendus Chimie*, 13(1-2): 40-51.

Joshi, I and Eley, A. (1988). The *in-vitro* effect of a Titanium implant on oral microflora: Comparison with other metallic compounds. *Journal of Medical Microbiology*, 27(2): 105-107.

Jovanović, B. (2011). *Immunotoxicology of titanium dioxide and hydroxylated fullerenes engineered nanoparticles in fish models*. Ames, Iowa: Iowa State University].

Jovanović, B., Anastasova, L., Rowe, W., Zhang, Y., Clapp, R and Palić, D. (2011). Effects of nanosized titanium dioxide on innate immune system of fathead minnow. *Ecotoxicology and Environmental Safety*, 74(4): 675-683.

Kadenbach, B., Ramzan, R and Vogt, S. (2009). Degenerative diseases, oxidative stress and cytochrome C oxidase function. *Trends in Molecular Medicine*, 15(4): 139-147.

Kaida, T., Kobayashi, K., Adachi, M and Suzuki, F. (2004). Optical characteristics of titanium oxide interference film and the film laminated with oxides and their applications for cosmetics. *Journal of Cosmetic Science,* 55: 219–220.

Kang, J., Kim, M., Lee, J., Hong, H and Chung, W. (2009). Titanium dioxide nanoparticles induce apoptosis through the JNK/p38-caspase-8-Bid pathway in phytohemagglutinin-stimulated human lymphocytes. *Biochemical and Biophysical Research Communications*, 386(4): 682-687.

Kantarci, A., Oyaizu, K and Dyke, E. (2003). Neutrophil-mediated tissue injury in periodontal disease pathogenesis: Findings from localized aggressive periodontitis. *Journal of Periodontology*, 74(1): 66-75.

Kaplanski, G., Marin, V., Montero-Julian, F., Mantovani, A and Farnarier, C. (2003), IL-6: a regulator of the transition from neutrophil to monocyte recruitment during inflammation. *Trends in Immunology,* 24(1): 25-9.

Kasai, Y., Iida, R and Uchida A. **(2003).** Metal concentrations in the serum and hair of patients with titanium alloy spinal implants. *Spine,* 15(12):1320-6.

Kasemo, B. (1983). Biocompatibility of titanium implants: Surface Science Aspects. *The Journal of Prosthetic Dentistry*, 49(6): 832-837.

Kawai, T and Akira, S. (2009). The roles of TLRs, RLRs and NLRs in pathogen recognition. *International Immunology*, 21(4): 317-337.

Kessenbrock, K., Krumbholz, M., Schönermarck, U., Back, W., Gross, L and Werb, Z. (2009). Netting neutrophils in autoimmune small-vessel vasculitis. *Nature Medicine*, 15(6): 623-625.

Klebanoff, J. (2005). Myeloperoxidase: Friend and foe. *Journal of leukocyte Biology*, 77(5): 598-625.

Klinge, B., Hultin, M and Berglundh, T. (2005). Peri-implantitis. *The Dental Clinics of North America*, 49(3): 661-676.

Klokkevold, R and Newman, G. (2000). Current status of dental implants: A periodontal perspective. *The International Journal of Oral & Maxillofacial Implants*, 15(1): 56-65.

Knight, S., Carmona-Rivera, C and Kaplan, J. (2012). Proteins derived from neutrophil extracellular traps may serve as self-antigens and mediate organ damage in autoimmune diseases. *Immunol*ogy, 3: 380.

Kobayashi, T and Seguchi, H. **(1999).** Novel insight into current models of NADPH oxidase regulation, assembly and localization in human polymorphonuclear leukocytes. *Histopathology,* 14: 1295-308.

Koike, M and Fujii, H. (2001). *In-vitro* assessment of corrosive properties of Titanium as a biomaterial. *Journal of Oral Rehabilitation*, 28(6): 540-548.

Krautgartner, D and Vitkov, L. (2009). Visualization of Neutrophil Extracellular Traps in TEM. *Microscopy*, 39(4), 367-372.

Kroll, A., Mike, P., Hahn, D and Schenekenburger, J. (2009). Current *in-vitro* methods in nanoparticle risk assessment: Limitations and challenges. *European Journal of Pharmaceuticsw and Biopharmaceutics,* 72: 370-377.

Kruger, J. (1979) Fundamental aspects of corrosion of metallic implants. In corrosion and degradation of implant materials. *ASTM International,* 684: 107-113.

Kruger, J., Long, G., Zhang, Z and Tanaka, D. (1990). The use of x-ray absorption spectroscopic techniques to study the influence of alloying elements on passive films. *Corrosion Science*, 31, 111–120.

Kumar, V and Sharma, A. (2010). Neutrophils: Cinderella of innate immune system. *International Immunopharmacology*, 10(11): 1325-1334.

Kumazawa, R., Watari, F., Takashi, N., Tanimura, Y and Totsuka, Y. (2002). Effects of Ti ions and particles on neutrophil function and morphology. *Biomaterials,* 23(3): 3757-3764.

Lai, J., Lai, M., Jandhyam, S., Dukhande, V., Bhushan, A and Daniels, C. (2008). Exposure to titanium dioxide and other metallic oxide nanoparticles induces cytotoxicity on human neural cells and fibroblasts. *International Journal of Nanomedicine*, 3(4): 533–545.

Lalor, A., Revell, A., Gray, B., Wright, S., Railton, T and Freeman MA. (1991). Sensitivity to titanium. A cause of implant failure? *Journal of Bone Joint Surgery,* 73(1): 25-8.

Lande, R., Liu, Y., Wang, Y., Chatterjee, B., Facchinetti, V and Gregorio, V. (2007). Plasmacytoid dendritic cells sense self-DNA coupled with antimicrobial peptide. *Nature*, 449(7162): 564-569.

Lande, R., Liu, Y., Gregorio, J., Conrad, C., Frasca, L and Facchinetti, V. (2011). Neutrophils activate plasmacytoid dendritic cells by releasing self-DNA-peptide complexes in Systemic Lupus Erythematosus. *Science Translational Medicine*, 3(73), 7319-7319.

Lang, P., Wetzel, C., Stich, H and Caffesse, G. (1994). Histologic probe penetration in healthy and inflamed peri-implant tissues. *Clinical Oral Implants Research,* 5(4): 191-201.

Lappalainen, J., Juvonen, R., Nurmi, J and Karp, M. (2001). Automated color correction method for Vibrio fischeri toxicity test. Comparison of standard and kinetic assays. *Chemosphere*, 45(4-5): 635-41.

Larmonier, C., Midura-Kiela, M., Ramalingam, M., Laubitz, D., Janikashvili, N., Larmonier, N and Ghishan, F. (2011). Modulation of neutrophil motility by curcumin: Implications for inflammatory bowel disease. *Inflammatory Bowel Disease,* 17(2): 503-515.

Larsson, J., Persson, C., Tengvall, P and Lundqvist-Gustafsson, H. (2003). Anti-inflammatory effects of a titanium-peroxy gel: role of oxygen metabolites and apoptosis. *Journal of Biomaterials Research,* 68(3): 448-57.

L'Azou, B., Jorly, J., On, D., Sellier, E., Moisan, F and Fleury-Feith, J. (2008). In vitro effects of nanoparticles on renal cells. *Particle and Fibre Toxicology*, 5(1): 22.

Leonhardt, A., Adolfsson, B., Lekholm, U., Wikstrom, M and Dahlen, G. (1993). A longitudinal microbiological study on osseointegrated titanium implants in partially edentulotis patients. *Clinical Oral Implants Research*, 4(3): 113-120.

Li, Y., Wong, C., Xiong, J., Hodgson, P and Wen, C. (2010). Cytotoxicity of titanium and titanium alloying elements. *Journal of Dental Research*, 89(5): 493-497.

Lindhe, J and Meyle, J. (2008). Peri-implant diseases: Consensus report of the sixth European workshop on periodontology. *Journal of Clinical Periodontology*, 35: 282-285.

Lim, B., Kuiper, W., Katchky, A., Goldberg, H and Glogauer, M. (2011). Rac2 is required for the formation of Neutrophil Extracellular Traps. *Journal of leukocyte Biology*, 90(4): 771-776.

Lippincott-Schwartz, J. (2005). Cell Motility. *Current Protocols in Cell Biology,* 12:1201-1210.

Liu, H and Webster, T. J. (2006). Nanomedicine for implants: a review of studies and necessary experimental tools. *Biomaterials,* 28: 354-69.

Liu, S., Xu, L., Zhang, T., Ren, G and Yang Z. (2010). Oxidative stress and apoptosis induced by nanosized titanium dioxide in PC12 cells. *Toxicology,* 12, 267(1-3): 172-7.

Lobinski, R., Moulin, C and Ortega, R. (2006). Imaging and speciation of trace elements in biological environment. *Biochemistry,* 88(11):1591-1704.

Long, C., Tajuba, J., Sama, P., Saleh, N., Swartz, C and Parker, J. (2007). Nanosize titanium dioxide stimulates Reactive Oxygen Species in brain microglia and damages neurons. *Environmental Health Perspectives*, 115(11): 1631–1637.

Lovern, B and Klaper, R. (2006). Daphnia magna mortality when exposed to titanium dioxide and fullerene (C60) nanoparticles. *Environmental Toxicology Chemistry,* 25(4): 1132-7.

Lundqvist, H. (1996). Isoluminol-enhanced chemiluminescence: A sensitive method to study the release of superoxide anion from human neutrophils. *Free Radical Biology and Medicine*, 20(6), 785-792.

Luster, A. (1998). Mechanisms of disease. Chemokines-chemotactic cytokines that mediate inflammation. *The New England Journal of Medicine,* 12: 436-445.

Maloney, J., Smith, L., Castro, F and Schurman, J. (1993). Fibroblast response to metallic debris in vitro. Enzyme induction, cell proliferation and toxicity. *Journal of Bone Joint Surgery,* 75(6): 835-44.

Manzenreiter, R., Kienberger, F., Hannig, M., Studnicka, M., Vitkov, L and Hart, D. (2011). Ultrastructural characterization of cystic fibrosis sputum using atomic force and scanning electron microscopy. *Journal of Cystic Fibrosis*, 11(2): 84-92.

Martinelli, S., Urosevic, M., Daryadel, A., Oberholzer, A., Baumann, C., Fey, F., Dummer, R., Simon, U and Yousefi, S. (2004). Induction of genes mediating interferon-dependent extracellular trap formation during neutrophil differentiation. *Journal of Biological Chemistry,* 279(42): 44123-32.

Matthews, J., Wright, H., Roberts, A., Cooper, P and Chapple, C. (2007a). Hyperactivity and reactivity of peripheral blood neutrophils in chronic periodontitis. *Clinical and Experimental Immunology,* 147(2): 255-264.

Matthews, J., Wright, H., Roberts, A., Ling-Mountford, A., Cooper, P and Chapple, I. (2007b). Neutrophil hyper-responsiveness in periodontitis. *Journal of Dental Research,* 86(8): 718-722.

May, R and Machesky, L. (2001). Phagocytosis and the actin cytoskeleton. *Journal of Cell Science,* 114(6), 1061-77.

McQuillan, D. (1970). Interpretation of hydrogen solutions in bcc early transition metals. *The Journal of Chemical Physics*, 53(1): 156.

McRae, R., Bagchi, P., Sumalekshmy, S and Fahrni, J. (2009). In situ imaging of metals in cells and tissues. *Chemistry Review,* 109(10): 4780-827.

Medical Devices Agency. (2002). JRI Furlong modular cemented total hip replacement system-atypical pain associated with corrosion of the polished titanium alloy femoral stem.

Mee, K and Adelstein, J. (1981). Predominance of core histones in formation of DNA--protein crosslinks in gamma-irradiated chromatin. *Proceedings of the National Academy of Sciences,*78(4): 2194-8.

Meffert, R. (1996). Periodontitis vs. peri-implantitis: The same disease? The same treatment? *Critical Reviews in Oral Biology & Medicine*, 7(3): 278-291.

Meijer, M., Pruchniak, M., Arazna, M and Demkow, U. (2012). Experimental immunology Extracellular Traps: How to isolate and quantify extracellular DNA (ET-DNA). *Central European Journal of Immunology*, *37*(4), 321-325.

Menegazzi, R., Decleva, E and Pietro, D. (2012). Killing by Neutrophil Extracellular Traps: Fact or folklore? *Blood,* 119(5): 1214-16.

Meng, B and Yang, X. (2013). Titanium particles enhanced osteoclast differentiation and osteoclast bone resorption activity in vitro. *Journal of Dentistry and Oral Hygiene*, 5(2): 7-12.

Menini, R., Dion, M., So, K., Gauthier, M and Lefebvre, L. (2005). Surface and corrosion electrochemical characterization of titanium foams for implant applications. *Journal of The Electrochemical Society*, 153(1): B13.

Metchnikoff, E. (1893). *Lectures on the comparative pathology of inflammation delivered at the Pasteur Institute in 1891*. London: Kegan Paul.

Metchnikoff, E. (1905). *Immunity in infective diseases*. Cambridge: University press.

Metzler, K., Fuchs, T., Nauseef, W., Reumaux, D., Roesler, J and Schulze, I. (2011). Myeloperoxidase is required for neutrophil extracellular trap formation: implications for innate immunity. *Blood*, 117(3): 953-9.

Miller, S., Pietras, M., Uricchio, H., Hirano, K., Rao, S., Lin, H., O'Connell, M., Iwakura, Y., Cheung, L., Cheng, G and Modlin, L. (2007). Inflammasome-mediated production of IL-1beta is required for neutrophil recruitment against Staphylococcus aureus in vivo. *Journal of Immunology,* 179(10): 6933-42.

Mombelli, A., Oosten, A., Schürch, E and Lang, P. (1987). The microbiota associated with successful or failing osseointegrated titanium implants. *Oral Microbiology and Immunology*, 2(4): 145-151.

Mombelli, A., Marxer, M., Gaberthüel, T., Grander, U and Lang, P. (1995). The microbiota of osseointegrated implants in patients with a history of periodontal disease. *Journal of Clinical Periodontology*, 22(2): 124-130.

Moseley, R., Waddington, R and Embery, G. (1997). Degradation of glycosaminoglycans by Reactive Oxygen Species derived from stimulated polymorphonuclear leukocytes. *Biochimica et Biophysica Acta (BBA) - Molecular Basis of Disease*, 1362(2-3): 221-231.

Mosselmans, F., Atkinson, D., Rosell, R., Gregory, R., Keylock, J and Leicester, J. (2009). I18–The microfocus spectroscopy beamline at The Diamond Light Source. *Journal of Synchrotron Radiation*, 16(6): 818-824.

Mountjoy, G., Pickup, D., Wallidge, G., Cole, J., Newport, R and Smith, M. (1999). In-situ high-temperature XANES observations of rapid and reversible changes in Ti coordination in titania–silica xerogels. *Chemical Physics Letters*, 1, 150–154.

Mudali, U., Sridhar, M and Raj, B. (2003). Corrosion of bio-implants. *Sadhana*, 28(3-4): 601-637.

Muinonen-Martin, A., Veltman, D., Kalna, G and Insall, R. (2010). An improved chamber for direct visualisation of chemotaxis. *Nature Cell Biology,* 5(12): 193-200.

Nathan, C. (2006). Neutrophils and immunity: Challenges and opportunities. *Nature Reviews Immunology*, 6(3): 173-182.

Nathan, C and Bussel, C. (2013). Beyond oxidative stress: an immunologist's guide to reactive oxygen species. *Nature Review Immunology*, 13: 349-361.

Neeli, I., Dwivedi, N., Khan, S and Radic, M. (2009). Regulation of extracellular chromatin release from neutrophils. *Journal of Innate Immunity*, 1(3): 194-201.

Nel, A. (2006). Toxic potential of materials at the nanolevel. *Science*, 311(5761): 622-627.

Neumanann, A. (2009). Biomaterials for craniofacial reconstruction. *German Medical Science Current Topics in Otorhinolaryngology, Head and Neck Surgery*, 8(1): S48-63.

Newton, A. C. (1995). Protein Kinase C: Structure, function and regulation. *Journal of Biological Chemistry,* 270(48): 28495-28498.

Niinomi, M. (2003). Recent research and development in titanium alloys for biomedical applications and healthcare goods. *Science and Technology of Advanced Materials*, 4(5): 445-454.

Noguchi, T., Takemoto, S., Hattori, M., Yoshinari, M., Kawada, E and Oda, Y. (2008). Discoloration and dissolution of titanium and titanium alloys with immersion in peroxide- or fluoride-containing solutions. *Dental Materials Journal,* 27(1): 117-23.

Noll, M. (1974). Subunit structure of chromatin. *Nature*, 251(5472): 249-251.

Oehmcke, S., Mörgelin, M and Herwald, H. (2009). Activation of the human contact system on Neutrophil Extracellular Traps. *Journal of Innate Immunity*, 1(3): 225-230.

O'Flaherty, T., Kreutzer, L., Showell, S., Becker, L and Ward, A. (1978). Desensitization of the neutrophil aggregation response to chemotactic factors. *Journal of Pathology,* 93(3): 693-706.

Okafor, C., Haleem-Smith, H., Laqueriere, P., Manner, A and Tuan, S. (2006). Particulate endocytosis mediates biological responses of human mesenchymal stem cells to titanium wear debris. *Journal of Orthopaedic Research,* 24(3): 461-73.

Oklu, R., Albadawi, H., Jones, E., Yoo, J and Watkins, T. (2013). Reduced hind limb ischemia-reperfusion injury in Toll-like receptor-4 mutant mice is associated with decreased neutrophil extracellular traps. Journal of Vascular Surgery, 214(13): 552-561.

Olmedo, G., Tasat, R., Evelson, P., Guglielmotti, B and Cabrini, L. (2008). Biological response of tissues with macrophagic activity to titanium dioxide.

Journal of Biomedical Materials Research Part A, 84A(4): 1087-1093.

Onuma, K., Ogawara, S and Su, N. (2009). Nano-scaled particles of titanium dioxide convert benign mouse fibrosarcoma cells into aggressive tumor cells. *The American Journal of Pathology*, 175(5): 2171-83.

Ortega, R., Deves, G and Carmona, A. (2009). Bio-metals imaging and speciation in cells using proton and synchrotron radiation X-ray microspectroscopy. *Journal of the Royal Society Interface,* 5: S749-58.

Osano, E., Kishi, J and Takahashi, Y. (2003). Phagocytosis of titanium particles and necrosis in TNF-alpha-resistant mouse sarcoma L929 cells. *Toxicolology In Vitro*, 17(1): 41-7.

Palmer, L., Cooper, P., Ling, M., Wright, H., Huissoon, A and Chapple, I. (2012). Hypochlorous acid regulates neutrophil extracellular trap release in humans. *The Journal of Translational Immunology*, 167: 261-268.

Papayannopoulos, V., Metzler, D., Hakkim, A and Zychlinsky, A. (2010). Neutrophil elastase and myeloperoxidase regulate the formation of Neutrophil Extracellular Traps. *The Journal of Cell Biology*, 191(3): 677-691.

Park, M., Shigenaga, K., Degan, P., Korn, S., Kitzler, W and Wehr, M. (1992). Assay of excised oxidative DNA lesions: isolation of 8-oxoguanine and its nucleoside derivatives from biological fluids with a monoclonal antibody column. *Journal of Immunology,* 23(1): 184.

Park, E., Yi, J., Chung, K., Ryu, D., Choi, J and Park, K. (2008). Oxidative stress and apoptosis induced by titanium dioxide nanoparticles in cultured BEAS-2B cells. *Toxicology Letters*, 180(3): 222-229.

Parker, H., Albert, A., Kettle, A and Winterbourn, C. (2012). Myeloperoxidase associated with neutrophil extracellular traps is active and mediates bacterial killing in the presence of hydrogen peroxide. *Journal of leukocyte biology*, 91(3): 369-76.

Parsonage, G., Filer, A., Bik, M., Hardie, D., Lax, S., Howlett, K., Church, D., Raza, K., Wong, H., Trebilcock, E., Scheel-Toellner, D., Salmon, M., Lord, M and Buckley, D. (2008). Prolonged, granulocyte-macrophage colony-stimulating factor-dependent, neutrophil survival following rheumatoid synovial fibroblast activation by IL-17 and TNF-α. *Arthritis Research Therapy,* 10 (2): R47.

Peng, L., Barczak, J., Barbeau, A., Xiao, Y., LaTempa, J and Grimes, A. (2010). Whole genome expression analysis reveals differential effects of TiO nanotubes on vascular cells. *Nano Letters*, 10(1): 143-148.

Peters, K., Unger, R. E., Kirkpatrick, C. J., Gatti, A. M and Monari, E. (2004). Effects Of nano-scaled particles on endothelial cell function in vitro:

Studies on viability, proliferation and inflammation. *Journal of Materials Science: Materials in Medicine*, 15(4): 321-325.

Petibois, C and Guidi, M. (2008). Bioimaging of cells and tissues using accelerator-based sources. *Analytical Bioanalysis Chemistry,* 391(5):1599-608.

Pierre, C. A. (2010). *Endocytosis, Phagocytosis, and Innate Immune Responses: a dissertation*. Massachusetts: University of Massachusetts Medical School.

Pilsczek, F., Salina, K., Poon, C., Fahey, B., Yipp, C and Sibley, S. (2010). A novel mechanism of rapid nuclear neutrophil extracellular trap formation in response to Staphylococcus aureus. *Journal of Immunology*, 185(12), 7413-25.

Pioletti, P., Takei, H., Kwon, Y., Wood, D. and Sung, P. (1999). The cytotoxic effect of titanium particles phagocytosed by osteoblasts. *Journal of Biomedical Materials Research*, 46(3): 399-407.

Pontoriero, R., Tonelli, P., Carnevale, G., Mombelli, A., Nyman, R and Lang, P. (1994). Experimentally induced peri-implant mucositis. A clinical study in humans. *Clinical Oral Implants Research*, 5(4): 254-259.

Punshon, T., Jackson, P., Lanzirotti, A., Hopkins, A., Bertsch, M and Burger, J. (2005). Application of synchrotron X-ray microbeam spectroscopy to the determination of metal distribution and speciation in biological tissues. *Spectroscopy Letters,* 38(3):343-373.

Quirynen, M., Vogels, R., Peeters, W., Steenberghe, D., Naert, I and Haffajee, A. (2006). Dynamics of initial subgingival colonization of 'pristine' peri-implant pockets. *Clinical Oral Implants Research*, 17(1): 25-37.

Rae, T. (1978). The haemolytic action of particulate metals (Cd, Cr, Co, Fe, Mo, Ni, Ta, Ti, Zn, Co-Cr Alloy). *The Journal of Pathology*, *125*(2): 81-89.

Rahman, Q., Lohani, M., Dopp, E., Pemsel, H., Jonas, L., Weiss, G and Schiffmann, D. (2002). Evidence that ultrafine titanium dioxide induces micronuclei and apoptosis in Syrian hamster embryo fibroblasts. *Environonmental Health Perspective,* 110(8): 797–800.

Ramos-Kichik, V., Mondragón-Flores, R., Mondragón-Castelán, M., Gonzalez-Pozos, S., Muñiz-Hernandez, S and Rojas-Espinosa, O. (2009). Neutrophil Extracellular Traps are induced by Mycobacterium Tuberculosis. *Tuberculosis*, 89(1), 29-37.

Rams, T and. Feik, S. (1990). *Staphylococci* in human periodontal diseases. *Oral Microbiology Immunology,* 32: 529.

Ratner, D. (2001). Replacing and renewing: Synthetic materials, biomimetics, and tissue engineering in implant dentistry. *Journal of Dental Education*, 65(12):

1340-1347.

Ravel, B and Newville, M. (2005) Athena, Artemis, Hephaestus: Data analysis for X-ray absorption spectroscopy using IFEFFIT. *Journal of Synchrotron Radiation,* 12: 537-541.

Remer, A., Bricic, M and Jungi, W. (2003). Toll-like receptor-4 is involved in eliciting an LPS-induced oxidative burst in neutrophils. *Immunology Letters*, 85(1): 75-80.

Remijsen, Q., Willems, J., Delforge, M., Noppen, S., Rycke, D., Parthoens, E., Asselbergh, B., Wirawan, E and Vanden, T. (2010). Neutrophil Extracellular Trap cell death requires both autophagy and superoxide generation. *Cell research*, *21*(2), 290-304.

Remijsen, Q., Kuijpers, W., Wirawan, E., Lippens, S., Vandenabeele, P and Vanden, T. (2011). Dying for a cause: NETosis, mechanisms behind an antimicrobial cell death modality. *Infection and Immunity,* 18(4): 581-8.

Renvert, S., Roos-Jansåker, A. Lindahl, C., Renvert, H and Persson, R. (2007). Infection at titanium implants with or without a clinical diagnosis of inflammation. *Clinical Oral Implants Research*, 18: 509–516.

Renwick, L. (2001). Impairment of alveolar macrophage phagocytosis by ultrafine particles. *Toxicology and Applied Pharmacology*, *172*(2): 119-127.

Riyapa, D., Buddhisa, S., Korbsrisate, S., Cuccui, J., Wren, W., Stevens, P and Lertmemongkolchai G. (2012). Neutrophil extracellular traps exhibit antibacterial activity against burkholderia pseudomallei and are influenced by bacterial and host factors. *Infection and Immunity,* 80(11): 3921-9.

Roberfroid, B and Calderon, P. (1995). *Free radicals and oxidation phenomena in biological systems*. New York: M. Dekker.

Robinson, J. M. (2008). Reactive Oxygen Species in phagocytic leukocytes. *Histochemistry and Cell Biology*, 130(2): 281-297.

Rothen-Rutishauser, B., Mueller, L., Blank, F., Brandenberger, C., Muehlfeld, C and Gehr, P. (2008). A newly developed in vitro model of the human epithelial airway barrier to study the toxic potential of nanoparticles. *Journal of Toxicology,* 25(3): 191-6.

Rubio, C., Garcia-Alonso, C., Alonso, C., Alobera, A., Clemente, C., Munuera, L andEscudero, L. (2008). Determination of metallic traces in kidneys, livers, lungs and spleens of rats with metallic implants after a long implantation time. *Journal of Materials Science: Materials in Medicine*, 19(1): 369-375.

Saffarzadeh, M., Juenemann, C., Queisser, A., Lochnit, G and Barreto, G. (2012) Neutrophil Extracellular Traps directly induce epithelial and endothelial cell death: A predominant role of histones. *PLoS Immunity,* 7(2): 366.

Sargeant, A and Goswami, T. (2007). Hip implants-Paper VI-Ion concentrations. *Materials and Design*, 28(1): 155-171.

Sarmiento-González, A., Encinar, R., Marchante-Gayón, M and Sanz-Medel, A. (2009). Titanium levels in the organs and blood of rats with a titanium implant, in the absence of wear, as determined by double-focusing ICP-MS. *Analytical Chemistry,* 393(1): 335-43.

Sayes, M. (2006). Correlating nanoscale titania structure with toxicity: A cytotoxicity and inflammatory response study with human dermal fibroblasts and human lung epithelial cells. *Toxicological Sciences*, 92(1), 174-185.

Sbarra, J and Karnovsky, L. (1959). The biochemical basis of phagocytosis. Metabolic changes during the ingestion of particles by polymorphonuclear leukocytes. *Journal of Biological Chemisty,* 234(6): 1355-62.

Scales, T. (1991). Black staining around titanium alloy prostheses; an orthopaedic enigma. *Journal of Bone and Joint Surgery*, 73(1): B534-6.

Schanen, C., Karakoti, S., Seal, S., Drake, I., Warren, L and Self, T. (2009). Exposure to titanium dioxide nanomaterials provokes inflammation of human immune construct. *ACS Nanoscience*, 3(9): 2523-2532.

Schroeder, A., Vanderzypen, E., Stich, H and Sutter, F. (1981). The reactions of bone, connective tissue, and epithelium to endosteal implants with titanium-sprayed surfaces. *Journal of Maxillofacial Surgery*, 9: 15-25.

Segal, W. (2005). How neutrophils kill microbes. *Annual Review of Immunology*, 23(1): 197-223.

Seligmann, E and Gallin, I. (1980). Use of lipophilic probes of membrane potential to assess human neutrophil activation. Abnormality in chronic granulomatous disease. *Journal of Clinical Investigation,* 66, 493-503.

Shanbhag, S., Jacobs, J., Black, J., Galante, O and Glant, T. (1995). Human monocyte response to particulate biomaterials generated in vivo and in vitro. *Journal of Orthopaedic Research,* 13(5):792-801.

Shi, X., Ding, M., Ye, J., Wang, S., Leonard, S., Zang, L., Castranova, V., Vallyathan, V., Chiu, A and Liu, K. (1999). Cr (IV) causes activation of nuclear transcription factor-kappa B, DNA strand breaks and dG hydroxylation via free radical reactions. Journal of Inorganic Biochemistry, 75(1): 37-44.

Shreir, L., Jarman, R and Burstein, G. (1993). *Corrosion*. Oxford: Butterworth-Heinemann.

Socransky, S., Haffajee, D., Cugini, A., Smith, C and Kent, L. (1998). Microbial complexes in sub-gingival plaque. *Journal of Clinical Periodontology,* 25(2): 134-144.

Soto, K., Garza, K and Murr, L. (2007). Cytotoxic effects of aggregated nanomaterials. *Acta Biomaterialia*, 3(3): 351-358.

Souto, M and Burstein, G. T. (1996). A preliminary investigation into the microscopic depassivation of passive titanium implant materials in vitro. *Journal of Materials Science: Materials in Medicine*, 7(6): 337-343.

Stearns, C., Paulauskis, D and Godleski, J. (2001). Endocytosis of ultrafine particles by A549 cells. *Journal of Respiratory Cell Molecular Biology,* 24(2): 108-15.

Stevens, P., Winston, J and Dyke, K. (1978). In vitro evaluation of opsonic and cellular granulocyte function by luminol-dependent chemiluminescence: utility in patients with severe neutropenia and cellular deficiency states. *Infection and Immunity,* 22(1): 41-51.

Stevens, A., Lowe, S., Wheater, R., Young, B and Burkitt, G. (2002). *Wheater's Basic Histopathology: A Colour Atlas and Text,* Michigan, Churchill Livingstone.

Squier, K., Sehnert, J and Cohen, J. (1995). Apoptosis in leukocytes. *Journal of Leukocyte Biology,* 57:2–10.

Sunny, C and Sharma, P. (1991). Titanium-protein interaction: changes with oxide layer thickness. *Journal of Biomaterials Applications*, 6(1): 89-98.

Takei, H., Araki, A., Watanabe, H., Ichinose, A and Sendo, F. (1996). Rapid killing of human neutrophils by the potent activator phorbol 12-myristate 13-acetate (PMA) accompanied by changes different from typical apoptosis or necrosis. *Journal of Leukocyte Biology,* 59: 229–240.

Tamura, K., Takashi, N., Kumazawa, R., Watari, F and Totsuka, Y. (2002). Effects of particle size on cell function and morphology in Titanium and Nickel. *Materials Transactions*, 43(12): 3052-3057.

Tang, L and Eaton, W. (1995). Inflammatory responses to biomaterials. *Journal of Clinical Pathology*, 103(4): 466-71.

Tapper, H. (1996). The secretion of preformed granules by macrophages and neutrophils. *Journal of Leukocyte Biology,* 59(5): 613-622.

Tengvall, P., Elwing, H and Lundstrom, I. (1989). Titanium gel made from metallic titanium and hydrogen peroxide. *Journal of Colloid and Interface Science*, *130*(2): 405-413.

Tengvall, P., Lundstrom, I., Sjoqvist, L., Elwing, H and Bjursten, L. (1989). Titanium-hydrogen peroxide interaction: Model studies of the influence of the inflammatory response on titanium implants. *Biomaterials*, 10(3): 166-175.

Teronen, O., Konttinen, Y., Lindqvist, C., Salo, T., Ingman, T., Lauhio, A., Ding, S and Santavirta, S. (1997). Human neutrophil collagenase MMP-8 in peri-implant sulcus fluid and its inhibition by clodronate. *Journal of Dental Research*, 76(9): 1529-1537.

Teufelhofer, O., Weiss, R., Parzefall, W., Schulte-Hermann, R., Micksche, M., Berger, W and Elbling, L. (2003). Promyelocytic HL60 cells express NADPH oxidase and are excellent targets in a rapid spectrophotometric microplate assay for extracellular superoxide. *Toxological Sciences,* 76(2): 376-383.

Thomas, R., Shukla, D and Latham, D. (2004). Corrosion of cemented titanium femoral stems. *Journal of Bone Joint Surgery,* 86(7): 974-8.

Thorek, L and Tsourkas, A. (2008). Size, charge and concentration dependent uptake of iron oxide particles by non-phagocytic cells. *Biomaterials*, 29(26): 3583-3590.

Tillack, K., Breiden, P., Martin, R and Sospedra, M. (2012). T lymphocyte priming by neutrophil extracellular traps links innate and adaptive immune responses. *Journal of Immunology*, *188*(7): 3150-9.

Tirado-Miranda, M., Schmitt, A., Callejas-Fernández, J and Fernández-Barbero, A. (2003). The aggregation behaviour of protein-coated particles: a light scattering study. *European Biophysics Journal,* 32(2): 128-36.

Tong, Z., Eric, B., Dallas, M., Hung, W., Stebe, K and Konstantopoulos, K. (2012). Chemotaxis of cell populations through confined spaces at single cell resoloution. *Nature Cell Biology,* 7(1): 960-1012.

Tsutsui, T., Kawaguchi, H., Fujino, A., Sakai, A., Kaji, H and Nakamura, T. (1999). Exposure of Macrophage-like cells to Titanium particles does not affect bone resorption, but inhibits bone formation. *Journal of Orthopaedic Science*, 4(1): 32-38.

Tuan, S., Lee, Y., Konttinen, T., Wilkinson, M and Smith, L. (2008). What are the local and systemic biologic reactions and mediators to wear debris and what host factors determine or modulate the biologic response to wear particles? *Journal of the American Academy of Orthopaedic Surgeons*, 16(1): S42-S48.

Uchino, T., Tokunaga, H. and Utsumi, H. (2002). Quantitative determination of OH radical generation and its cytotoxicity induced by TiO(2)-UVA treatment. *Toxicology In Vitro*, 16(5): 629-35.

Uo, M., Asakura, K., Yokoyama, A., Ishikawa, M., Tamura, K., Totsuka, Y., Akasaka, T and Watari, F. (2007). X-ray absorption fine structure (XAFS) analysis of titanium-implanted soft tissue. Dental Materials Journal, 26(2): 268-73.

Urban, R., Jacobs, J., Tomlinson, M., Gavrilovic, J., Black, J and Peoch, M. (2000). Dissemination of wear particles to the liver, spleen and abdominal lymph nodes of patients with hip or knee replacement. *The Journal of Bone and Joint Surgery,* 82: 457-476.

Urban, F., Reichard, U., Brinkmann, V and Zychlinsky, A. (2006). Neutrophil Extracellular Traps capture and kill *Candida Albicans* yeast and hyphal forms. *Cellular Microbiology*, 8(4): 668-676.

Urban, F., Zychlinsky, A., Jungblut, R., Brinkmann, V., Nacken, W and Goosmann, C. (2009). Neutrophil Extracellular Traps contain Calprotectin, a cytosolic protein complex involved in host defense against *Candida Albicans*. *PLoS Pathogens*, 5(10): 639.

Vamanu, I., Høl, P., Allouni, Z., Elsayed, S and Gjerdet, N. (2008). Formation of potential titanium antigens based on protein binding to titanium dioxide nanoparticles. *International Journal of Nanomedicine*, 3(1): 69-74.

Vicentini, B., Sinigaglia, D and Taccani, G. (1975). Crevice corrosion of titanium. Behaviour of galvanic cell between shielded and unshielded titanium in sulphuric acid. *Corrosion Science*, 15(6-12): 479-492.

Vitkov, L., Klappacher, M., Hannig, M and Krautgartner, W. D. (2009). Extracellular Neutrophil Traps in Periodontitis. *Journal of Periodontal Research*, 44(5): 664-672.

Von Köckritz-Blickwede, M., Goldmann, O., Thulin, P., Heinemann, K., Norrby-Teglund, A., Rohde, M and Medina, E. (2008). Phagocytosis-independent antimicrobial activity of mast cells by means of extracellular trap formation. *Blood,* 111(6): 3070-80.

Wagner, J and Roth, R. (2000). Neutrophil migration mechanisms, with an emphasis on the pulmonary vasculature. *The American Society for Pharmacology and Experimental Therapeutics,* 52(3): 349-368.

Wang, J., Li, B., Gao, Y., Jia, G., Ma, Y., Wang, T., Ma, Y., Jia, G., Gao, Y., Li, B., Sun, J., Li, Y., Jiao, F., Zhao, Y and Chai, Z. (2007). Acute toxicity and bio-distribution of different sized titanium dioxide particles in mice after oral administration. *Toxicology Letters*, 168(2): 176-185.

Wang, J., Fan, Y., Gao, Y., Hu, Q and Wang, T. (2009). TiO_2 nanoparticles translocation and potential toxicological effect in rats after intraarticular injection. *Biomaterials*, 30(27): 4590-4600.

Wang, Y., Allis, D., Li, M., Coonrod, A., Grigoryev, A and Han, H. (2009). Histone hypercitrullination mediates chromatin decondensation and Neutrophil Extracellular Trap Formation. *The Journal of Cell Biology*, 184(2): 205-213.

Warheit, D. (1997). Inhalation of high concentrations of low toxicity dusts in rats results in impaired pulmonary clearance mechanisms and persistent inflammation. *Toxicology and Applied Pharmacology*, 145(1): 10-22.

Wazen, J., Young, L., Farrugia, C., Chandrasekhar, S., Ghossaini, N., Borik, J., Soneru, C and Spitzer, B. (2008). Successes and complications of the Baha System. *Otology & Neurotology*, 29(8): 1115-1119.

Weng, T., Waldo, S and Penner-Hahn, E. (2005). A method for normalization of X-ray Absorption Spectra. *Journal of Synchrotron Radiation*, 12(4): 506-510.

Williams, D. (1981). Implants in dental and maxillofacial surgery. *Biomaterials*, 2(3): 133-146.

Williams, D. F. (1987). *Definitions in biomaterials: Proceedings of a consensus conference of the European Society for Biomaterials.* Amsterdam: Elsevier.

Williams, D. F. (1994). Titanium: epitome of biocompatibility or cause for concern. *The Journal Of Bone And Joint Surgery*, 76(3): 348-349.

Willmott, P. (2011). *An introduction to synchrotron radiation techniques and applications*. Chichester, West Sussex, U.K.: Wiley.

Witko-Sarsat, V., Rieu, P., Descamps-Latscha, B., Lesavre, P and Halbwachs-Mecarelli, L. (2000). Neutrophils: Molecules, functions and pathophysiological aspects. *Lab Investigation,* 80(5): 617-653.

Wright, H., Matthews, J., Chapple, I., Ling-Mountford, N and Cooper, P. (2008). Periodontitis associates with a type 1 IFN signature in peripheral blood neutrophils. *Journal of Immunology,* 181(8): 5775-5784.

Wright, H., Moots, R., Bucknall, R and Edwards, W. (2010). Neutrophil function in inflammation and inflammatory diseases. *Rheumatology*, 49(9): 1618-1631.

Wu, J., Chen, H., Li, L., Wu, W and Sung, L. (2005) Influence of different-sized titanium particles loading on osteoblastic differentiation and mineralization. *Journal of Biomaterials Medical Research,* 22(1): 30-4.

Wu, J., Guo, Y., He, X and Chen, H. (2011). Effect of titanium particle size on osteogenic differentiation of Bone Marrow–Derived Mesenchymal Stem cells. *Key Engineering Materials*, *474*: 1939-1942.

Xing, Z., Schwab, P., Alley, F., Hasty, A and Smith, A. (2008). Titanium particles that have undergone phagocytosis by macrophages lose the ability to activate other macrophages. *Journal of Biomedical Materials Research,* 85(1): 37-41.

Xu, J., Lupu, F., Esmon, L., Taylor, B., Semeraro, F and Ammollo, T. (2009). Extracellular histones are major mediators of death in Sepsis. *Nature Medicine*, *15*: 1318-13321.

Yamaguchi, M., Yoshida, H and Nohta, H. (2002). Luminol-type chemiluminescence derivatization reagents for liquid chromatography and capillary electrophoresis. *Journal of Chromatography A*, 950(1-2): 1-19.

Yokota, A., Yukawa, K., Yamamoto, A., Sugiyama, K., Suemura, M., Tashiro, Y., Kishimoto, T and Kikutani, H. (1992). Two forms of the low affinity Fc receptor for IgE differentially mediate endocytosis and phagocytosis: identification of the critical cytoplasmic domains. *Proceedings of National Academy of Sciences,* 50, 30-5034.

Zhang, P and Sun, P. (2004). Photocatalytic killing effect of TiO_2 nanoparticles on Ls-174-t human colon carcinoma cells. *Journal of Gastroenterology,* 10: 3191–3193.

APPENDIX I

11.1 Selection of volunteers

Healthy volunteers were recruited from Birmingham Dental School, University of Birmingham, UK. Ethical approval was obtained from School of Medicine and Dentistry, University of Birmingham Dental Hospital, UK and donors gave their informed consent. Exclusion criteria included volunteers were non-diabetic, non-smokers, no special dietary requirements, did not consume or use any recreational drugs and did not have any course of non-steroidal anti-inflammatory drugs (NSAID's) in the past 24 hours prior to blood collection.

11.2 Collection and isolation of peripheral blood neutrophils (PBN)

The following section details the isolation of peripheral blood neutrophils (PBN) from whole blood. At least 18 mL or more blood was collected from the ante-cubital fossa into lithium heparin coated tubes (171 U/mL) through a vacutainer (Greiner, Bio-one Ltd, Stonehouse, UK). PBN were extracted using discontinuous Percoll® (1.13 g/mL) (17-0891-01; GE Healthcare, Buckinghamshire, UK) density centrifugation (Matthews et al., 2007) (section 11.3).

11.3 Percoll® density gradients preparation

The isolation of cells of interest by Percoll® density gradient is based on the differences in size or buoyant density existing in a population of cells. Therefore, two Percoll® densities (δ=1.079 and 1.098 g/mL) were prepared (Table 11.1).

Table 11.1 Reagents and volumes used to prepare Percoll® densities (δ=1.079 and 1.098 g/mL)

Density	Volume in mL for Percoll® density 1.079 g/mL	Volume in mL for Percoll® density 1.098 g/mL
Percoll®	19.708	24.823
Water	11.792	6.677
1.5 M NaCl	3.500	3.500

Discontinuous Percoll® gradient was prepared by layering 8 mL of 1.098 Percoll® density underneath 8 mL of 1.079 Percoll® density in a 25 mL centrifuge tube. These were stored at 4 °C until use.

Percoll® forms self-generated gradients with centrifugation in 1.5 M NaCl (S9625; Sigma-Aldrich, UK) as consists of colloidal silica particles of 15-30 nm diameter (23% w/w in water) that are coated with polyvinylpyrrolidone (PVP) (Sigma-Aldrich, Chemical Company, Poole, UK). Also another advantage of using Percoll® is that its inert nature prevents interfering with downstream assays in comparison to dextran/ficoll method which can pre-activate neutrophils.

11.4 Lysis buffer

1 L of lysis buffer was made by adding 8.3 g NH_4Cl (A9434; Sigma-Aldrich), 1 g $KHCO_3$ (P9144; Sigma-Aldrich), 0.04 g $C_{10}H_{14}N_2Na_2O_8 \cdot 2H_2O$ (E5134; Sigma-Aldrich) and 2.5 g Bovine Serum Albumin (BSA) (A4530 Sigma-Aldrich) to 1 L of water (Versol, Somerset, UK) and stored at 4 °C until use. Buffer was replenished after 30 days as degradable.

11.5 Phosphate buffered saline (PBS)

1 L of PBS was made by combining 7.75 g NaCl (S9625; Sigma-Aldrich), 0.2 g KH_2PO_4 (P5379; Sigma-Aldrich) and 1.5 g K_2HPO_4 (P8281; Sigma-Aldrich) in 1 L distilled water. The buffer pH was adjusted to 7.3, autoclaved and stored at 4 °C.

11.6 Neutrophil isolation

Whole blood (~6 mL) was layered on top of percoll gradients (section 11.3) and centrifuged for 8 mins at 150 rcf, followed by 10 mins at 1200 rcf. The plasma, lymphocyte and monocyte layers separated were carefully removed and discarded by manual aspiration using a plastic pasteur pipette. The neutrophil layer located at the top of the red blood cell layer was transferred, again using a plastic pasteur pipette, to a 50 mL centrifuge tube containing 15 mL lysis buffer (section 11.4). The tube was gently inverted to mix, and incubated at room temperature for 5 mins until red blood cells had lysed. This was then centrifuged for 6 mins at 500 rcf to pellet the neutrophils. The supernatant was discarded and the pellet was re-suspended in 3 mLs of lysis buffer and incubated for 5 mins at room temperature prior to re-centrifugation at 500 rcf for 6 mins. The supernatant was removed; the pellet was washed in 3 mLs of PBS (section 11.5), and centrifuged once more for 6 mins at 500 rcf before re-suspension in 3 mLs of PBS.

11.7 Cell viability

Cells were counted using a light microscope (LeitzLaborlux s, Germany) and haemocytometer (Neubauer, Reichart, Germany). Cell viability was determined by trypan blue exclusion (1:1 mix of cells with trypan blue) (T8154; Sigma-Aldrich, UK) immediately prior to assay and was typically >98%.

Neutrophils of interest were used immediately by re-suspending in either PBS or RPMI-1640 for *ex-vivo* neutrophil functional assays (Chapters 5-8).

APPENDIX II

12.1 Bacterial stimuli preparation

Bacteria were used as control stimuli for neutrophil functional assays (Chapters 5-8). Bacteria were grown in broth cultures and rinsed twice by centrifugation at 1087 rcf for 40 mins. The supernatant was removed and the pellet was then re-suspended in sterile PBS (Appendix I) following bacterial number estimation using spectrophotometry (section 12.11). Bacterial suspensions were then diluted in sterile PBS and stored at -30 °C/- 80 °C respectively until further use.

12.2 Mannitol salt agar (MSA)

MSA (ThermoFisher Scientific, Oxford, UK) contains 7.5% NaCl which inhibits growth of gram negative bacteria. Therefore gram positive bacteria were grown according to manufacturer's instructions. Briefly, 55.5 g of MSA was dissolved in 500 mL of distilled water. Post autoclaving at 121 °C for 15 mins the agar was cooled to 50 °C in a water bath. Agar was poured into Petri dishes (101VR20; Sterilin, Newport, UK) allowing around 25 mins settling time and then stored at 4 °C until further use.

12.3 Horse blood agar

5% defibrinated horse blood (SR0050B; Oxoid) was aseptically added to tryptone soya agar (CM0131; Oxoid) prepared according to manufacturer's instructions. 40 g of tryptone soya agar was dissolved in 1 L of distilled water and autoclaved at

121 °C for 15 mins. The agar was then cooled to 50 °C in a water bath. Agar was pored into petri dishes (101VR20; Sterilin, Newport, UK) allowing to equilibrate at room temperature for 1 hr and then stored at 4 °C until further use.

12.4 Tryptone soya broth

Tryptone soya broth (ThermoFisher Scientific, Oxford, UK) was prepared according to the manufactures instructions. 111 g of tryptone soya broth was dissolved in 1 L of distilled water and autoclaved.

12.5 Opsonisation of *S. aureus* (Ops *Sa*)

Staphylococcus aureus (ATCC 9144) was cultured on MSA (section 12.2). Sterile tryptone soya broth (section 12.4) was inoculated by transfer of bacterial growth from agar plate (section 12.2) using a flame sterilised loop. Cultures were grown in an anaerobic chamber comprised of CO_2 9.97%, hydrogen 9.92% with nitrogen balance at 37 °C (Don Whitley Scientific, Molecular Atmosphere Controlled System, CAL-3200, Shipley UK). After overnight growth, bacteria were pelleted by centrifugation at 3800 rcf for 5 mins, the supernatant was removed and the pellet was re-suspended in sterile PBS. This was repeated three times. After the third centrifugation step the bacterial pellet was re-suspended in 3% formaldehyde (P6148; SigmaAldrich, UK) in PBS and incubated at room temperature for 1 hr to fix. The bacteria were again washed three times by centrifugation and re-suspended in sterile PBS. Bacterial concentration was then estimated by spectrophotometry (section 12.11) and diluted in additional sterile PBS to give a

suspension of $1x10^9$ bacteria per mL. The bacteria were then heat killed by incubating at 80 °C for 20 mins. This bacterial suspension was then treated with 33 µL of Vigam liquid (5 mg/mL IgG; Bio Products Laboratory, Hertfordshire, UK) per mL of bacteria and incubated overnight at room temperature with constant agitation to allow opsonization. *Staphylococcus aureus* is a gram positive bacterium and was opsonised with IgG to enable stimulation of cellular Fc-γ receptors (Fc-γR). Finally, bacteria were again rinsed twice in sterile PBS by centrifugation and stored at -80 °C. Bacterial numbers were again estimated by spectrophotometry to re-suspend in PBS to give $6x10^8$ bacteria/mL.

12.6 *Fusobacterium Nucleatum* (*FN*)

The periodontopathogen *F. Nucleatum* (ATCC 10953; LGC Standards, Germany) supplied as freeze dried bacterial powder was dissolved in 3 mL brain heart infusion broth supplemented with 10% serum (BO0129E; Oxoid). 100 µL of the above suspension was streaked onto horse blood agar plates (section 12.3) and incubated for 48 hrs in an anaerobic chamber of CO_2 9.97%, hydrogen 9.92% with nitrogen balance at 37 °C (Don Whitley Scientific, Molecular Atmosphere Controlled System, CAL-3200, Shipley UK). In addition, another plate was inoculated to be left at aerobic conditions at 37 °C to determine purity.

After growth of bacterial cultures on agar plates, a single bacterial colony was inoculated in 1 L sterile brain infusion broth using a flame sterilised loop and again grown in anaerobic chamber for 48 hrs as described above. After incubation, 1 mL of this bacterial suspension was further diluted in 1 L broth and

streaked in new agar plates for bacterial quantification. The number of bacteria present on the agar plates was used to approximate the number of bacteria present in the broth culture. Subsequently then bacteria was isolated from broth cultures by centrifugation, washed three times in PBS and heat treated at 80 °C for 20 mins prior to dilution with additional sterile PBS to give a final stock suspension of $4x10^8$ cells/mL, which was stored at -30 °C until further use.

12.7 Identification of bacteria

The identification of bacteria was verified by streak plating out to single colonies which were primarily gram stained later to observe microscopic cell morphology. This method aided in distinguishing between *Streptococci* and *Staphylococci* species. The reference system used for identification was Bergey's manual of determinative bacteriology.

12.8 Crystal violet solution

10 g of crystal violet (C0775; Sigma-Aldrich) was dissolved in 100 mL of 95% ethanol. 20 mL of this was mixed with 80 mL of 1% ammonium oxalate (A8545; Sigma-Aldrich) in distilled water and allowed to stand for several weeks prior to use.

12.9 Carbol fuchsin

Strong carbol fuchsin (351874U; Birmingham Dental Hospital) was diluted 1:9 in distilled water.

12.10 Gram staining procedure

Gram staining was performed by placing a drop of sterile 85% saline on a microscope slide. A sterile loop was used to transfer bacterial colonies and is further emulsified in this saline drop. This bacterial suspension was dried by passing the slide several times through a flame to fix the bacteria. The bacteria were then covered with crystal violet for 30 secs, rinsed under tap water, Lugols iodine (L6146; Sigma-Aldrich) was applied for 15 secs, rinsed, flooded with acetone and washed immediately, then treated with carbol fuchsin (section 12.9) for 15 secs and rinsed. The slide was blotted dry and viewed under oil immersion microscope (LeitzDialux 22, Germany). This procedure distinguishes between gram positive and negative bacteria as gram staining using crystal violet stains gram positive bacteria species purple as rich in peptidoglycan outer layer. Whereas gram negative bacteria are counter stained pink with carbol fuchsin as these species have an outer lipid membrane which is further removed by acetone.

12.11 Determination of bacterial growth by spectrophotometry

Cell growth was estimated using a spectrophotometer (Jenway 6300) by measuring the optical density at 600 nm (OD_{600nm}). Non-inoculated samples of media were used to correct for media changes in absorbance at OD_{600nm} not due to bacterial growth. The OD_{600nm} values that were used to estimate bacterial growth were calculated by the Forysth Institute, Boston.

Appendix III

Raman spectra of the Ti oxide powders used in the current study are displayed. Spectra were obtained using a Renishaw inVia Raman microscope (Renishaw Plc, Wotton-under-Edge, UK) with an excitation wavelength of λ=633 nm. Anatase (~30 nm) and rutile (~50 nm) powders matched standard spectra and the mixed oxide (~66 nm) species contains peak assignments consistent with an admix of rutile and anatase (anatase fraction is likely to be larger).

(a) Rutile (~50 nm) powder

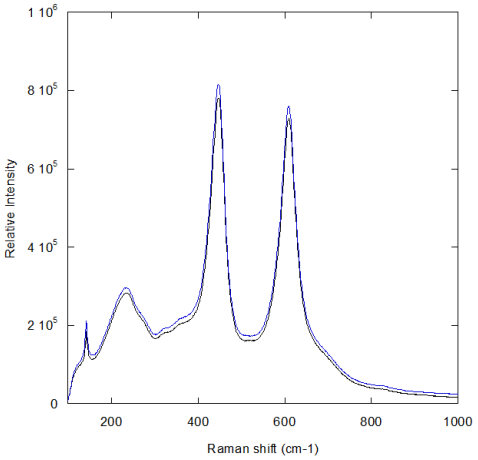

(b) Anatase (~30 nm) powder

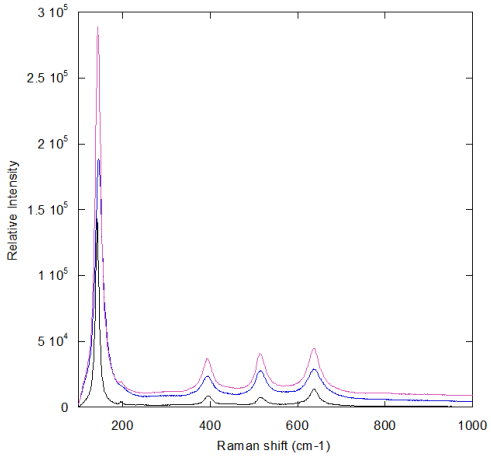

(c) Mixed oxide (~66 nm) species

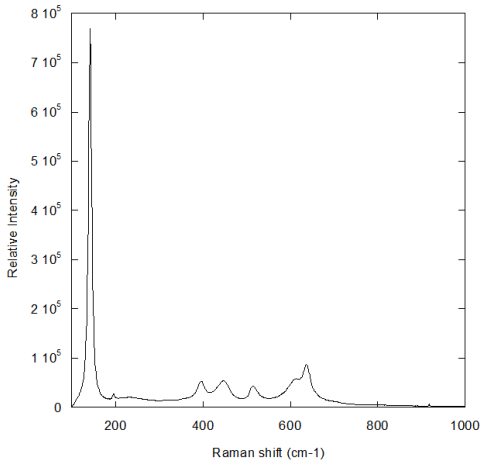

Appendix IV

INFLAMMATORY CYTOKINE RELEASE FROM HUMAN NEUTROPHILS EXPOSED TO TITANIUM IMPLANT DERIVATIVES

13.1 PREFACE

An Enzyme Linked Immunosorbant Assay (ELISA) was employed for *ex-vivo* measurement of inflammatory cytokines (IL-1β and IL-6) release in supernatants collected at 0, 8, 16, and 24 hrs from neutrophils challenged with micron and nano sized Ti implant derivatives (oxide or metallic) at concentrations of 2000, 200, 20 and 2 ppm and compared with control conditions. Given the evidence of a significant decrease in ROS and NET production from neutrophils co-stimulated with Ops *Sa* (Fc-γR mediated) and Ti (oxide or metallic), the impact on the release of IL-1β and IL-6 cytokines was also measured from cells exposed to similar stimuli and compared with stimulated controls.

13.2 INTRODUCTION

13.2.1 Neutrophil cytokine release

Alongside phagocytosis and reactive oxygen species (ROS) production (Amulic et al., 2012), neutrophils have the capacity to produce and cause a cascade release of a variety of pro- and anti-inflammatory mediators which possess a broad spectrum of biological activities. Cytokines are amongst the most well studied inflammatory signalling molecules involved in acute and chronic inflammatory responses (Edwards, 1994 & Hatanaka et al., 2006). A cytokine is a small protein less than 20kDa which serves with a hormone like function which enables immune cells to communicate with each other (Luster, 1998). During an inflammatory response numerous cytokines are generated which influence the release of other cytokines and also affect neutrophil functions (such as respiratory burst, degranulation and expression of plasma membrane receptors) (Cassatella, 1995).

It is accepted that the cytokine cascade is highly complex involving expression of integrins on leukocytes and activation of numerous pathways (Cassatella, 1995). The release of any specific cytokine has a variety of roles in the inflammatory processes (Edwards, 1994) and with this respect, IL-1β cytokine which is an integral unit of the IL-1 family is one of the most widely studied inflammatory cytokines (Hatanaka et al., 2006, Miller et al., 2007, Wright et al., 2010 & Yazdi et al., 2010). It's secretion through the NLRP3 inflammasome pathway in neutrophils is recognised as potent mediators of inflammation (Yazdi et al., 2010).

In addition, IL-1β is reported to be specifically involved in neutrophil activation and recruitment against *S. aureus* infection *in-vivo* (Miller et al., 2007).

In addition to IL-1β function in neutrophils, IL-6 is another ubiquitous pro-inflammatory cytokine released by the neutrophil via the STAT3 pathway (Fielding et al., 2008). The biological mechnisms of IL-6 release are complex, although its release at inflammatory sites is recognised to regulate transition of neutrophils infiltrates to monocyte recruitment which is a hallmark of acute inflammation (Kaplanski et al., 2003). In addition, the precise functionality of IL-6 in neutrophils is still not categorised although it has been reported to modulate neutrophil function and is shown to delay neutrophil apoptosis thus resulting in prolonged ROS release (Biffi et al., 1996).

13.2.2 Measurement of cytokine release

ELISA is a valuable tool which enables simple and accurate quantification of inflammatory cytokines in cell culture supernatants through antibodies and enzymatic detection reactions (Edwards, 1994 & Kobayashi et al., 2002). Limited studies have been performed to detect the release of various cytokines from Ti oxide stimulated neutrophils (Tamura et al., 2002, Goncalves et al., 2010 & Pierre, 2010). However, recently some investigators have also reported the interference of nanoparticles with enzymatic immunoassays such as ELISA (Kroll et al., 2008).

The impact Ti stimulation (oxide or metallic) on the release of both IL-1β and IL-6 cytokines is poorly established (Yazdi et al., 2010). Therefore, these findings would provide further insights into understanding the pro-inflammatory potential of Ti interactions with neutrophils in the peri-implant environment and will help to elucidate mechanistic pathways determining the influence of Ti exposure on neutrophil function.

13.3 METHODS

13.3.1 Lipopolysaccharide (LPS) preparation

A component of gram negative bacteria cell wall are LPS, which activate TLR-4/2 in conjunction with CD14, MD-2 and LPS binding protein. LPS (L4654; Sigma-Aldrich) provided in lyophilized powder was suspended in PBS for use at a concentration of 10 μg/mL.

13.3.2 Cell purification and culture conditions

Isolated neutrophils (2.5×10^6 cells/mL) (Appendix I) were re-suspended in RPMI-1640 supplemented with 0.3 g/L glutamine, 2.32 g/L HEPES, 2 g/L sodium bicarbonate, 100 μg/mL streptomycin, 100 U/mL penicillin. Cells were subsequently cultured in 37 °C in a 5% CO_2 atmosphere for up to 24 hrs with and without opsonised *S.aureus*, *F.nucleatum* and LPS (10 μg/mL) as control stimuli. Ti (oxide or metallic) at concentrations of 2000, 200, 20 and 2 ppm dispersed in RPMI were employed as experimental stimuli. In addition, neutrophils were co-stimulated with Ops-*Sa* and Ti stimuli. Supernatants were removed at 0, 8, 20 and

24 hrs following centrifugation at 5000 rcf for 5 mins and stored at -80 °C. IL-1β and IL-6 release in the collected supernatants was determined by ELISA kits specific for humans -(IL-1β, Ebiosciences, Australia and IL-6 2bscientific, USA). The experiment was repeated five times with neutrophils sourced from different healthy volunteers.

13.3.3 Measurement of Pro-Inflammatory Cytokine IL-1β Release

The assay was performed in 96-well transparent plate (Corning Costar 9018,UK) strictly according to the manufacture's instructions. Plates were coated with 100 µL of the capture antibody and stored overnight at 4 °C. Prior to addition of the analyte to be tested, the plate was washed with PBS-Tween20 five times following subsequent addition of 200 µL of 5% PBS-BSA per well for 1 hr at room temperature. Liquid from the wells was then aspirated and the plate was washed again five times. 100 µL of the analyte to be tested and known concentrations IL-1β analyte were added per well and stored overnight at -4 °C for maximal sensitivity. After overnight incubation, aspiration and repeated washing was conducted five times. 100 µL of IL-1β detection antibody was added to the wells and incubated at room temperature for 1 hr. Liquid from the plate was aspirated and washed again five times with PBS-Tween20 to remove any unbound antibody-enzyme reagent. 100 µL of HRP was added per well for 30 mins following subsequent aspiration and wash with PBS-Tween20 seven times. 100 µL of substrate TMB solution (provided in the kit) was added per well and incubated at room temperature for 15 mins (protected from light). Immediately, 50 µL of 1 M H_2SO_4 solution was added per well and the plate was read using a

microplate reader set at optical density of 450 nm (Bio-rad 550, UK) and corrected at 570 nm respectively. The detection limit was less than 4 pg/ml. All samples were assayed in duplicate.

13.3.4 Measurement of Pro-Inflammatory Cytokine IL-6 Release

The assay was performed in 96-well plate (Corning Costar 9018, UK) strictly according to the manufacture's instructions. Plates were coated with 100 µL of capture antibody and stored overnight at 4 ^{o}C followed by washing twice with PBS-Tween followed by adding 250 µL of 5% PBS-BSA to the wells for two hrs at room temperature. Plates were then aspirated and left at room temperature to dry for at least 24 hrs. Post coating with the capture antibody and 5% BSA, 100 µL of the standard, control, or sample were added per well. The tested samples for IL-6 were incubated for at least 1 hr with 50 µL of IL-6 detection antibody. Post one hr incubation, the plate was aspirated and washed at least three times with PBS-Tween 20 to remove any unbound antibody-enzyme reagent. 100 µL of HRP was added to the wells for 20 min at room temperature and again aspirated and washed with PBS-Tween as above. Then 100 µL of substrate TMB solution (provided in the kit) was added to each well and then incubated and protected from light at room temperature for 15 mins. 100 µL of 1M H_2SO_4 solution was added to each well immediately after 15 mins to stop the reaction. The optical density of each well was immediately read using a microplate reader set to read at 450 nm (Bio-rad 550, UK) respectively. The detection limit for IL-6 assay was 2 pg/mL. All samples were assayed in duplicates.

13.4 RESULTS

13.4.1 *Ex-vivo* cytokine (IL-1β and IL-6) release quantification from stimulated neutrophils

The maximum release of pro-inflammatory cytokines IL-1β and IL-6 in supernatants collected from stimulated neutrophils at 0, 8, 16 and 24 hrs is presented in the form of histogram plots (Figure 13.1).

Increased release of IL-1β and IL-6 was observed from neutrophils stimulated with the positive controls, Ops *Sa* (Fc R mediated), LPS and FN (TLR4 mediated) when compared with unstimulated neutrophils. The magnitude of cytokine release increased with time. In addition, a higher order of magnitude of IL-6 inflammatory cytokine release was observed from all stimulated conditions in comparison to IL-1β release. Amongst, the positive controls employed the highest order of magnitude cytokine release was observed in response to Ops *Sa*.

Following Ti stimulation neutrophils released IL-1β and IL-6 in a dose dependent pattern however, the magnitude of the cytokine release was observed to be much lower than positive control stimulated neutrophils. In addition, similar to control stimulated cells, the orders of IL-6 cytokine release were also observed to be higher than IL-1β. A series of experiments were conducted to identify the impact of the Ti stimuli on the ELISA assay. The findings (not shown) demonstrated that the Ti stimuli interrupted the assay significantly (presumed to bind to the antibody) leading to aberrant results which could not be safely interpreted. This

phenomenon is rarely reported but has recently been acknowledged in the literature.

Figure 13.1 Representative histogram plots demonstrating maximum release of IL-1β and IL-6 cytokines in supernatants collected from stimulated neutrophils at various time points